



Universität Hamburg
DER FORSCHUNG | DER LEHRE | DER BILDUNG

FAKULTÄT
FÜR MATHEMATIK, INFORMATIK
UND NATURWISSENSCHAFTEN

Symmetry-Adapted Matrix-Product-State Approach to Quantum Magnetism

Dissertation

zur Erlangung des Doktorgrades an der
Fakultät für Mathematik, Informatik und Naturwissenschaften
Fachbereich Physik
Universität Hamburg

vorgelegt von

Cassian Plorin

Hamburg, 2024

| | |
|---|---|
| Gutachter der Dissertation: | Prof. Dr. Michael Potthoff Prof. Dr. Tim Wehling |
| Zusammensetzung der Prüfungskommission: | Prof. Dr. Daniela Pfannkuche Prof. Dr. Michael Potthoff Prof. Dr. Tim Wehling Prof. Dr. Alexander Lichtenstein Prof. Dr. Henning Moritz |
| Vorsitzende der Prüfungskommission: | Prof. Dr. Daniela Pfannkuche |
| Datum der Disputation: | 8. November 2024 |
| Vorsitzender des Fach-Promotionsausschusses PHYSIK: | Prof. Dr. Wolfgang Parak |
| Leiter des Fachbereichs PHYSIK: | Prof. Dr. Markus Drescher |
| Dekan der Fakultät MIN: | Prof. Dr.-Ing. Norbert Ritter |

Für meinen Opa.

Abstract

In this thesis the computational technique *Variation of Matrix Product States* is examined with a special focus on the implementation of a non-Abelian $SU(2)$ symmetry and the efficient construction and compression of so-called matrix product operators needed for calculations building upon matrix product states. This method is applied to determine quantum-mechanical groundstates of various systems, namely magnetically frustrated molecules, the interacting protons and neutrons in an atomic nucleus, and a superconducting host with magnetic adatoms as impurities.

The antiferromagnetic Heisenberg model on the frustrated C_{60} fullerene geometry yields a spin-singlet groundstate with a short-range and exponentially decaying spin correlation. The same model is investigated on another frustrated geometry: the sodalite cage molecule, which is a molecular version of a capped kagome lattice. The groundstate is found to be a degenerate singlet of spin that breaks the spatial symmetry of the molecule. The particular arrangement of atoms in this molecule allows for localized magnons, which give rise to broad magnetization plateaus.

The nuclear-pairing problem, i. e., the effective interaction between protons and neutrons in atomic nuclei, can be mapped onto a lattice model and then be studied using the above-mentioned method, which was originally developed for the description of condensed-matter systems. It turns out that for singlet coupling of the nucleons the groundstate exhibits surprisingly low entanglement and is therefore well-suited for an investigation based on matrix product states. The experimental values for the so-called even-odd mass differences for tin and lead can be reproduced with excellent agreement. The entanglement structure of the nuclei for different fillings can be used to detect magic numbers for nucleons. Since these physical systems are not inherently one-dimensional, it is essential to use efficiently constructed and compressed matrix product operators, because the mapping to a chain introduces long-range hopping.

For two quantum spin- $1/2$ impurities located on top of a one-dimensional conventionally superconducting host of electrons described in terms of a Kondo impurity model with a BCS host system, the competition between Kondo-singlet formation and indirect magnetic exchange of the RKKY-type is studied. For weak exchange couplings J the impurities are subject to an indirect magnetic exchange mediated by the substrate. An emerging indirect magnetic exchange coupling J_{RKKY} is derived using second-order perturbation theory in J . For an even atomic distance between the impurities and with increasing superconducting pairing strength $|\Delta|$, the emergent coupling changes its sign, leading to a phase transition between an RKKY singlet and an RKKY triplet. For stronger exchange couplings the system exhibits a partial-Kondo-screening phase in which only one impurity is screened. Finally, for large exchange couplings, the system enters a local-Kondo-singlet phase, in which both impurities are screened individually. For an odd impurity distance there is a smooth crossover between an RKKY singlet and a singlet with local Kondo screening.

By considering a toy model with only three lattice sites, the Kondo-vs.-RKKY physics in a quantum box is studied for a conventional superconductor. Here the finite-size gap is large and the finite-size Kondo effect dominates at very weak J and $|\Delta|$. This model is also investigated by means of a self-consistent approach in which the system can adjust the local pairing strength. The topology of the self-consistent phase diagram is the same as for the toy model with preset pairing strength.

Kurzzusammenfassung

In dieser Arbeit wird die numerische Technik *Variation von Matrixproduktzuständen* mit einem besonderen Augenmerk auf die Implementierung einer nicht-abelschen $SU(2)$ -Symmetrie sowie der effizienten Konstruktion und Kompression sogenannter Matrixproduktoperatoren dargestellt. Die Methode wird angewandt, um die quantenmechanischen Grundzustände verschiedener Systeme zu bestimmen: magnetisch frustrierte Moleküle, die wechselwirkenden Protonen und Neutronen in Atomkernen, sowie ein supraleitendes Substrat mit magnetischen Adatomen, die als Störstellen auf dem Substrat platziert werden.

Das antiferromagnetische Heisenberg-Modell auf der frustrierten C_{60} -Geometrie liefert einen Spin-Singulett-Grundzustand mit einer kurzreichweitigen und exponentiell abfallenden Spinkorrelation. Dasselbe Modell wird mit dem Sodalite-Cage-Molekül auf einer weiteren käfigförmigen frustrierten Geometrie betrachtet, die dem Kagome-Gitter ähnelt. In diesem Fall ist der Grundzustand gegeben durch ein entartetes Spin-Singulett, das die räumliche Symmetrie des Moleküls bricht. Die besondere Anordnung der Atome in diesem Molekül lässt das Auftreten von lokalisierten Magnonen zu, welche zu breiten Plateaus in der Magnetisierungskurve führen.

Das Kernpaarungsproblem, also die effektive Wechselwirkung zwischen Protonen und Neutronen in Atomkernen, kann auf ein Gittermodell abgebildet und dann mit der obengenannten Methode untersucht werden, die ursprünglich für die theoretische Beschreibung von Systemen kondensierter Materie entwickelt wurde. Es stellt sich heraus, dass bei Singulett-Kopplung der Nukleonen der Grundzustand sehr wenig Quantenverschränkung aufweist und damit sehr gut für eine Untersuchung mithilfe von Matrixproduktzuständen geeignet ist. Die experimentellen Werte der sogenannten Even-Odd-Massenunterschiede für Zinn und Blei können mit hervorragender Genauigkeit reproduziert werden. Die Struktur der Verschränkung für verschiedene Füllgrade kann genutzt werden, um magische Zahlen für die Nukleonen zu finden. Da die betrachteten Systeme nicht inhärent eindimensional sind, ist es nötig, die beteiligten Matrixproduktoperatoren effizient zu konstruieren und zu komprimieren, denn die Abbildung auf eine lineare Kette erfordert langreichweitiges Hopping.

Für zwei Quanten-Spins mit Länge $1/2$, die auf einem eindimensionalen konventionell supraleitenden Substrat von Elektronen platziert werden – beschrieben durch ein Kondo-Störstellenmodell mit BCS-Supraleitungstermen für das Substrat – wird der Wettstreit zwischen Kondo-Singulett-Bildung und indirektem magnetischen Austausch vom RKKY-Typ untersucht. Für kleine Austauschwechselwirkungen J unterliegen die Störstellen einer indirekten magnetischen Wechselwirkung durch das Substrat. Eine emergente Austauschwechselwirkung J_{RKKY} wird mittels einer Störungstheorie-Rechnung bis zur zweiten Ordnung in der Stärke der Austauschwechselwirkung hergeleitet. Für einen geraden atomaren Abstand der Störstellen und für anwachsende supraleitende Paarungsstärke $|\Delta|$ wechselt diese emergente Austauschwechselwirkung ihr Vorzeichen, sodass das System einen Phasenübergang zwischen einem RKKY-Singulett und einem RKKY-Triplett aufweist. Für stärkere Austauschwechselwirkungen zeigt das System eine partielle Kondo-Abschirmung, bei welcher nur eine der beiden Störstellen mit dem Substrat ein Singulett bildet und die andere ungekoppelt bleibt. Für noch größere Austauschwechselwirkungen geht das System schließlich in einen Zustand über, in dem beide Störstellen unabhängig voneinander durch das Substrat abgeschirmt werden. Für einen ungeraden Störstellen-Abstand wird ein stetiger Übergang zwischen einem RKKY-Singulett-Regime und einem lokalen Kondo-Abschirmungs-Regime gefunden.

Durch Betrachtung eines Modells mit nur drei Gitterplätzen wird die Kondo-vs.-RKKY-Physik für kleinste konventionell supraleitende Systeme untersucht. Dabei ist die Energielücke, die auf die endliche Systemgröße zurückzuführen ist, groß, und der Finite-Size-Kondoeffekt dominiert für kleine Parameter J und $|\Delta|$. Für dieses Modell wird außerdem ein selbstkonsistenter Ansatz gewählt, bei welchem das System seine lokalen Paarungsstärken flexibel anpassen kann. Die Topologie beider Phasendiagramme ist identisch.

Table of Contents

| | |
|---|------------|
| 1 Introduction | 1 |
| 2 Variation of Matrix Product States | 5 |
| 2.1 Basic Concepts | 5 |
| 2.2 Angular Momentum in Quantum Mechanics | 22 |
| 2.3 Symmetries in Matrix Product States | 30 |
| 2.4 Construction & Compression of Matrix Product Operators | 48 |
| 3 Applications of Compressed Matrix Product Operators | 54 |
| 3.1 The Antiferromagnetic $S = 1/2$ Heisenberg Model on the C_{60} Fullerene Geometry | 54 |
| 3.2 Magnetic Properties of a Capped Kagome Molecule with 60 Quantum Spins | 59 |
| 3.3 Matrix-Product-State Approach to the Generalized Nuclear-Pairing Hamiltonian | 63 |
| 4 Kondo Screening and Indirect Magnetic Exchange through a Conventional Superconductor | 69 |
| 4.1 Model & Charge Pseudospins | 69 |
| 4.2 VMPS Results | 71 |
| 4.3 Perturbation Theory in the Exchange Coupling. | 78 |
| 4.4 Discussion: Quantum Box, Thermodynamical Limit and Self-Consistency | 85 |
| 5 Conclusion | 93 |
| A Appendix | 99 |
| A.1 Hilbert Spaces of MPS and MPO Bond Indices | 99 |
| A.2 Minimizing the Frobenius Scalar Product. | 101 |
| A.3 Properties of Clebsch–Gordan Coefficients | 104 |
| A.4 Reduced Matrix Elements | 106 |
| A.5 Product of $SU(2)$ -Symmetric Matrix Product Operators | 110 |
| A.6 Localized Magnons | 116 |
| A.7 Calculations for Perturbation Theory in J around the BCS Groundstate | 119 |
| A.8 Diagonalization of the 3-Site Toy Model | 122 |
| Bibliography | 125 |
| List of Publications | 133 |

1 – Introduction

Motivation

It is fascinating to consider what ancient thinkers postulated about the nature of the world. Take Thales of Miletus, for instance, who believed that magnetic stones possess a soul because they are able to move. While it is certainly challenging to disprove such a claim, we will not be placing magnets on a couch in the hopes that they reveal their secrets to us anytime soon. Instead, we turn our attention to a significantly more modern concept – one that, from a philosophical standpoint, is perhaps no less mysterious and intriguing than the quest to understand the origins of consciousness: quantum physics.

From the perspective of a modern physicist, at a fundamental level, the situation appears to be quite straightforward: through the Coulomb interaction, atomic nuclei attract electrons, while the same interaction also causes the electrons to repel each other. From this seemingly simple microscopic theory and the corresponding Hamilton operator for the constituents of atoms emerges a plethora of physical phenomena. P. W. Anderson wrote about the emergence of previously unknown phenomena in his very renowned article “More is different” [1], that at another scale of complexity, a system may exhibit behavior which is quite impossible to synthesize and predict from the elementary parts of the system only. In the context of condensed-matter theory, the emergence of novel effects originates from collective behavior and various competing or cooperating coupling mechanisms between many particles. This interplay often leads to the spontaneous breaking of symmetries that were present in the microscopic theory. Prime examples are the crystallization of atoms into a regular lattice, which breaks the full spatial symmetry of the Coulomb interaction down to a discrete translational symmetry, or superconductors, in which the phase symmetry of quantum electromagnetism is broken. Beyond these, the rich phenomenology of condensed-matter systems offers more: exotic, non-Fermi-liquid states of matter such as spin glasses or strange metals, and correlation effects such as the correlation-induced Mott insulator or high-temperature superconductivity [2–4]. The latter can be found, e. g., in doped cuprates or as metastable photo-induced superconductivity in fullerenes [5–10].

The first description of ferromagnetism is often attributed to above-mentioned Thales, who is said to have discovered magnetic stones in the region of Magnesia in ancient Greece more than two millennia ago. But although this kind of magnetism has attracted scientific interest for such a long time, only with the advent of quantum mechanics a rigorous description has become possible. The significance of quantum mechanics is encapsulated in the Bohr-van Leeuwen theorem [11, 12], which, in colloquial terms, states that magnetism is exclusively a quantum-mechanical phenomenon, because within classical physics the thermal average of the magnetization would need to be zero. However, quantum magnetism encompasses a multitude of phenomena and ordering schemes. In addition to ferromagnetism, which is present in the elementary materials iron, cobalt, nickel, and gadolinium, these include antiferromagnetism, diamagnetism, and paramagnetism.

Very roughly, one can distinguish between dia- and paramagnetism on the one hand and ferro- and antiferromagnetism on the other hand [13]. The former describes how a solid reacts to external magnetic fields with a magnetization of a previously magnetically unordered system. In a diamagnet, the electrons orbiting the nuclei induce a magnetic moment, which according to Lenz’ law is oriented antiparallel to the external magnetic field, thus mitigating the field in the solid. In paramagnetic systems there are permanent magnetic moments, but they are unordered and only align due to the external field. In contrast, the latter two are subtypes of collective collinear magnetism, in which the quantum-mechanical exchange interaction of magnetic moments causes an intrinsic magnetic order for temperatures lower than a certain critical value. For ferromagnetic materials, the interaction favors the parallel alignment of magnetic moments, so that the magnetic moments add up and yield an extensive magnetization that breaks the rotational symmetry by selecting a distinct direction. Antiferromagnets tend to have antiparallel magnetic moments and therefore have no macroscopic magnetization,

which, however, does not imply the absence of magnetic order. Unlike with a ferromagnetic order, the staggered alignment of antiferromagnetism is not compatible with each lattice. This is the reason for geometry-induced magnetic frustration. Additionally, there exists a magnetic order in between antiferromagnetism and ferromagnetism: ferrimagnetic systems are usually made of different species of atoms, or at least their lattice structure divides into inequivalent sublattices. While they exhibit an antiferromagnetic coupling between the inequivalent magnetic moments, one outweighs the other in number or magnitude, so that there is a net magnetization.

Since the formation of magnetic moments in a solid is due to electrons and, in particular, their spin, the theoretical treatment of collective magnetism focusses on the electronic structure. Theoretical physicists try to find simple models from which complex magnetic phenomena emerge. Itinerant magnetic moments are caused by electrons that can move through a solid, while localized magnetic moments appear for electrons which are immobile. To illustrate, consider a solid made of nickel, which has the electron configuration $\text{Ni} = [\text{Ar}] 3d^8 4s^2$ or $[\text{Ar}] 3d^9 4s^1$. The 3d and 4s orbitals overlap and form a band of delocalized states, allowing electrons to move through the lattice. The itinerant electrons of such a material can be described in terms of the Hubbard model [14], which is a second-quantized tight-binding Hamilton operator that contains a hopping term for electrons from one lattice site to a neighboring site, thereby optimizing their energy via delocalization, and a Coulomb interaction for electrons at the same site. A qualitatively different physical situation appears in europium(II) oxide. Each europium atom donates two electrons to oxygen, so that it comes with an electron configuration $\text{Eu}^{2+} = [\text{Xe}] 4f^7$. Since the 4f orbitals are more localized, the electrons are less mobile. By Hund's rule, the electronic spins add up, so that each europium atom contributes a total magnetic moment of length $7/2$. This situation is described by the Heisenberg model [15], which assumes localized magnetic moments at each site. These localized magnetic moments interact via a Heisenberg exchange coupling that can be ferromagnetic or antiferromagnetic. The Kondo lattice model (and its close relative, the Anderson impurity model [16, 17]) is suited for a mixed setup, in which localized magnetic moments as well as itinerant magnetic moments appear [18]. Typically, a local exchange coupling between the localized and itinerant magnetic moments is assumed. Rather than via a direct exchange, the localized magnetic moments predominantly interact via an indirect magnetic exchange mediated by the itinerant electrons [19–22]. Gadolinium with $\text{Gd} = [\text{Xe}] 4f^7 5d^1 6s^2$ is an example for such a material. The seven 4f electrons create a localized spin- $7/2$, while the 5d and 6s orbitals generate partially filled conduction bands for itinerant magnetic moments. The Kondo lattice model is the prototypical model to study heavy-fermion physics [23, 24]. Coming back to Thales' intuition of magnetism, one could possibly say that the souls of these magnetic materials can be captured in either a Hubbard, Heisenberg, or Kondo model.

An intriguing question concerns the simultaneous presence of multiple collective phenomena. A superconductor serves as an ideal diamagnet, repelling magnetic fields from the bulk of the material. One may then ask which effect dominates when a system exhibits conventional superconductivity as well as collective magnetism due to direct or indirect magnetic exchange. Among other goals, this thesis aims at a substantial contribution to this long-standing and still controversially discussed subject.

However, even for the conceptually strongly simplified point of view provided by the mentioned effective model Hamilton operators, a solution of the many-body Schrödinger equation is not accessible due to the complexity inherent to the model systems themselves. Full diagonalization of the Hamilton matrices for hundreds of particles exceeds the computational limits due to exponential scaling, not to mention real macroscopic systems with 10^{23} particles. At this point, more sophisticated computational methods come into play. In the following, a small excerpt of the core ideas of important and influential techniques to tackle the quantum many-body problem is given. The *Hartree-Fock* method treats interactions on a mean-field level by replacing parts of the dynamic variables of a Hamilton operator by expectation values [25, 26]. This way, the dynamical variables only couple to an averaged value of all other parts of the system. The method comes from a time before the advent of computers in theoretical physics, yet it helps to overcome the computational problem of exponentially large matrices by allowing to restrict calculations to the single-particle Hilbert space, which only grows linearly in the system size. However, the decoupling of interaction terms is both the main advantage and disadvantage, because the method

does not capture correlation effects, which are crucial for the occurrence of many interesting phenomena. The *Density Functional Theory* focusses on the electron density in the system's groundstate, and aims to derive it from a non-interacting system with an effective potential [27–29]. While in principle the existence of such a system is guaranteed by the Hohenberg-Kohn theorem and the Kohn-Sham construction, in practice it is challenging to find well-suited approximations to the exchange-correlation functional that incorporates the full electronic interaction into a single-particle potential. Density functional theory was established in the 1960s and 1970s and is still widely used for ab-initio calculations nowadays. In contrast, Monte Carlo methods do not attempt to solve the full problem, but perform a random sampling of datapoints to find a good approximative result. Originating from the Manhattan Project [30], stochastic sampling algorithms inspired from Monte Carlo methods are used in various different contexts. Starting from the 1960s, the *Quantum Monte Carlo* method was applied to study quantum-mechanical problems in condensed-matter physics [31–33]. The occurring sign problem excludes several physical situations from being solved by this ansatz, as the “signal-to-noise ratio” of the sampling is dissatisfying. This happens in particular for fermions or frustrated systems. The idea of *Dynamical Mean-Field Theory* is to map an interacting lattice system onto an impurity model with only a single correlated site [34–36], which is computationally less demanding and can be solved with a suited technique, for example exact diagonalization or Quantum Monte Carlo. The motivation behind this is that in infinite dimensions, the self-energy functional of electrons becomes local, so that the local lattice Green's function becomes identical to the impurity Green's function of the impurity model for properly chosen bath parameters that are obtained from a self-consistency condition. [37]. While strictly speaking this holds true only for an infinite lattice coordination number, dynamical mean-field theory has achieved very good results for lattices in three spatial dimensions.

The method of choice for low-dimensional systems is *Variation of Matrix Product States*, at least if one is interested in energetically low-lying states. The basic idea of this method is to skillfully truncate the reduced density matrix of the groundstate for any division of the system, so that as much information as possible about entanglement in the system is retained during the process. The algorithm can be formulated as a variational ansatz employing matrix product states. The method is particularly well-known for its ability to determine groundstates of strongly correlated systems in one dimension at zero temperature very accurately. Therefore, this method fills a niche that is not covered by the other methods: density functional theory is not optimally suited for strongly correlated systems, Quantum Monte Carlo suffers from the sign problem for fermionic systems, and the infinite-dimension approximation of dynamical mean-field theory applies poorly here. Moreover, the Green's-function based dynamical mean-field theory runs into problems in cases where non-local correlations are important. On the other hand, variation of matrix product states encounters problems when excited or thermal states are of interest.

In my PhD thesis, I present the concept of variation of matrix product states and show applications of this technique to physical problems in rather different fields. The overarching theme is quantum magnetism: beyond the already mentioned competition of superconductivity and direct and indirect magnetic exchange as well as spin frustration in frustrated geometries, the pairing in atomic nuclei is also brought to the realm of quantum magnetism by mapping it onto an abstract Heisenberg model.

Organization of this thesis

This thesis is organized as follows: in Chapter 2, a fairly comprehensive overview of the computational method *Variation of Matrix Product States* (VMPS) is given. This tensor-network based variational technique is the method I have used for most of the calculations during my PhD research time. The program code was originally developed by two former group members, R. Rausch and M. Peschke, but of course it is still subject to enhancement and progress. The first section of the chapter sets the stage and introduces the main idea of matrix product representations and the well-known groundstate algorithm. After a brief summary of the theory of angular momentum in quantum mechanics, special emphasis is put on the incorporation of symmetries in these tensor networks. As this reflects a large part of the conceptual understanding, detailed calculations are presented in this section. Finally, this rather long methodical chapter ends with the handling of matrix product operators. It contains a description of efficient ways to construct and compress matrix product operators, which was my main contribution to the program code project.

Chapter 3 highlights exemplary applications of our VMPS method to different physical problems. The results were obtained in a collaboration and are published in three research articles [CP1, CP2, CP4], of which I am a co-author. In this thesis, summarizing overviews of these publications are given. The physical problems range from magnetically frustrated fullerene molecules to nuclear physics. A common property of the fullerene molecules and the nuclear-pairing problem in atomic nuclei is that these systems are not inherently one-dimensional, so that the Hamilton operator and its square cannot be chosen as short-ranged operators even by a smart choice of lattice site numbering. Thus, it was only with efficiently constructed and compressed matrix product operators that these problems came into reach for VMPS. The first section is concerned with the antiferromagnetic Heisenberg model on the fullerene molecule C_{60} . In the second section results are presented for a similar yet hypothetical molecule, which, as a molecular relative of the capped kagome lattice, also features a non-bipartite and thus frustrated geometry. The third section deals with our approach to apply the matrix-product-state technique to nuclear physics, namely investigating the nuclear-pairing Hamilton operator by means of VMPS.

Chapter 4 is dedicated to the interplay of quantum magnetism and superconductivity. To this end, a BCS superconductor is investigated with quantum impurity spins placed on it. In particular, the mechanisms of RKKY-like indirect magnetic exchange and Kondo-like screening of impurity spins are studied. In the first section, the model and its symmetries are introduced, while in the second section VMPS results are presented and discussed. The third section shows a perturbative treatment of the exchange coupling of the impurity spins to the substrate from which the emergent RKKY coupling can be obtained. In the fourth section, the discussion is broadened by the additional question of system sizes and finite-size gaps, as well as a self-consistent treatment of the BCS theory. These results are published in [CP5].

Finally, in Chapter 5 the results presented in this thesis are summarized and connections between these topics are drawn. Moreover, an outlook with ideas for future research is given.

The Appendix contains several analytic calculations, which were too long and unhandy for the main part, but which are crucial for the understanding.

2 – Variation of Matrix Product States

2.1 – Basic Concepts

The quantum many-body problem

The quantum-mechanical description of interacting particles is accompanied by the challenge of dealing with large Hilbert spaces. In order to solve the eigenvalue problem for the time-independent Schrödinger equation, i. e., $\hat{H}|\psi\rangle = E|\psi\rangle$, the problem is shifted to the diagonalization of a matrix of dimension $D \times D$ with D the dimension of the Hilbert space by switching to a matrix representation of the Hamilton operator.

Usually the entire Hilbert space of a many-body system is made up of a tensor product of smaller Hilbert spaces:

$$\mathcal{H} = \mathcal{H}_{\text{loc}}(1) \otimes \mathcal{H}_{\text{loc}}(2) \otimes \cdots \otimes \mathcal{H}_{\text{loc}}(L). \quad (2.1)$$

These smaller Hilbert spaces, which are called *local Hilbert spaces* in the context of this thesis, may be thought of as Hilbert spaces of individual particles or, in a common condensed-matter setup, they describe the spatially localized orbitals derived from Wannier functions in a tight-binding approximation. In this situation, within the formalism of second quantization, the local Hilbert space characterizes the different electronic configurations of a lattice site. This formalism also allows for the incorporation of correct commutation relations for indistinguishable particles. The local Hilbert spaces may become even more abstract – e. g., this concept will be used to distinguish different angular momentum shells in a nucleus later in this thesis. The local Hilbert spaces $\mathcal{H}_{\text{loc}}(\ell) = \text{span}(|n_\ell\rangle \mid 1 \leq n_\ell \leq d_\ell)$ with dimension d_ℓ may or may not be isomorphic. For translationally symmetric lattices in condensed matter, the local Hilbert spaces are often copies of each other.

The problem of the exact-diagonalization approach described above becomes apparent when looking at the involved matrix dimension. The dimension of the entire Hilbert space grows exponentially in the system size:

$$D = \prod_{\ell=1}^L d_\ell = d^L \quad \text{for } d_\ell = d. \quad (2.2)$$

The method of numerical diagonalization is limited to small systems by this exponential growth. The physical state of the entire system can be written down as a linear combination in the basis corresponding to the local Hilbert spaces:

$$|\Psi\rangle = \sum_{n_1, \dots, n_L} \psi_{n_1 \dots n_L} |n_1, \dots, n_L\rangle. \quad (2.3)$$

The complexity of the problem manifests itself in the appearance of the coefficients $\psi_{n_1 \dots n_L}$, which form a tensor of order L . Each index of the tensor connects to a state $|n_\ell\rangle$ in a local Hilbert space. In general, this tensor cannot be separated into a product of multiple tensors of order 1. If this is possible, such a state is called a product state, as it can be written as a product of states in the local Hilbert spaces:

$$\begin{aligned} |\Psi\rangle &= \sum_{n_1, \dots, n_L} \psi(1)_{n_1} \cdots \psi(L)_{n_L} |n_1\rangle \otimes \cdots \otimes |n_L\rangle = \left(\sum_{n_1} \psi(1)_{n_1} |n_1\rangle \right) \otimes \cdots \otimes \left(\sum_{n_L} \psi(L)_{n_L} |n_L\rangle \right) \\ &= |\psi(1)\rangle \otimes \cdots \otimes |\psi(L)\rangle. \end{aligned} \quad (2.4)$$

Two remarks are in order. First, in the case of second quantization the splitting of an occupation number state into individual states, $|n_1, n_2\rangle = |n_1\rangle \otimes |n_2\rangle$, is a suggestive notation used in this thesis that should always

be understood as nothing more than an expression of the fact that the occupation numbers for different modes are independent of each other. Second, for indistinguishable particles the (anti-)symmetrization sometimes prevents states from being in a product state form, although within second quantization, they are product states. For example one may consider two fermions in orbitals ψ_1 and ψ_2 , where the corresponding fermionic creation operators are \hat{c}_1^\dagger and \hat{c}_2^\dagger :

$$|\Psi\rangle = \frac{1}{\sqrt{2}} (|\psi_1\rangle \otimes |\psi_2\rangle - |\psi_2\rangle \otimes |\psi_1\rangle) = \hat{c}_1^\dagger \hat{c}_2^\dagger |0, 0\rangle^{(-)} = |1, 1\rangle^{(-)}. \quad (2.5)$$

Here, the minus sign marks anti-symmetrized occupation number states. The first-quantized state as a Slater determinant cannot be written in a product state form, whereas the second-quantized state is in a simple product state form. The same ambiguity holds true for other choices of local Hilbert spaces, which in this context corresponds to a unitary transformation of creators and annihilators from one set of quantum numbers to another: while a state in reciprocal space may be a product state, this does not have to be true for its Fourier transform. Therefore, the notion of product states depends on the choice of factorization of the entire Hilbert space into local Hilbert spaces.

In the following, the local Hilbert spaces can often be thought of as modes belonging to different quantum numbers (such as lattice site, crystal momentum, or more abstract combinations), with the two possible states being an unoccupied or an occupied mode.

Single-particle physics

In a tight-binding description of electrons on a lattice, a general Hamilton operator is given by

$$\hat{H} = \hat{H}_0 + \hat{V} = \sum_{\alpha, \beta} t_{\alpha\beta} \hat{c}_\alpha^\dagger \hat{c}_\beta + \frac{1}{2} \sum_{\alpha, \beta, \gamma, \lambda} U_{\alpha\beta\gamma\lambda} \hat{c}_\alpha^\dagger \hat{c}_\beta^\dagger \hat{c}_\lambda \hat{c}_\gamma. \quad (2.6)$$

The electron creation and annihilation operators fulfill fermionic commutation relations, i. e., $\{\hat{c}_\alpha, \hat{c}_\beta\} = 0$ and $\{\hat{c}_\alpha, \hat{c}_\beta^\dagger\} = \delta_{\alpha\beta}$. The indices α may split into orbital and spin degrees of freedom. In the simplest case of a one-orbital model, $\alpha = (i, \sigma)$ describes the lattice site i and the spin projection σ of a particle.

The term \hat{H}_0 , which is of second order in creators and annihilators, is called the *hopping term* and the term \hat{V} , which is of fourth order, is called the *interaction term*. Hermiticity of the Hamilton operator requires the hopping amplitudes to form a Hermitian matrix: $t_{\alpha\beta} = t_{\beta\alpha}^*$. This can be used to arrive at a simpler form of the hopping term: using the fact that the Hermitian hopping matrix is diagonalized by a unitary matrix, $\mathbf{t} = \mathbf{U}\boldsymbol{\varepsilon}\mathbf{U}^\dagger$, the action of the unitary transformation matrices can be shifted to the creators and annihilators to define a new set of fermionic operators for quasiparticles:

$$\hat{H}_0 = \sum_{\alpha, \beta} t_{\alpha\beta} \hat{c}_\alpha^\dagger \hat{c}_\beta = \sum_{\alpha, \beta, \gamma} U_{\alpha\gamma} \varepsilon_\gamma U_{\beta\gamma}^* \hat{c}_\alpha^\dagger \hat{c}_\beta = \sum_{\gamma} \varepsilon_\gamma \hat{d}_\gamma^\dagger \hat{d}_\gamma \quad \text{with} \quad \hat{d}_\alpha = \sum_{\beta} U_{\beta\alpha}^* \hat{c}_\beta, \quad (2.7)$$

$$\{\hat{d}_\alpha, \hat{d}_\beta\} = \sum_{\gamma, \lambda} U_{\gamma\alpha}^* U_{\lambda\beta} \{\hat{c}_\gamma, \hat{c}_\lambda\} = 0, \quad \{\hat{d}_\alpha, \hat{d}_\beta^\dagger\} = \sum_{\gamma, \lambda} U_{\gamma\alpha}^* U_{\lambda\beta} \{\hat{c}_\gamma, \hat{c}_\lambda^\dagger\} = \sum_{\gamma} U_{\gamma\alpha}^* U_{\gamma\beta} = \delta_{\alpha\beta}. \quad (2.8)$$

Since the new creation and annihilation operators also obey the fermionic commutation relations, another Fock space with its corresponding occupation number representation can be built from them. In the absence of an interaction term, the Hamilton operator from Equation (2.7) is now in its diagonal form and its eigenstates can easily be read off:

$$|\Psi\rangle = \hat{d}_{\alpha_1}^\dagger \cdots \hat{d}_{\alpha_N}^\dagger |\text{vac}\rangle \quad \text{with} \quad \alpha_n \neq \alpha_m \quad \text{for} \quad n \neq m \quad \Rightarrow \quad \hat{H}_0 |\Psi\rangle = \sum_{n=1}^N \varepsilon_{\alpha_n} |\Psi\rangle. \quad (2.9)$$

Since the occupation number states form a basis of the entire Hilbert space, all eigenstates of the Hamilton operator are in this simple Slater determinant form or, in the case of degeneracies, can at least be chosen in such a way.

The groundstate for a fixed number of particles N has the form that, starting from the vacuum state, the N quasiparticle modes with the lowest single-particle energies ε_α are filled with one fermion each. In the local Hilbert space decomposition that corresponds to the new quasiparticle occupations, i. e., $\mathcal{H}_{\text{loc}}(\ell) = \text{span}(|\text{vac}\rangle, \hat{d}_{\alpha_\ell}^\dagger |\text{vac}\rangle)$, the eigenstates are product states. Within this choice of local Hilbert spaces, all modes decouple and can be treated individually. In this sense, quadratic Hamilton operators imply single-particle physics. Indeed, this also holds true for Hamilton operators that contain products of two fermionic creators or annihilators and are thus not particle-number conserving because they can be brought to a particle-number conserving form by means of a Bogoliubov transformation [38, 39].

This simple procedure of decoupling generally fails in the presence of interactions: after diagonalizing the hopping part, the interaction part still couples different modes to each other. Thus the eigenstates of the Hamilton operator are not just Slater determinants, but a priori unknown linear combinations of those. In the single-particle case, instead of diagonalizing the entire $d^L \times d^L$ Hamilton matrix, one could restrict the diagonalization to the $L \times L$ hopping matrix, for which the number of rows and columns grows only linearly with the number of orbitals L . In the case of interactions, this trick is no longer possible and one has to deal with the full exponential complexity of the many-body problem.

Considering expectation values provides another perspective: in this context, Hamilton operators with only hopping terms are also often referred to as *free systems*. For these free systems, Wick's theorem states that the expectation value of every n -tuple of creation and annihilation operators factorizes into a sum of products of expectation values of two operators [40], for example

$$\langle \hat{c}_\alpha^\dagger \hat{c}_\beta^\dagger \hat{c}_\lambda \hat{c}_\gamma \rangle^{(0)} = \langle \hat{c}_\alpha^\dagger \hat{c}_\beta^\dagger \rangle^{(0)} \langle \hat{c}_\lambda \hat{c}_\gamma \rangle^{(0)} + \langle \hat{c}_\alpha^\dagger \hat{c}_\gamma \rangle^{(0)} \langle \hat{c}_\beta^\dagger \hat{c}_\lambda \rangle^{(0)} - \langle \hat{c}_\alpha^\dagger \hat{c}_\lambda \rangle^{(0)} \langle \hat{c}_\beta^\dagger \hat{c}_\gamma \rangle^{(0)}. \quad (2.10)$$

This means that higher-order correlation functions can be built from single-particle correlation functions in the case of free systems and do not yield any new information, whereas for interacting systems, the correlation functions of higher order are non-trivial.

Entanglement entropy

Entanglement entropy is a measure of how entangled two subsystems are in a state $|\Psi\rangle$. Although being called an entropy, it is not related to any lack of knowledge about the system but rather to the quantum-mechanical nature of the state. It is a manifestation of the Shannon information gained through measurement processes [41]. A state is highly entangled if measurements and thus projections in one part of the system strongly affect the quantum state in the other part. The prime example of a highly entangled state is a spin singlet formed out of two spins of length $S = 1/2$: a priori, for both spins there is an equal probability to measure the projection as up or down. If, however, one spin is found to be up, the other spin is guaranteed to be in the down state and vice versa. On the other hand, for product states measuring one part of the system and thus projecting the respective subpart of the state has no influence on the rest of the state, so a product state is not entangled.

To define the entanglement entropy, one first has to determine a partition of the total system into two parts: $\mathcal{H} = \mathcal{H}_A \otimes \mathcal{H}_B$. The state can then be written as

$$|\Psi\rangle = \sum_{a,b} \psi_{ab} |a\rangle^{(A)} \otimes |b\rangle^{(B)}, \quad (2.11)$$

where $|a\rangle^{(A)} \in \mathcal{H}_A$ and $|b\rangle^{(B)} \in \mathcal{H}_B$ are orthonormal basis vectors. The reduced density operator of subsystem A can be defined from the pure-state density operator by tracing out subsystem B :

$$\hat{\rho}_A : \mathcal{H}_A \rightarrow \mathcal{H}_A \quad \text{with} \quad \hat{\rho}_A = \text{tr}_B (|\Psi\rangle\langle\Psi|). \quad (2.12)$$

The entanglement entropy between A and B is then defined as

$$S_{AB} = -\text{tr}_A (\hat{\rho}_A \ln (\hat{\rho}_A)). \quad (2.13)$$

To investigate this quantity further, the concept of *Singular Value Decomposition* (SVD) is useful: each $n \times m$ matrix \mathbf{M} can be decomposed into a product of three matrices $\mathbf{M} = \mathbf{U}\mathbf{D}\mathbf{V}^\dagger$, where \mathbf{U} is an $n \times n$ unitary matrix, \mathbf{V} is an $m \times m$ unitary matrix, and \mathbf{D} is an $n \times m$ diagonal matrix, i. e., $D_{ij} = D_{ii}\delta_{ij}$. The entries of the diagonal matrix are non-negative. The number of non-zero entries, which are called singular values, is the rank of the matrix \mathbf{M} with $\text{rk}(\mathbf{M}) \leq \min(n, m)$.

Applying a singular value decomposition to the $\dim(\mathcal{H}_A) \times \dim(\mathcal{H}_B)$ matrix ψ with singular values σ_i yields an adapted choice of basis states (Schmidt decomposition [42]):

$$\begin{aligned} \psi_{ab} &= \sum_{a', b'} U_{aa'} D_{a'b'} V_{bb'}^* = \sum_{i=1}^{\text{rk}(\psi)} \sigma_i U_{ai} V_{bi}^* \\ \Rightarrow |\Psi\rangle &= \sum_{i=1}^{\text{rk}(\psi)} \sigma_i \left(\sum_a U_{ai} |a\rangle^{(A)} \right) \otimes \left(\sum_b V_{bi}^* |b\rangle^{(B)} \right) = \sum_{i=1}^{\text{rk}(\psi)} \sigma_i |i\rangle^{(A,U)} \otimes |i\rangle^{(B,V^*)}. \end{aligned} \quad (2.14)$$

From the normalization constraint $\langle\Psi|\Psi\rangle = 1$ follows that $\sum_{i=1}^{\text{rk}(\psi)} |\sigma_i|^2 = 1$. Multiplying an orthonormal basis with a unitary matrix preserves the orthonormality. Thus, for calculation of traces these bases can be chosen:

$$\hat{\rho}_A = \sum_{i=1}^{\dim(\mathcal{H}_B)} \sum_{(B,V^*)} \langle i|\Psi\rangle\langle\Psi|i\rangle^{(B,V^*)} = \sum_{i=1}^{\text{rk}(\psi)} |\sigma_i|^2 |i\rangle^{(A,U)} \langle i|^{(A,U)}, \quad (2.15)$$

$$\begin{aligned} S_{AB} &= - \sum_{i=1}^{\dim(\mathcal{H}_A)} \sum_{(A,U)} \langle i|\hat{\rho}_A \ln (\hat{\rho}_A) |i\rangle^{(A,U)} = - \sum_{k=0}^{\infty} \ln_k \sum_{i=1}^{\dim(\mathcal{H}_A)} \langle i|\hat{\rho}_A^{k+1} |i\rangle^{(A,U)} = - \sum_{k=0}^{\infty} \ln_k \sum_{i=1}^{\text{rk}(\psi)} |\sigma_i|^{2(k+1)} \\ &= - \sum_{i=1}^{\text{rk}(\psi)} |\sigma_i|^2 \ln (|\sigma_i|^2), \end{aligned} \quad (2.16)$$

where a formal series expansion $\ln(x) = \sum_{k=0}^{\infty} \ln_k x^k$ of the logarithm was used. Interchanging subsystems A and B shows that $S_{AB} = S_{BA}$. Furthermore, unitary basis transformations within a subsystem do not change the value of the entanglement entropy. In this sense, this quantity is well-defined. However, one may note that this definition requires a pure state $|\Psi\rangle$ and does not work for mixed states.

Equation (2.16) together with the normalization constraint shows that the entanglement entropy ranges from 0 to $\ln(\min(\dim(\mathcal{H}_A), \dim(\mathcal{H}_B)))$. The latter is the case if all singular values of the coefficient matrix are equal. If $|\Psi\rangle$ is a pure tensor with respect to the partitioning of the system, i. e., $|\Psi\rangle = |a\rangle^{(A)} \otimes |b\rangle^{(B)}$, then the entanglement entropy between subsystems A and B is zero:

$$\hat{\rho}_A = |a\rangle^{(A)} \langle a|, \quad \hat{\rho}_A^k = \hat{\rho}_A \quad \text{for all } k \in \mathbb{N}^*, \quad (2.17)$$

$$S_{AB} = -\text{tr}_A (\hat{\rho}_A \ln (\hat{\rho}_A)) = - \sum_{k=0}^{\infty} \ln_k \text{tr}_A (\hat{\rho}_A^{k+1}) = -\text{tr}_A (\hat{\rho}_A \ln(1)) = 0. \quad (2.18)$$

This means that a product state has vanishing entanglement entropy, regardless of the partitioning of the system. However, this does not mean that eigenstates of interacting systems have to have a large amount of entanglement entropy: indeed, for example the groundstates of a ferromagnetically coupled Heisenberg model, of a next-nearest neighbor antiferromagnetic Heisenberg chain at the Majumdar-Ghosh point [43, 44] or the groundstate of the AKLT model [45] exhibit very low entanglement.

Matrix product states

In the following, a method called *Variation of Matrix Product States* (VMPS) is presented. This method utilizes tensor networks to efficiently represent and manipulate quantum many-body objects such as states, operators and matrix elements. It is closely related to the *Density-Matrix Renormalization Group* (DMRG), which was proposed by S. White in 1992 [46, 47]. Indeed, some years after its original formulation it was noticed that the DMRG algorithm that searches for groundstates of finite systems can be reformulated using matrix product states. The rest of the section is devoted to clarifying what matrix product states are and how they are used to find groundstates of quantum many-body systems. It loosely follows the results from the two reviews by U. Schollwöck [48, 49], supplemented by own calculations with a focus on the needs of this thesis.

The first step is to define what a *Matrix Product State* (MPS) is: the main idea is to represent the tensor ψ of order L from Equation (2.3) with components $\psi_{n_1 \dots n_L}$ as a network of tensors of lower order. The local Hilbert spaces are thought to be arranged in a chain, where the leftmost site corresponds to $\mathcal{H}_{\text{loc}}(1)$ and the rightmost site corresponds to $\mathcal{H}_{\text{loc}}(L)$. The connections between two adjacent local Hilbert spaces are called *bonds* henceforth. For each site ℓ there is a tensor $\mathbf{A}(\ell)$ of order 3, with one index belonging to the physical index n_ℓ and two indices $i_{\ell-1}$ and i_ℓ that connect to the neighboring tensors $\mathbf{A}(\ell-1)$ and $\mathbf{A}(\ell+1)$ and thus constitute the two bonds of the site ℓ . Given a tensor ψ belonging to a state $|\Psi\rangle$, successively applying singular value decomposition brings it into such a form:

1. Start at site $\ell = 1$: Define a matrix $\mathbf{M}(1) \in \text{Mat}(d, d^{L-1})$ with entries $M(1)_{(i_0 n_1)(n_2 \dots n_L i_L)} = \psi_{n_1 \dots n_L}$. Indices within parantheses are meant to be combined to a single index by means of the Kronecker product. Two dummy indices $i_0 = 1$ and $i_L = 1$ were introduced with index domains of size $\chi_0 = \chi_L = 1$.
2. A singular value decomposition of $\mathbf{M}(\ell) \in \text{Mat}(\chi_{\ell-1} \cdot d, d^{L-\ell})$ yields $\mathbf{M}(\ell) = \mathbf{U}(\ell) \mathbf{D}(\ell) \mathbf{V}^\dagger(\ell)$, respectively in components:

$$\begin{aligned} M(\ell)_{(i_{\ell-1} n_\ell)(n_{\ell+1} \dots n_L i_L)} &= \sum_{i'_{\ell-1}, n'_\ell, \dots, n'_L, i'_L} U(\ell)_{(i_{\ell-1} n_\ell)(i'_{\ell-1} n'_\ell)} D(\ell)_{(i'_{\ell-1} n'_\ell)(n'_{\ell+1} \dots n'_L i'_L)} V^\dagger(\ell)_{(n'_{\ell+1} \dots n'_L i'_L)(n_{\ell+1} \dots n_L i_L)} \\ &= \sum_{i'_{\ell-1}, n'_\ell, i_\ell} U(\ell)_{(i_{\ell-1} n_\ell)(i'_{\ell-1} n'_\ell)} \bar{D}(\ell)_{(i'_{\ell-1} n'_\ell) i_\ell} \bar{V}^\dagger(\ell)_{i_\ell (n_{\ell+1} \dots n_L i_L)}. \end{aligned} \quad (2.19)$$

The diagonal matrix $\mathbf{D}(\ell)$ has at most $\chi_{\ell-1} \cdot d$ non-vanishing entries. The truncated matrix $\bar{\mathbf{D}}(\ell)$ is created by leaving out the zero columns in $\mathbf{D}(\ell)$. For $\bar{\mathbf{V}}^\dagger(\ell)$ the corresponding rows are left out. The index i_ℓ runs over the remaining values, its index domain is $i_\ell \in \{1, \dots, \chi_\ell\}$ with $\chi_\ell \leq \chi_{\ell-1} \cdot d \leq d^\ell$.

3. Define:

$$\begin{aligned} M(\ell+1)_{(i_\ell n_{\ell+1})(n_{\ell+2} \dots n_L i_L)} &= \bar{V}^\dagger(\ell)_{i_\ell (n_{\ell+1} \dots n_L i_L)}, \\ A(\ell)_{i_{\ell-1} n_\ell}^{i_\ell} &= \sum_{i'_{\ell-1}, n'_\ell} U(\ell)_{(i_{\ell-1} n_\ell)(i'_{\ell-1} n'_\ell)} \bar{D}(\ell)_{(i'_{\ell-1} n'_\ell) i_\ell}. \end{aligned} \quad (2.20)$$

For the tensors $\mathbf{A}(\ell)$ (also called the *MPS Tensors*) the convention used is that incoming indices are written as subscript and outgoing indices are written as superscript. The newly defined MPS bond indices i_ℓ start from a tensor $\mathbf{A}(\ell)$ and end at the next tensor $\mathbf{A}(\ell+1)$. The physical indices n_ℓ of the local Hilbert

spaces, that in order to construct the state $|\Psi\rangle$ have to be combined with ket states $|n_\ell\rangle$, are chosen to be incoming for the MPS tensors. Indices which connect to bra states $\langle n_\ell|$ have to be outgoing. Now it follows:

$$M(\ell)_{(i_{\ell-1}n_\ell)(n_{\ell+1}\dots n_L i_L)} = \sum_{i_\ell} A(\ell)_{i_{\ell-1}n_\ell}^{i_\ell} M(\ell+1)_{(i_\ell n_{\ell+1})(n_{\ell+2}\dots n_L i_L)}. \quad (2.21)$$

4. The steps 2 and 3 are repeated for the next site until the entire tensor ψ can be written (with trivial $M(L+1) \in \text{Mat}(1, 1)$, $M(L+1)_{11} = 1$) as follows:

$$\begin{aligned} \psi_{n_1\dots n_L} &= \sum_{i_0, \dots, i_L} A(1)_{i_0 n_1}^{i_1} \cdots A(L)_{i_{L-1} n_L}^{i_L}, \quad \text{and thus} \\ |\Psi\rangle &= \sum_{\substack{n_1, \dots, n_L, \\ i_0, \dots, i_L}} A(1)_{i_0 n_1}^{i_1} \cdots A(L)_{i_{L-1} n_L}^{i_L} |n_1\rangle \otimes \cdots \otimes |n_L\rangle. \end{aligned} \quad (2.22)$$

From Equation (2.20) it is obvious that the MPS tensors have full rank, i. e., when the incoming indices $i_{\ell-1}$ and n_ℓ are grouped together, the resulting matrix has full rank χ_ℓ . This means that no redundant information is kept. The MPS representation of a dual state is quite similar to that of a state, with all the directions of indices inverted and the MPS tensors adjoint:

$$\langle\Psi| = \sum_{\substack{n_1, \dots, n_L, \\ i_0, \dots, i_L}} A^\dagger(1)_{i_1}^{i_0 n_1} \cdots A^\dagger(L)_{i_L}^{i_{L-1} n_L} \langle n_1| \otimes \cdots \otimes \langle n_L|. \quad (2.23)$$

Explicit formulas for tensor networks can be quite long and tedious, so it is quite common to introduce a graphical representation of the expressions. Tensors of order n are depicted as objects with n legs each corresponding to an index, and if the legs of two tensors are connected, this means that the respective index is summed over. Although many expressions in this thesis are written down as explicit formulas, these graphical representations are provided as an aid to visualizing what is happening. For example, the process of transforming a huge tensor of order L into an MPS-like tensor network is shown in Figure 1.

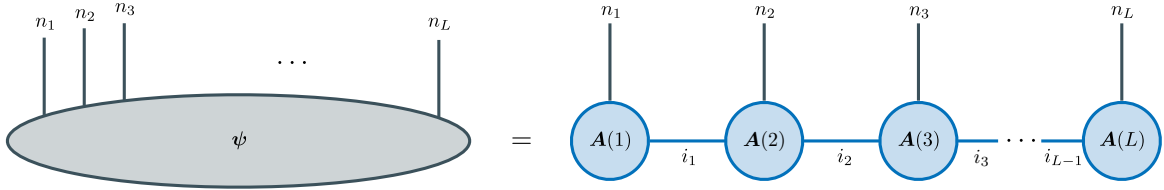


Figure 1: Visualization of the decomposition from Equation (2.22). A general tensor of high order is brought into an MPS form.

Since for fixed physical index n_ℓ the MPS tensor constitutes a matrix $\mathbf{A}(\ell)_{n_\ell} \in \text{Mat}(\chi_{\ell-1}, \chi_\ell)$ and the state could be rewritten as

$$|\Psi\rangle = \left(\sum_{n_1} \mathbf{A}(1)_{n_1} |n_1\rangle \right) \otimes \cdots \otimes \left(\sum_{n_L} \mathbf{A}(L)_{n_L} |n_L\rangle \right), \quad (2.24)$$

such a state is called a matrix product state. If the matrices $\mathbf{A}(\ell)_{n_\ell}$ were simply numbers, one would arrive at a product state. However, in this case the “coefficients” of an MPS are still matrices in the MPS bond indices i_ℓ , so that this representation of a state is not restricted to product states. The indices take values from their domain $\{1, \dots, \chi_\ell\}$. The domain size χ_ℓ is also called the bond dimension. The bond dimension is a very important quantity in VMPS since it controls the amount of entanglement an MPS can encode as well as the

computational effort needed to perform calculations. In the construction described above the bond dimensions obey $\chi_\ell \leq \min(d^\ell, d^{L-\ell})$, which means that in order to be able to bring any state to this form, a maximum bond dimension $\chi = \max(\chi_0, \dots, \chi_L) \leq d^{\lfloor \frac{L}{2} \rfloor}$ is sufficient. In this procedure it was assumed that all local Hilbert spaces have the same dimension d , but generalization to different situations is straightforward.

In practice, however, this theoretical limit of the bond dimension is too high for most numerical calculations. In order to achieve computational accessibility even for larger system sizes, the bond dimension has to be truncated. By keeping only the χ_{trunc} largest singular values of each MPS tensor, one constructs an MPS approximation for a given state $|\Psi\rangle$. A justification for this approach will be provided later. The quality of this approximation depends on the chosen bond dimension: for $\chi_{\text{trunc}} = 1$ all MPS indices become trivial and the matrix product state turns into a product state without any entanglement. For $\chi_{\text{trunc}} = \chi_{\text{exact}}$ the MPS is an exact representation of the quantum state with all its entanglement.

An MPS representation of a state is not unique: of course it is possible to apply any invertible matrix to the outgoing MPS index of a tensor, as long as the inverse of that matrix is applied to the incoming MPS index of the next tensor, so that in the whole tensor network both matrices cancel each other out and the bond remains unchanged. This is used to define a canonical form of an MPS, in which for a chosen so-called *pivot site* p all tensors on sites left to p are left-normalized and all tensors to the right are right-normalized. To bring an MPS $|\Psi\rangle$ into its canonical form, the following procedure is applied:

Left-normalization of sites 1 to $p - 1$:

1. Start at site $\ell = 1$ and define $\overline{\mathbf{D}}(0), \mathbf{V}^\dagger(0) \in \text{Mat}(1, 1)$ with $\overline{\mathbf{D}}(0)_{1,1} = \mathbf{V}^\dagger(0)_{1,1} = 1$.
2. Multiply the MPS tensor at site ℓ with $\overline{\mathbf{D}}(\ell-1)\mathbf{V}^\dagger(\ell-1)$ and block the result to a matrix $\mathbf{M}(\ell) \in \text{Mat}(\chi_{\ell-1}d_\ell, \chi_\ell)$:

$$\mathbf{M}(\ell)_{(i_{\ell-1}n_\ell)i_\ell} = \sum_{i'_{\ell-1}, i''_{\ell-1}} \overline{\mathbf{D}}(\ell-1)_{i_{\ell-1}i'_{\ell-1}} \mathbf{V}^\dagger(\ell-1)_{i'_{\ell-1}i''_{\ell-1}} A(\ell)_{i''_{\ell-1}n_\ell}^{i_\ell}. \quad (2.25)$$

3. Singular value decomposition of $\mathbf{M}(\ell) = \mathbf{U}(\ell)\mathbf{D}(\ell)\mathbf{V}^\dagger(\ell)$, where $\mathbf{U}(\ell) \in \text{Mat}(\chi_{\ell-1}d_\ell, \chi_{\ell-1}d_\ell)$ and $\mathbf{V}^\dagger(\ell) \in \text{Mat}(\chi_\ell, \chi_\ell)$ are unitary and $\mathbf{D}(\ell) \in \text{Mat}(\chi_{\ell-1}d_\ell, \chi_\ell)$ is diagonal.
4. The last rows of $\mathbf{D}(\ell)$ are zero rows, because $\chi_{\ell-1}d_\ell \geq \chi_\ell$ (this is always true, because for an MPS without redundant information the bond dimension grows at most by a factor of the local Hilbert space dimension). These trivial rows are left out and the corresponding columns of $\mathbf{U}(\ell)$ are truncated to arrive at $\overline{\mathbf{U}}(\ell) \in \text{Mat}(\chi_{\ell-1}d_\ell, \chi_\ell)$ and $\overline{\mathbf{D}}(\ell) \in \text{Mat}(\chi_\ell, \chi_\ell)$.

Due to unitarity of $\mathbf{U}(\ell)$ one finds $\overline{\mathbf{U}}^\dagger(\ell)\overline{\mathbf{U}}(\ell) = \mathbf{1}_{\chi_\ell}$, but $\overline{\mathbf{U}}(\ell)\overline{\mathbf{U}}^\dagger(\ell) \neq \mathbf{1}_{\chi_{\ell-1}d_\ell}$.

5. Reshape $\overline{\mathbf{U}}(\ell)$ to an MPS tensor $\mathbf{L}(\ell)$ with $L(\ell)_{i_{\ell-1}n_\ell}^{i_\ell} = \overline{\mathbf{U}}(\ell)_{(i_{\ell-1}n_\ell)i_\ell}$. This yields:

$$\sum_{i'_{\ell-1}, i''_{\ell-1}} \overline{\mathbf{D}}(\ell-1)_{i_{\ell-1}i'_{\ell-1}} \mathbf{V}^\dagger(\ell-1)_{i'_{\ell-1}i''_{\ell-1}} A(\ell)_{i''_{\ell-1}n_\ell}^{i_\ell} = \sum_{i'_\ell, i''_\ell} L(\ell)_{i_{\ell-1}n_\ell}^{i''_\ell} \overline{\mathbf{D}}(\ell)_{i'_\ell i''_\ell} \mathbf{V}^\dagger(\ell)_{i'_\ell i_\ell}. \quad (2.26)$$

It follows:

$$\sum_{i_{\ell-1}, n_\ell} L^\dagger(\ell)_{i'_\ell}^{i_{\ell-1}n_\ell} L(\ell)_{i_{\ell-1}n_\ell}^{i_\ell} = \sum_{i_{\ell-1}, n_\ell} \overline{\mathbf{U}}^\dagger(\ell)_{i'_\ell(i_{\ell-1}n_\ell)} \overline{\mathbf{U}}(\ell)_{(i_{\ell-1}n_\ell)i_\ell} = \delta_{i'_\ell i_\ell}. \quad (2.27)$$

6. The steps 2 to 5 are repeated for the next site $\ell + 1$ until $\ell = p - 1$.

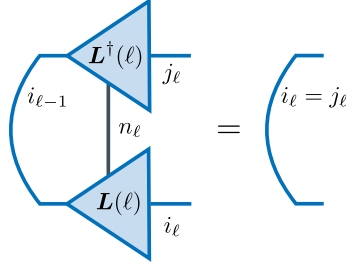


Figure 2: Visualization of the left-normalization condition of an MPS tensor. Left-normalized MPS tensors are depicted as triangles with their tip pointing to the left.

Equation (2.27) is the left-normalization condition. For the graphical notation, left-normalized MPS tensors are depicted as left-pointing triangles. Figure 2 shows a possible visualization of the left-normalization condition. The matrix product state is now given by

$$|\Psi\rangle = \sum_{n_1, \dots, n_L} \mathbf{L}(1)_{n_1} \cdots \mathbf{L}(p-1)_{n_{p-1}} \overline{\mathbf{D}}(p-1) \mathbf{V}^\dagger(p-1) \mathbf{A}(p)_{n_p} \mathbf{A}(p+1)_{n_{p+1}} \cdots \mathbf{A}(L)_{n_L} |n_1\rangle \otimes \cdots \otimes |n_L\rangle. \quad (2.28)$$

Right-normalization of sites L to $p+1$:

1. Start at site $\ell = L$ and define $\mathbf{U}(L+1), \overline{\mathbf{D}}(L+1) \in \text{Mat}(1, 1)$ with $\mathbf{U}(L+1)_{1,1} = \overline{\mathbf{D}}(L+1)_{1,1} = 1$.
2. Multiply the MPS tensor at site ℓ with $\mathbf{U}(\ell+1)\overline{\mathbf{D}}(\ell+1)$ and block the result to a matrix $\mathbf{M}(\ell) \in \text{Mat}(\chi_{\ell-1}, \chi_\ell d_\ell)$:

$$\mathbf{M}(\ell)_{i_{\ell-1}(i_\ell n_\ell)} = \sum_{i'_\ell, i''_\ell} A(\ell)_{i_{\ell-1} n_\ell}^{i''_\ell} U(\ell+1)_{i''_\ell i'_\ell} \overline{\mathbf{D}}(\ell+1)_{i'_\ell i_\ell}. \quad (2.29)$$

3. Singular value decomposition of $\mathbf{M}(\ell) = \mathbf{U}(\ell)\mathbf{D}(\ell)\mathbf{V}^\dagger(\ell)$, where $\mathbf{U}(\ell) \in \text{Mat}(\chi_{\ell-1}, \chi_{\ell-1})$ and $\mathbf{V}^\dagger(\ell) \in \text{Mat}(\chi_\ell d_\ell, \chi_\ell d_\ell)$ are unitary and $\mathbf{D}(\ell) \in \text{Mat}(\chi_{\ell-1}, \chi_\ell d_\ell)$ is diagonal.
4. The last columns of $\mathbf{D}(\ell)$ are zero columns, because $\chi_\ell d_\ell \geq \chi_{\ell-1}$ (this is always true, because for an MPS without redundant information the bond dimension grows at most by a factor of the local Hilbert space dimension – also if the MPS is built from right to left). These trivial columns are left out and the corresponding rows of $\mathbf{V}^\dagger(\ell)$ are truncated to arrive at $\overline{\mathbf{D}}(\ell) \in \text{Mat}(\chi_{\ell-1}, \chi_{\ell-1})$ and $\overline{\mathbf{V}}^\dagger(\ell) \in \text{Mat}(\chi_{\ell-1}, \chi_\ell d_\ell)$. Due to unitarity of $\mathbf{V}^\dagger(\ell)$ one finds $\overline{\mathbf{V}}^\dagger(\ell)\overline{\mathbf{V}}(\ell) = \mathbb{1}_{\chi_{\ell-1}}$, but $\overline{\mathbf{V}}(\ell)\overline{\mathbf{V}}^\dagger(\ell) \neq \mathbb{1}_{\chi_\ell d_\ell}$.
5. Reshape $\overline{\mathbf{V}}^\dagger(\ell)$ to an MPS tensor $\mathbf{R}(\ell)$ with $R(\ell)_{i_{\ell-1} n_\ell}^{i_\ell} = \overline{\mathbf{V}}^\dagger(\ell)_{i_{\ell-1}(i_\ell n_\ell)}$. This yields:

$$\sum_{i'_\ell, i''_\ell} A(\ell)_{i_{\ell-1} n_\ell}^{i''_\ell} U(\ell+1)_{i''_\ell i'_\ell} \overline{\mathbf{D}}(\ell+1)_{i'_\ell i_\ell} = \sum_{i'_{\ell-1}, i''_{\ell-1}} U(\ell)_{i_{\ell-1} i'_{\ell-1}} \overline{\mathbf{D}}(\ell)_{i'_{\ell-1} i''_{\ell-1}} R(\ell)_{i''_{\ell-1} n_\ell}^{i_\ell}. \quad (2.30)$$

It follows:

$$\sum_{i_\ell, n_\ell} R(\ell)_{i_{\ell-1} n_\ell}^{i_\ell} R^\dagger(\ell)_{i_\ell}^{i'_{\ell-1} n_\ell} = \sum_{i_\ell, n_\ell} \overline{\mathbf{V}}^\dagger(\ell)_{i_{\ell-1}(i_\ell n_\ell)} \overline{\mathbf{V}}(\ell)_{(i_\ell n_\ell) i'_{\ell-1}} = \delta_{i_{\ell-1} i'_{\ell-1}}. \quad (2.31)$$

6. The steps 2 to 5 are repeated for the next site $\ell - 1$ until $\ell = p + 1$.

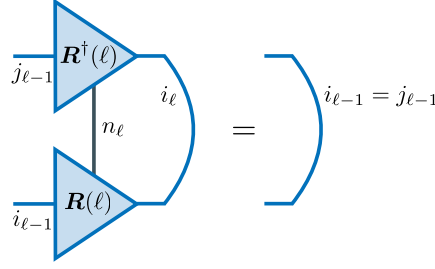


Figure 3: Visualization of the right-normalization condition of an MPS tensor. Right-normalized MPS tensors are depicted as triangles with their tip pointing to the right.

Equation (2.31) is the right-normalization condition. For the graphical notation, right-normalized MPS tensors are depicted as right-pointing triangles. Figure 3 shows a possible visualization of the right-normalization condition. If one now sets the central MPS tensor

$$C(p)_{i_{p-1}i_p}^{i'_p} = \sum_{i'_{p-1}, i''_{p-1}, i'_p, i''_p} \bar{D}(p-1)_{i_{p-1}i'_{p-1}} V^\dagger(p-1)_{i'_{p-1}i''_{p-1}} A(p)_{i''_{p-1}n_p}^{i'_p} U(p+1)_{i'_p i''_p} \bar{D}(p+1)_{i''_p i_p} \quad (2.32)$$

at the pivot site p , the matrix product state is in its canonical form (Figure 4):

$$|\Psi\rangle = \sum_{n_1, \dots, n_L} \mathbf{L}(1)_{n_1} \cdots \mathbf{L}(p-1)_{n_{p-1}} \mathbf{C}(p)_{n_p} \mathbf{R}(p+1)_{n_{p+1}} \cdots \mathbf{R}(L)_{n_L} |n_1\rangle \otimes \cdots \otimes |n_L\rangle. \quad (2.33)$$

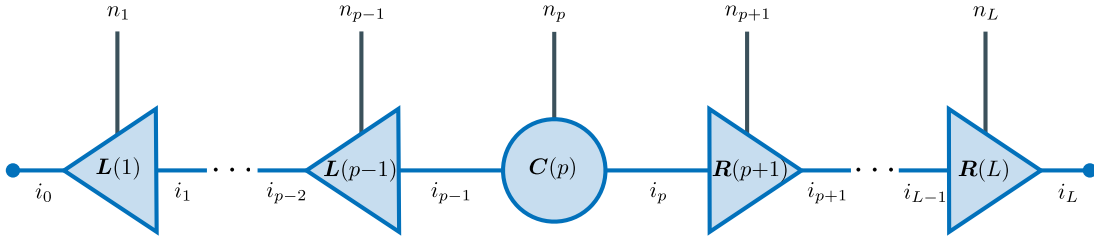


Figure 4: Visualization of an MPS in its canonical form around a pivot site p .

The canonical form of an MPS is particularly suitable for the calculation of the norm of an MPS:

$$\begin{aligned} \langle \Psi | \Psi \rangle &= \sum_{\substack{n_1, \dots, n_L, \\ m_1, \dots, m_L}} \text{tr} \left(\mathbf{R}^\dagger(L)^{m_L} \cdots \mathbf{R}^\dagger(p+1)^{m_{p+1}} \mathbf{C}^\dagger(p)^{m_p} \mathbf{L}^\dagger(p-1)^{m_{p-1}} \cdots \mathbf{L}^\dagger(1)^{m_1} \right. \\ &\quad \left. \cdots \mathbf{L}(1)_{n_1} \cdots \mathbf{L}(p-1)_{n_{p-1}} \mathbf{C}(p)_{n_p} \mathbf{R}(p+1)_{n_{p+1}} \cdots \mathbf{R}(L)_{n_L} \right) \langle m_1 | n_1 \rangle \cdots \langle m_L | n_L \rangle \\ &= \sum_{n_1, \dots, n_L} \text{tr} \left(\mathbf{C}^\dagger(p)^{n_p} \mathbf{L}^\dagger(p-1)^{n_{p-1}} \cdots \mathbf{L}^\dagger(1)^{n_1} \mathbf{L}(1)_{n_1} \cdots \mathbf{L}(p-1)_{n_{p-1}} \right. \\ &\quad \left. \cdot \mathbf{C}(p)_{n_p} \mathbf{R}(p+1)_{n_{p+1}} \cdots \mathbf{R}(L)_{n_L} \mathbf{R}^\dagger(L)^{n_L} \cdots \mathbf{R}^\dagger(p+1)^{n_{p+1}} \right) \\ &= \sum_{n_p} \text{tr} \left(\mathbf{C}^\dagger(p)^{n_p} \mathbf{C}(p)_{n_p} \right) = \sum_{n_p, i_{p-1}, i_p} |C(p)_{i_{p-1}i_p}^{i_p}|^2. \end{aligned} \quad (2.34)$$

In the graphical language, the norm is given by a tensor network of a bra and a ket MPS, whose physical indices are joined together. Therefore, all MPS bonds and physical bonds have to be summed over – or in the language of tensor networks, they have to be contracted. Repeated application of the left- and right-normalization conditions is shown in Figure 5.

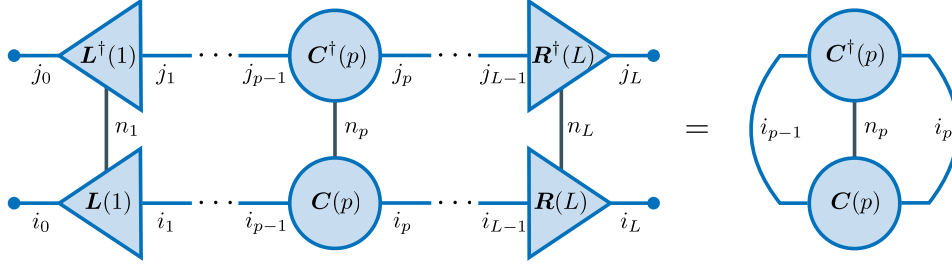


Figure 5: Visualization of the contraction of a tensor network for the norm of an MPS in its canonical form.

For a better understanding of the MPS bond indices, one can recursively define a sequence of artificial Hilbert spaces which are spanned by the MPS indices at each bond:

$$\begin{aligned} \mathcal{H}_{\text{MPS}}(0) &= \text{span}(|i_0\rangle | i_0 = 1) \quad \text{with } |i_0\rangle = 1, \quad \text{and for } 1 \leq \ell \leq L: \\ \mathcal{H}_{\text{MPS}}(\ell) &= \text{span}(|i_\ell\rangle | 1 \leq i_\ell \leq \chi_\ell) \quad \text{with } |i_\ell\rangle = \sum_{n_\ell, i_{\ell-1}} A(\ell)_{i_{\ell-1} n_\ell}^{i_\ell} |i_{\ell-1}\rangle \otimes |n_\ell\rangle. \end{aligned} \quad (2.35)$$

The space spanned by the $|i_\ell\rangle$ is a χ_ℓ dimensional subspace of the first ℓ local Hilbert spaces $\mathcal{H}_{\text{loc}}(1) \otimes \cdots \otimes \mathcal{H}_{\text{loc}}(\ell)$. A state $|i_\ell\rangle$ describes the progress of representing a state $|\Psi\rangle$ with respect to the first local Hilbert spaces. The last MPS Hilbert space $\mathcal{H}_{\text{MPS}}(L)$ is one-dimensional with $|i_L\rangle = |\Psi\rangle$.

Analogously to the MPS Hilbert spaces being constructed by starting from the leftmost site and going right, the MPS Hilbert spaces constructed from right to left can be defined:

$$\begin{aligned} \tilde{\mathcal{H}}_{\text{MPS}}(L+1) &= \text{span}(\widetilde{|i_L\rangle} | i_L = 1) \quad \text{with } \widetilde{|i_L\rangle} = 1, \quad \text{and for } 1 \leq \ell \leq L: \\ \tilde{\mathcal{H}}_{\text{MPS}}(\ell) &= \text{span}(\widetilde{|i_{\ell-1}\rangle} | 1 \leq i_{\ell-1} \leq \chi_{\ell-1}) \quad \text{with } \widetilde{|i_{\ell-1}\rangle} = \sum_{n_\ell, i_\ell} A(\ell)_{i_{\ell-1} n_\ell}^{i_\ell} |n_\ell\rangle \otimes \widetilde{|i_\ell\rangle}. \end{aligned} \quad (2.36)$$

Right-to-left MPS Hilbert spaces are marked with a tilde to distinguish them from left-to-right MPS Hilbert spaces. $\tilde{\mathcal{H}}_{\text{MPS}}(\ell)$ is a subspace of $\mathcal{H}_{\text{loc}}(\ell) \otimes \cdots \otimes \mathcal{H}_{\text{loc}}(L)$ and $\widetilde{|i_0\rangle} = |\Psi\rangle$ arrives at the full MPS. In the Appendix A.1 it is shown that proper left- and right-normalization leads to the MPS states being orthonormal bases of their respective Hilbert spaces. With the definitions of Equation (2.35) and Equation (2.36) at hand, any MPS for each $\ell \in \{1, \dots, L\}$ can be written as

$$|\Psi\rangle = \sum_{n_\ell, i_{\ell-1}, i_\ell} A(\ell)_{i_{\ell-1} n_\ell}^{i_\ell} |i_{\ell-1}\rangle \otimes |n_\ell\rangle \otimes \widetilde{|i_\ell\rangle} = \sum_{i_\ell} |i_\ell\rangle \otimes \widetilde{|i_\ell\rangle}, \quad (2.37)$$

depending on whether one wishes to write the local physical state explicitly, or incorporate it into the left part of the system. A large bond dimension means that due to large entanglement many different states of each site of the bond couple to their respective counterparts. This procedure also provides another perspective on the MPS tensors: via Equation (2.35) the MPS tensors iteratively select which part of the physical Hilbert space $\mathcal{H}_{\text{loc}}(1) \otimes \cdots \otimes \mathcal{H}_{\text{loc}}(\ell)$ is used for the construction of the MPS and which part is left out.

Compression of matrix product states

Given a partitioning of a system $\mathcal{H} = \mathcal{H}_A \otimes \mathcal{H}_B$ and a state $|\Psi\rangle = \sum_{a,b} \psi_{ab} |a\rangle^{(A)} \otimes |b\rangle^{(B)}$ written in the orthonormal tensor product basis, one may wish to approximate the state by another state $|\Phi\rangle = \sum_{a,b} \phi_{ab} |a\rangle^{(A)} \otimes |b\rangle^{(B)}$, where the matrix $\phi \in \text{Mat}(\dim(\mathcal{H}_A), \dim(\mathcal{H}_B))$ has lower rank than the matrix $\psi \in \text{Mat}(\dim(\mathcal{H}_A), \dim(\mathcal{H}_B))$. For $\text{rk}(\psi) = r \leq \min(\dim(\mathcal{H}_A), \dim(\mathcal{H}_B))$, the goal is to find the best approximation in terms of a matrix of lower rank $\text{rk}(\phi) = k < r$. The number of non-zero entries in the diagonal matrices of the singular value decompositions $\psi = \mathbf{U}_\psi \mathbf{D}_\psi \mathbf{V}_\psi^\dagger$ and $\phi = \mathbf{U}_\phi \mathbf{D}_\phi \mathbf{V}_\phi^\dagger$ corresponds to the rank of the matrix. An optimal approximation

minimizes the distance between both states while keeping the norm of the approximation fixed. The Lagrange function that describes the distance between both states and ensures the correct norm of the approximation is then given by

$$\begin{aligned}
 \mathcal{L} &= \|\Psi\rangle - |\Phi\rangle\|_{\mathcal{H}}^2 + \lambda \left(\|\Phi\rangle\|_{\mathcal{H}}^2 - 1 \right) = \langle\Psi|\Psi\rangle - \langle\Phi|\Psi\rangle - \langle\Psi|\Phi\rangle + \langle\Phi|\Phi\rangle + \lambda (\langle\Phi|\Phi\rangle - 1) \\
 &= \text{tr}(\psi^\dagger\psi - \psi^\dagger\phi - \phi^\dagger\psi + \phi^\dagger\phi) + \lambda (\text{tr}(\phi^\dagger\phi) - 1) \\
 &= \text{tr}(\mathbf{D}_\psi^\dagger \mathbf{D}_\psi + \mathbf{D}_\phi^\dagger \mathbf{D}_\phi - \mathbf{V}_\phi^\dagger \mathbf{V}_\psi \mathbf{D}_\psi^\dagger (\mathbf{U}_\phi^\dagger \mathbf{U}_\psi)^\dagger \mathbf{D}_\phi - \mathbf{D}_\phi^\dagger \mathbf{U}_\phi^\dagger \mathbf{U}_\psi \mathbf{D}_\psi (\mathbf{V}_\phi^\dagger \mathbf{V}_\psi)^\dagger) + \lambda (\text{tr}(\mathbf{D}_\phi^\dagger \mathbf{D}_\phi) - 1) \\
 &= 2 - 2 \text{Re} \left(\text{tr}(\mathbf{D}_\phi^\dagger \mathbf{U} \mathbf{D}_\psi \mathbf{V}^\dagger) \right) + (\lambda + 1) (\text{tr}(\mathbf{D}_\phi^\dagger \mathbf{D}_\phi) - 1) \quad \text{with } \mathbf{U} = \mathbf{U}_\phi^\dagger \mathbf{U}_\psi, \mathbf{V} = \mathbf{V}_\phi^\dagger \mathbf{V}_\psi. \quad (2.38)
 \end{aligned}$$

In Appendix A.2 it is shown that for properly ordered diagonal elements of \mathbf{D}_ϕ the term depending on the unitary matrices is minimized for $\mathbf{U} = \mathbf{1}_n, \mathbf{V} = \mathbf{1}_m$. In this case:

$$\begin{aligned}
 \mathcal{L}(\sigma_1(\phi), \dots, \sigma_k(\phi), \lambda) &= \text{tr} \left((\mathbf{D}_\psi^\dagger - \mathbf{D}_\phi^\dagger) (\mathbf{D}_\psi - \mathbf{D}_\phi) \right) + \lambda (\text{tr}(\mathbf{D}_\phi^\dagger \mathbf{D}_\phi) - 1) \\
 &= \sum_{i=1}^k \left((\lambda + 1) \sigma_i^2(\mathbf{D}_\phi) - 2\sigma_i(\mathbf{D}_\psi) \sigma_i(\mathbf{D}_\phi) \right) - \lambda + 1, \quad (2.39)
 \end{aligned}$$

where $\sigma_i(\mathbf{M})$ describes the i -th singular value of a matrix \mathbf{M} . The gradient with respect to the k singular values of Φ and λ yields:

$$(\lambda + 1) \sigma_i(\Phi) = \sigma_i(\Psi) \quad \text{for } 1 \leq i \leq k \quad \text{and} \quad \sum_{i=1}^k \sigma_i^2(\Phi) = 1. \quad (2.40)$$

Let $\epsilon^2 = \sum_{i=k+1}^r \sigma_i^2(\Psi)$ be the sum over truncated singular value squares, then this is solved by $\lambda = \sqrt{1 - \epsilon^2} - 1$ and $\sigma_i(\Phi) = \frac{\sigma_i(\Psi)}{\sqrt{1 - \epsilon^2}}$, i. e., the optimal approximation consists of keeping only the k largest singular values of the original matrix Ψ and scaling them to keep the norm (the edge case solution $\lambda = -1$ can be shown to result in an at most equally good approximation by using the Cauchy–Schwarz inequality). Interestingly, the same result is achieved when the normalization constraint is disregarded in the optimization process and only performed afterwards: the Eckart–Young–Mirsky theorem [50, 51] states that the best approximation of a matrix by a matrix of smaller rank is that matrix where the smallest singular values are discarded. The approximation is controlled by the truncated weight ϵ , since

$$\|\Psi\rangle - |\Phi\rangle\|_{\mathcal{H}} = \sqrt{2 - 2\sqrt{1 - \epsilon^2}} \leq \sqrt{2}\epsilon. \quad (2.41)$$

Now let $|\Psi\rangle$ be a canonical matrix product state with a pivot site p as in Equation (2.37), where the states $|i_{p-1}\rangle \otimes |n_p\rangle$ form an ONB for $\mathcal{H}_{\text{MPS}}(p-1) \otimes \mathcal{H}_{\text{loc}}(p)$ and the states $|\tilde{i}_p\rangle$ form an ONB for $\tilde{\mathcal{H}}_{\text{MPS}}(p)$. With the above approximation at hand, a procedure to reduce the bond dimension of an MPS can be formulated: starting with a canonical MPS with pivot site $p = 1$, one joins the incoming indices of the MPS tensor together and performs an SVD of the corresponding matrix. Only the χ_{trunc} largest singular values are kept. The left unitary matrix is taken as the new MPS tensor at that site, and the diagonal matrix of singular values and the right unitary matrix are multiplied onto the next MPS tensor, thus bringing the MPS to the canonical form with the pivot site shifted by one site. This is repeated for the entire MPS, which then gives an approximation of the original MPS.

This can be useful or even necessary, for example, when the sum of two matrix product states is needed: given two states $|\Psi\rangle$ and $|\Phi\rangle$ which are in MPS form with respect to the same local Hilbert space, then one can easily build an MPS for the sum $\alpha|\Psi\rangle + \beta|\Phi\rangle$ by taking the direct sum of their MPS tensors $\mathbf{A}(\ell)$ and $\mathbf{B}(\ell)$

for fixed physical indices:

$$\alpha |\Psi\rangle + \beta |\Phi\rangle = \sum_{n_1, \dots, n_L} \begin{pmatrix} \alpha & \beta \end{pmatrix} \begin{pmatrix} \mathbf{A}^{(1)n_1} & 0 \\ 0 & \mathbf{B}^{(1)n_1} \end{pmatrix} \cdots \begin{pmatrix} \mathbf{A}^{(L)n_L} & 0 \\ 0 & \mathbf{B}^{(L)n_L} \end{pmatrix} \begin{pmatrix} 1 \\ 1 \end{pmatrix} |n_1\rangle \otimes \cdots \otimes |n_L\rangle. \quad (2.42)$$

Of course the bond dimension of the result is given by the sum of both bond dimensions. If this larger bond dimension is no longer computationally feasible, the SVD compression detailed above may provide a remedy.

Matrix product operators

Operators can also be brought into a matrix product form. A general operator acting on the entire Hilbert space takes the following form in the basis of the local Hilbert spaces:

$$\hat{O} = \sum_{\substack{n_1, \dots, n_L, \\ m_1, \dots, m_L}} O_{n_1 m_1 \dots n_L m_L} |m_1, \dots, m_L\rangle \langle n_1, \dots, n_L|. \quad (2.43)$$

The only difference to a state is the appearance of two physical indices for each local Hilbert space. This means that if the two physical indices are merged together by means of a Kronecker product, the operator tensor $O_{n_1 m_1 \dots n_L m_L}$ of order $2L$ can be transformed into a tensor network in exactly the same way as a state. Afterwards, the two physical indices at each site have to be split, leading to fourth order tensors $\mathbf{W}(\ell)$ that appear in the matrix product operator (MPO) description:

$$\hat{O} = \sum_{\substack{n_1, \dots, n_L, \\ m_1, \dots, m_L, \\ k_0, \dots, k_L}} W(1)_{k_0 m_1}^{k_1 n_1} \cdots W(L)_{k_{L-1} m_L}^{k_L n_L} |m_1\rangle \langle n_1| \otimes \cdots \otimes |m_L\rangle \langle n_L|. \quad (2.44)$$

The MPO tensors $\mathbf{W}(\ell)$ have two physical indices for the physical states as well as an incoming and an outgoing MPO bond index that appear in the same fashion as the MPS bond indices i_ℓ . Their bond dimension is μ_ℓ , with $\mu_0 = \mu_L = 1$ being trivial and $\mu = \max(\mu_0, \dots, \mu_L)$. Often the bond dimension needed for an exact representation of an operator is not very high as compared to typical MPS bond dimensions, because common operators describe one- or two-particle interactions between adjacent sites, leading to low entanglement in the operator. Nevertheless, MPO bond dimensions can become quite large in certain cases, in particular for products of operators. In Section 2.4 a more efficient way to construct and losslessly compress MPOs is presented. The MPO bond indices also define artificial MPO Hilbert spaces constructed from left to right $\mathcal{H}_{\text{MPO}}(\ell)$, and from right to left $\tilde{\mathcal{H}}_{\text{MPO}}(\ell)$ (details can be found in Appendix A.1).

The same graphical notation used for matrix product states can also be applied to matrix product operators. The tensor network for an operator is shown in Figure 6.

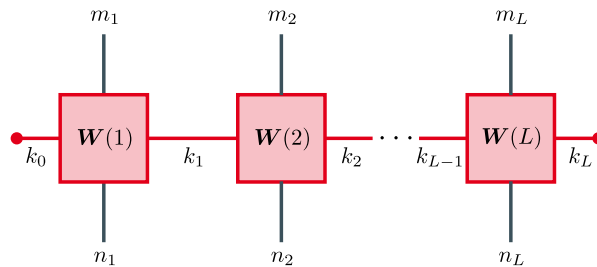


Figure 6: Visualization of a matrix product operator. The MPO tensors $\mathbf{W}(\ell)$ consist of four legs: incoming MPO index $k_{\ell-1}$ and physical index m_ℓ and outgoing MPO index k_ℓ and physical index n_ℓ .

With the MPS and MPO representation at hand, it is straightforward to write down a matrix element, in formulas as well as graphically (Figure 7):

$$\begin{aligned}
 \langle \Phi | \widehat{O} | \Psi \rangle &= \sum_{\substack{n_1, \dots, n_L, \\ m_1, \dots, m_L, \\ n'_1, \dots, n'_L, \\ m'_1, \dots, m'_L}} \mathbf{B}^\dagger(1)^{m_1} \dots \mathbf{B}^\dagger(L)^{m_L} \mathbf{W}(1)_{m'_1}^{n'_1} \dots \mathbf{W}(L)_{m'_L}^{n'_L} \mathbf{A}(1)_{n_1} \dots \mathbf{A}(L)_{n_L} \\
 &\quad \cdot \langle m_1 | m'_1 \rangle \langle n'_1 | n_1 \rangle \dots \langle m_L | m'_L \rangle \langle n'_L | n_L \rangle \\
 &= \sum_{\substack{n_1, \dots, n_L, \\ m_1, \dots, m_L}} \sum_{\substack{i_0, \dots, i_L, \\ j_0, \dots, j_L, \\ k_0, \dots, k_L}} \mathbf{B}^\dagger(1)_{j_1}^{j_0 m_1} \dots \mathbf{B}^\dagger(L)_{j_L}^{j_{L-1} m_L} \mathbf{W}(1)_{k_0 m_1}^{k_1 n_1} \dots \mathbf{W}(L)_{k_{L-1} m_L}^{k_L n_L} \mathbf{A}(1)_{i_0 n_1}^{i_1} \dots \mathbf{A}(L)_{i_{L-1} n_L}^{i_L}. \quad (2.45)
 \end{aligned}$$

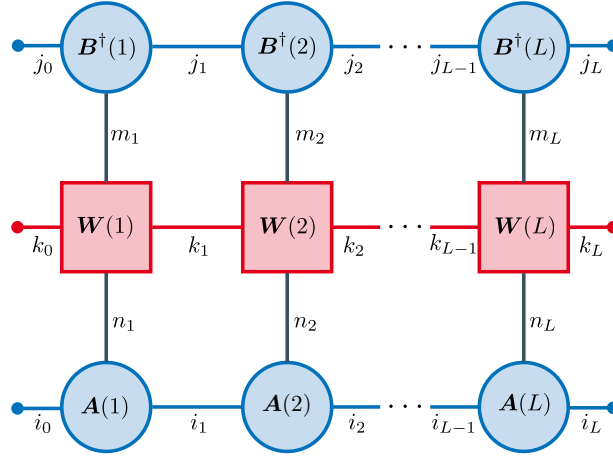


Figure 7: Visualization of a tensor network consisting of a bra MPS $\langle \Phi |$, a ket MPS $|\Psi\rangle$ and an operator \widehat{O} . In order to calculate the matrix element, all indices have to be contracted.

The organization of the complete contraction of the tensor network in Figure 7 is still a formidable task. The first thing to note is that contracting all the MPS and MPO bond indices first does not benefit from the special matrix product representation, because after these contractions one would have to contract tensors with L , $2L$ and L indices. Instead of that, the rule of thumb is to sum over the local Hilbert spaces first. Indeed, one performs all “vertical” sums at the leftmost or rightmost site ℓ first, and then uses the result to incorporate the next site. In doing so, the sequential structure of the matrix product representation is exploited efficiently and sums over the entire Hilbert space of dimension D are avoided at the price of performing $\mathcal{O}(L)$ contractions within local Hilbert spaces, which are of much smaller dimension d_ℓ . In a more formal way, the contraction process can be done making use of environment tensors (Figure 8) that hold the information about all contractions performed so far:

$$\begin{aligned}
 \text{Left environment: } E(0)_{j_0}^{i_0 k_0} &= 1, \quad \text{and for } 1 \leq \ell \leq L : \\
 E(\ell)_{j_\ell}^{i_\ell k_\ell} &= \sum_{\substack{n_\ell, m_\ell, i_{\ell-1}, \\ k_{\ell-1}, j_{\ell-1}}} E(\ell-1)_{j_{\ell-1}}^{i_{\ell-1} k_{\ell-1}} \mathbf{B}^\dagger(\ell)_{j_\ell}^{j_{\ell-1} m_\ell} \mathbf{W}(\ell)_{k_{\ell-1} m_\ell}^{k_\ell n_\ell} \mathbf{A}(\ell)_{i_{\ell-1} n_\ell}^{i_\ell}. \quad (2.46)
 \end{aligned}$$

$$\begin{aligned}
 \text{Right environment: } F(L+1)_{i_L k_L}^{j_L} &= 1, \quad \text{and for } 1 \leq \ell \leq L : \\
 F(\ell)_{i_{\ell-1} k_{\ell-1}}^{j_{\ell-1}} &= \sum_{\substack{n_\ell, m_\ell, i_\ell, \\ k_\ell, j_\ell}} \mathbf{B}^\dagger(\ell)_{j_\ell}^{j_{\ell-1} m_\ell} \mathbf{W}(\ell)_{k_{\ell-1} m_\ell}^{k_\ell n_\ell} \mathbf{A}(\ell)_{i_{\ell-1} n_\ell}^{i_\ell} F(\ell+1)_{i_\ell k_\ell}^{j_\ell}. \quad (2.47)
 \end{aligned}$$

It is self-evident that $E(L)_{j_\ell k_\ell}^{i_\ell}$ as well as $F(1)_{i_0 k_0}^{j_0}$ are scalars that coincide with the matrix element. The shifting of the environment, i. e., contracting $\mathbf{E}(\ell-1)$ with $\mathbf{A}(\ell)$, $\mathbf{W}(\ell)$ and $\mathbf{B}^\dagger(\ell)$ to gain the next $\mathbf{E}(\ell)$, is an operation that naively takes $\mathcal{O}(\chi_{\ell-1}^2 \chi_\ell^2 \mu_{\ell-1} \mu_\ell d_\ell^2) \sim \mathcal{O}(\chi^4 \mu^2 d^2)$ operations. Contracting the indices one after another is computationally significantly cheaper:

1. Contract $\mathbf{E}(\ell-1)$ and $\mathbf{A}(\ell)$ $\rightarrow \mathcal{O}(\chi_{\ell-1}^2 \chi_\ell \mu_{\ell-1} d_\ell) \sim \mathcal{O}(\chi^3 \mu d)$
2. Contract the result from step 1 and $\mathbf{W}(\ell)$ $\rightarrow \mathcal{O}(\chi_{\ell-1} \chi_\ell \mu_{\ell-1} \mu_\ell d_\ell^2) \sim \mathcal{O}(\chi^2 \mu^2 d^2)$
3. Contract the result from step 2 and $\mathbf{B}^\dagger(\ell)$ $\rightarrow \mathcal{O}(\chi_{\ell-1} \chi_\ell^2 \mu_\ell d_\ell^2) \sim \mathcal{O}(\chi^3 \mu d^2)$

Since in general the MPS bond dimension is the largest value, this contraction order reduces the computational effort by a factor of roughly $\chi\mu$. A similar contraction order for the right environment ensures an economical usage of the computational resources, too. Since L updates of the environments have to be performed, this contraction for a matrix element tensor network scales like $\mathcal{O}(L\chi^3\mu d^2)$, which for finite bond dimensions is much less than the exponential scaling behavior $\mathcal{O}(d^L)$ of tensors of order L .

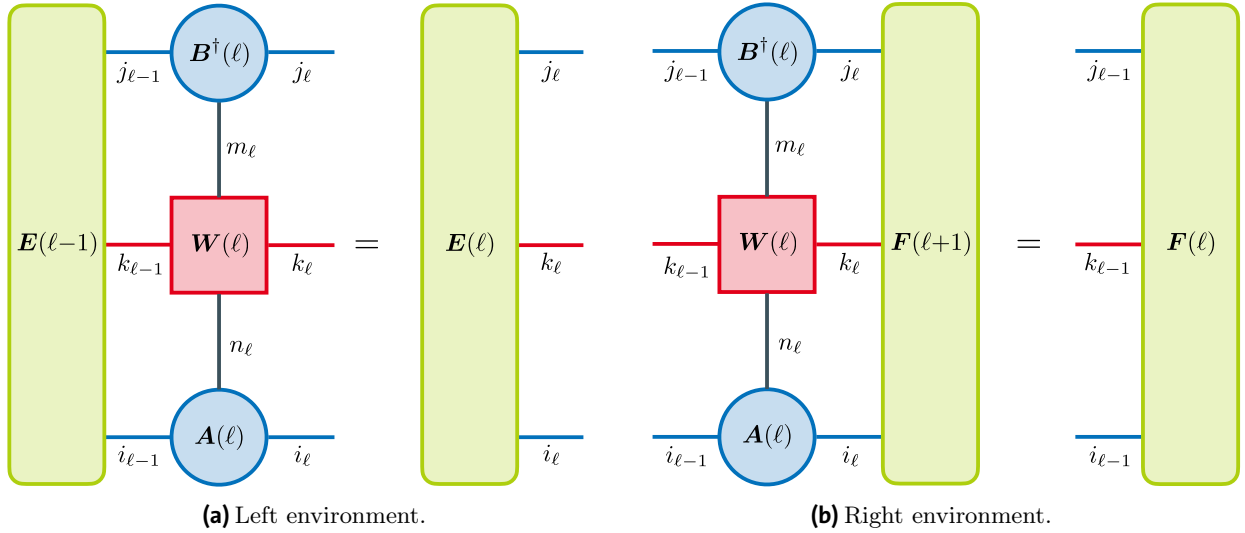


Figure 8: Visualization of the iterative update conditions for the environment tensors.

Variational algorithms

In principle, left and right environments are straightforwardly generalized to cases without an MPO (overlap of two states) or with more than one MPO. The latter, however, is computationally quite expensive, and it may be a better choice to bring the operators into the form of a single MPO first. The product of two MPOs can be calculated one site after another by taking the tensor product of the respective MPO bond indices and contracting both MPO tensors along their common physical index as shown in Figure 9a. The same holds true for the application of an MPO onto an MPS: iterative contraction of the MPO tensors and the MPS tensors along the physical index for fixed bond indices leads to a faithful MPS representation of the state after application of the operator. However, the bond dimensions of both objects multiply due to the tensor product of the bond indices.

Instead of performing operations on matrix product states exactly and compressing them afterwards, there exists another approach that makes more use of the special structure of the matrix product states: without calculating the actual result of an MPS operation, one makes the variational ansatz of an MPS of fixed bond dimension and optimizes the parameters of the trial MPS so that it is a good approximation. In that sense, this approach is more in-situ as it does not involve any matrix product states of much higher bond dimension

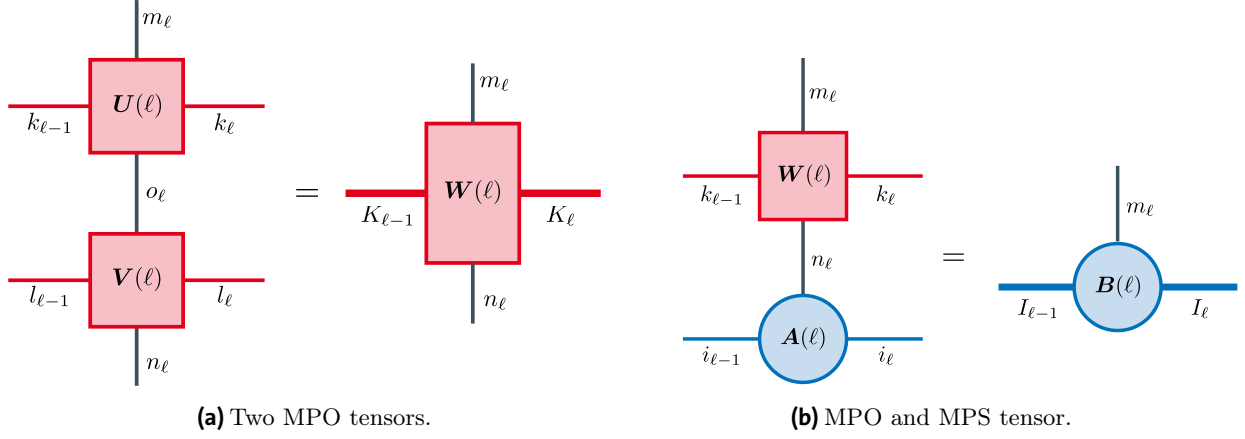


Figure 9: Visualization of exact products of local MPO and MPS tensors. The respective bond indices are combined into a tensor product.

than the original one. If $\mathcal{F}(|\Psi\rangle)$ denotes an abstract operation on an MPS $|\Psi\rangle$ and $|\Phi(\mathbf{A}(1), \dots, \mathbf{A}(L))\rangle$ is the variational ansatz MPS, one usually minimizes the functional $\| |\Phi\rangle - \mathcal{F}(|\Psi\rangle) \|_{\mathcal{H}}$ under the normalization constraint $\langle \Phi | \Phi \rangle = 1$ on the manifold of matrix product states of bond dimension χ_{target} or smaller.

Optimizing all MPS tensors $\mathbf{A}(1)$ to $\mathbf{A}(L)$ at the same time usually exceeds the limits of computational resources. Instead, one performs local optimizations one site at a time. For example, one may start with an arbitrarily initialized MPS and first optimize the functional

$$\mathcal{L}(\mathbf{A}(1), \dots, \mathbf{A}(L), \lambda) = \| |\Phi(\mathbf{A}(1), \dots, \mathbf{A}(L))\rangle - \mathcal{F}(|\Psi\rangle) \|_{\mathcal{H}}^2 + \lambda \left(\| |\Phi(\mathbf{A}(1), \dots, \mathbf{A}(L))\rangle \|_{\mathcal{H}}^2 - 1 \right) \quad (2.48)$$

at site $\ell = 1$, leading to a new value of $\mathbf{A}(1)$, and then move to the next site. When the right end of the chain is reached, the direction is reversed and the next site to optimize is again $\ell = L - 1$. The reason behind this is that these local optimizations can only be optimal with respect to their instantaneous environments, and after these have changed, there might be an adapted optimum. Therefore, many iterations are performed until the ansatz MPS does not change significantly anymore. The local optimizations decrease the value of the functional, yet it is not clear that a global minimum will be reached. Some standard techniques such as mixing with solutions from previous iterations or adding noise can become necessary if algorithms get stuck in local minima. These sequences of local optimizations from left to right and then back from right to left are called *sweeps* in the context of VMPS. If organized efficiently, this algorithm exploits the structure of the matrix product states as it only involves local operations within the local Hilbert spaces instead of the entire Hilbert space.

The local optimization conditions can easily be formulated using the graphical notation for tensor networks. Derivation with respect to either the MPS tensor or their respective complex conjugate (the Wirtinger calculus [52] states that they should be treated as independent variables) breaks down to deleting a corresponding MPS tensor in the tensor network, because tensor networks are inherently linear in the tensors they are constructed from. In particular, if the sweeping process is accompanied by proper normalizations to have the MPS always in the canonical form with the current site as pivot site, the tensor network for the norm of the trial MPS is drastically simplified.

A natural application for this procedure would be to find an MPS representation of another MPS with a smaller bond dimension – thus it is an alternative to SVD compression. Beyond that, for the application of an operator \hat{O} onto an MPS $|\Psi\rangle$, the local optimization condition that arises from derivation with respect to $\mathbf{A}^\dagger(p)$ is a simple equation. The new MPS tensor $\mathbf{A}(p)$ can be computed directly from the contraction of the left environment, the right environment, the MPO tensor and the MPS tensor, as can be seen in Figure 10. The prefactor is adjusted such that $\sum_{n_p, i_{p-1}, i_p} |A(p)_{i_{p-1} n_p}^{i_p}|^2 = 1$.

$$\begin{aligned}
 \mathcal{L} &= (\lambda + 1) \left(\begin{array}{c} \text{---} \text{A}^\dagger(p) \text{---} \\ | \\ \text{---} \text{A}(p) \text{---} \end{array} \right) - \left(\begin{array}{c} \text{---} \text{E}_{\psi(p-1)} \text{---} \\ | \\ \text{---} \text{A}^\dagger(p) \text{---} \\ | \\ \text{---} \text{W}(p) \text{---} \\ | \\ \text{---} \text{A}_{\psi(p)} \text{---} \\ | \\ \text{---} \text{F}_{\psi(p+1)} \text{---} \end{array} \right) + h.c. + \langle \Psi | \hat{O}^\dagger \hat{O} | \Psi \rangle - \lambda \\
 \\
 \frac{\partial \mathcal{L}}{\partial \text{A}^\dagger(p)} = 0 &\Rightarrow \begin{array}{c} | \\ \text{---} \text{A}(p) \text{---} \end{array} = \frac{1}{\lambda + 1} \begin{array}{c} \text{---} \text{E}_{\psi(p-1)} \text{---} \\ | \\ \text{---} \text{W}(p) \text{---} \\ | \\ \text{---} \text{A}_{\psi(p)} \text{---} \\ | \\ \text{---} \text{F}_{\psi(p+1)} \text{---} \end{array}
 \end{aligned}$$

Figure 10: Local optimization condition for variationally determining an approximation to $\hat{O}|\Psi\rangle$.

Analogously, the local optimization condition for a weighted sum $\alpha|\Psi\rangle + \beta|\Theta\rangle$ of two matrix product states (with $\|\alpha|\Psi\rangle + \beta|\Theta\rangle\|_{\mathcal{H}} = 1$) is visualized in Figure 11. Another very important use case for variational algorithms is detailed in the next section.

$$\begin{aligned}
 \mathcal{L} &= (\lambda + 1) \left(\begin{array}{c} \text{---} \text{A}^\dagger(p) \text{---} \\ | \\ \text{---} \text{A}(p) \text{---} \end{array} \right) - \left(\begin{array}{c} \text{---} \text{E}_{\psi(p-1)} \text{---} \\ | \\ \text{---} \text{A}^\dagger(p) \text{---} \\ | \\ \text{---} \text{A}_{\psi(p)} \text{---} \\ | \\ \text{---} \text{F}_{\psi(p+1)} \text{---} \end{array} - \beta \begin{array}{c} \text{---} \text{E}_{\Theta(p-1)} \text{---} \\ | \\ \text{---} \text{A}^\dagger(p) \text{---} \\ | \\ \text{---} \text{A}_{\Theta(p)} \text{---} \\ | \\ \text{---} \text{F}_{\Theta(p+1)} \text{---} \end{array} + h.c. \right) + 1 - \lambda \\
 \\
 \frac{\partial \mathcal{L}}{\partial \text{A}^\dagger(p)} = 0 &\Rightarrow \begin{array}{c} | \\ \text{---} \text{A}(p) \text{---} \end{array} = \frac{\alpha}{\lambda + 1} \begin{array}{c} \text{---} \text{E}_{\psi(p-1)} \text{---} \\ | \\ \text{---} \text{A}_{\psi(p)} \text{---} \\ | \\ \text{---} \text{F}_{\psi(p+1)} \text{---} \end{array} + \frac{\beta}{\lambda + 1} \begin{array}{c} \text{---} \text{E}_{\Theta(p-1)} \text{---} \\ | \\ \text{---} \text{A}_{\Theta(p)} \text{---} \\ | \\ \text{---} \text{F}_{\Theta(p+1)} \text{---} \end{array}
 \end{aligned}$$

Figure 11: Local optimization condition for variationally determining an approximation to $\alpha|\Psi\rangle + \beta|\Theta\rangle$.

Groundstate algorithm & area law

Probably the most prominent application of the variational principle with respect to matrix product states deals with the search for groundstates of condensed-matter systems. The original formulation of DMRG provided a method to numerically investigate low-energy physics of interacting quantum systems, and VMPS continues to address this generally still very challenging task. The idea is quite simple: find an MPS representation of a system's groundstate by means of local optimizations. In order to do so, sweeping algorithms are applied to the tensor network $\langle \Psi | \hat{H} | \Psi \rangle$. Starting with an arbitrarily initialized matrix product state of bond dimension χ , the state is brought into canonical form with the leftmost site as the pivot site. Afterwards, starting from the rightmost site, the contraction environment tensors $\mathbf{F}(L)$ to $\mathbf{F}(2)$ of the MPS and the MPO representation of the Hamiltonian operator are calculated and saved. The trivial tensors $\mathbf{E}(0)$ and $\mathbf{F}(L+1)$ are set to 1.

In the next step and all following steps, the left and right contraction environment tensors are contracted with the local MPO tensor $\mathbf{W}(p)$, forming an object $\mathbf{H}(p)$ that takes into account the local part of the Hamiltonian operator as well as the action of all non-local parts of the Hamiltonian operator with respect to the current MPS tensors. $\mathbf{H}(p)$ is connected to the local MPS tensors $\mathbf{A}(p)$ and $\mathbf{A}^\dagger(p)$ via three indices each. This structure is reminiscent of vector-matrix-vector multiplication. If the constraint of normalization is added via a Lagrangian parameter λ , taking the derivative of the functional $\mathcal{L} = \langle \Psi | \hat{H} | \Psi \rangle - \lambda (\langle \Psi | \Psi \rangle - 1)$ with respect to $\mathbf{A}^\dagger(p)$ leads to an eigenvalue equation, for which the eigenvector of the matrix $\mathbf{H}(p) \in \text{Mat}(\chi_{p-1}\chi_p d_p, \chi_{p-1}\chi_p d_p)$ with the lowest eigenvalue has to be found (Figure 12). This eigenvector can be obtained with the help of the Lanczos algorithm [53], which offers an iterative and numerically feasible method to calculate eigenvectors at the extremal points of the spectrum of a matrix.

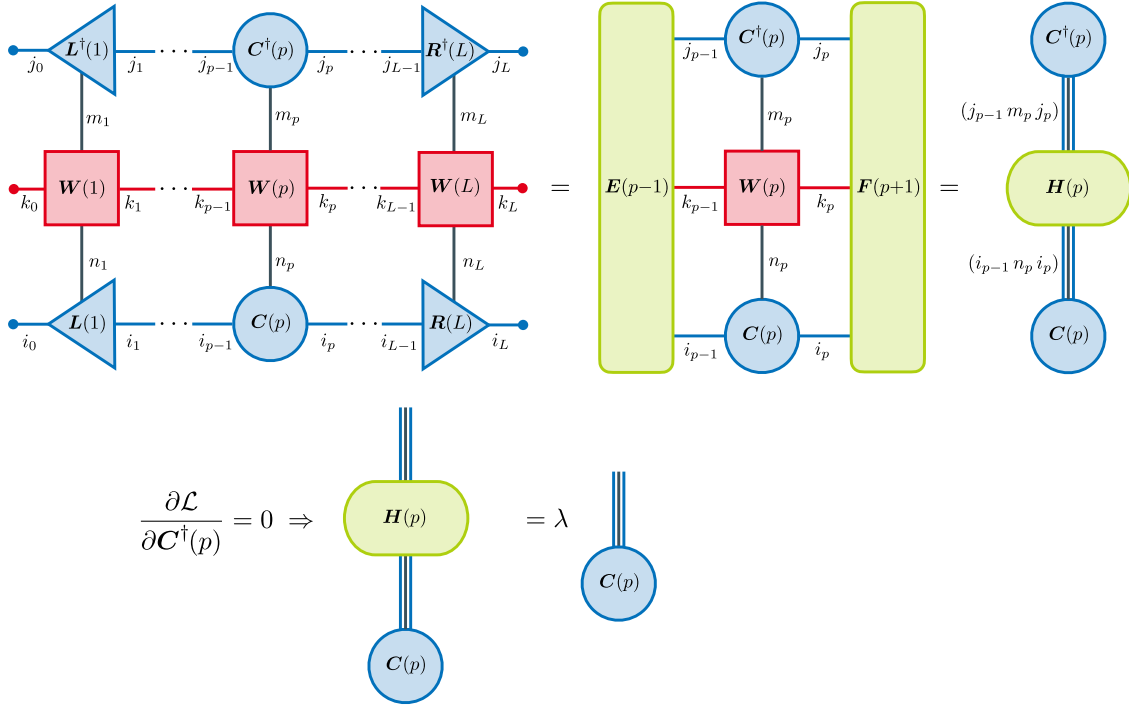


Figure 12: Tensor network for variationally determining an approximate groundstate.

The normalized eigenvector is then used to build the new MPS tensor $\mathbf{A}(p)$, and the pivot site is shifted to the next site. Since the environment contraction tensors were stored during the initial setup, one only needs to perform an SVD of the MPS tensor in order to move the pivot and afterwards one environment contraction to include the updated site. The energy of the MPS cannot increase during this local energy minimization. This local optimization of every site is performed in each sweep until convergence is reached. Convergence can be measured using the standard deviation of energy:

$$\Delta E^2 = \langle \Psi | \hat{H}^2 | \Psi \rangle - \langle \Psi | \hat{H} | \Psi \rangle^2. \quad (2.49)$$

When the matrix product state approaches an energy eigenstate, this quantity decreases until it finally reaches zero. However, one has to keep in mind that this variational algorithm does not change the bond dimension of the MPS representation, it just optimizes the variational ansatz. If the groundstate of the system cannot be represented faithfully by an MPS of this bond dimension, one cannot expect the groundstate to be reached. Instead, one has to increase the bond dimension. There are several approaches for how to dynamically increase the bond dimension during sweeping, e.g., a two-site algorithm that takes into account two pivot sites at the same time and thus deals with matrices with $\chi_{p-1}\chi_{p+1}d_p d_{p+1}$ rows and columns. By dividing this two-site

tensor into two local MPS tensors $\mathbf{A}(p)$ and $\mathbf{A}(p+1)$, the bond dimension χ_p between them can be resized. A standard procedure is to start with a comparatively small bond dimension, perform numerically demanding two-site optimizations during the first sweeps to let the bond dimension grow, and afterwards find the best approximation within the bond dimension using the one-site algorithm for later sweeps until the variational energy does not improve anymore.

The fundamental reason why matrix product states provide a well-suited platform for the description of one-dimensional systems in particular is the fact that a certain class of groundstates obeys a so called *area law* [54–56]. In order to formulate the area law, the notion of locality has to be introduced: a second-quantized Hamilton operator on a D dimensional lattice is called local if it couples only modes corresponding to sites within a limited spatial distance (the notion of locality can also be extended to other choices of Hilbert space factorizations). An example would be the Hamilton operator of a Hubbard model that contains nearest-neighbor hopping terms and an on-site interaction term. The area law then states that for gapped systems, i. e., systems with a finite energy gap between the groundstate and the first excited state, the groundstate exhibits an area-like scaling of its entanglement entropy. This means that if one chooses a subsystem of length l (and thus l^D lattice sites) and determines the entanglement entropy of the groundstate between the subsystem and the rest of the system, this quantity scales as $S \sim l^{D-1}$. Naively one might think that entanglement is an extensive measure that scales with the number of lattice sites, yet in the groundstate for gapped local Hamilton operators, the entanglement is also local, which leads to the point that only lattice sites adjacent to the boundaries of the subsystem contribute to the entanglement entropy. Hence, the entanglement entropy is subject to a surface or area scaling instead of a volume scaling. If the state exhibits a lot of entanglement, a high bond dimension is needed because the entanglement entropy is bounded by it ($S \leq \ln(\chi)$) and only a high bond dimension allows for large entanglement between the system parts to the left and right of an MPS bond.

For one-dimensional systems, the above argument guarantees that the bond dimension needed for an exact representation of the system’s groundstate is finite, irrespective of the system size. It also explains why the VMPS method is less effective in higher dimensions: the growth of the entanglement entropy for the groundstates with system size leads to the necessity of a higher and numerically more demanding bond dimension. Given computational limitations, matrix product states are limited to small systems in higher dimensions. Of course, even for one-dimensional systems, the suitability of the MPS description depends on the arrangement of local Hilbert spaces. For local Hamilton operators of condensed-matter systems, a good approach will be to recreate the system’s geometry with local Hilbert spaces describing the occupation at the corresponding lattice site. More abstract local Hilbert spaces, such as modes labelled by crystal momentum or other quantum numbers, may require testing of different site numberings if their entanglement structure is not clear a priori.

The tensor-network language of matrix product states allows for further useful algorithms such as real time evolution [57–61], imaginary time evolution for finite temperature [62, 63], uniform matrix product states for translationally invariant systems in the thermodynamic limit [64–66] or approaches to bring VMPS to higher dimensions [67–69]. However, describing these in detail is beyond the scope of this thesis.

2.2 – Angular Momentum in Quantum Mechanics

Angular momentum operators and their eigenstates

In the following, a brief overview of the concept of angular momentum and rotations and, in particular, the notations used in this thesis will be given. In quantum mechanics, orbital angular momentum appears in the context of spatial rotations as an analogue to classical angular momentum. However, the spin constitutes an angular momentum, too. Indeed, any set of three operators $\hat{J}^{(x)}$, $\hat{J}^{(y)}$ and $\hat{J}^{(z)}$ that obey the commutation

relations

$$\left[\widehat{\mathcal{J}}^{(x)}, \widehat{\mathcal{J}}^{(y)} \right] = i\widehat{\mathcal{J}}^{(z)} \quad \text{and cyclic permutations of } (x, y, z) \quad (2.50)$$

is called angular momentum (the reduced Planck constant \hbar is set to 1 henceforth). The three components of the angular momentum do not commute, but they commute with the square of their magnitude, given by $\widehat{\mathcal{J}}^2 = (\widehat{\mathcal{J}}^{(x)})^2 + (\widehat{\mathcal{J}}^{(y)})^2 + (\widehat{\mathcal{J}}^{(z)})^2$. Hence, it is possible to choose a basis for the Hilbert space that consists of common eigenstates of $\widehat{\mathcal{J}}^2$ and any one component. Typically the z component is chosen, such that each quantum state is labelled by $|j, \alpha, m\rangle$, where j (called the *angular momentum quantum number*) and m (called the *projection quantum number*) describe the action of the angular momentum operators on the state, i.e.,

$$\begin{aligned} \widehat{\mathcal{J}}^2 |j, \alpha, m\rangle &= j(j+1) |j, \alpha, m\rangle & \text{with } 2j \in \mathbb{N}, \\ \widehat{\mathcal{J}}^{(z)} |j, \alpha, m\rangle &= m |j, \alpha, m\rangle & \text{with } m \in \{-j, -j+1, \dots, +j\}, \end{aligned} \quad (2.51)$$

and α describes any further quantum numbers that may be necessary to characterize the state (*degeneracy quantum number*). These quantum numbers are chosen in such a way that the states form an ONB: $\langle j', \alpha', m' | j, \alpha, m \rangle = \delta_{jj'} \delta_{\alpha\alpha'} \delta_{mm'}$. A very common description makes use of *ladder operators* $\widehat{\mathcal{J}}^{(\pm)} = \widehat{\mathcal{J}}^{(x)} \pm i\widehat{\mathcal{J}}^{(y)}$, which increment or decrement the projection quantum number:

$$\widehat{\mathcal{J}}^{(\pm)} |j, \alpha, m\rangle = \sqrt{(j \mp m)(j \pm m + 1)} |j, \alpha, m \pm 1\rangle. \quad (2.52)$$

Here another constraint for the degeneracy quantum numbers occurs: the application of $\widehat{\mathcal{J}}^{(\pm)}$ changes neither the angular momentum nor the degeneracy quantum number. While the former is an inevitable consequence of $[\widehat{\mathcal{J}}^2, \widehat{\mathcal{J}}^{(\pm)}] = 0$, the latter restricts the choice of the degeneracy quantum numbers such that they do not depend on the projection quantum numbers. If the choice of degeneracy quantum numbers is altered from one set $\{\alpha\}$ to another set $\{\beta\}$, then the matrix elements are independent of the projection quantum numbers:

$$\begin{aligned} |j, \beta, m\rangle &= \sum_{j', \alpha, m'} \langle j', \alpha, m' | j, \beta, m \rangle |j', \alpha, m'\rangle = \sum_{\alpha} \langle j, \alpha, m | j, \beta, m \rangle |j, \alpha, m\rangle \\ \Rightarrow \widehat{\mathcal{J}}^{(\pm)} |j, \beta, m\rangle &= \sum_{\alpha} \langle j, \alpha, m | j, \beta, m \rangle \sqrt{(j \mp m)(j \pm m + 1)} |j, \alpha, m \pm 1\rangle \\ &= \sqrt{(j \mp m)(j \pm m + 1)} |j, \beta, m \pm 1\rangle = \sqrt{(j \mp m)(j \pm m + 1)} \sum_{\alpha} \langle j, \alpha, m \pm 1 | j, \beta, m \pm 1 \rangle |j, \alpha, m \pm 1\rangle. \end{aligned}$$

Projection onto $\langle j, \alpha, m \pm 1 |$ yields

$$\langle j, \alpha, m | j, \beta, m \rangle = \langle j, \alpha, m \pm 1 | j, \beta, m \pm 1 \rangle = \langle\langle j, \alpha || j, \beta \rangle\rangle, \quad (2.53)$$

where $\langle\langle \cdot || \cdot \rangle\rangle$ denotes a reduced scalar product that only depends on the angular momentum and the degeneracy quantum numbers. This argument will be used several times in the further course of this thesis.

From a group theoretical perspective, the underlying symmetry group is $SU(2)$ and the operators $\widehat{\mathcal{J}}^{(x)}$, $\widehat{\mathcal{J}}^{(y)}$ and $\widehat{\mathcal{J}}^{(z)}$ are generators of the corresponding Lie algebra $\mathfrak{su}(2)$ with $\widehat{\mathcal{J}}^2$ the Casimir element of this Lie algebra. Via exponential mapping, elements from the Lie algebra are represented on the Hilbert space as unitary operators. The action of the group $SU(2)$ on the Hilbert space describes rotations. In fact, every element $g \in SU(2)$ corresponds to a rotation with Euler angles α , β and γ . A commonly used representation [70] of g

on the Hilbert space is given by

$$\widehat{U}_g = \exp\left(-i\alpha_g \widehat{J}^{(z)}\right) \exp\left(-i\beta_g \widehat{J}^{(y)}\right) \exp\left(-i\gamma_g \widehat{J}^{(z)}\right). \quad (2.54)$$

The aforementioned total momentum quantum number j labels irreducible representations of the group $SU(2)$, and the degeneracy quantum number α distinguishes between different equivalent representations in the case of multiplicity $\mathfrak{D}(j) > 1$. The projection quantum numbers m label the states within an irreducible representation. For $SU(2)$ (as opposed to $SO(3)$) half-integer numbers are possible for j . Thus the Hilbert space can be completely decomposed into $2j + 1$ -dimensional carrier spaces $V_\alpha^{[j]} = \text{span}(|j, \alpha, m\rangle \mid -j \leq m \leq +j)$ of irreducible representations:

$$\mathcal{H} = \bigoplus_j \bigoplus_{\alpha=1}^{\mathfrak{D}(j)} V_\alpha^{[j]} \quad \text{with } \widehat{U}_\alpha^{[j]} : V_\alpha^{[j]} \rightarrow V_\alpha^{[j]} \quad \text{and} \quad \left(\widehat{U}_\alpha^{[j]}, \widehat{U}_{\alpha'}^{[j']}\right) \text{ equivalent} \Leftrightarrow j = j'. \quad (2.55)$$

All equivalent irreducible representations are specified to be the same henceforth, so that the degeneracy index on the operator can be dropped. With this, a rotation g acts on an angular momentum eigenstate as

$$\widehat{U}_g |j, \alpha, m\rangle = \sum_{j', \alpha', m'} \langle j', \alpha', m' | \exp\left(-i\alpha_g \widehat{J}^{(z)}\right) \exp\left(-i\beta_g \widehat{J}^{(y)}\right) \exp\left(-i\gamma_g \widehat{J}^{(z)}\right) |j, \alpha, m\rangle |j', \alpha', m'\rangle,$$

where

$$\langle j', \alpha', m' | \exp\left(-i\alpha_g \widehat{J}^{(z)}\right) \exp\left(-i\beta_g \widehat{J}^{(y)}\right) \exp\left(-i\gamma_g \widehat{J}^{(z)}\right) |j, \alpha, m\rangle = \delta_{jj'} \delta_{\alpha\alpha'} D_{m'm}^{[j]} \quad (2.56)$$

are the elements of the g -dependent Wigner D-matrix $\mathbf{D} = \bigoplus_j \mathbf{D}^{[j]}$, so that one arrives at

$$\widehat{U}_g |j, \alpha, m\rangle = \sum_{m'} D_{m'm}^{[j]} |j, \alpha, m'\rangle, \quad (2.57)$$

and for a bra state one finds

$$\langle j, \alpha, m | \widehat{U}_g^\dagger = \sum_{m'} (D_{m'm}^{[j]})^* \langle j, \alpha, m' |. \quad (2.58)$$

The Wigner D-matrix is a matrix representation of $SU(2)$ on the Hilbert space equipped with an angular momentum eigenstate basis, which can be derived from the abstract representation $SU(2) \rightarrow \text{End}(\mathcal{H})$ with $g \mapsto \widehat{U}_g : \mathcal{H} \rightarrow \mathcal{H}$, by calculating the corresponding matrix elements.

Coupling of angular momenta

When two systems with angular momentum operators $\widehat{\mathbf{j}}_1$ and $\widehat{\mathbf{j}}_2$ are brought together and described in terms of their tensor product space, the operator $\widehat{\mathbf{J}} = \widehat{\mathbf{j}}_1 \otimes \text{id} + \text{id} \otimes \widehat{\mathbf{j}}_2$ (in the following the identity operators are omitted for simplicity) forms a total angular momentum operator on the space spanned by the tensor product basis. However, these states are not eigenstates of

$$\widehat{J}^2 = \widehat{j}_1^2 + \widehat{j}_2^2 + 2\widehat{\mathbf{j}}_1 \cdot \widehat{\mathbf{j}}_2 = \widehat{j}_1^2 + \widehat{j}_2^2 + \widehat{j}_1^{(+)} \widehat{j}_2^{(-)} + \widehat{j}_1^{(-)} \widehat{j}_2^{(+)} + 2\widehat{j}_1^{(z)} \widehat{j}_2^{(z)}, \quad (2.59)$$

since this operator does not commute with $\widehat{j}_1^{(z)}$ and $\widehat{j}_2^{(z)}$. Common eigenstates of the total angular momentum, its projection and the two constituent angular momenta can be found – for fixed $j_1, j_2, \alpha_1, \alpha_2$ they are given

by

$$\begin{aligned} |J(j_1, j_2), (\alpha_1, \alpha_2), M\rangle &= \sum_{m_1, m_2} \langle j_1, \alpha_1, m_1; j_2, \alpha_2, m_2 | J(j_1, j_2), (\alpha_1, \alpha_2), M \rangle |j_1, \alpha_1, m_1\rangle \otimes |j_2, \alpha_2, m_2\rangle \\ &= \sum_{m_1, m_2} \Gamma_{m_1 m_2 \rightarrow M}^{j_1 j_2 \rightarrow J} |j_1, \alpha_1, m_1\rangle \otimes |j_2, \alpha_2, m_2\rangle. \end{aligned} \quad (2.60)$$

The appearing coefficients $\Gamma_{m_1 m_2 \rightarrow M}^{j_1 j_2 \rightarrow J}$ are called Clebsch–Gordan coefficients. They are matrix elements of a unitary matrix transforming from a decoupled tensor product basis to a basis with coupled angular momenta. They depend only on angular momentum and projection quantum numbers, the relevant symmetries of Clebsch–Gordan coefficients are given in Appendix A.3. One of the most important implications is the triangle rule which states that two angular momenta can couple to total angular momenta $|j_1 - j_2| \leq J \leq j_1 + j_2$. This can also be seen from a group theoretical perspective. The tensor product representation for SU(2) irreducible representations labelled by j_1 and j_2 reads:

$$\widehat{U}^{[j_1]} \otimes \widehat{U}^{[j_2]} = \bigoplus_J n_{j_1 j_2 \rightarrow J} \widehat{U}^{[J]} \quad \text{where} \quad n_{j_1 j_2 \rightarrow J} = \begin{cases} 1 & |j_1 - j_2| \leq J \leq j_1 + j_2, \\ 0 & \text{otherwise.} \end{cases} \quad (2.61)$$

The fact that $n_{j_1 j_2 \rightarrow J} \leq 1$ signifies that SU(2) has no outer multiplicity [71], because each irreducible representation occurs at most once (of course, if irreducible representations which appear equivalently multiple times are multiplied, the result will also contain multiple equivalent irreducible representations).

If any other choice of degeneracy quantum numbers is made than just the concatenation of the two individual degeneracy quantum numbers, the above statement about projection independence of the matrix elements from Equation (2.53) holds, so that a general state with coupled angular momentum takes the form

$$|J(j_1, j_2), \mathcal{A}, M\rangle = \sum_{\substack{\alpha_1, m_1, \\ \alpha_2, m_2}} \langle J(j_1, j_2), \mathcal{A} | J(j_1, j_2), (\alpha_1, \alpha_2) \rangle \Gamma_{m_1 m_2 \rightarrow M}^{j_1 j_2 \rightarrow J} |j_1, \alpha_1, m_1\rangle \otimes |j_2, \alpha_2, m_2\rangle. \quad (2.62)$$

When more than two angular momenta are coupled, the order of the pairwise couplings becomes crucial for the explicit states. This circumstance is reflected in the so-called recoupling symbols. In Section 2.3 it will be shown that these appear quite often for contractions of tensor networks that exhibit an SU(2) symmetry, as they involve sums over projection quantum numbers of Clebsch–Gordan coefficients.

The coupling order of three angular momenta is taken into account by Wigner 6j-symbols, which, up to a prefactor, are given by the scalar product of two differently ordered angular momenta couplings leading to the same total angular momentum J (the overlap is diagonal in and otherwise independent of other quantum numbers, so that the degeneracy indices can be ignored for a moment). For three initial angular momenta j_1, j_2, j_3 , one either couples j_1 and j_2 first to an angular momentum J_{12} , and afterwards couples J_{12} and j_3 to the total angular momentum J , or in a first step j_2 and j_3 are combined to J_{23} and j_1 is added afterwards. The overlap of two such states is diagonal in the projection quantum number and does not actually depend on its value, as can be seen from application of $\widehat{J}^{(z)}$ and $\widehat{J}^{(\pm)}$:

$$\begin{aligned} \langle J(J_{12}, j_3), M | \widehat{J}^{(z)} | J(j_1, J_{23}), M' \rangle &= M \langle J(J_{12}, j_3), M | J(j_1, J_{23}), M' \rangle = M' \langle J(J_{12}, j_3), M | J(j_1, J_{23}), M' \rangle \\ \Rightarrow \langle J(J_{12}, j_3), M | J(j_1, J_{23}), M' \rangle &= \delta_{MM'} \langle J(J_{12}, j_3), M | J(j_1, J_{23}), M \rangle, \quad \text{and} \\ \langle J(J_{12}, j_3), M + 1 | \widehat{J}^{(+)} | J(j_1, J_{23}), M \rangle &= \sqrt{(J - M)(J + M + 1)} \langle J(J_{12}, j_3), M + 1 | J(j_1, J_{23}), M + 1 \rangle \\ &= \sqrt{(J - M)(J + M + 1)} \langle J(J_{12}, j_3), M | J(j_1, J_{23}), M \rangle \\ \Rightarrow \langle J(J_{12}, j_3), M | J(j_1, J_{23}), M \rangle &= \langle J(J_{12}, j_3), J | J(j_1, J_{23}), J \rangle. \end{aligned} \quad (2.63)$$

Now this scalar product can be evaluated by decoupling of the combined angular momenta:

$$\begin{aligned}
& \langle J(J_{12}(j_1, j_2), j_3), M | J(j_1, J_{23}(j_2, j_3)), M \rangle \\
&= \sum_{\substack{M_{12}, m_3, \\ m_1, M_{23}}} \langle J(J_{12}, j_3), M | J_{12}, M_{12}; j_3, m_3 \rangle \langle J_{12}(j_1, j_2), M_{12}; j_3, m_3 | j_1, m_1; J_{23}(j_2, j_3), M_{23} \rangle \\
&\quad \cdot \langle j_1, m_1; J_{23}, M_{23} | J(j_1, J_{23}), M \rangle \\
&= \sum_{\substack{M_{12}, m_3, \\ m_1, M_{23}}} \Gamma_{M_{12} m_3 \rightarrow M}^{J_{12} j_3 \rightarrow J} \Gamma_{m_1 M_{23} \rightarrow M}^{j_1 J_{23} \rightarrow J} \langle J_{12}(j_1, j_2), M_{12}; j_3, m_3 | j_1, m_1; J_{23}, M_{23} \rangle \\
&= \sum_{\substack{M_{12}, m_3, m'_1, m'_2, \\ m_1, M_{23} m''_2, m''_3}} \Gamma_{M_{12} m_3 \rightarrow M}^{J_{12} j_3 \rightarrow J} \Gamma_{m_1 M_{23} \rightarrow M}^{j_1 J_{23} \rightarrow J} \langle J_{12}(j_1, j_2), M_{12} | j_1, m'_1; j_2, m'_2 \rangle \\
&\quad \cdot \langle j_1, m'_1; j_2, m'_2; j_3, m_3 | j_1, m_1; j_2, m''_2; j_3, m'_3 \rangle \langle j_2, m''_2; j_3, m'_3 | J_{23}, M_{23} \rangle \\
&= \sum_{\substack{m_1, m_2, m_3, \\ M_{12}, M_{23}}} \Gamma_{M_{12} m_3 \rightarrow M}^{J_{12} j_3 \rightarrow J} \Gamma_{m_1 M_{23} \rightarrow M}^{j_1 J_{23} \rightarrow J} \Gamma_{m_1 m_2 \rightarrow M_{12}}^{j_1 j_2 \rightarrow J_{12}} \Gamma_{m_2 m_3 \rightarrow M_{23}}^{j_2 j_3 \rightarrow J_{23}}. \tag{2.64}
\end{aligned}$$

The Wigner 6j-symbol is defined as

$$\begin{aligned}
\left\{ \begin{array}{ccc} j_1 & j_2 & J_{12} \\ j_3 & J & J_{23} \end{array} \right\} &= \frac{(-1)^{j_1+j_2+j_3+J}}{\sqrt{(2J_{12}+1)(2J_{23}+1)}} \langle J(J_{12}(j_1, j_2), j_3), M | J(j_1, J_{23}(j_2, j_3)), M \rangle \\
&= \frac{(-1)^{j_1+j_2+j_3+J}}{\sqrt{(2J_{12}+1)(2J_{23}+1)}} \sum_{\substack{m_1, m_2, m_3, \\ M_{12}, M_{23}}} \Gamma_{m_1 m_2 \rightarrow M_{12}}^{j_1 j_2 \rightarrow J_{12}} \Gamma_{M_{12} m_3 \rightarrow M}^{J_{12} j_3 \rightarrow J} \Gamma_{m_2 m_3 \rightarrow M_{23}}^{j_2 j_3 \rightarrow J_{23}} \Gamma_{m_1 M_{23} \rightarrow M}^{j_1 J_{23} \rightarrow J}. \tag{2.65}
\end{aligned}$$

Analogously, for the coupling of four initial angular momenta with four intermediate steps, one defines Wigner 9j-symbols:

$$\begin{aligned}
\left\{ \begin{array}{ccc} j_1 & j_2 & J_{12} \\ j_3 & j_4 & J_{34} \\ J_{13} & J_{24} & J \end{array} \right\} &= \frac{\langle J(J_{12}(j_1, j_2), J_{34}(j_3, j_4)), M | J(J_{13}(j_1, j_3), J_{24}(j_2, j_4)), M \rangle}{\sqrt{(2J_{12}+1)(2J_{34}+1)(2J_{13}+1)(2J_{24}+1)}} \\
&= \sum_{\substack{m_1, m_2, m_3, m_4, \\ M_{12}, M_{34}, M_{13}, M_{24}}} \frac{\Gamma_{m_1 m_2 \rightarrow M_{12}}^{j_1 j_2 \rightarrow J_{12}} \Gamma_{m_3 m_4 \rightarrow M_{34}}^{j_3 j_4 \rightarrow J_{34}} \Gamma_{M_{12} M_{34} \rightarrow M}^{J_{12} J_{34} \rightarrow J} \Gamma_{m_1 m_3 \rightarrow M_{13}}^{j_1 j_3 \rightarrow J_{13}} \Gamma_{m_2 m_4 \rightarrow M_{24}}^{j_2 j_4 \rightarrow J_{24}} \Gamma_{M_{13} M_{24} \rightarrow M}^{J_{13} J_{24} \rightarrow J}}{\sqrt{(2J_{12}+1)(2J_{34}+1)(2J_{13}+1)(2J_{24}+1)}}. \tag{2.66}
\end{aligned}$$

Irreducible tensor operators and Wigner–Eckart theorem

An operator \widehat{O} transforms under the action of $g \in \text{SU}(2)$ as

$$\widehat{O}' = \widehat{U}_g \widehat{O} \widehat{U}_g^\dagger. \tag{2.67}$$

Operators that are symmetric under the action of $\text{SU}(2)$ are invariant under this transformation. This is the case, e. g., for Hamilton operators that exhibit a $\text{SU}(2)$ symmetry:

$$\widehat{H}' = \widehat{U}_g \widehat{H} \widehat{U}_g^\dagger = \widehat{H} \quad \text{for all } g \in \text{SU}(2). \tag{2.68}$$

The generators $\widehat{J}^{(x)}$, $\widehat{J}^{(y)}$ and $\widehat{J}^{(z)}$ are not symmetric on their own, but they are twisted into one another under the action of the group. Thus the three operators span an invariant subspace (of the space of operators $\text{End}(\mathcal{H})$). To account for this common transformation behavior of a set of operators, the concept of an *Irreducible Tensor Operator* is introduced. A set of operators is called an irreducible tensor operator, if its components transform

under the action of the group corresponding to an irreducible representation of that group:

$$\begin{aligned} \widehat{T}^{[j]} &= \begin{pmatrix} \widehat{T}_{+j}^{[j]} \\ \vdots \\ \widehat{T}_{-j}^{[j]} \end{pmatrix} \text{ is called an irreducible tensor operator of rank } j \\ :\Leftrightarrow \widehat{U}_g \widehat{T}_m^{[j]} \widehat{U}_g^\dagger &= \sum_{m'} D_{m'm}^{[j]} \widehat{T}_{m'}^{[j]} \text{ for all } g \in \text{SU}(2) \text{ and } -j \leq m \leq +j, \\ \text{where } D_{m'm}^{[j]} &= \langle j, \alpha, m' | \widehat{U}_g | j, \alpha, m \rangle \text{ is a matrix representation of SU}(2) \text{ on } V_\alpha^{[j]} \subset \mathcal{H}. \end{aligned} \quad (2.69)$$

Again, using the standard Euler-angle representation, the matrix representation is given by the Wigner D-matrix. Irreducible tensor operators of rank 0 are scalar operators which commute with every symmetry transformation. From the definition of irreducible tensor operators, commutation relations for the components can be derived by expanding in orders of an arbitrarily chosen real number φ :

$$\begin{aligned} \widehat{U} = \exp(i\varphi \widehat{J}^{(z)}) : \exp(i\varphi \widehat{J}^{(z)}) \widehat{T}_m^{[j]} \exp(-i\varphi \widehat{J}^{(z)}) &= \widehat{T}_m^{[j]} + i\varphi [\widehat{J}^{(z)}, \widehat{T}_m^{[j]}] + \mathcal{O}(\varphi^2) \\ &= \sum_{m'} \langle j, m' | \exp(i\varphi \widehat{J}^{(z)}) | j, m \rangle \widehat{T}_{m'}^{[j]} = \widehat{T}_m^{[j]} + i\varphi m \widehat{T}_m^{[j]} + \mathcal{O}(\varphi^2) \\ \Rightarrow [\widehat{J}^{(z)}, \widehat{T}_m^{[j]}] &= m \widehat{T}_m^{[j]}, \\ \widehat{U} = \exp(i\varphi \widehat{J}^{(\pm)}) : \exp(i\varphi \widehat{J}^{(\pm)}) \widehat{T}_m^{[j]} \exp(-i\varphi \widehat{J}^{(\pm)}) &= \widehat{T}_m^{[j]} + i\varphi [\widehat{J}^{(\pm)}, \widehat{T}_m^{[j]}] + \mathcal{O}(\varphi^2) \\ &= \sum_{m'} \langle j, m' | \exp(i\varphi \widehat{J}^{(\pm)}) | j, m \rangle \widehat{T}_{m'}^{[j]} = \widehat{T}_m^{[j]} + i\varphi \sqrt{(j \mp m)(j \pm m + 1)} \widehat{T}_{m \pm 1}^{[j]} + \mathcal{O}(\varphi^2) \\ \Rightarrow [\widehat{J}^{(\pm)}, \widehat{T}_m^{[j]}] &= \sqrt{(j \mp m)(j \pm m + 1)} \widehat{T}_{m \pm 1}^{[j]}. \end{aligned} \quad (2.70)$$

These commutation relations resemble the action of the angular momentum operators on angular momentum eigenstates given in Equation (2.51) and Equation (2.52). In fact, it is sufficient for a set of $2j + 1$ operators to obey these commutation relations to be an irreducible tensor operator of rank j [72].

Given two irreducible tensor operators $\widehat{R}^{[j]}$ and $\widehat{S}^{[j']}$, one can define a product-like concatenation of these operators that again constitutes an irreducible tensor operator [73]. However, this product is not unique, because different non-trivial irreducible tensor operators with rank J ranging from $|j - j'|$ to $j + j'$ may result. From the perspective of angular momentum coupling, this may seem obvious: angular momenta can in general be coupled to a variety of different resulting angular momenta. In order to achieve a well-defined product, it is therefore necessary to specify the rank of the result:

$$\widehat{T}_M^{[J]} = \left(\widehat{R}^{[j]} \star \widehat{S}^{[j']} \right)_M^{[J]} := \sum_{m, m'} \Gamma_{m m' \rightarrow M}^{j j' \rightarrow J} \widehat{R}_m^{[j]} \circ \widehat{S}_{m'}^{[j']}. \quad (2.71)$$

This definition indeed gives an irreducible tensor operator of rank J :

$$\begin{aligned} [\widehat{J}^{(z)}, \widehat{T}_M^{[J]}] &= \sum_{m, m'} \Gamma_{m m' \rightarrow M}^{j j' \rightarrow J} \left([\widehat{J}^{(z)}, \widehat{R}_m^{[j]}] \widehat{S}_{m'}^{[j']} + \widehat{R}_m^{[j]} [\widehat{J}^{(z)}, \widehat{S}_{m'}^{[j']}] \right) \\ &= \sum_{m, m'} (m + m') \Gamma_{m m' \rightarrow M}^{j j' \rightarrow J} \widehat{R}_m^{[j]} \widehat{S}_{m'}^{[j']} = M \widehat{T}_M^{[J]}, \end{aligned}$$

$$\begin{aligned}
 [\hat{\mathcal{J}}^{(\pm)}, \hat{T}_M^{[J]}] &= \sum_{m,m'} \Gamma_{mm'}^{j j' \rightarrow J} \left([\hat{\mathcal{J}}^{(\pm)}, \hat{R}_m^{[j]} \hat{S}_{m'}^{[j']} + \hat{R}_m^{[j]} [\hat{\mathcal{J}}^{(\pm)}, \hat{S}_{m'}^{[j]}] \right) \\
 &= \sum_{m,m'} \Gamma_{mm'}^{j j' \rightarrow J} \left(\sqrt{(j \mp m)(j \pm m + 1)} \hat{R}_{m \pm 1}^{[j]} \hat{S}_{m'}^{[j']} + \sqrt{(j' \mp m')(j' \pm m' + 1)} \hat{R}_m^{[j]} \hat{S}_{m' \pm 1}^{[j']} \right) \\
 &= \sum_{m=-j \mp 1}^{j \mp 1} \sum_{m'=-j'}^{j'} \Gamma_{mm'}^{j j' \rightarrow J} \sqrt{(j \mp m)(j \pm m + 1)} \hat{R}_{m \pm 1}^{[j]} \hat{S}_{m'}^{[j']} \\
 &\quad + \sum_{m=-j}^j \sum_{m'=-j' \mp 1}^{j' \mp 1} \Gamma_{mm'}^{j j' \rightarrow J} \sqrt{(j' \mp m')(j' \pm m' + 1)} \hat{R}_m^{[j]} \hat{S}_{m' \pm 1}^{[j']} \\
 &= \sum_{m=-j}^j \sum_{m'=-j'}^{j'} \left(\Gamma_{m \mp 1 m'}^{j j' \rightarrow J} \sqrt{(j \pm m)(j \mp m + 1)} + \Gamma_{m m' \mp 1}^{j j' \rightarrow J} \sqrt{(j' \pm m')(j' \mp m' + 1)} \right) \hat{R}_m^{[j]} \hat{S}_{m'}^{[j']} \\
 &= \sum_{m,m'} \sqrt{(J \mp M)(J \pm M + 1)} \Gamma_{mm'}^{j j' \rightarrow J} \hat{R}_m^{[j]} \hat{S}_{m'}^{[j']} = \sqrt{(J \mp M)(J \pm M + 1)} \hat{T}_{M \pm 1}^{[J]}. \tag{2.72}
 \end{aligned}$$

The adjoint of an irreducible tensor operator can also be constructed. In addition to taking the adjoint of the individual components, the order has to be reversed and a phase factor is acquired – in order to avoid confusion, the adjoint of an irreducible tensor operator is marked with a ‡:

$$(\hat{T}_m^\ddagger)^{[j]} = (-1)^{j-m} \left(\hat{T}_{-m}^{[j]} \right)^\dagger, \tag{2.73}$$

because the so-defined components again obey the right commutation relations:

$$\begin{aligned}
 [\hat{\mathcal{J}}^{(z)}, (\hat{T}_m^\ddagger)^{[j]}] &= (-1)^{j-m} [\hat{T}_{-m}^{[j]}, \hat{\mathcal{J}}^{(z)}]^\dagger = (-1)^{j-m} \cdot m \left(\hat{T}_{-m}^{[j]} \right)^\dagger = m (\hat{T}_m^\ddagger)^{[j]}, \\
 [\hat{\mathcal{J}}^{(\pm)}, (\hat{T}_m^\ddagger)^{[j]}] &= (-1)^{j-m} [\hat{T}_{-m}^{[j]}, \hat{\mathcal{J}}^{(\mp)}]^\dagger = (-1)^{j-m+1} \cdot \sqrt{(j \pm (-m))(j \mp (-m) + 1)} \left(\hat{T}_{-m \mp 1}^{[j]} \right)^\dagger \\
 &= \sqrt{(j \mp m)(j \pm m + 1)} (\hat{T}_{m \pm 1}^\ddagger)^{[j]}. \tag{2.74}
 \end{aligned}$$

Taking the adjoint twice gives $\left((\hat{T}_m^\ddagger)^{[j]} \right)^\ddagger = (-1)^{2j} \hat{T}_m^{[j]}$ – this means that for tensor operators of half-integer rank, taking the adjoint twice results in an additional minus sign.

Lastly, a particular irreducible tensor operator is presented, which will be useful for later calculations. For fixed values j, j', α and α' , one can define

$$\hat{T}_n^{[k]} = \sum_{m,m'} \Gamma_{mn \rightarrow m'}^{j k \rightarrow j'} |j', \alpha', m'\rangle \langle j, \alpha, m|. \tag{2.75}$$

For $|j - j'| \leq k \leq j + j'$, this constitutes an irreducible tensor operator of rank k , as can directly be seen:

$$\begin{aligned}
 [\hat{\mathcal{J}}^{(z)}, \hat{T}_n^{[k]}] &= \sum_{m,m'} \Gamma_{mn \rightarrow m'}^{j k \rightarrow j'} (m' - m) |j', \alpha', m'\rangle \langle j, \alpha, m| = n \hat{T}_n^{[k]}, \\
 [\hat{\mathcal{J}}^{(\pm)}, \hat{T}_n^{[k]}] &= \sum_{m,m'} \Gamma_{mn \rightarrow m'}^{j k \rightarrow j'} \left(\sqrt{(j' \mp m')(j' \pm m' + 1)} |j', \alpha', m' \pm 1\rangle \langle j, \alpha, m| \right. \\
 &\quad \left. - |j', \alpha', m'\rangle \langle j, \alpha, m \mp 1| \sqrt{(j \pm m)(j \mp m + 1)} \right) \\
 &= \sum_{m,m'} \left(\sqrt{(j' \pm m')(j' \mp m' + 1)} \Gamma_{mn \rightarrow m' \mp 1}^{j k \rightarrow j'} - \sqrt{(j \mp m)(j \pm m + 1)} \Gamma_{m \pm 1 n \rightarrow m}^{j k \rightarrow j'} \right) |j', \alpha', m'\rangle \langle j, \alpha, m| \\
 &= \sqrt{(k \mp n)(k \pm n + 1)} \hat{T}_{n \pm 1}^{[k]}. \tag{2.76}
 \end{aligned}$$

The main use of irreducible tensor operators is the extension of selection rules for matrix elements. While it is obvious that a matrix element of a SU(2)-symmetric Hamilton operator with two angular momentum eigenstates of different angular momentum vanishes, the Wigner–Eckart theorem generalizes this concept to the case of irreducible tensor operators of higher rank. It states that matrix elements of irreducible tensor operators break down into a product of a Clebsch–Gordan coefficient and a reduced matrix element:

$$\langle j', \alpha', m' | \widehat{T}_n^{[k]} | j, \alpha, m \rangle = \Gamma_{mn \rightarrow m'}^{j k \rightarrow j'} \langle j', \alpha' | \widehat{\mathbf{T}}^{[k]} || j, \alpha \rangle. \quad (2.77)$$

The reduced matrix elements depend only on the quantum numbers characterizing the irreducible representations, while the Clebsch–Gordan coefficient solely depends on angular momentum and projection quantum numbers and takes care of the symmetry properties of the matrix element.

To prove the Wigner–Eckart theorem [70], for a fixed irreducible tensor operator $\widehat{\mathbf{T}}^{[k]}$ of rank k and fixed quantum numbers j and α these states are defined:

$$|\Psi_{j'm'}\rangle = \sum_{n,m} \Gamma_{mn \rightarrow m'}^{j k \rightarrow j'} \widehat{T}_n^{[k]} | j, \alpha, m \rangle. \quad (2.78)$$

These states obey

$$\begin{aligned} \widehat{J}^{(z)} |\Psi_{j'm'}\rangle &= \sum_{n,m} \Gamma_{mn \rightarrow m'}^{j k \rightarrow j'} \left([\widehat{J}^{(z)}, \widehat{T}_n^{[k]}] | j, \alpha, m \rangle + \widehat{T}_n^{[k]} \widehat{J}^{(z)} | j, \alpha, m \rangle \right) \\ &= \sum_{n,m} \Gamma_{mn \rightarrow m'}^{j k \rightarrow j'} \left(n \widehat{T}_n^{[k]} | j, \alpha, m \rangle + m \widehat{T}_n^{[k]} | j, \alpha, m \rangle \right) = \sum_{n,m} (n+m) \Gamma_{mn \rightarrow m'}^{j k \rightarrow j'} \widehat{T}_n^{[k]} | j, \alpha, m \rangle = m' |\Psi_{j'm'}\rangle, \\ \widehat{J}^{(\pm)} |\Psi_{j'm'}\rangle &= \sum_{n,m} \Gamma_{mn \rightarrow m'}^{j k \rightarrow j'} \left([\widehat{J}^{(\pm)}, \widehat{T}_n^{[k]}] | j, \alpha, m \rangle + \widehat{T}_n^{[k]} \widehat{J}^{(\pm)} | j, \alpha, m \rangle \right) \\ &= \sum_{n,m} \Gamma_{mn \rightarrow m'}^{j k \rightarrow j'} \left(\sqrt{(k \mp n)(k \pm n + 1)} \widehat{T}_{n \pm 1}^{[k]} | j, \alpha, m \rangle + \sqrt{(j \mp m)(j \pm m + 1)} \widehat{T}_n^{[k]} | j, \alpha, m \pm 1 \rangle \right) \\ &= \sum_{n,k} \sqrt{(j' \pm m')(j' \mp m' + 1)} \Gamma_{mn \rightarrow m' \mp 1}^{j k \rightarrow j'} \widehat{T}_n^{[k]} | j, \alpha, m \rangle = \sqrt{(j' \pm m')(j' \mp m' + 1)} |\Psi_{j',m' \pm 1}\rangle. \end{aligned} \quad (2.79)$$

Thus, $|\Psi_{j'm'}\rangle$ is an angular momentum eigenstate with angular momentum j' and projection m' . It can be written as a linear combination of corresponding basis states:

$$|\Psi_{j'm'}\rangle = \sum_{\alpha'} X(j, \alpha, k, j', \alpha') | j', \alpha', m' \rangle. \quad (2.80)$$

Since the state $|\Psi_{j'm'}\rangle$ depends on j , α and k , the coefficients also depend on these parameters. However, they cannot depend on the projection quantum number m' as argued above. Summing over all states constructed this way yields:

$$\begin{aligned} &\sum_{j'',m''} \Gamma_{mn \rightarrow m''}^{j k \rightarrow j''} \langle j', \alpha', m' | \Psi_{j''m''} \rangle \\ &= \sum_{j'',m''} \Gamma_{mn \rightarrow m''}^{j k \rightarrow j''} \sum_{\alpha''} X(j, \alpha, k, j'', \alpha'') \langle j', \alpha', m' | j'', \alpha'', m'' \rangle = \Gamma_{mn \rightarrow m'}^{j k \rightarrow j'} X(j, \alpha, k, j', \alpha') \\ &= \sum_{j'',m''} \Gamma_{mn \rightarrow m''}^{j k \rightarrow j''} \sum_{\tilde{n}, \tilde{m}} \Gamma_{\tilde{m} \tilde{n} \rightarrow m''}^{j k \rightarrow j''} \langle j', \alpha', m' | \widehat{T}_{\tilde{n}}^{[k]} | j, \alpha, \tilde{m} \rangle = \langle j', \alpha', m' | \widehat{T}_n^{[k]} | j, \alpha, m \rangle. \end{aligned} \quad (2.81)$$

From comparison of the second and the last row follows the Wigner–Eckart theorem with the identification of $X(j, \alpha, k, j', \alpha') = \langle\langle j', \alpha' | \widehat{\mathbf{T}}^{[k]} | j, \alpha \rangle\rangle$ as a reduced matrix element. More properties of reduced matrix elements and their arithmetic rules are presented in Appendix A.4.

2.3 – Symmetries in Matrix Product States

Advantages of symmetry-adapted implementations

If a physical system exhibits symmetry, this can and should also be exploited in the construction of matrix product states. Doing so offers two decisive advantages. First, a symmetry-adapted basis choice reduces the computational effort, since the tensors for matrix product states and matrix product operators as well as contraction environments factorize in the sense of the Wigner–Eckart theorem and a symmetry-related part can be contracted in advance, while the reduced part of the tensor network generally has a lower bond dimension. Second, only the correct implementation of symmetries makes it possible to variationally search for a groundstate in a selected subspace with the desired quantum numbers of the symmetry and ensures that the result does not contain any numerical admixtures of states from another subspace.

Applications include U(1) symmetries (particle number conservation, or rotational symmetry around the z axis) and SU(2) symmetries (spin rotation symmetry). These two symmetries differ in their implementation, since the Abelian symmetry U(1) only has one-dimensional irreducible representations, while the non-Abelian SU(2) symmetry also requires higher-dimensional irreducible representations.

For a symmetry-adapted description, not only the physical states have to be chosen sensibly, but also the auxiliary bond indices for matrix product states and matrix product operators acquire a physical meaning. They are divided into physical quantum numbers that characterize the irreducible representation of the symmetry group according to which the corresponding states transform, indices that count the states within an invariant subspace, and further degeneracy indices. The latter offer the possibility to achieve large bond dimensions and to encode entanglement adapted to the underlying system, while the former two index types are to a certain extent conditioned by the symmetry group and indicate which transitions are compatible with the symmetry.

First, the integration of a U(1) symmetry in the context of matrix product states will be discussed, before generalizing the findings for the non-Abelian SU(2) symmetry in the next step. The proposed algorithms were introduced by I. McCulloch [73], and later this theory was developed further and generalized by A. Weichselbaum [71]. Again, the general line of argumentation is taken from there and is supplemented with own calculations specific to the application in this thesis.

U(1) symmetry in VMPS

If the physical system under consideration is subject to a U(1) symmetry, e. g., the U(1) symmetry that corresponds to particle number conservation, its local Hilbert space states can be characterized by a quantum number n and a degeneracy index ν which takes values from 1 to $\mathfrak{D}(n)$ and distinguishes between different states that belong to the same quantum number. Henceforth, in the context of VMPS, quantum numbers that refer to a particular irreducible representation are labelled with (non-italic) Latin letters, and degeneracy indices which take care of the multiplicity of an irreducible representation are written in Greek letters. Combinations of both indices are denoted as bold Latin letters, i. e., $\mathbf{n}_\ell = (n_\ell, \nu_\ell)$. Since for Abelian symmetries the irreducible representations are one-dimensional, no internal quantum number appears. Thus, the local Hilbert spaces take the form

$$\mathcal{H}_{\text{loc}}(\ell) = \text{span} \left(|n_\ell, \nu_\ell\rangle \mid \nu_\ell \in \{1, \dots, \mathfrak{D}(n_\ell)\} \right). \quad (2.82)$$

Since the MPS and MPO bond indices are constructed using local Hilbert space indices and since they mediate between two local Hilbert spaces that are equipped with a symmetry-adapted basis, they split in the same way into a quantum number and a degeneracy index: $\mathbf{i}_\ell = (i_\ell, \alpha_\ell)$ with $1 \leq \alpha_\ell \leq \mathfrak{D}(i_\ell)$, and $\mathbf{k}_\ell = (k_\ell, \gamma_\ell)$ with $1 \leq \gamma_\ell \leq \mathfrak{D}(k_\ell)$. In order to describe a state with a large amount of entanglement, the multiplicity $\mathfrak{D}(i_\ell)$ of MPS bond indices has to be increased. Taking more and more possible values for the quantum number i_ℓ into consideration does not provide a better-suited variational ansatz once all relevant quantum numbers appear.

In the case of particle number conservation, the quantum numbers n_ℓ , i_ℓ and k_ℓ describe the particle number. In particular, the MPS bond index i_ℓ indicates how many particles the matrix product state has acquired from the local Hilbert spaces $\mathcal{H}_{\text{loc}}(1)$ to $\mathcal{H}_{\text{loc}}(\ell)$. Thus, the first index $\mathbf{i}_0 = (0, 1)$ has to contain zero particles, and the last MPS bond index can only take the value $\mathbf{i}_L = (s, 1)$, where s is the total particle number of the state:

$$\begin{aligned} |\Psi^{[s]}\rangle &= \sum_{\substack{i_0=0, \alpha_0=1, \\ i_L=s, \alpha_L=1}} \sum_{\substack{i_0, \dots, i_L, \\ \alpha_0, \dots, \alpha_L}} A(1)_{i_0 \alpha_0 n_1 \nu_1}^{i_1 \alpha_1} \cdots A(L)_{i_{L-1} \alpha_{L-1} n_L \nu_L}^{i_L \alpha_L} |n_1, \nu_1\rangle \otimes \cdots \otimes |n_L, \nu_L\rangle \\ &= \sum_{\substack{i_0=(0,1), \\ i_L=(s,1)}} A(1)_{i_0 n_1}^{i_1} \cdots A(L)_{i_{L-1} n_L}^{i_L} |\mathbf{n}_1; \dots; \mathbf{n}_L\rangle. \end{aligned} \quad (2.83)$$

The MPS is constructed starting from a non-degenerate state with zero particles and ends at a non-degenerate state with s particles. The total quantum number s can be chosen and targeted, which simply means that all quantum number sequences that do not ultimately lead to the targeted quantum number are neglected.

The MPS tensors have to satisfy the symmetry in that sense that the amount of incoming particles has to be the same as the number of outgoing particles:

$$A(\ell)_{i_{\ell-1} n_\ell}^{i_\ell} = \delta_{i_{\ell-1} + n_\ell, i_\ell} A(\ell)_{i_{\ell-1} n_\ell}^{i_\ell}. \quad (2.84)$$

A lot of entries of the MPS tensors can a priori be set to zero due to this symmetry requirement.

Operators also carry quantum numbers, depending on how the application of the operator affects the quantum numbers of the states. In the specific example of particle number conservation, a creation operator increases the number of particles by one, so that creators have a total quantum number of $+1$. For the analogous reason, annihilators carry the quantum number -1 . Whilst Hamilton operators obeying a certain $U(1)$ symmetry are operators of total quantum number 0 , in general, any total quantum number r is possible. These operator quantum numbers provide a criterion for when a matrix element must vanish due to symmetry:

$$\langle \Phi^{[s']} | \hat{O}^{[r]} | \Psi^{[s]} \rangle = \delta_{s+r, s'} \langle \Phi^{[s']} | \hat{O}^{[r]} | \Psi^{[s]} \rangle. \quad (2.85)$$

An MPO representation of an operator \hat{O} starts from non-degenerate $\mathbf{k}_0 = (0, 1)$ and ends at non-degenerate $\mathbf{k}_L = (r, 1)$:

$$\begin{aligned} \hat{O}^{[r]} &= \sum_{\substack{k_0=0, \gamma_0=1, \\ k_L=r, \gamma_L=1}} \sum_{\substack{k_0, \dots, k_L, \\ \gamma_0, \dots, \gamma_L}} \sum_{\substack{n_1, \dots, n_L, m_1, \dots, m_L, \\ \nu_1, \dots, \nu_L, \mu_1, \dots, \mu_L}} W(1)_{k_0 \gamma_0 m_1 \mu_1}^{k_1 \gamma_1 n_1 \nu_1} \cdots W(L)_{k_{L-1} \gamma_{L-1} m_L \mu_L}^{k_L \gamma_L n_L \nu_L} |m_1, \mu_1\rangle \langle n_1, \nu_1| \otimes \cdots \otimes |m_L, \mu_L\rangle \langle n_L, \nu_L| \\ &= \sum_{\substack{k_0=(0,1), \\ k_L=(r,1)}} W(1)_{k_0 m_1}^{k_1 n_1} \cdots W(L)_{k_{L-1} m_L}^{k_L n_L} |\mathbf{m}_1; \dots; \mathbf{m}_L\rangle \langle \mathbf{n}_1; \dots; \mathbf{n}_L|. \end{aligned} \quad (2.86)$$

The symmetry-induced constraints for the MPO tensors appear in a similar fashion: when applying the local part of an operator changes the physical index from n_ℓ to m_ℓ (for example by destroying a particle, $m_\ell = n_\ell - 1$), the MPO bond index has to increase accordingly: $k_\ell = k_{\ell-1} + m_\ell - n_\ell$ (due to the choice of incoming and outgoing indices for matrix product states, the physical index n_ℓ is outgoing for MPO tensors, but corresponds to the physical state before the application of the operator – this might be confusing). This also has the obvious consequence for the contraction environments that the sum of incoming and outgoing quantum number indices have to be the same:

$$\begin{aligned} W(\ell)_{\mathbf{k}_{\ell-1}\mathbf{m}_\ell}^{\mathbf{k}_\ell\mathbf{n}_\ell} &= \delta_{\mathbf{k}_{\ell-1}+\mathbf{m}_\ell, \mathbf{k}_\ell+\mathbf{n}_\ell} W(\ell)_{\mathbf{k}_{\ell-1}\mathbf{m}_\ell}^{\mathbf{k}_\ell\mathbf{n}_\ell}, \\ E(\ell)_{\mathbf{j}_\ell}^{\mathbf{i}_\ell\mathbf{k}_\ell} &= \delta_{\mathbf{i}_\ell+\mathbf{k}_\ell, \mathbf{j}_\ell} E(\ell)_{\mathbf{j}_\ell}^{\mathbf{i}_\ell\mathbf{k}_\ell}, \\ F(\ell)_{\mathbf{i}_{\ell-1}\mathbf{k}_{\ell-1}}^{\mathbf{j}_{\ell-1}} &= \delta_{\mathbf{i}_{\ell-1}+\mathbf{k}_{\ell-1}, \mathbf{j}_{\ell-1}} F(\ell)_{\mathbf{i}_{\ell-1}\mathbf{k}_{\ell-1}}^{\mathbf{j}_{\ell-1}}. \end{aligned} \quad (2.87)$$

If these constraints are taken into account for the implementation, the algorithms for tensor networks are manifestly symmetric, which leads to computational benefit as well as higher stability and precision.

Structure of SU(2)-symmetric matrix product states

In the presence of an SU(2) symmetry the states acquire another quantum number: in addition to the main quantum number and the degeneracy, a secondary quantum number comes into play which indicates the state in a given irreducible representation. This secondary quantum number corresponds to the projection of angular momentum and is henceforth assigned a superscript (z). A common application is the $SU(2)_{\text{spin}}$ which is the symmetry group behind spin rotations, but there are more operators obeying the angular momentum commutation relations and thus constituting an SU(2) symmetry, such as $SU(2)_{\text{charge}}$ which acts on charge pseudospins (later in this section). The local Hilbert spaces take the following form for a symmetry-adapted basis choice:

$$\mathcal{H}_{\text{loc}}(\ell) = \text{span} \left(\left| \mathbf{n}_\ell, \nu_\ell, \mathbf{n}_\ell^{(z)} \right\rangle \mid \nu_\ell \in \{1, \dots, \mathfrak{D}(\mathbf{n}_\ell)\}, \mathbf{n}_\ell^{(z)} \in \{-\mathbf{n}_\ell, \dots, +\mathbf{n}_\ell\} \right),$$

$$\text{with } d_\ell = \dim(\mathcal{H}_{\text{loc}}(\ell)) = \sum_{\mathbf{n}_\ell} \mathfrak{D}(\mathbf{n}_\ell)(2\mathbf{n}_\ell + 1). \quad (2.88)$$

The degeneracy index ν_ℓ , which labels equivalent irreducible representations of the SU(2) symmetry, can contain quantum numbers of other symmetries of the system. Projection quantum numbers are not part of composite indices, which are just made of the angular momentum quantum number and the degeneracy.

The angular momentum and projection quantum number of a quantum state are inherited by the corresponding MPS representation: the MPS starts at the leftmost site as a non-degenerate singlet state and ends at the rightmost site as a non-degenerate state with angular momentum quantum number $\mathbf{i}_L = \mathbf{s}$ and projection quantum number $\mathbf{i}_L^{(z)} = \mathbf{s}^{(z)}$. It only makes sense to talk about a multiplet of $2\mathbf{s} + 1$ matrix product states, of which the total projection quantum number selects one particular. For a given multiplet of states, the sums over the dummy bond indices at the edges are restricted to $\mathbf{i}_0 = (0, 1)$ and $\mathbf{i}_L = (\mathbf{s}, 1)$ unless specified otherwise. The MPS Hilbert spaces read

$$\mathcal{H}_{\text{MPS}}(\ell) = \text{span} \left(\left| \mathbf{i}_\ell, \alpha_\ell, \mathbf{i}_\ell^{(z)} \right\rangle \mid \alpha_\ell \in \{1, \dots, \mathfrak{D}(\mathbf{i}_\ell)\}, \mathbf{i}_\ell^{(z)} \in \{-\mathbf{i}_\ell, \dots, +\mathbf{i}_\ell\} \right),$$

$$\text{with } \chi_\ell = \sum_{\mathbf{i}_\ell} \mathfrak{D}(\mathbf{i}_\ell)(2\mathbf{i}_\ell + 1). \quad (2.89)$$

From the recursive definition of the MPS basis,

$$|\mathbf{i}_\ell, \mathbf{i}_\ell^{(z)}\rangle = \sum_{\substack{\mathbf{i}_{\ell-1}, \mathbf{n}_\ell, \\ \mathbf{i}_{\ell-1}^{(z)}, \mathbf{n}_\ell^{(z)}}} A(\ell)_{\mathbf{i}_{\ell-1} \mathbf{i}_{\ell-1}^{(z)} \mathbf{n}_\ell \mathbf{n}_\ell^{(z)}}^{\mathbf{i}_\ell \mathbf{i}_\ell^{(z)}} |\mathbf{i}_{\ell-1}, \mathbf{i}_{\ell-1}^{(z)}\rangle \otimes |\mathbf{n}_\ell, \mathbf{n}_\ell^{(z)}\rangle, \quad (2.90)$$

one can deduce with the help of Equation (2.62) that the $SU(2)$ -symmetric MPS tensors factorize into a Clebsch–Gordan coefficient and a reduced MPS tensor that depends solely on the composite indices and not on the projection quantum numbers:

$$A(\ell)_{\mathbf{i}_{\ell-1} \mathbf{i}_{\ell-1}^{(z)} \mathbf{n}_\ell \mathbf{n}_\ell^{(z)}}^{\mathbf{i}_\ell \mathbf{i}_\ell^{(z)}} = \Gamma_{\mathbf{i}_{\ell-1}^{(z)} \mathbf{n}_\ell^{(z)} \rightarrow \mathbf{i}_\ell^{(z)}}^{\mathbf{i}_{\ell-1} \mathbf{n}_\ell \rightarrow \mathbf{i}_\ell} \cdot \bar{A}(\ell)_{\mathbf{i}_{\ell-1} \mathbf{n}_\ell}^{\mathbf{i}_\ell}. \quad (2.91)$$

This ensures correct transformation behavior of the MPS tensors, i. e., MPS tensors are invariant if all angular momentum indices are contracted with the matrix D of their corresponding irreducible representation (as in Equation (A.13)):

$$\sum_{\mathbf{i}'_{\ell-1}, \mathbf{n}'_\ell, \mathbf{i}'_\ell} D_{\mathbf{i}'_{\ell-1} \mathbf{i}'_{\ell-1}^{(z)}}^{[\mathbf{i}_{\ell-1}]} D_{\mathbf{n}'_\ell \mathbf{n}'_\ell^{(z)}}^{[\mathbf{n}_\ell]} \left(D_{\mathbf{i}'_\ell \mathbf{i}'_\ell^{(z)}}^{[\mathbf{i}_\ell]} \right)^* A(\ell)_{\mathbf{i}'_{\ell-1} \mathbf{i}'_{\ell-1}^{(z)} \mathbf{n}'_\ell \mathbf{n}'_\ell^{(z)}}^{\mathbf{i}'_\ell \mathbf{i}'_\ell^{(z)}} = A(\ell)_{\mathbf{i}_{\ell-1} \mathbf{i}_{\ell-1}^{(z)} \mathbf{n}_\ell \mathbf{n}_\ell^{(z)}}^{\mathbf{i}_\ell \mathbf{i}_\ell^{(z)}}. \quad (2.92)$$

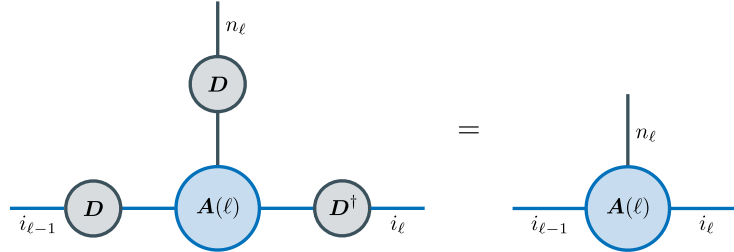


Figure 13: Visualization of the transformation behavior of MPS tensors from Equation (2.92).

An MPS with angular momentum s and projection $s^{(z)}$ then takes the following form:

$$|\Psi_{s^{(z)}}^{[s]}\rangle = \sum_{\substack{\mathbf{i}_0, \dots, \mathbf{i}_L, \\ \mathbf{i}_0^{(z)}, \dots, \mathbf{i}_L^{(z)}}}^{\mathbf{i}_L^{(z)} = s^{(z)}} \sum_{\substack{\mathbf{n}_1, \dots, \mathbf{n}_L, \\ \mathbf{n}_1^{(z)}, \dots, \mathbf{n}_L^{(z)}}} A(1)_{\mathbf{i}_0 \mathbf{i}_0^{(z)} \mathbf{n}_1 \mathbf{n}_1^{(z)}}^{\mathbf{i}_1 \mathbf{i}_1^{(z)}} \cdots A(L)_{\mathbf{i}_{L-1} \mathbf{i}_{L-1}^{(z)} \mathbf{n}_L \mathbf{n}_L^{(z)}}^{\mathbf{i}_L \mathbf{i}_L^{(z)}} |\mathbf{n}_1, \mathbf{n}_1^{(z)}; \dots; \mathbf{n}_L, \mathbf{n}_L^{(z)}\rangle. \quad (2.93)$$

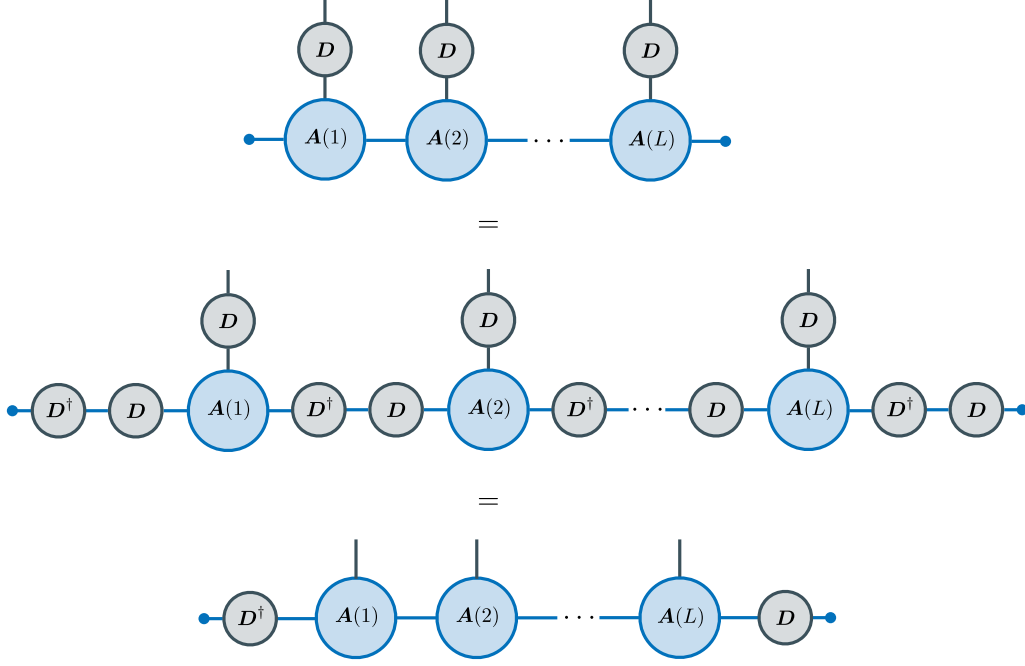


Figure 14: Transformation behavior of MPS under the action of $g \in \text{SU}(2)$. The leftmost transformation matrix is trivial due to $i_0 = 0$, the rightmost transformation matrix ensures the expected transformation behavior since $i_L = s$.

It transforms under the action of a symmetry operation $g \in \text{SU}(2)$ as expected:

$$\begin{aligned}
 \widehat{U}_g \left| \Psi_{s^{(z)}}^{[s]} \right\rangle &= \sum_{\substack{i_L^{(z)}=s^{(z)} \\ i_0, \dots, i_L, \\ i_0^{(z)}, \dots, i_L^{(z)}}} \sum_{\substack{\mathbf{n}_1, \dots, \mathbf{n}_L, \\ n_1^{(z)}, \dots, n_L^{(z)}, \\ n_0', \dots, n_L'}} A(1)_{i_0 i_0^{(z)} \mathbf{n}_1 n_1^{(z)}}^{i_1 i_1^{(z)}} \cdots A(L)_{i_{L-1} i_{L-1}^{(z)} \mathbf{n}_L n_L^{(z)}}^{i_L i_L^{(z)}} D_{n_1' n_1^{(z)}}^{[n_1]} \cdots D_{n_L' n_L^{(z)}}^{[n_L]} \left| \mathbf{n}_1, n_1^{(z)}; \dots; \mathbf{n}_L, n_L^{(z)} \right\rangle \\
 &= \sum_{\substack{i_0, \dots, i_L, \\ \mathbf{n}_1, \dots, \mathbf{n}_L, \\ i_0^{(z)}, \dots, i_L^{(z)}, \\ i_0^{(z)}, \dots, i_{L-1}^{(z)}, \\ i_0^{(z)}, \dots, i_{L-1}^{(z)}}} \sum_{\substack{\mathbf{n}_1, \dots, \mathbf{n}_L, \\ n_1^{(z)}, \dots, n_L^{(z)}, \\ n_1', \dots, n_L'}} \left(D_{i_0' i_0^{(z)} i_0^{(z)}}^{[i_0]} \right)^* D_{i_0' i_0^{(z)} i_0^{(z)}}^{[i_0]} D_{n_1' n_1^{(z)}}^{[n_1]} A(1)_{i_0 i_0^{(z)} \mathbf{n}_1 n_1^{(z)}}^{i_1 i_1^{(z)}} \left(D_{i_1' i_1^{(z)} i_1^{(z)}}^{[i_1]} \right)^* D_{i_1' i_1^{(z)} i_1^{(z)}}^{[i_1]} \cdots \\
 &\quad \cdots \left(D_{i_{L-1}' i_{L-1}^{(z)} i_{L-1}^{(z)}}^{[i_{L-1}]} \right)^* D_{i_{L-1}' i_{L-1}^{(z)} i_{L-1}^{(z)}}^{[i_{L-1}]} D_{n_L' n_L^{(z)}}^{[n_L]} A(L)_{i_{L-1} i_{L-1}^{(z)} \mathbf{n}_L n_L^{(z)}}^{i_L i_L^{(z)}} \left| \mathbf{n}_1, n_1^{(z)}; \dots; \mathbf{n}_L, n_L^{(z)} \right\rangle \\
 &= \sum_{\substack{i_0, \dots, i_L, \\ \mathbf{n}_1, \dots, \mathbf{n}_L, \\ i_0^{(z)}, \dots, i_{L-1}^{(z)}, \\ i_0^{(z)}, \dots, i_{L-1}^{(z)}, \\ i_0^{(z)}, \dots, i_{L-1}^{(z)}}} \sum_{\substack{\mathbf{n}_1, \dots, \mathbf{n}_L, \\ n_1^{(z)}, \dots, n_L^{(z)}, \\ n_1', \dots, n_L'}} \left(D_{i_0' i_0^{(z)} i_0^{(z)}}^{[i_0]} \right)^* A(1)_{i_0 i_0^{(z)} \mathbf{n}_1 n_1^{(z)}}^{i_1 i_1^{(z)}} \cdots A(L-1)_{i_{L-2} i_{L-2}^{(z)} \mathbf{n}_{L-1} n_{L-1}^{(z)}}^{i_{L-1} i_{L-1}^{(z)}} \\
 &\quad \cdot D_{i_{L-1}' i_{L-1}^{(z)} i_{L-1}^{(z)}}^{[i_{L-1}]} D_{n_L' n_L^{(z)}}^{[n_L]} A(L)_{i_{L-1} i_{L-1}^{(z)} \mathbf{n}_L n_L^{(z)}}^{i_L s} \left| \mathbf{n}_1, n_1^{(z)}; \dots; \mathbf{n}_L, n_L^{(z)} \right\rangle \\
 &= \left(D_{00}^{[0]} \right)^* \sum_{\substack{i_0, \dots, i_L, \\ \mathbf{n}_1, \dots, \mathbf{n}_L, \\ i_0^{(z)}, \dots, i_{L-1}^{(z)}, \\ i_0^{(z)}, \dots, i_{L-1}^{(z)}, \\ i_0^{(z)}, \dots, i_{L-1}^{(z)}}} \sum_{\substack{\mathbf{n}_1, \dots, \mathbf{n}_L, \\ n_1^{(z)}, \dots, n_L^{(z)}, \\ n_1', \dots, n_L'}} A(1)_{i_0 i_0^{(z)} \mathbf{n}_1 n_1^{(z)}}^{i_1 i_1^{(z)}} \cdots A(L-1)_{i_{L-2} i_{L-2}^{(z)} \mathbf{n}_{L-1} n_{L-1}^{(z)}}^{i_{L-1} i_{L-1}^{(z)}} \\
 &\quad \cdot \sum_{i_L^{(z)}, s'} A(L)_{i_{L-1} i_{L-1}^{(z)} \mathbf{n}_L n_L^{(z)}}^{i_L i_L^{(z)}} \delta_{i_L^{(z)} s'} \delta_{i_L^{(z)} s'} D_{s' s^{(z)}}^{[s]} \left| \mathbf{n}_1, n_1^{(z)}; \dots; \mathbf{n}_L, n_L^{(z)} \right\rangle \\
 &= \sum_{s^{(z)}} D_{s^{(z)} s^{(z)}}^{[s]} \sum_{\substack{i_0, \dots, i_L, \\ i_0^{(z)}, \dots, i_L^{(z)}, \\ i_0^{(z)}, \dots, i_L^{(z)}}} \sum_{\substack{\mathbf{n}_1, \dots, \mathbf{n}_L, \\ n_1^{(z)}, \dots, n_L^{(z)}, \\ n_1^{(z)}, \dots, n_L^{(z)}}} A(1)_{i_0 i_0^{(z)} \mathbf{n}_1 n_1^{(z)}}^{i_1 i_1^{(z)}} \cdots A(L)_{i_{L-1} i_{L-1}^{(z)} \mathbf{n}_L n_L^{(z)}}^{i_L i_L^{(z)}} \left| \mathbf{n}_1, n_1^{(z)}; \dots; \mathbf{n}_L, n_L^{(z)} \right\rangle \\
 &= \sum_{s^{(z)}} D_{s^{(z)} s^{(z)}}^{[s]} \left| \Psi_{s^{(z)}}^{[s]} \right\rangle.
 \end{aligned} \tag{2.94}$$

The MPS tensors for a bra state

$$\left\langle \phi_{s^{(z)}}^{[s]} \right| = \sum_{\substack{j_L^{(z)}=s^{(z)} \\ j_0^{(z)}, \dots, j_L^{(z)}, m_1^{(z)}, \dots, m_L^{(z)} \\ j_0^{(z)}, \dots, j_L^{(z)}, m_1^{(z)}, \dots, m_L^{(z)}}} B^\dagger(1)_{j_0^{(z)} j_1^{(z)}}^{j_0^{(z)} m_1^{(z)}} \dots B^\dagger(L)_{j_L^{(z)} j_{L-1}^{(z)}}^{j_L^{(z)} m_L^{(z)}} \left\langle \mathbf{m}_1, m_1^{(z)}; \dots; \mathbf{m}_L, m_L^{(z)} \right| \quad (2.95)$$

also factorize into a reduced adjoint MPS tensor and a Clebsch–Gordan coefficient:

$$B^\dagger(\ell)_{j_\ell^{(z)} j_{\ell-1}^{(z)}}^{j_{\ell-1}^{(z)} m_\ell^{(z)}} = \Gamma_{j_{\ell-1}^{(z)} m_\ell^{(z)} \rightarrow j_\ell^{(z)}}^{j_{\ell-1}^{(z)} m_\ell^{(z)}} \cdot \bar{B}^\dagger(\ell)_{j_\ell^{(z)}}^{j_{\ell-1}^{(z)} m_\ell^{(z)}}. \quad (2.96)$$

Structure of SU(2)-symmetric matrix product operators

Just as with the matrix product states, the MPO bond indices are subject to a splitting into an angular momentum quantum number k_ℓ , a degeneracy index γ_ℓ and a projection quantum number $k_\ell^{(z)}$, where the former two, $\mathbf{k}_\ell = (k_\ell, \gamma_\ell)$, are needed to identify the irreducible representation. Since irreducible tensor operators are inherently SU(2) symmetric, these are the operators one should consider for a symmetry-respecting implementation of VMPS. Irreducible tensor operators are built from local irreducible tensor operators via the product rule in Equation (2.71) for these operators. The component $r^{(z)}$ of an operator with rank r constructed this way can be written as

$$\begin{aligned} \hat{\mathcal{O}}_{r^{(z)}}^{[r]} &= \left(\left(\dots \left(\hat{\mathcal{O}}^{[t_1]}(1) \star \hat{\mathcal{O}}^{[t_2]}(2) \right)^{[k_2]} \star \hat{\mathcal{O}}^{[t_3]}(3) \right)^{[k_3]} \star \dots \star \hat{\mathcal{O}}^{[t_L]}(L) \right)^{[k_L]} \\ &= \sum_{\substack{k_0^{(z)}, \dots, k_L^{(z)} \\ t_1^{(z)}, \dots, t_L^{(z)}}} \Gamma_{k_0^{(z)} t_1^{(z)} \rightarrow k_1^{(z)}}^{k_0^{(z)} t_1^{(z)}} \hat{\mathcal{O}}_{t_1^{(z)}}^{[t_1]}(1) \otimes \Gamma_{k_1^{(z)} t_2^{(z)} \rightarrow k_2^{(z)}}^{k_1^{(z)} t_2^{(z)}} \hat{\mathcal{O}}_{t_2^{(z)}}^{[t_2]}(2) \otimes \dots \otimes \Gamma_{k_{L-1}^{(z)} t_L^{(z)} \rightarrow k_L^{(z)}}^{k_{L-1}^{(z)} t_L^{(z)}} \hat{\mathcal{O}}_{t_L^{(z)}}^{[t_L]}(L). \end{aligned} \quad (2.97)$$

Here, the indices t_ℓ refer to the rank of the local irreducible tensor operators, and the indices $(k_0 = 0, k_1 = t_1, k_2, \dots, k_{L-1}, k_L = r)$ constitute a sequence of ranks of irreducible tensor operators constructed recursively one after another by concatenating the operator acting on the local Hilbert space of a corresponding site. In general, an irreducible tensor operator acting on the entire Hilbert space can be a sum of these elementary operators:

$$\hat{\mathcal{O}}_{r^{(z)}}^{[r]} = \sum_{x=1}^X \left(\hat{\mathcal{O}}_{r^{(z)}}^{[r]} \right)_x. \quad (2.98)$$

By allowing for multiple operators to be added, and thus diminishing uniqueness of the local operators, degeneracy indices come into play. The first and last MPO bond indices, however, have to be non-degenerate, i. e., $\gamma_0 = \gamma_L = 1$. Thus, once again, the sums over the dummy bond indices at the edges are restricted to $\mathbf{k}_0 = (0, 1)$ and $\mathbf{k}_L = (r, 1)$ unless specified otherwise. The MPO Hilbert spaces read

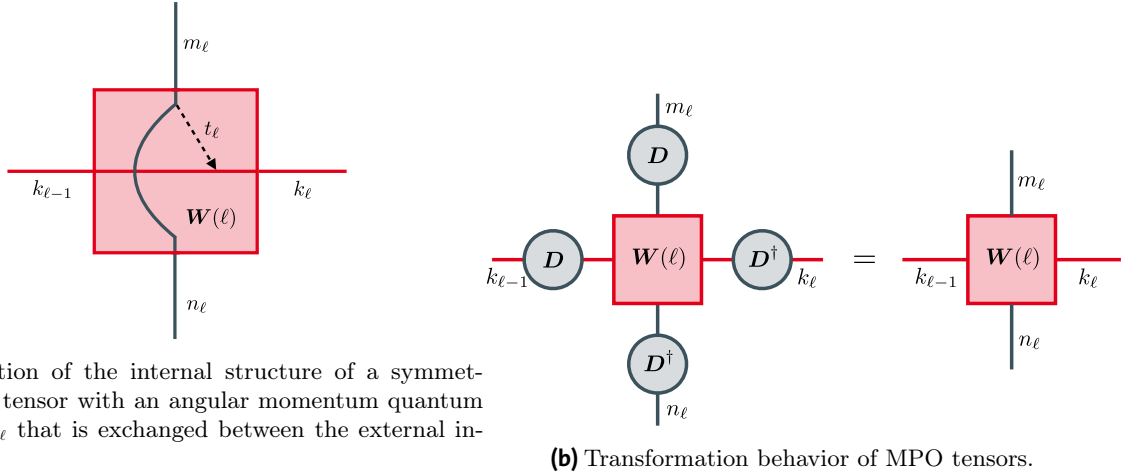
$$\mathcal{H}_{\text{MPO}}(\ell) = \text{span} \left(\left| k_\ell, \gamma_\ell, k_\ell^{(z)} \right\rangle \mid \gamma_\ell \in \{1, \dots, \mathfrak{D}(k_\ell)\}, k_\ell^{(z)} \in \{-k_\ell, \dots, +k_\ell\} \right),$$

$$\text{with } \mu_\ell = \sum_{k_\ell} \mathfrak{D}(k_\ell)(2k_\ell + 1). \quad (2.99)$$

The definition of MPO tensors can be given with Equation (2.98) in mind. For each summand x , the degeneracies are adjusted to $(\gamma_0 = 1, \gamma_1 = x, \dots, \gamma_{L-1} = x, \gamma_L = 1)$, and then one obtains

$$\begin{aligned} W(\ell)_{\mathbf{k}_{\ell-1} \mathbf{k}_{\ell-1}^{(z)} \mathbf{m}_{\ell} \mathbf{m}_{\ell}^{(z)}}^{\mathbf{k}_{\ell} \mathbf{k}_{\ell}^{(z)} \mathbf{n}_{\ell} \mathbf{n}_{\ell}^{(z)}} &= \langle \mathbf{m}_{\ell}, \mathbf{m}_{\ell}^{(z)} | \sum_{\mathbf{t}_{\ell}^{(z)}} \Gamma_{\mathbf{k}_{\ell-1}^{(z)} \mathbf{t}_{\ell}^{(z)} \rightarrow \mathbf{k}_{\ell}^{(z)}} \widehat{\mathcal{O}}_{\mathbf{t}_{\ell}^{(z)}}^{[t_{\ell}]}(\ell)_x | \mathbf{n}_{\ell}, \mathbf{n}_{\ell}^{(z)} \rangle \\ &= \sum_{\mathbf{t}_{\ell}, \mathbf{t}_{\ell}^{(z)}} \Gamma_{\mathbf{k}_{\ell-1}^{(z)} \mathbf{t}_{\ell}^{(z)} \rightarrow \mathbf{k}_{\ell}^{(z)}} \Gamma_{\mathbf{n}_{\ell}^{(z)} \mathbf{t}_{\ell}^{(z)} \rightarrow \mathbf{m}_{\ell}^{(z)}} \langle \langle \mathbf{m}_{\ell} | \widehat{\mathcal{O}}^{[t_{\ell}]}(\ell)_x | \mathbf{n}_{\ell} \rangle \rangle. \end{aligned} \quad (2.100)$$

Here the Wigner–Eckart theorem was used to factorize the matrix element into a Clebsch–Gordan coefficient and a reduced matrix element $\overline{W}^{[t_{\ell}]}(\ell)_{\mathbf{k}_{\ell-1} \mathbf{m}_{\ell}}^{\mathbf{k}_{\ell} \mathbf{n}_{\ell}}$ (that also depends on $\mathbf{k}_{\ell-1}$ and \mathbf{k}_{ℓ} via the quantum number branch in Equation (2.97)). The occurrence of an internal angular momentum quantum number t_{ℓ} and its projection $t_{\ell}^{(z)}$ is a consequence of the fact that the MPO tensors have four external indices – as opposed to MPS tensors, which only have three. Therefore, since angular momentum coupling happens pairwise, the incoming physical angular momentum m_{ℓ} and bond index $k_{\ell-1}$ are coupled to an intermediate angular momentum t_{ℓ} that splits into an outgoing physical angular momentum n_{ℓ} and an outgoing bond quantum number k_{ℓ} . This internal quantum number is not fixed, but may take several values which are summed over. At each vertex, a Clebsch–Gordan coefficient enters the expression as a weight factor. This process is visualized in Figure 15a.



(a) Visualization of the internal structure of a symmetric MPO tensor with an angular momentum quantum number t_{ℓ} that is exchanged between the external indices.

(b) Transformation behavior of MPO tensors.

Figure 15: Visualization of the structure of MPO tensors in the presence of an $SU(2)$ symmetry.

From the above definition of MPS tensors one obtains

$$\sum_{\substack{\mathbf{k}_0, \dots, \mathbf{k}_L, \\ \mathbf{k}_0^{(z)}, \dots, \mathbf{k}_L^{(z)}}} W(1)_{\mathbf{k}_0 \mathbf{k}_0^{(z)} \mathbf{m}_1 \mathbf{m}_1^{(z)}}^{\mathbf{k}_1 \mathbf{k}_1^{(z)} \mathbf{n}_1 \mathbf{n}_1^{(z)}} \cdots W(L)_{\mathbf{k}_{L-1} \mathbf{k}_{L-1}^{(z)} \mathbf{m}_L \mathbf{m}_L^{(z)}}^{\mathbf{k}_L \mathbf{k}_L^{(z)} \mathbf{n}_L \mathbf{n}_L^{(z)}} = \langle \mathbf{m}_1, \mathbf{m}_1^{(z)}; \dots; \mathbf{m}_L, \mathbf{m}_L^{(z)} | \widehat{\mathcal{O}}_{\mathbf{r}^{(z)}}^{[r]} | \mathbf{n}_1, \mathbf{n}_1^{(z)}; \dots; \mathbf{n}_L, \mathbf{n}_L^{(z)} \rangle,$$

or equivalently,

$$\widehat{\mathcal{O}}_{\mathbf{r}^{(z)}}^{[r]} = \sum_{\substack{\mathbf{k}_0, \dots, \mathbf{k}_L, \\ \mathbf{n}_1, \dots, \mathbf{n}_L, \\ \mathbf{m}_1, \dots, \mathbf{m}_L}} \sum_{\substack{\mathbf{k}_0^{(z)}, \dots, \mathbf{k}_L^{(z)}, \\ \mathbf{n}_1^{(z)}, \dots, \mathbf{n}_L^{(z)}, \\ \mathbf{m}_1^{(z)}, \dots, \mathbf{m}_L^{(z)}}} W(1)_{\mathbf{k}_0 \mathbf{k}_0^{(z)} \mathbf{m}_1 \mathbf{m}_1^{(z)}}^{\mathbf{k}_1 \mathbf{k}_1^{(z)} \mathbf{n}_1 \mathbf{n}_1^{(z)}} \cdots W(L)_{\mathbf{k}_{L-1} \mathbf{k}_{L-1}^{(z)} \mathbf{m}_L \mathbf{m}_L^{(z)}}^{\mathbf{k}_L \mathbf{k}_L^{(z)} \mathbf{n}_L \mathbf{n}_L^{(z)}} | \mathbf{m}_1, \mathbf{m}_1^{(z)}; \dots; \mathbf{m}_L, \mathbf{m}_L^{(z)} \rangle \langle \mathbf{n}_1, \mathbf{n}_1^{(z)}; \dots; \mathbf{n}_L, \mathbf{n}_L^{(z)} |. \quad (2.101)$$

Therefore, these MPO tensors are a sensible choice for a matrix product representation of the operator $\widehat{\mathcal{O}}_{\mathbf{r}^{(z)}}^{[r]}$. With the transformation properties of Clebsch–Gordan coefficients, the transformation behavior under the

action of an $SU(2)$ rotation of the MPO tensors can be deduced (Figure 15b):

$$W(\ell)_{\mathbf{k}_{\ell-1} \mathbf{k}_{\ell-1}^{(z)} \mathbf{m}_{\ell} \mathbf{m}_{\ell}^{(z)}}^{\mathbf{k}_{\ell} \mathbf{k}_{\ell}^{(z)} \mathbf{n}_{\ell} \mathbf{n}_{\ell}^{(z)}} = \sum_{\mathbf{k}'_{\ell-1}, \mathbf{k}'_{\ell}, \mathbf{m}'_{\ell}, \mathbf{n}'_{\ell}} D_{\mathbf{k}_{\ell-1} \mathbf{k}'_{\ell-1}}^{[\mathbf{k}_{\ell-1}]} D_{\mathbf{m}_{\ell} \mathbf{m}'_{\ell}}^{[\mathbf{m}_{\ell}]} W(\ell)_{\mathbf{k}_{\ell-1} \mathbf{k}'_{\ell-1} \mathbf{m}_{\ell} \mathbf{m}'_{\ell}}^{\mathbf{k}_{\ell} \mathbf{k}'_{\ell} \mathbf{n}_{\ell} \mathbf{n}'_{\ell}} \left(D_{\mathbf{k}_{\ell} \mathbf{k}'_{\ell}}^{[\mathbf{k}_{\ell}]} \right)^* \left(D_{\mathbf{n}_{\ell} \mathbf{n}'_{\ell}}^{[\mathbf{n}_{\ell}]} \right)^*. \quad (2.102)$$

The reduced MPO tensors can be calculated directly from the full MPO tensors:

$$\begin{aligned} & \frac{(2t_{\ell} + 1)^2}{(2k_{\ell} + 1)(2m_{\ell} + 1)} \sum_{\substack{\mathbf{k}_{\ell-1}^{(z)}, \mathbf{k}_{\ell}^{(z)}, \\ \mathbf{n}_{\ell}^{(z)}, \mathbf{m}_{\ell}^{(z)}}} \Gamma_{\mathbf{n}_{\ell}^{(z)} \mathbf{t}_{\ell}^{(z)} \rightarrow \mathbf{m}_{\ell}^{(z)}}^{\mathbf{n}_{\ell} \mathbf{t}_{\ell} \rightarrow \mathbf{m}_{\ell}} \Gamma_{\mathbf{k}_{\ell-1}^{(z)} \mathbf{t}_{\ell}^{(z)} \rightarrow \mathbf{k}_{\ell}^{(z)}}^{\mathbf{k}_{\ell-1} \mathbf{t}_{\ell} \rightarrow \mathbf{k}_{\ell}} W(\ell)_{\mathbf{k}_{\ell-1} \mathbf{k}_{\ell-1} \mathbf{m}_{\ell} \mathbf{m}_{\ell}^{(z)}}^{\mathbf{k}_{\ell} \mathbf{k}_{\ell}^{(z)} \mathbf{n}_{\ell} \mathbf{n}_{\ell}^{(z)}} \\ &= \frac{(2t_{\ell} + 1)^2}{(2k_{\ell} + 1)(2m_{\ell} + 1)} \sum_{\substack{\mathbf{k}_{\ell-1}^{(z)}, \mathbf{k}_{\ell}^{(z)}, \\ \mathbf{n}_{\ell}^{(z)}, \mathbf{m}_{\ell}^{(z)}}} \Gamma_{\mathbf{n}_{\ell}^{(z)} \mathbf{t}_{\ell}^{(z)} \rightarrow \mathbf{m}_{\ell}^{(z)}}^{\mathbf{n}_{\ell} \mathbf{t}_{\ell} \rightarrow \mathbf{m}_{\ell}} \Gamma_{\mathbf{k}_{\ell-1}^{(z)} \mathbf{t}_{\ell}^{(z)} \rightarrow \mathbf{k}_{\ell}^{(z)}}^{\mathbf{k}_{\ell-1} \mathbf{t}_{\ell} \rightarrow \mathbf{k}_{\ell}} \sum_{\mathbf{t}'_{\ell}, \mathbf{t}_{\ell}} \overline{W}^{[\mathbf{t}'_{\ell}]}(\ell)_{\mathbf{k}_{\ell-1} \mathbf{m}_{\ell}}^{\mathbf{k}_{\ell} \mathbf{n}_{\ell}} \Gamma_{\mathbf{n}_{\ell}^{(z)} \mathbf{t}'_{\ell} \rightarrow \mathbf{m}_{\ell}^{(z)}}^{\mathbf{n}_{\ell} \mathbf{t}'_{\ell} \rightarrow \mathbf{m}_{\ell}} \Gamma_{\mathbf{k}_{\ell-1}^{(z)} \mathbf{t}'_{\ell} \rightarrow \mathbf{k}_{\ell}^{(z)}}^{\mathbf{k}_{\ell-1} \mathbf{t}'_{\ell} \rightarrow \mathbf{k}_{\ell}} \\ &= \sum_{\mathbf{t}'_{\ell}, \mathbf{t}_{\ell}} \overline{W}^{[\mathbf{t}'_{\ell}]}(\ell)_{\mathbf{k}_{\ell-1} \mathbf{m}_{\ell}}^{\mathbf{k}_{\ell} \mathbf{n}_{\ell}} \delta_{\mathbf{t}_{\ell} \mathbf{t}'_{\ell}} \delta_{\mathbf{t}_{\ell}^{(z)} \mathbf{t}'_{\ell}^{(z)}} = \overline{W}^{[\mathbf{t}_{\ell}]}(\ell)_{\mathbf{k}_{\ell-1} \mathbf{m}_{\ell}}^{\mathbf{k}_{\ell} \mathbf{n}_{\ell}}. \end{aligned} \quad (2.103)$$

The MPO tensors for the product of two operators as in Figure 9a can be obtained from the reduced MPO tensors as well. Let $U(\ell)$ and $V(\ell)$ be the MPO tensors of the two operators, then the MPO tensors of the product read (a detailed derivation can be found in Appendix A.5)

$$\begin{aligned} W(\ell)_{\mathbf{K}_{\ell-1} \mathbf{K}_{\ell-1}^{(z)} \mathbf{m}_{\ell} \mathbf{m}_{\ell}^{(z)}}^{\mathbf{K}_{\ell} \mathbf{K}_{\ell}^{(z)} \mathbf{n}_{\ell} \mathbf{n}_{\ell}^{(z)}} &= \sum_{\mathbf{T}_{\ell}, \mathbf{T}_{\ell}^{(z)}} \Gamma_{\mathbf{K}_{\ell-1}^{(z)} \mathbf{T}_{\ell}^{(z)} \rightarrow \mathbf{K}_{\ell}^{(z)}}^{\mathbf{K}_{\ell-1} \mathbf{T}_{\ell} \rightarrow \mathbf{K}_{\ell}} \Gamma_{\mathbf{n}_{\ell}^{(z)} \mathbf{T}_{\ell}^{(z)} \rightarrow \mathbf{m}_{\ell}^{(z)}}^{\mathbf{n}_{\ell} \mathbf{T}_{\ell} \rightarrow \mathbf{m}_{\ell}} \overline{W}^{[\mathbf{T}_{\ell}]}(\ell)_{\mathbf{K}_{\ell-1} \mathbf{m}_{\ell}}^{\mathbf{K}_{\ell} \mathbf{n}_{\ell}} \quad \text{where} \\ \overline{W}^{[\mathbf{T}_{\ell}]}(\ell)_{\mathbf{K}_{\ell-1} \mathbf{m}_{\ell}}^{\mathbf{K}_{\ell} \mathbf{n}_{\ell}} &= \sum_{\substack{\mathbf{k}_{\ell-1}, \mathbf{l}_{\ell-1}, \\ \mathbf{k}_{\ell}, \mathbf{l}_{\ell}, \\ \mathbf{o}_{\ell}, \mathbf{t}_{\ell}, \mathbf{x}_{\ell}}} \overline{U}^{[\mathbf{t}_{\ell}]}(\ell)_{\mathbf{k}_{\ell-1} \mathbf{m}_{\ell}}^{\mathbf{k}_{\ell} \mathbf{o}_{\ell}} \overline{V}^{[\mathbf{x}_{\ell}]}(\ell)_{\mathbf{l}_{\ell-1} \mathbf{o}_{\ell}}^{\mathbf{l}_{\ell} \mathbf{n}_{\ell}} \langle \langle \mathbf{K}_{\ell-1} \parallel \mathbf{k}_{\ell-1} ; \mathbf{l}_{\ell-1} \rangle \rangle \langle \langle \mathbf{k}_{\ell} ; \mathbf{l}_{\ell} \parallel \mathbf{K}_{\ell} \rangle \rangle \\ &\quad \cdot \begin{bmatrix} \mathbf{n}_{\ell} & \mathbf{x}_{\ell} & \mathbf{o}_{\ell} \\ \mathbf{t}_{\ell} & \mathbf{m}_{\ell} & \mathbf{T}_{\ell} \end{bmatrix} \begin{bmatrix} \mathbf{k}_{\ell-1} & \mathbf{l}_{\ell-1} & \mathbf{K}_{\ell-1} \\ \mathbf{t}_{\ell} & \mathbf{x}_{\ell} & \mathbf{T}_{\ell} \\ \mathbf{k}_{\ell} & \mathbf{l}_{\ell} & \mathbf{K}_{\ell} \end{bmatrix}. \end{aligned} \quad (2.104)$$

Structure of $SU(2)$ -symmetric contraction environments

For a fully symmetric tensor-network description it is somewhat problematic that in matrix elements of the form $\langle \Phi_{\mathbf{s}'^{(z)}}^{[\mathbf{s}']} | \widehat{\mathcal{O}}_{\mathbf{r}^{(z)}}^{[\mathbf{r}]} | \Psi_{\mathbf{s}^{(z)}}^{[\mathbf{s}]} \rangle$ (where the physical states are components of multiplets of states and the operator is an irreducible tensor operator) the projection quantum numbers of the physical states and the operator stand out. It is algorithmically more reasonable to compute the reduced matrix element $\langle \langle \Phi^{[\mathbf{s}']} | \widehat{\mathcal{O}}^{[\mathbf{r}]} | \Psi^{[\mathbf{s}]} \rangle \rangle$ and multiply the Clebsch–Gordan coefficient afterwards. The reduced matrix element can be obtained from

$$\begin{aligned} \sum_{\mathbf{s}^{(z)}, \mathbf{r}^{(z)}, \mathbf{s}'^{(z)}} \langle \Phi_{\mathbf{s}'^{(z)}}^{[\mathbf{s}']} | \widehat{\mathcal{O}}_{\mathbf{r}^{(z)}}^{[\mathbf{r}]} | \Psi_{\mathbf{s}^{(z)}}^{[\mathbf{s}]} \rangle \Gamma_{\mathbf{s}^{(z)} \mathbf{r}^{(z)} \rightarrow \mathbf{s}'^{(z)}}^{\mathbf{s} \mathbf{r} \rightarrow \mathbf{s}'} &= \sum_{\mathbf{s}^{(z)}, \mathbf{r}^{(z)}, \mathbf{s}'^{(z)}} \langle \langle \Phi^{[\mathbf{s}']} | \widehat{\mathcal{O}}^{[\mathbf{r}]} | \Psi^{[\mathbf{s}]} \rangle \rangle \left(\Gamma_{\mathbf{s}^{(z)} \mathbf{r}^{(z)} \rightarrow \mathbf{s}'^{(z)}}^{\mathbf{s} \mathbf{r} \rightarrow \mathbf{s}'} \right)^2 \\ &= (2s' + 1) \langle \langle \Phi^{[\mathbf{s}']} | \widehat{\mathcal{O}}^{[\mathbf{r}]} | \Psi^{[\mathbf{s}]} \rangle \rangle. \end{aligned} \quad (2.105)$$

This expression is the result of the full contraction of a tensor network in which the last projection quantum numbers $\mathbf{i}_L^{(z)}$, $\mathbf{j}_L^{(z)}$ and $\mathbf{k}_L^{(z)}$ are connected to a tensor of Clebsch–Gordan coefficients and thus summed over (the angular momentum quantum numbers and degeneracy indices remain fixed: $\mathbf{i}_L = (s, 1)$, $\mathbf{j}_L = (s', 1)$ and $\mathbf{k}_L = (r, 1)$). This can be achieved by absorbing these Clebsch–Gordan coefficients into the previously trivial environment tensor $\mathbf{F}(L+1)$.

Now the transformation behavior of the contraction environment tensors can be investigated. With the graphical notation at hand, it becomes quite easy to organize the unitary transformation matrices that represent a symmetry operation $g \in \text{SU}(2)$ in Figure 16. After inserting unities, with the help of the already known transformation rules for MPS and MPO tensors, the transformation of the indices of the contraction environment tensor $\mathbf{E}(\ell)$ can be shifted to the previous one $\mathbf{E}(\ell-1)$. Due to the recursive definition of contraction environments, if any of these is invariant with respect to the index transformations, all following tensors will inherit this property. Since the leftmost dummy contraction environment $\mathbf{E}(0)$ is just a scalar, it is invariant under transformations of its dummy indices, and because of that, all left contraction environment tensors are invariant under this transformation. For the right environment, the same applies: the rightmost tensor fulfills the transformation behavior as it is built from Clebsch–Gordan coefficients, and all other right environment tensors inherit this property from it (Figure 17).

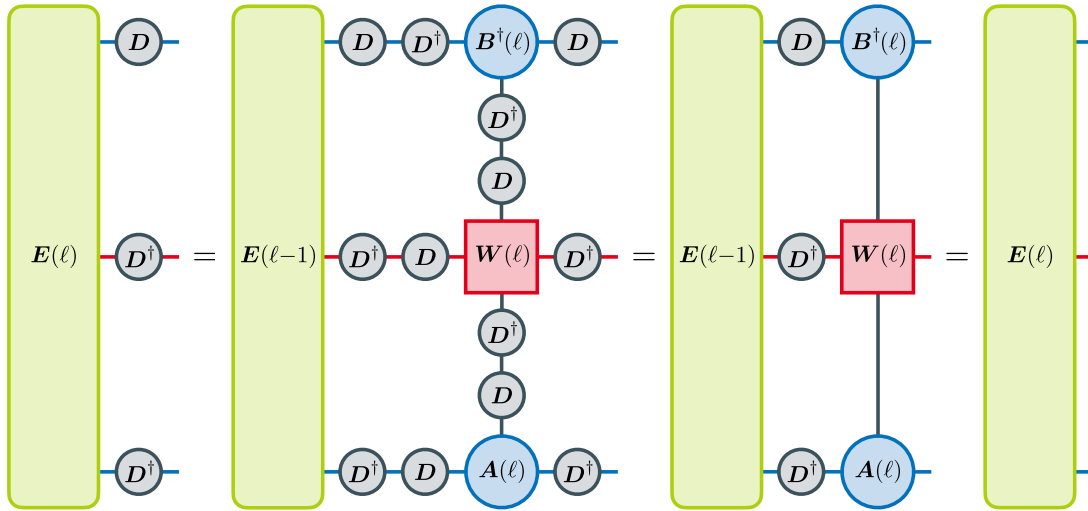


Figure 16: Transformation behavior of the left contraction environment tensors.

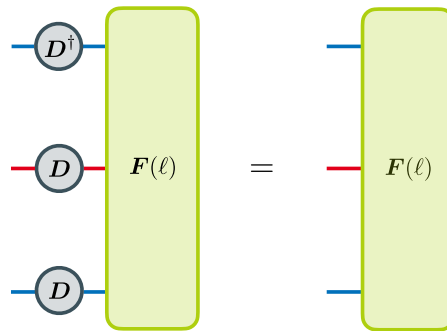


Figure 17: Transformation behavior of the right contraction environment tensors.

In a second step, this transformation behavior is used to define a set of operators that involve the left contraction environment tensors and investigate the effect the group action has on this set of operators:

$$\begin{aligned}\widehat{\mathcal{E}}(\mathbf{k}_\ell, \mathbf{k}_\ell^{(z)}) &= \sum_{\mathbf{i}_\ell, \mathbf{j}_\ell, \mathbf{i}_\ell^{(z)}, \mathbf{j}_\ell^{(z)}} E(\ell) \begin{matrix} \mathbf{i}_\ell \mathbf{i}_\ell^{(z)} \mathbf{k}_\ell \mathbf{k}_\ell^{(z)} \\ \mathbf{j}_\ell \mathbf{j}_\ell^{(z)} \end{matrix} \left| \mathbf{j}_\ell, \mathbf{j}_\ell^{(z)} \right\rangle \left\langle \mathbf{i}_\ell, \mathbf{i}_\ell^{(z)} \right| \quad \text{with} \\ \widehat{U}_g \widehat{\mathcal{E}}(\mathbf{k}_\ell, \mathbf{k}_\ell^{(z)}) \widehat{U}_g^\dagger &= \sum_{\substack{\mathbf{i}_\ell, \mathbf{j}_\ell, \\ \mathbf{i}_\ell^{(z)}, \mathbf{j}_\ell^{(z)}, \mathbf{i}'_\ell, \mathbf{j}'_\ell}} E(\ell) \begin{matrix} \mathbf{i}_\ell \mathbf{i}_\ell^{(z)} \mathbf{k}_\ell \mathbf{k}_\ell^{(z)} \\ \mathbf{j}_\ell \mathbf{j}_\ell^{(z)} \end{matrix} D_{\mathbf{j}'_\ell \mathbf{j}_\ell^{(z)}}^{[\mathbf{j}_\ell]} \left(D_{\mathbf{i}'_\ell \mathbf{i}_\ell^{(z)}}^{[\mathbf{i}_\ell]} \right)^* \left| \mathbf{j}'_\ell, \mathbf{j}'_\ell^{(z)} \right\rangle \left\langle \mathbf{i}'_\ell, \mathbf{i}'_\ell^{(z)} \right| \\ &= \sum_{\substack{\mathbf{i}_\ell, \mathbf{j}_\ell, \\ \mathbf{i}_\ell^{(z)}, \mathbf{j}_\ell^{(z)}, \mathbf{k}'_\ell}} D_{\mathbf{k}'_\ell \mathbf{k}_\ell^{(z)}}^{[\mathbf{k}_\ell]} E(\ell) \begin{matrix} \mathbf{i}_\ell \mathbf{i}_\ell^{(z)} \mathbf{k}_\ell \mathbf{k}_\ell^{(z)} \\ \mathbf{j}_\ell \mathbf{j}_\ell^{(z)} \end{matrix} \left| \mathbf{j}_\ell, \mathbf{j}_\ell^{(z)} \right\rangle \left\langle \mathbf{i}_\ell, \mathbf{i}_\ell^{(z)} \right| = \sum_{\mathbf{k}'_\ell} D_{\mathbf{k}'_\ell \mathbf{k}_\ell^{(z)}}^{[\mathbf{k}_\ell]} \widehat{\mathcal{E}}(\mathbf{k}_\ell, \mathbf{k}'_\ell). \quad (2.106)\end{aligned}$$

Analogously, one finds for the right-environment counterpart

$$\begin{aligned}\widehat{\mathcal{F}}(\mathbf{k}_{\ell-1}, \mathbf{k}_{\ell-1}^{(z)}) &= \sum_{\mathbf{i}_{\ell-1}, \mathbf{j}_{\ell-1}, \mathbf{i}_{\ell-1}^{(z)}, \mathbf{j}_{\ell-1}^{(z)}} F(\ell) \begin{matrix} \mathbf{j}_{\ell-1} \mathbf{j}_{\ell-1}^{(z)} \\ \mathbf{i}_{\ell-1} \mathbf{i}_{\ell-1}^{(z)} \mathbf{k}_{\ell-1} \mathbf{k}_{\ell-1}^{(z)} \end{matrix} \left| \mathbf{j}_{\ell-1}, \mathbf{j}_{\ell-1}^{(z)} \right\rangle \left\langle \mathbf{i}_{\ell-1}, \mathbf{i}_{\ell-1}^{(z)} \right| \quad \text{with} \\ \widehat{U}_g \widehat{\mathcal{F}}(\mathbf{k}_{\ell-1}, \mathbf{k}_{\ell-1}^{(z)}) \widehat{U}_g^\dagger &= \sum_{\mathbf{k}'_{\ell-1}} D_{\mathbf{k}'_{\ell-1} \mathbf{k}_{\ell-1}^{(z)}}^{[\mathbf{k}_{\ell-1}]} \widehat{\mathcal{F}}(\mathbf{k}_{\ell-1}, \mathbf{k}'_{\ell-1}). \quad (2.107)\end{aligned}$$

Therefore, $\widehat{\mathcal{E}}(\mathbf{k}_\ell, \mathbf{k}_\ell^{(z)})$ is the $\mathbf{k}_\ell^{(z)}$ component of an irreducible tensor operator of rank \mathbf{k}_ℓ and $\widehat{\mathcal{F}}(\mathbf{k}_{\ell-1}, \mathbf{k}_{\ell-1}^{(z)})$ is the $\mathbf{k}_{\ell-1}^{(z)}$ component of an irreducible tensor operator of rank $\mathbf{k}_{\ell-1}$. Application of the Wigner–Eckart theorem yields

$$\begin{aligned}\left\langle \mathbf{j}_\ell, \mathbf{j}_\ell^{(z)} \right| \widehat{\mathcal{E}}(\mathbf{k}_\ell, \mathbf{k}_\ell^{(z)}) \left| \mathbf{i}_\ell, \mathbf{i}_\ell^{(z)} \right\rangle &= E(\ell) \begin{matrix} \mathbf{i}_\ell \mathbf{i}_\ell^{(z)} \mathbf{k}_\ell \mathbf{k}_\ell^{(z)} \\ \mathbf{j}_\ell \mathbf{j}_\ell^{(z)} \end{matrix} = \Gamma_{\mathbf{i}_\ell^{(z)} \mathbf{k}_\ell^{(z)} \rightarrow \mathbf{j}_\ell^{(z)}}^{\mathbf{i}_\ell \mathbf{k}_\ell \rightarrow \mathbf{j}_\ell} \cdot \overline{E}(\ell) \begin{matrix} \mathbf{i}_\ell \mathbf{k}_\ell \\ \mathbf{j}_\ell \end{matrix} \quad \text{and} \\ \left\langle \mathbf{j}_{\ell-1}, \mathbf{j}_{\ell-1}^{(z)} \right| \widehat{\mathcal{F}}(\mathbf{k}_{\ell-1}, \mathbf{k}_{\ell-1}^{(z)}) \left| \mathbf{i}_{\ell-1}, \mathbf{i}_{\ell-1}^{(z)} \right\rangle &= F(\ell) \begin{matrix} \mathbf{j}_{\ell-1} \mathbf{j}_{\ell-1}^{(z)} \\ \mathbf{i}_{\ell-1} \mathbf{i}_{\ell-1}^{(z)} \mathbf{k}_{\ell-1} \mathbf{k}_{\ell-1}^{(z)} \end{matrix} = \Gamma_{\mathbf{i}_{\ell-1}^{(z)} \mathbf{k}_{\ell-1}^{(z)} \rightarrow \mathbf{j}_{\ell-1}^{(z)}}^{\mathbf{i}_{\ell-1} \mathbf{k}_{\ell-1} \rightarrow \mathbf{j}_{\ell-1}} \cdot \overline{F}(\ell) \begin{matrix} \mathbf{j}_{\ell-1} \\ \mathbf{i}_{\ell-1} \mathbf{k}_{\ell-1} \end{matrix}. \quad (2.108)\end{aligned}$$

Using these factorizations, the third step is to find an expression for recursive calculation of the reduced environment tensors:

$$\begin{aligned}\overline{E}(\ell) \begin{matrix} \mathbf{i}_\ell \mathbf{k}_\ell \\ \mathbf{j}_\ell \end{matrix} &= \sum_{\mathbf{i}_\ell^{(z)}, \mathbf{k}_\ell^{(z)}} E(\ell) \begin{matrix} \mathbf{i}_\ell \mathbf{i}_\ell^{(z)} \mathbf{k}_\ell \mathbf{k}_\ell^{(z)} \\ \mathbf{j}_\ell \mathbf{j}_\ell^{(z)} \end{matrix} \Gamma_{\mathbf{i}_\ell^{(z)} \mathbf{k}_\ell^{(z)} \rightarrow \mathbf{j}_\ell^{(z)}}^{\mathbf{i}_\ell \mathbf{k}_\ell \rightarrow \mathbf{j}_\ell} \\ &= \sum_{\substack{\mathbf{i}_{\ell-1}, \mathbf{j}_{\ell-1}, \\ \mathbf{k}_{\ell-1}, \mathbf{n}_\ell, \mathbf{m}_\ell}} \sum_{\substack{\mathbf{i}_{\ell-1}^{(z)}, \mathbf{j}_{\ell-1}^{(z)}, \\ \mathbf{k}_{\ell-1}^{(z)}, \mathbf{n}_\ell^{(z)}, \mathbf{m}_\ell^{(z)}, \\ \mathbf{i}_\ell^{(z)}, \mathbf{k}_\ell^{(z)}}} B^\dagger(\ell) \begin{matrix} \mathbf{j}_{\ell-1} \mathbf{j}_{\ell-1}^{(z)} \mathbf{m}_\ell \mathbf{m}_\ell^{(z)} \\ \mathbf{j}_\ell \mathbf{j}_\ell^{(z)} \end{matrix} W(\ell) \begin{matrix} \mathbf{k}_\ell \mathbf{k}_\ell^{(z)} \mathbf{n}_\ell \mathbf{n}_\ell^{(z)} \\ \mathbf{k}_{\ell-1} \mathbf{k}_{\ell-1}^{(z)} \mathbf{m}_\ell \mathbf{m}_\ell^{(z)} \end{matrix} A(\ell) \begin{matrix} \mathbf{i}_\ell \mathbf{i}_\ell^{(z)} \\ \mathbf{i}_{\ell-1} \mathbf{i}_{\ell-1}^{(z)} \mathbf{n}_\ell \mathbf{n}_\ell^{(z)} \end{matrix} E(\ell-1) \begin{matrix} \mathbf{i}_{\ell-1} \mathbf{i}_{\ell-1}^{(z)} \mathbf{k}_{\ell-1} \mathbf{k}_{\ell-1}^{(z)} \\ \mathbf{j}_{\ell-1} \mathbf{j}_{\ell-1}^{(z)} \end{matrix} \Gamma_{\mathbf{i}_{\ell-1}^{(z)} \mathbf{k}_{\ell-1}^{(z)} \rightarrow \mathbf{j}_{\ell-1}^{(z)}}^{\mathbf{i}_{\ell-1} \mathbf{k}_{\ell-1} \rightarrow \mathbf{j}_{\ell-1}} \\ &= \sum_{\substack{\mathbf{i}_{\ell-1}, \mathbf{j}_{\ell-1}, \mathbf{k}_{\ell-1}, \\ \mathbf{n}_\ell, \mathbf{m}_\ell, \mathbf{t}_\ell}} \overline{B}^\dagger(\ell) \begin{matrix} \mathbf{j}_{\ell-1} \mathbf{j}_{\ell-1}^{(z)} \mathbf{m}_\ell \mathbf{m}_\ell^{(z)} \\ \mathbf{j}_\ell \mathbf{j}_\ell^{(z)} \end{matrix} \overline{W}^{[t_\ell]}(\ell) \begin{matrix} \mathbf{k}_\ell \mathbf{n}_\ell \\ \mathbf{k}_{\ell-1} \mathbf{m}_\ell \end{matrix} \overline{A}(\ell) \begin{matrix} \mathbf{i}_\ell \\ \mathbf{i}_{\ell-1} \mathbf{n}_\ell \end{matrix} \overline{E}(\ell-1) \begin{matrix} \mathbf{i}_{\ell-1} \mathbf{k}_{\ell-1} \\ \mathbf{j}_{\ell-1} \end{matrix} \\ &\quad \cdot \sum_{\substack{\mathbf{i}_{\ell-1}^{(z)}, \mathbf{j}_{\ell-1}^{(z)}, \mathbf{k}_{\ell-1}^{(z)}, \\ \mathbf{n}_\ell^{(z)}, \mathbf{m}_\ell^{(z)}, \mathbf{t}_\ell^{(z)}, \\ \mathbf{i}_\ell^{(z)}, \mathbf{k}_\ell^{(z)}}} \Gamma_{\mathbf{i}_{\ell-1}^{(z)} \mathbf{k}_{\ell-1}^{(z)} \rightarrow \mathbf{j}_{\ell-1}^{(z)}}^{\mathbf{i}_{\ell-1} \mathbf{k}_{\ell-1} \rightarrow \mathbf{j}_{\ell-1}} \Gamma_{\mathbf{i}_{\ell-1}^{(z)} \mathbf{k}_{\ell-1}^{(z)} \rightarrow \mathbf{j}_{\ell-1}^{(z)}}^{\mathbf{i}_{\ell-1} \mathbf{k}_{\ell-1} \rightarrow \mathbf{j}_{\ell-1}} \Gamma_{\mathbf{j}_{\ell-1}^{(z)} \mathbf{m}_\ell^{(z)} \rightarrow \mathbf{j}_\ell^{(z)}}^{\mathbf{j}_{\ell-1} \mathbf{m}_\ell \rightarrow \mathbf{j}_\ell} \Gamma_{\mathbf{i}_{\ell-1}^{(z)} \mathbf{n}_\ell^{(z)} \rightarrow \mathbf{i}_\ell^{(z)}}^{\mathbf{i}_{\ell-1} \mathbf{n}_\ell \rightarrow \mathbf{i}_\ell} \Gamma_{\mathbf{n}_\ell^{(z)} \mathbf{t}_\ell^{(z)} \rightarrow \mathbf{m}_\ell^{(z)}}^{\mathbf{n}_\ell \mathbf{t}_\ell \rightarrow \mathbf{m}_\ell} \Gamma_{\mathbf{k}_{\ell-1}^{(z)} \mathbf{t}_\ell^{(z)} \rightarrow \mathbf{k}_\ell^{(z)}}^{\mathbf{k}_{\ell-1} \mathbf{t}_\ell \rightarrow \mathbf{k}_\ell} \\ &= \sum_{\substack{\mathbf{i}_{\ell-1}, \mathbf{j}_{\ell-1}, \mathbf{k}_{\ell-1}, \\ \mathbf{n}_\ell, \mathbf{m}_\ell, \mathbf{t}_\ell}} \overline{B}^\dagger(\ell) \begin{matrix} \mathbf{j}_{\ell-1} \mathbf{j}_{\ell-1}^{(z)} \mathbf{m}_\ell \mathbf{m}_\ell^{(z)} \\ \mathbf{j}_\ell \mathbf{j}_\ell^{(z)} \end{matrix} \overline{W}^{[t_\ell]}(\ell) \begin{matrix} \mathbf{k}_\ell \mathbf{n}_\ell \\ \mathbf{k}_{\ell-1} \mathbf{m}_\ell \end{matrix} \overline{A}(\ell) \begin{matrix} \mathbf{i}_\ell \\ \mathbf{i}_{\ell-1} \mathbf{n}_\ell \end{matrix} \overline{E}(\ell-1) \begin{matrix} \mathbf{i}_{\ell-1} \mathbf{k}_{\ell-1} \\ \mathbf{j}_{\ell-1} \end{matrix} \cdot \begin{bmatrix} \mathbf{i}_{\ell-1} & \mathbf{k}_{\ell-1} & \mathbf{j}_{\ell-1} \\ \mathbf{n}_\ell & \mathbf{t}_\ell & \mathbf{m}_\ell \\ \mathbf{i}_\ell & \mathbf{k}_\ell & \mathbf{j}_\ell \end{bmatrix}. \quad (2.109)\end{aligned}$$

and

$$\begin{aligned}
 \overline{F}(\ell)^{j_{\ell-1} k_{\ell-1}} &= \frac{1}{2j_{\ell-1} + 1} \sum_{i_{\ell-1}^{(z)}, j_{\ell-1}^{(z)}, k_{\ell-1}^{(z)}} F(\ell)^{j_{\ell-1} i_{\ell-1}^{(z)} k_{\ell-1}^{(z)}} \Gamma_{i_{\ell-1}^{(z)} k_{\ell-1}^{(z)} \rightarrow j_{\ell-1}^{(z)}}^{i_{\ell-1} k_{\ell-1} \rightarrow j_{\ell-1}} \\
 &= \frac{1}{2j_{\ell-1} + 1} \sum_{\substack{\mathbf{i}_{\ell}, \mathbf{j}_{\ell}, \\ \mathbf{k}_{\ell}, \mathbf{n}_{\ell}, \mathbf{m}_{\ell}}} \sum_{\substack{i_{\ell}^{(z)}, j_{\ell}^{(z)}, \\ k_{\ell}^{(z)}, n_{\ell}^{(z)}, m_{\ell}^{(z)}, \\ i_{\ell-1}^{(z)}, j_{\ell-1}^{(z)}, k_{\ell-1}^{(z)}}} B^{\dagger}(\ell)^{j_{\ell} i_{\ell}^{(z)} k_{\ell}^{(z)}} W(\ell)^{k_{\ell} k_{\ell}^{(z)} n_{\ell} n_{\ell}^{(z)}} A(\ell)^{i_{\ell} i_{\ell}^{(z)}} F(\ell+1)^{j_{\ell} j_{\ell}^{(z)}} \Gamma_{i_{\ell-1}^{(z)} k_{\ell-1}^{(z)} \rightarrow j_{\ell-1}^{(z)}}^{i_{\ell-1} k_{\ell-1} \rightarrow j_{\ell-1}} \\
 &= \frac{1}{2j_{\ell-1} + 1} \sum_{\substack{\mathbf{i}_{\ell}, \mathbf{j}_{\ell}, \mathbf{k}_{\ell}, \\ \mathbf{n}_{\ell}, \mathbf{m}_{\ell}, \mathbf{t}_{\ell}}} \overline{B}^{\dagger}(\ell)^{j_{\ell} i_{\ell}^{(z)} k_{\ell}^{(z)}} \overline{W}^{[t_{\ell}]}(\ell)^{k_{\ell} n_{\ell} m_{\ell}} \overline{A}(\ell)^{i_{\ell} i_{\ell}^{(z)}} \overline{F}(\ell+1)^{j_{\ell} j_{\ell}^{(z)}} \\
 &\quad \cdot \sum_{\substack{i_{\ell}^{(z)}, j_{\ell}^{(z)}, k_{\ell}^{(z)}, \\ n_{\ell}^{(z)}, m_{\ell}^{(z)}, t_{\ell}^{(z)}, \\ i_{\ell-1}^{(z)}, j_{\ell-1}^{(z)}, k_{\ell-1}^{(z)}}} \Gamma_{i_{\ell}^{(z)} k_{\ell}^{(z)} \rightarrow j_{\ell}^{(z)}}^{i_{\ell} k_{\ell} \rightarrow j_{\ell}} \Gamma_{i_{\ell-1}^{(z)} k_{\ell-1}^{(z)} \rightarrow j_{\ell-1}^{(z)}}^{i_{\ell-1} k_{\ell-1} \rightarrow j_{\ell-1}} \Gamma_{j_{\ell-1}^{(z)} m_{\ell}^{(z)} \rightarrow j_{\ell}^{(z)}}^{j_{\ell-1} m_{\ell} \rightarrow j_{\ell}} \Gamma_{i_{\ell-1}^{(z)} n_{\ell}^{(z)} \rightarrow i_{\ell}^{(z)}}^{i_{\ell-1} n_{\ell} \rightarrow i_{\ell}} \Gamma_{n_{\ell}^{(z)} t_{\ell}^{(z)} \rightarrow m_{\ell}^{(z)}}^{n_{\ell} t_{\ell} \rightarrow m_{\ell}} \Gamma_{k_{\ell-1}^{(z)} t_{\ell}^{(z)} \rightarrow k_{\ell}^{(z)}}^{k_{\ell-1} t_{\ell} \rightarrow k_{\ell}} \\
 &= \sum_{\substack{\mathbf{i}_{\ell}, \mathbf{j}_{\ell}, \mathbf{k}_{\ell}, \\ \mathbf{n}_{\ell}, \mathbf{m}_{\ell}, \mathbf{t}_{\ell}}} \overline{B}^{\dagger}(\ell)^{j_{\ell} i_{\ell}^{(z)} k_{\ell}^{(z)}} \overline{W}^{[t_{\ell}]}(\ell)^{k_{\ell} n_{\ell} m_{\ell}} \overline{A}(\ell)^{i_{\ell} i_{\ell}^{(z)}} \overline{F}(\ell+1)^{j_{\ell} j_{\ell}^{(z)}} \cdot \frac{2j_{\ell} + 1}{2j_{\ell-1} + 1} \begin{bmatrix} i_{\ell-1} & k_{\ell-1} & j_{\ell-1} \\ n_{\ell} & t_{\ell} & m_{\ell} \\ i_{\ell} & k_{\ell} & j_{\ell} \end{bmatrix}. \tag{2.110}
 \end{aligned}$$

Contractions can be calculated as if there was no internal dimension of the irreducible representations at all, with the only adjustment being a Wigner 9j-symbol and a quotient of two irreducible representation dimensions in the case of the right environment tensors.

With all these ingredients, the reduced matrix element is readily available:

$$\begin{aligned}
 \langle\langle \Phi^{[s']} | | \widehat{O}^{[r]} | | \Psi^{[s]} \rangle\rangle &= \frac{1}{2s' + 1} \sum_{\substack{\mathbf{i}_{\ell}, \mathbf{j}_{\ell}, \mathbf{k}_{\ell}, \\ i_{\ell}^{(z)}, j_{\ell}^{(z)}, k_{\ell}^{(z)}}} E(\ell)^{i_{\ell} i_{\ell}^{(z)} k_{\ell} k_{\ell}^{(z)}} F(\ell+1)^{j_{\ell} j_{\ell}^{(z)}} \\
 &= \frac{1}{2s' + 1} \sum_{\mathbf{i}_{\ell}, \mathbf{j}_{\ell}, \mathbf{k}_{\ell}} \overline{E}(\ell)^{i_{\ell} k_{\ell}} \overline{F}(\ell+1)^{j_{\ell} j_{\ell}^{(z)}} \sum_{i_{\ell}^{(z)}, j_{\ell}^{(z)}, k_{\ell}^{(z)}} \left(\Gamma_{i_{\ell}^{(z)} k_{\ell}^{(z)} \rightarrow j_{\ell}^{(z)}}^{i_{\ell} k_{\ell} \rightarrow j_{\ell}} \right)^2 \\
 &= \sum_{\mathbf{i}_{\ell}, \mathbf{j}_{\ell}, \mathbf{k}_{\ell}} \overline{E}(\ell)^{i_{\ell} k_{\ell}} \overline{F}(\ell+1)^{j_{\ell} j_{\ell}^{(z)}} \frac{2j_{\ell} + 1}{2s' + 1} \text{ for arbitrary } \ell \in \{1, \dots, L\}. \tag{2.111}
 \end{aligned}$$

The formula for the product of two MPOs (Equation (2.104)) can be used to bring in principle any product of operators into a single MPO form, so that for the determination of matrix elements, only contraction tensors of order 3 are involved. Since then all relevant expressions can be evaluated in terms of reduced tensors, the manifestly SU(2)-symmetric implementation of VMPS simplifies to a procedure quite similar to the implementation of the Abelian symmetry U(1): the internal structure of the irreducible representations, i. e., the multiplets of states and tensor operators, can be separated from the indices that label each irreducible representation. This part of the tensor network is already fixed by symmetry requirements and can be computed beforehand. The results are Wigner symbols, which are available in standard programming libraries such as GNU Scientific Library [74]. The triangle rule for coupling of angular momenta reduces the amount of quantum number blocks that can be connected. The variational algorithms as well as MPS compression by SVD are straightforwardly generalized to the case of an SU(2) symmetry. Thus, the symmetric implementation reduces the dimensionality of the involved Hilbert spaces, while at the same time it guarantees the correct total quantum number of a state without admixtures from other quantum numbers.

Generalized symmetry framework

The formalism for the treatment of a non-Abelian symmetry, namely the appearance of coupling coefficients that arise whenever two irreducible representations are merged, can also be applied to the Abelian symmetry $U(1)$. Here, many expressions are quite trivial, because the irreducible representations are one-dimensional, and the product of two irreducible representations is uniquely determined – as opposed to the case of angular momentum coupling, where all intermediate quantum numbers that obey the triangle rule are allowed. For the irreducible representations $\widehat{U}^{[n]} : V_{\nu}^{[n]} \rightarrow V_{\nu}^{[n]}$ (equivalent representations are assumed to be equal)

$$\widehat{U}^{[n]} \otimes \widehat{U}^{[n']} = \widehat{U}^{[n+n']} : V_{\nu''}^{[n+n']} \rightarrow V_{\nu''}^{[n+n']}, \quad (2.112)$$

holds, where ν'' is a degeneracy index that corresponds to the coupling of the carrier spaces, $V_{\nu}^{[n]} \otimes V_{\nu'}^{[n']} = V_{\nu''}^{[n+n']}$. Since no projection quantum numbers appear, the $U(1)$ coupling coefficients that replace the Clebsch–Gordan coefficients are given by

$$\Gamma^{n \ n' \rightarrow N} = \delta_{n+n', N} \quad (2.113)$$

One can also define irreducible tensor operators for $U(1)$. Due to one-dimensionality of irreducible representations, these irreducible tensor operators are not built from a set of operators anymore, but are given by a single operator each. Still the defining property is the commutation relation with the generating operator of the symmetry, which in the case of particle number conservation is the particle number operator $\widehat{N} = \sum_{i\sigma} \widehat{c}_{i\sigma}^\dagger \widehat{c}_{i\sigma}$.

$$\left[\widehat{N}, \widehat{c}_{i\sigma} \right] = -\widehat{c}_{i\sigma} \quad \Rightarrow \quad \widehat{c}_{i\sigma} = (\widehat{c}_{i\sigma})^{[-1]} \quad \text{irreducible tensor operator of rank } -1. \quad (2.114)$$

The $U(1)$ version of the Wigner–Eckart theorem is obvious, because for any $\varphi \in \mathbb{R}$ the following equation holds:

$$\begin{aligned} \langle \Phi^{[s']} | \widehat{O}^{[r]} | \Psi^{[s]} \rangle &= \langle \Phi^{[s']} | \exp(-i\varphi \widehat{N}) \exp(i\varphi \widehat{N}) \widehat{O}^{[r]} \exp(-i\varphi \widehat{N}) \exp(i\varphi \widehat{N}) | \Psi^{[s]} \rangle \\ &= \langle \Phi^{[s']} | \exp(-i\varphi s') \exp(i\varphi r) \widehat{O}^{[r]} \exp(-i\varphi s) | \Psi^{[s]} \rangle = \exp(i\varphi(s+r-s')) \langle \Phi^{[s']} | \widehat{O}^{[r]} | \Psi^{[s]} \rangle, \\ \Rightarrow \quad s+r &= s' \quad \text{or} \quad \langle \Phi^{[s']} | \widehat{O}^{[r]} | \Psi^{[s]} \rangle = 0, \\ \Rightarrow \quad \langle \Phi^{[s']} | \widehat{O}^{[r]} | \Psi^{[s]} \rangle &= \Gamma^{s \ r \rightarrow s'} \langle \langle \Phi^{[s']} | \widehat{O}^{[r]} | \Psi^{[s]} \rangle \rangle \quad \text{with} \quad \langle \langle \Phi^{[s']} | \widehat{O}^{[r]} | \Psi^{[s]} \rangle \rangle = \langle \Phi^{[s']} | \widehat{O}^{[r]} | \Psi^{[s]} \rangle. \end{aligned} \quad (2.115)$$

The tensors that appear in the context of VMPS are listed here for completeness. The Clebsch–Gordan coefficients actually only say when an expression must vanish for symmetry reasons, the reduced tensors coincide with the original ones.

$$\begin{aligned} A(\ell)_{i_{\ell-1} \mathbf{n}_\ell}^{i_\ell} &= \Gamma^{i_{\ell-1} \mathbf{n}_\ell \rightarrow i_\ell} \overline{A}(\ell)_{i_{\ell-1} \mathbf{n}_\ell}^{i_\ell}, & B^\dagger(\ell)_{j_\ell}^{j_{\ell-1} \mathbf{m}_\ell} &= \Gamma^{j_{\ell-1} \mathbf{m}_\ell \rightarrow j_\ell} \overline{B}^\dagger(\ell)_{j_\ell}^{j_{\ell-1} \mathbf{m}_\ell}, \\ W(\ell)_{\mathbf{k}_{\ell-1} \mathbf{m}_\ell}^{\mathbf{k}_\ell \mathbf{n}_\ell} &= \sum_{t_\ell} \Gamma^{\mathbf{k}_{\ell-1} t_\ell \rightarrow \mathbf{k}_\ell} \Gamma^{\mathbf{n}_\ell t_\ell \rightarrow \mathbf{m}_\ell} \overline{W}^{[t_\ell]}(\ell)_{\mathbf{k}_{\ell-1} \mathbf{m}_\ell}^{\mathbf{k}_\ell \mathbf{n}_\ell}, \\ E(\ell)_{j_\ell}^{i_\ell \mathbf{k}_\ell} &= \Gamma^{i_\ell \mathbf{k}_\ell \rightarrow j_\ell} \overline{E}(\ell)_{j_\ell}^{i_\ell \mathbf{k}_\ell}, & F(\ell)_{i_{\ell-1} \mathbf{k}_{\ell-1}}^{j_{\ell-1}} &= \Gamma^{i_{\ell-1} \mathbf{k}_{\ell-1} \rightarrow j_{\ell-1}} \overline{F}(\ell)_{i_{\ell-1} \mathbf{k}_{\ell-1}}^{j_{\ell-1}} \end{aligned} \quad (2.116)$$

The analogs of Wigner 6j-symbols and Wigner 9j-symbols are given by

$$\left\{ \begin{array}{ccc} n_1 & n_2 & N_{12} \\ n_3 & N & N_{23} \end{array} \right\} = \delta_{n_1+n_2, N_{12}} \delta_{n_2+n_3, N_{23}} \delta_{n_1+n_2+n_3, N},$$

$$\left\{ \begin{array}{ccc} n_1 & n_2 & N_{12} \\ n_3 & n_4 & N_{34} \\ N_{13} & N_{24} & N \end{array} \right\} = \delta_{n_1+n_2, N_{12}} \delta_{n_3+n_4, N_{34}} \delta_{n_1+n_3, N_{13}} \delta_{n_2+n_4, N_{24}} \delta_{n_1+n_2+n_3+n_4, N}. \quad (2.117)$$

They coincide with the rescaled ones because there is no internal dimension.

With these adaptations, U(1) symmetries can be handled in the same framework as SU(2) symmetries. For systems in which neither a U(1) nor an SU(2) can be exploited, the coupling coefficients are trivial as there are no selection rules for coupling any indices. Moreover, if two symmetries are present at the same time, e. g., SU(2)_{spin} and U(1)_{charge} could be symmetries of the model under consideration, and their generators commute, this framework also allows for product symmetries. In this case, the quantum number of one symmetry are part of the degeneracy indices of the other symmetry. The coupling coefficients of the product symmetry are then given by the product of the individual coupling coefficients. This is motivated by the Wigner–Eckart theorem: considering the symmetries one after another, in a first step matrix elements factorize into a Clebsch–Gordan coefficient and a reduced matrix element, in which the internal indices of irreducible representations of the first symmetry are absent. However, this reduced matrix element is not a reduced matrix element with respect to the second symmetry, as the degeneracies of the first symmetry still contain internal indices of the irreducible representations of the second symmetry. Thus, the Wigner–Eckart theorem can be applied another time, leading to another Clebsch–Gordan coefficient.

Example: Spin-SU(2)

A possible definition of generators of the $\mathfrak{su}(2)$ angular-momentum algebra can be given in terms of fermionic annihilation and creation operators via the operators of total spin:

$$\begin{aligned} \hat{J}_S^{(x)} &= \frac{1}{2} \sum_{\ell=1}^L \left(\hat{c}_{\ell\uparrow}^\dagger \hat{c}_{\ell\downarrow} + \hat{c}_{\ell\downarrow}^\dagger \hat{c}_{\ell\uparrow} \right) & \Rightarrow & \quad \tilde{J}_S^{(+)} = \hat{J}_S^{(x)} + i\tilde{J}_S^{(y)} = \sum_{\ell=1}^L \hat{c}_{\ell\uparrow}^\dagger \hat{c}_{\ell\downarrow}, \\ \hat{J}_S^{(y)} &= \frac{1}{2i} \sum_{\ell=1}^L \left(\hat{c}_{\ell\uparrow}^\dagger \hat{c}_{\ell\downarrow} - \hat{c}_{\ell\downarrow}^\dagger \hat{c}_{\ell\uparrow} \right) & \Rightarrow & \quad \tilde{J}_S^{(-)} = \hat{J}_S^{(x)} - i\tilde{J}_S^{(y)} = \sum_{\ell=1}^L \hat{c}_{\ell\downarrow}^\dagger \hat{c}_{\ell\uparrow}, \\ \hat{J}_S^{(z)} &= \frac{1}{2} \sum_{\ell=1}^L \left(\hat{c}_{\ell\uparrow}^\dagger \hat{c}_{\ell\uparrow} - \hat{c}_{\ell\downarrow}^\dagger \hat{c}_{\ell\downarrow} \right), & & \quad (2.118) \end{aligned}$$

with the derived commutation relations

$$\begin{aligned} [\hat{J}_S^{(+)}, \hat{J}_S^{(-)}] &= \sum_{\ell, \ell'=1}^L \left[\hat{c}_{\ell\uparrow}^\dagger \hat{c}_{\ell\downarrow}, \hat{c}_{\ell'\downarrow}^\dagger \hat{c}_{\ell'\uparrow} \right] = \sum_{\ell, \ell'=1}^L \left(\delta_{\ell\ell'} \hat{c}_{\ell\uparrow}^\dagger \hat{c}_{\ell'\uparrow} - \delta_{\ell\ell'} \hat{c}_{\ell\downarrow}^\dagger \hat{c}_{\ell'\downarrow} \right) = 2\hat{J}_S^{(z)}, \\ [\hat{J}_S^{(z)}, \hat{J}_S^{(+)}] &= \frac{1}{2} \sum_{\ell, \ell'=1}^L \left[\hat{c}_{\ell\uparrow}^\dagger \hat{c}_{\ell\uparrow} - \hat{c}_{\ell\downarrow}^\dagger \hat{c}_{\ell\downarrow}, \hat{c}_{\ell'\uparrow}^\dagger \hat{c}_{\ell'\downarrow} \right] = \frac{1}{2} \sum_{\ell, \ell'=1}^L \left(\delta_{\ell\ell'} \hat{c}_{\ell\uparrow}^\dagger \hat{c}_{\ell'\downarrow} + \delta_{\ell\ell'} \hat{c}_{\ell\downarrow}^\dagger \hat{c}_{\ell'\uparrow} \right) = \hat{J}_S^{(+)}. \quad (2.119) \end{aligned}$$

The basis of a local Hilbert space of electrons in a Wannier orbital can be equipped with quantum numbers of this symmetry. The states are of the form $|n_\ell, \nu_\ell, n_\ell^{(z)}\rangle$, where n_ℓ is the angular momentum quantum number,

$\mathfrak{n}_\ell^{(z)}$ is the projection and $\nu_\ell \in \{1, \dots, \mathfrak{D}(\mathfrak{n}_\ell)\}$ is the degeneracy that occurs in the presence of multiplicity:

$$\begin{aligned} |0\rangle &= |0, 1, 0\rangle, \\ |\uparrow\rangle &= |\frac{1}{2}, 1, +\frac{1}{2}\rangle, \\ |\downarrow\rangle &= |\frac{1}{2}, 1, -\frac{1}{2}\rangle, \\ |\uparrow\downarrow\rangle &= |0, 2, 0\rangle. \end{aligned} \quad (2.120)$$

These states fulfill the desired eigenvalue equations $\widehat{J}_S^2 |\mathfrak{n}_\ell, \nu_\ell, \mathfrak{n}_\ell^{(z)}\rangle = \mathfrak{n}_\ell(\mathfrak{n}_\ell + 1) |\mathfrak{n}_\ell, \nu_\ell, \mathfrak{n}_\ell^{(z)}\rangle$ and $\widehat{J}_S^{(z)} |\mathfrak{n}_\ell, \nu_\ell, \mathfrak{n}_\ell^{(z)}\rangle = \mathfrak{n}_\ell^{(z)} |\mathfrak{n}_\ell, \nu_\ell, \mathfrak{n}_\ell^{(z)}\rangle$, and the ladder operators are used to explore the multiplet of states that belong to this irreducible representation, i. e., $\widehat{J}_S^{(\pm)} |\mathfrak{n}_\ell, \nu_\ell, \mathfrak{n}_\ell^{(z)}\rangle = \sqrt{(\mathfrak{n}_\ell \mp \mathfrak{n}_\ell^{(z)})(\mathfrak{n}_\ell \pm \mathfrak{n}_\ell^{(z)} + 1)} |\mathfrak{n}_\ell, \nu_\ell, \mathfrak{n}_\ell^{(z)} \pm 1\rangle$.

The local spin operator itself is not an irreducible tensor operator, but it can be rescaled to achieve this:

$$(\widehat{S}_\ell)^{[1]} = \begin{pmatrix} (\widehat{S}_\ell)_{+1}^{[1]} \\ (\widehat{S}_\ell)_0^{[1]} \\ (\widehat{S}_\ell)_{-1}^{[1]} \end{pmatrix} = \begin{pmatrix} -\frac{1}{\sqrt{2}} \widehat{J}_{S,\ell}^{(+)} \\ \widehat{J}_{S,\ell}^{(z)} \\ \frac{1}{\sqrt{2}} \widehat{J}_{S,\ell}^{(-)} \end{pmatrix}, \quad (2.121)$$

because these three operators obey the commutation relations for an irreducible tensor operator of rank 1:

$$\begin{aligned} [\widehat{J}_S^{(z)}, (\widehat{S}_\ell)_m^{[1]}] &= m (\widehat{S}_\ell)_m^{[1]}, \\ [\widehat{J}_S^{(\pm)}, (\widehat{S}_\ell)_m^{[1]}] &= \sqrt{(1 \mp m)(2 \pm m)} (\widehat{S}_\ell)_{m\pm 1}^{[1]}. \end{aligned} \quad (2.122)$$

The scalar product of two local spin operators $\widehat{J}_{S,\ell} \cdot \widehat{J}_{S,\ell'}$ can be expressed as an irreducible tensor operator as follows:

$$\begin{aligned} \left((\widehat{S}_\ell)^{[1]} \star (\widehat{S}_{\ell'})^{[1]} \right)^{[0]} &= \Gamma_{+1-1 \rightarrow 0}^1 (\widehat{S}_\ell)_{+1}^{[1]} (\widehat{S}_{\ell'})_{-1}^{[1]} + \Gamma_{00 \rightarrow 0}^{11} (\widehat{S}_\ell)_0^{[1]} (\widehat{S}_{\ell'})_0^{[1]} + \Gamma_{-1+1 \rightarrow 0}^1 (\widehat{S}_\ell)_{-1}^{[1]} (\widehat{S}_{\ell'})_{+1}^{[1]} \\ &= -\frac{1}{2\sqrt{3}} \left(\widehat{J}_{S,\ell}^{(+)} \widehat{J}_{S,\ell'}^{(-)} + 2\widehat{J}_{S,\ell}^{(z)} \widehat{J}_{S,\ell'}^{(z)} + \widehat{J}_{S,\ell}^{(-)} \widehat{J}_{S,\ell'}^{(+)} \right) = -\frac{1}{\sqrt{3}} \widehat{J}_{S,\ell} \cdot \widehat{J}_{S,\ell'}. \end{aligned} \quad (2.123)$$

Operators for higher spin correlation functions can be constructed in a similar way, for example this way:

$$\begin{aligned} &\sum_J \sqrt{2J+1} \left(\left((\widehat{S}_\ell)^{[1]} \star (\widehat{S}_\ell)^{[1]} \right)^{[J]} \star \left((\widehat{S}_{\ell'})^{[1]} \star (\widehat{S}_{\ell'})^{[1]} \right)^{[J]} \right)_0^{[0]} \\ &= \sum_{J,M} \sqrt{2J+1} \Gamma_{M-M \rightarrow 0}^J (\widehat{S}_\ell)_M^{[1]} (\widehat{S}_\ell)_M^{[1]} \left((\widehat{S}_{\ell'})^{[1]} \star (\widehat{S}_{\ell'})^{[1]} \right)_{-M}^{[J]} \\ &= \sum_{\substack{J,M, \\ m_1, m_2, m_3, m_4}} \sqrt{2J+1} \Gamma_{M-M \rightarrow 0}^J \Gamma_{m_1 m_2 \rightarrow M}^1 \Gamma_{m_3 m_4 \rightarrow -M}^1 (\widehat{S}_\ell)_{m_1}^{[1]} (\widehat{S}_\ell)_{m_2}^{[1]} (\widehat{S}_{\ell'})_{m_3}^{[1]} (\widehat{S}_{\ell'})_{m_4}^{[1]} \\ &= \sum_{\substack{m_1, m_2, \\ m_3, m_4}} (-1)^{m_1+m_2} \delta_{m_1, -m_3} \delta_{m_2, -m_4} (\widehat{S}_\ell)_{m_1}^{[1]} (\widehat{S}_\ell)_{m_2}^{[1]} (\widehat{S}_{\ell'})_{m_3}^{[1]} (\widehat{S}_{\ell'})_{m_4}^{[1]} \\ &= \left(\sum_m (-1)^m (\widehat{S}_\ell)_m^{[1]} (\widehat{S}_{\ell'})_{-m}^{[1]} \right)^2 = \left(\frac{1}{2} \widehat{J}_{S,\ell}^{(+)} \widehat{J}_{S,\ell'}^{(-)} + \widehat{J}_{S,\ell}^{(z)} \widehat{J}_{S,\ell'}^{(z)} + \frac{1}{2} \widehat{J}_{S,\ell}^{(-)} \widehat{J}_{S,\ell'}^{(+)} \right)^2 = \left(\widehat{J}_{S,\ell} \cdot \widehat{J}_{S,\ell'} \right)^2, \end{aligned} \quad (2.124)$$

since for integer J and M

$$\begin{aligned}
& \sum_{J,M} \sqrt{2J+1} \Gamma_{M-M \rightarrow 0}^J \Gamma_{m_1 m_2 \rightarrow M}^J \Gamma_{m_3 m_4 \rightarrow -M}^J \\
&= \sum_{J,M} \sqrt{2J+1} \cdot \frac{(-1)^{J-M}}{\sqrt{2J+1}} \Gamma_{m_1 m_2 \rightarrow M}^J \cdot (-1)^{2-J} \Gamma_{-m_3 -m_4 \rightarrow M}^J \\
&= \sum_{J,M} (-1)^M \Gamma_{m_1 m_2 \rightarrow M}^J \Gamma_{-m_3 -m_4 \rightarrow M}^J = (-1)^{m_1+m_2} \sum_{J,M} \langle 1, m_1; 1, m_2 | J, M \rangle \langle J, M | 1, -m_3; 1, -m_4 \rangle \\
&= (-1)^{m_1+m_2} \langle 1, m_1 | 1, -m_3 \rangle \langle 1, m_2 | 1, -m_4 \rangle = (-1)^{m_1+m_2} \delta_{m_1, -m_3} \delta_{m_2, -m_4}. \tag{2.125}
\end{aligned}$$

One can define an irreducible tensor operator of rank $\frac{1}{2}$ that contains fermionic annihilators:

$$(\widehat{\psi}_\ell)^{[\frac{1}{2}]} = \begin{pmatrix} (\widehat{\psi}_\ell)_{+\frac{1}{2}}^{[\frac{1}{2}]} \\ (\widehat{\psi}_\ell)_{-\frac{1}{2}}^{[\frac{1}{2}]} \end{pmatrix} = \begin{pmatrix} -\widehat{c}_{\ell\downarrow} \\ \widehat{c}_{\ell\uparrow} \end{pmatrix}, \tag{2.126}$$

and its adjoint with creators:

$$(\widehat{\psi}_\ell^\dagger)^{[\frac{1}{2}]} = \begin{pmatrix} (\widehat{\psi}_\ell^\dagger)_{+\frac{1}{2}}^{[\frac{1}{2}]} \\ (\widehat{\psi}_\ell^\dagger)_{-\frac{1}{2}}^{[\frac{1}{2}]} \end{pmatrix} = \begin{pmatrix} (-1)^{\frac{1}{2}-\frac{1}{2}} \left((\widehat{\psi}_\ell)_{-\frac{1}{2}}^{[\frac{1}{2}]} \right)^\dagger \\ (-1)^{\frac{1}{2}+\frac{1}{2}} \left((\widehat{\psi}_\ell)_{+\frac{1}{2}}^{[\frac{1}{2}]} \right)^\dagger \end{pmatrix} = \begin{pmatrix} \widehat{c}_{\ell\uparrow}^\dagger \\ \widehat{c}_{\ell\downarrow}^\dagger \end{pmatrix}. \tag{2.127}$$

This definition comes with a pitfall: the ordinary fermionic annihilators and creators cannot be locally evaluated irrespective of other lattice sites, because for the fermionic anticommutation relations, a sign factor appears in the definition of these operators. One chooses some ordering of the lattice sites, and all singly occupied sites that appear earlier in the ordering contribute a minus sign, i.e., the operator in total acquires a sign $(-1)^{n_1+\dots+n_{\ell-1}}$. Instead of incorporating this prefactor into the definition of creators and annihilators, here a standard trick is used in which the occupation dependent factors are taken into account explicitly as local operators $\widehat{s}_\ell = (-1)^{\widehat{n}_\ell}$, thus creating an operator that acts on all sites from 1 to ℓ , where the individual operators only act on their respective local Hilbert space: $\widehat{s}_1 \widehat{s}_2 \cdots \widehat{s}_{\ell-1} \widehat{c}_{\ell\sigma}$. Since the sign operator can be written as $\widehat{s}_\ell = \text{id} + \frac{8}{\sqrt{3}} \left((\widehat{\mathcal{S}}_\ell)^{[1]} \star (\widehat{\mathcal{S}}_\ell)^{[1]} \right)^{[0]}$, it is obvious that this operator is compatible with $\text{SU}(2)_{\text{spin}}$.

With the product rule for irreducible tensor operators, scalar operators of this form can be constructed:

$$\begin{aligned}
\left((\widehat{\psi}_\ell^\dagger)^{[\frac{1}{2}]} \star (\widehat{\psi}_{\ell'})^{[\frac{1}{2}]} \right)^{[0]} &= \Gamma_{+\frac{1}{2} -\frac{1}{2} \rightarrow 0}^{\frac{1}{2} \frac{1}{2}} \left((\widehat{\psi}_\ell^\dagger)_{+\frac{1}{2}}^{[\frac{1}{2}]} (\widehat{\psi}_{\ell'})_{-\frac{1}{2}}^{[\frac{1}{2}]} \right) + \Gamma_{-\frac{1}{2} +\frac{1}{2} \rightarrow 0}^{\frac{1}{2} \frac{1}{2}} \left((\widehat{\psi}_\ell^\dagger)_{-\frac{1}{2}}^{[\frac{1}{2}]} (\widehat{\psi}_{\ell'})_{+\frac{1}{2}}^{[\frac{1}{2}]} \right) \\
&= \frac{1}{\sqrt{2}} \left(\widehat{c}_{\ell\uparrow}^\dagger \widehat{c}_{\ell'\uparrow} + \widehat{c}_{\ell\downarrow}^\dagger \widehat{c}_{\ell'\downarrow} \right), \tag{2.128}
\end{aligned}$$

which means that all hopping terms that do not depend on the spin projection are irreducible tensor operators of rank 0 and thus are compatible with the $\text{SU}(2)_{\text{spin}}$ symmetry. Moreover, it is possible to construct a different irreducible tensor operator of rank 0, which comes into play for BCS-type superconductivity Hamilton operators:

$$\begin{aligned}
\left((\widehat{\psi}_\ell)^{[\frac{1}{2}]} \star (\widehat{\psi}_{\ell'})^{[\frac{1}{2}]} \right)^{[0]} &= \Gamma_{+\frac{1}{2} -\frac{1}{2} \rightarrow 0}^{\frac{1}{2} \frac{1}{2}} \left((\widehat{\psi}_\ell)_{+\frac{1}{2}}^{[\frac{1}{2}]} (\widehat{\psi}_{\ell'})_{-\frac{1}{2}}^{[\frac{1}{2}]} \right) + \Gamma_{-\frac{1}{2} +\frac{1}{2} \rightarrow 0}^{\frac{1}{2} \frac{1}{2}} \left((\widehat{\psi}_\ell)_{-\frac{1}{2}}^{[\frac{1}{2}]} (\widehat{\psi}_{\ell'})_{+\frac{1}{2}}^{[\frac{1}{2}]} \right) \\
&= -\frac{1}{\sqrt{2}} \left(\widehat{c}_{\ell\downarrow} \widehat{c}_{\ell'\uparrow} + \widehat{c}_{\ell\uparrow} \widehat{c}_{\ell'\downarrow} \right). \tag{2.129}
\end{aligned}$$

The reduced matrix elements for these elementary operators with respect to the above local basis are readily

obtained using the Wigner–Eckart theorem:

$$\begin{aligned}
 \langle\langle 0, 1 | (\widehat{\psi}_\ell)^{[1/2]} | 1/2, 1 \rangle\rangle &= \frac{1}{\Gamma_{\substack{1/2 & 1/2 & \rightarrow 0 \\ +1/2 & -1/2 & \rightarrow 0}}} \langle 0, 1, 0 | (\widehat{\psi}_\ell)^{[1/2]} | 1/2, 1, +1/2 \rangle = \sqrt{2} \langle 0 | \widehat{c}_{\ell\uparrow} | \uparrow \rangle = \sqrt{2}, \\
 \langle\langle 1/2, 1 | (\widehat{\psi}_\ell)^{[1/2]} | 0, 2 \rangle\rangle &= \frac{1}{\Gamma_{\substack{0 & 1/2 & \rightarrow 1/2 \\ 0 & -1/2 & \rightarrow -1/2}}} \langle 1/2, 1, -1/2 | (\widehat{\psi}_\ell)^{[1/2]} | 0, 2, 0 \rangle = \langle \downarrow | \widehat{c}_{\ell\uparrow} | \uparrow\downarrow \rangle = 1, \\
 \langle\langle 0, 2 | (\widehat{\psi}_\ell^\dagger)^{[1/2]} | 1/2, 1 \rangle\rangle &= (-1)^{1/2+1/2-0} \sqrt{\frac{1+1}{0+1}} \langle\langle 1/2, 1 | (\widehat{\psi}_\ell)^{[1/2]} | 0, 2 \rangle\rangle^* = -\sqrt{2}, \\
 \langle\langle 1/2, 1 | (\widehat{\psi}_\ell^\dagger)^{[1/2]} | 0, 1 \rangle\rangle &= (-1)^{0+1/2-1/2} \sqrt{\frac{0+1}{1+1}} \langle\langle 0, 1 | (\widehat{\psi}_\ell)^{[1/2]} | 1/2, 1 \rangle\rangle^* = 1.
 \end{aligned} \tag{2.130}$$

Example: Charge-SU(2)

For a bipartite hopping graph, i. e., a bipartition of all lattice sites into two subsets A and B such that sites from A are only connected to sites from B and vice versa, the system may have another SU(2) symmetry that is related to the particle number – depending on parameters such as chemical potential. Setting $\epsilon_\ell = +1$ for $\ell \in A$ and $\epsilon_\ell = -1$ for $\ell \in B$, one can define these operators that obey the $\mathfrak{su}(2)$ commutation relations:

$$\begin{aligned}
 \widehat{J}_C^{(x)} &= \sum_{\ell=1}^L \frac{\epsilon_\ell}{2} \left(\widehat{c}_{\ell\uparrow}^\dagger \widehat{c}_{\ell\downarrow}^\dagger + \widehat{c}_{\ell\downarrow} \widehat{c}_{\ell\uparrow} \right) & \Rightarrow & \widehat{J}_C^{(+)} = \widehat{J}_C^{(x)} + i\widehat{J}_C^{(y)} = \sum_{\ell=1}^L \epsilon_\ell \widehat{c}_{\ell\uparrow}^\dagger \widehat{c}_{\ell\downarrow}^\dagger, \\
 \widehat{J}_C^{(y)} &= \sum_{\ell=1}^L \frac{\epsilon_\ell}{2i} \left(\widehat{c}_{\ell\uparrow}^\dagger \widehat{c}_{\ell\downarrow}^\dagger - \widehat{c}_{\ell\downarrow} \widehat{c}_{\ell\uparrow} \right) & \Rightarrow & \widehat{J}_C^{(-)} = \widehat{J}_C^{(x)} - i\widehat{J}_C^{(y)} = \sum_{\ell=1}^L \epsilon_\ell \widehat{c}_{\ell\downarrow} \widehat{c}_{\ell\uparrow}, \\
 \widehat{J}_C^{(z)} &= \frac{1}{2} \sum_{\ell=1}^L \left(\widehat{c}_{\ell\uparrow}^\dagger \widehat{c}_{\ell\uparrow} - \widehat{c}_{\ell\downarrow} \widehat{c}_{\ell\downarrow}^\dagger \right),
 \end{aligned} \tag{2.131}$$

with

$$\begin{aligned}
 \left[\widehat{J}_C^{(+)} , \widehat{J}_C^{(-)} \right] &= \sum_{\ell, \ell'=1}^L \epsilon_\ell \epsilon_{\ell'} \left[\widehat{c}_{\ell\uparrow}^\dagger \widehat{c}_{\ell\downarrow}^\dagger , \widehat{c}_{\ell'\downarrow} \widehat{c}_{\ell'\uparrow} \right] = \sum_{\ell, \ell'=1}^L \epsilon_\ell \epsilon_{\ell'} \left(\delta_{\ell\ell'} \widehat{c}_{\ell\uparrow}^\dagger \widehat{c}_{\ell\uparrow} - \delta_{\ell\ell'} \widehat{c}_{\ell\downarrow} \widehat{c}_{\ell\downarrow}^\dagger \right) = 2\widehat{J}_C^{(z)}, \\
 \left[\widehat{J}_C^{(z)} , \widehat{J}_C^{(+)} \right] &= \sum_{\ell, \ell'=1}^L \frac{\epsilon_{\ell'}}{2} \left[\widehat{c}_{\ell\uparrow}^\dagger \widehat{c}_{\ell\uparrow} - \widehat{c}_{\ell\downarrow} \widehat{c}_{\ell\downarrow}^\dagger , \widehat{c}_{\ell'\uparrow}^\dagger \widehat{c}_{\ell'\downarrow} \right] = \sum_{\ell, \ell'=1}^L \frac{\epsilon_{\ell'}}{2} \left(\delta_{\ell\ell'} \widehat{c}_{\ell\uparrow}^\dagger \widehat{c}_{\ell\downarrow}^\dagger + \delta_{\ell\ell'} \widehat{c}_{\ell\downarrow} \widehat{c}_{\ell\uparrow} \right) = \widehat{J}_C^{(+)}.
 \end{aligned} \tag{2.132}$$

These operators are called charge-pseudospin operators, as they behave like spin operators do, but are not actual spin operators. The z component measures the particle number in relation to half-filling, and the ladder operators increase or decrease the particle number by two instead of increasing or decreasing the spin projection quantum number. If the charge-pseudospin symmetry is broken and only persists around one axis, the remaining symmetry is a $U(1)_{\text{charge}}$ symmetry. In particular, a $U(1)$ symmetry in the charge sector around the z axis corresponds to the usual particle number conservation. All the algebraic results for the treatment of angular momentum in quantum mechanics also apply to the case of charge-pseudospin. In particular, the irreducible representations can be labelled by a pseudospin quantum number, its projection (which corresponds to the particle number difference to half-filling), and a degeneracy label. The local basis of states $|\mathbf{n}_\ell, \nu_\ell, \mathbf{n}_\ell^{(z)}\rangle$ can thus also be written in terms of quantum numbers of this symmetry (here, a site-dependent prefactor ϵ_ℓ is inserted into the doubly occupied state):

$$\begin{aligned}
 |0\rangle &= |1/2, 1, -1/2\rangle, \\
 |\uparrow\rangle &= |0, 1, 0\rangle, \\
 |\downarrow\rangle &= |0, 2, 0\rangle, \\
 \epsilon_\ell |\uparrow\downarrow\rangle &= |1/2, 1, +1/2\rangle.
 \end{aligned} \tag{2.133}$$

For these states one also finds $\widehat{J}_C^2 |n_\ell, \nu_\ell, n_\ell^{(z)}\rangle = n_\ell(n_\ell + 1) |n_\ell, \nu_\ell, n_\ell^{(z)}\rangle$, $\widehat{J}_C^{(z)} |n_\ell, \nu_\ell, n_\ell^{(z)}\rangle = n_\ell^{(z)} |n_\ell, \nu_\ell, n_\ell^{(z)}\rangle$ and $\widehat{J}_C^{(\pm)} |n_\ell, \nu_\ell, n_\ell^{(z)}\rangle = \sqrt{(n_\ell \mp n_\ell^{(z)})(n_\ell \pm n_\ell^{(z)} + 1)} |n_\ell, \nu_\ell, n_\ell^{(z)} \pm 1\rangle$, as required. This also means that on the space spanned by these states one finds $\widehat{J}_S^2 + \widehat{J}_C^2 = \frac{3}{4} \text{id}$. Just as in the case of the spin operator, the local charge-pseudospin operator is not an irreducible tensor operator, but it can be rescaled:

$$(\widehat{C}_\ell)^{[1]} = \begin{pmatrix} (\widehat{C}_\ell)_1^{[1]} \\ (\widehat{C}_\ell)_0^{[1]} \\ (\widehat{C}_\ell)_{-1}^{[1]} \end{pmatrix} = \begin{pmatrix} -\frac{1}{\sqrt{2}} \widehat{J}_{C,\ell}^{(+)} \\ \widehat{J}_{C,\ell}^{(z)} \\ \frac{1}{\sqrt{2}} \widehat{J}_{C,\ell}^{(-)} \end{pmatrix},$$

$$\text{with } [\widehat{J}_C^{(z)}, (\widehat{C}_\ell)_m^{[1]}] = m (\widehat{C}_\ell)_m^{[1]}, \text{ and } [\widehat{J}_C^{(\pm)}, (\widehat{C}_\ell)_m^{[1]}] = \sqrt{(1 \mp m)(2 \pm m)} (\widehat{C}_\ell)_{m \pm 1}^{[1]}. \quad (2.134)$$

Of course, for this operator the identity $\widehat{J}_{C,\ell} \cdot \widehat{J}_{C,\ell'} = -\sqrt{3} \left((\widehat{C}_\ell)^{[1]} \star (\widehat{C}_{\ell'})^{[1]} \right)^{[0]}$ holds, too. The irreducible tensor operator of fermionic operators cannot be made of either creators or annihilators only, but must contain an annihilator and a creator:

$$\begin{aligned} (\widehat{\psi}_\ell)^{[1/2]} &= \begin{pmatrix} (\widehat{\psi}_\ell)_{+1/2}^{[1/2]} \\ (\widehat{\psi}_\ell)_{-1/2}^{[1/2]} \end{pmatrix} = \begin{pmatrix} \epsilon_{\ell} \widehat{c}_{\ell\downarrow}^\dagger \\ -\widehat{c}_{\ell\uparrow} \end{pmatrix}, \quad \text{and its adjoint} \\ (\widehat{\psi}_\ell^\dagger)^{[1/2]} &= \begin{pmatrix} (\widehat{\psi}_\ell^\dagger)_{+1/2}^{[1/2]} \\ (\widehat{\psi}_\ell^\dagger)_{-1/2}^{[1/2]} \end{pmatrix} = \begin{pmatrix} (-1)^{1/2-1/2} \left((\widehat{\psi}_\ell)_{-1/2}^{[1/2]} \right)^\dagger \\ (-1)^{1/2+1/2} \left((\widehat{\psi}_\ell^\dagger)_{+1/2}^{[1/2]} \right)^\dagger \end{pmatrix} = \begin{pmatrix} -\widehat{c}_{\ell\uparrow}^\dagger \\ -\epsilon_{\ell} \widehat{c}_{\ell\downarrow} \end{pmatrix}. \end{aligned} \quad (2.135)$$

Analogously to the spin case, the sign factors $\widehat{s}_1 \cdots \widehat{s}_{\ell-1}$ have to be split from the definition of the operators to make these act locally. The sign operators commute with the generators of $\text{SU}(2)_{\text{charge}}$ and are thus compatible with the symmetry.

The reduced matrix elements of the fermionic operators are given by

$$\begin{aligned} \langle\langle 0, 2 | (\widehat{\psi}_\ell)^{[1/2]} | 1/2, 1 \rangle\rangle &= \frac{1}{\Gamma_{+1/2-1/2 \rightarrow 0}^{1/2 \ 1/2 \rightarrow 0}} \langle 0, 2, 0 | (\widehat{\psi}_\ell)_{-1/2}^{[1/2]} | 1/2, 1, +1/2 \rangle = \sqrt{2} \langle \downarrow | -\widehat{c}_{\ell\uparrow} \epsilon_{\ell} | \uparrow \downarrow \rangle = -\sqrt{2} \epsilon_{\ell}, \\ \langle\langle 1/2, 1 | (\widehat{\psi}_\ell)^{[1/2]} | 0, 1 \rangle\rangle &= \frac{1}{\Gamma_{0-1/2 \rightarrow -1/2}^{0 \ 1/2 \rightarrow 1/2}} \langle 1/2, 1, -1/2 | (\widehat{\psi}_\ell)_{-1/2}^{[1/2]} | 0, 1, 0 \rangle = \langle 0 | -\widehat{c}_{\ell\uparrow} | \uparrow \rangle = -1, \\ \langle\langle 0, 1 | (\widehat{\psi}_\ell^\dagger)^{[1/2]} | 1/2, 1 \rangle\rangle &= (-1)^{1/2+1/2-0} \sqrt{\frac{1+1}{0+1}} \langle\langle 1/2, 1 | (\widehat{\psi}_\ell)^{[1/2]} | 0, 1 \rangle\rangle^* = \sqrt{2}, \\ \langle\langle 1/2, 1 | (\widehat{\psi}_\ell^\dagger)^{[1/2]} | 0, 2 \rangle\rangle &= (-1)^{0+1/2-1/2} \sqrt{\frac{0+1}{1+1}} \langle\langle 0, 2 | (\widehat{\psi}_\ell)^{[1/2]} | 1/2, 1 \rangle\rangle^* = -\epsilon_{\ell}. \end{aligned} \quad (2.136)$$

By multiplying these operators, the following hopping terms can be obtained:

$$\begin{aligned} \left((\widehat{\psi}_\ell^\dagger)^{[1/2]} \star (\widehat{\psi}_{\ell'})^{[1/2]} \right)^{[0]} &= \Gamma_{+1/2-1/2 \rightarrow 0}^{1/2 \ 1/2 \rightarrow 0} (\widehat{\psi}_\ell^\dagger)_{+1/2}^{[1/2]} (\widehat{\psi}_{\ell'})_{-1/2}^{[1/2]} + \Gamma_{-1/2+1/2 \rightarrow 0}^{1/2 \ 1/2 \rightarrow 0} (\widehat{\psi}_\ell^\dagger)_{-1/2}^{[1/2]} (\widehat{\psi}_{\ell'})_{+1/2}^{[1/2]} \\ &= \frac{1}{\sqrt{2}} \left(\widehat{c}_{\ell\uparrow}^\dagger \widehat{c}_{\ell'\uparrow} + \epsilon_{\ell} \epsilon_{\ell'} \widehat{c}_{\ell\downarrow} \widehat{c}_{\ell'\downarrow}^\dagger \right) = \frac{1}{\sqrt{2}} \left(\widehat{c}_{\ell\uparrow}^\dagger \widehat{c}_{\ell'\uparrow} - \epsilon_{\ell} \epsilon_{\ell'} \widehat{c}_{\ell\downarrow}^\dagger \widehat{c}_{\ell\downarrow} + \delta_{\ell\ell'} \right), \\ \left((\widehat{\psi}_\ell)^{[1/2]} \star (\widehat{\psi}_{\ell'})^{[1/2]} \right)^{[0]} &= \Gamma_{+1/2-1/2 \rightarrow 0}^{1/2 \ 1/2 \rightarrow 0} (\widehat{\psi}_\ell)_{+1/2}^{[1/2]} (\widehat{\psi}_{\ell'})_{-1/2}^{[1/2]} + \Gamma_{-1/2+1/2 \rightarrow 0}^{1/2 \ 1/2 \rightarrow 0} (\widehat{\psi}_\ell)_{-1/2}^{[1/2]} (\widehat{\psi}_{\ell'})_{+1/2}^{[1/2]} \\ &= \frac{1}{\sqrt{2}} \left(\epsilon_{\ell} \widehat{c}_{\ell\downarrow}^\dagger \widehat{c}_{\ell'\uparrow} + \epsilon_{\ell'} \widehat{c}_{\ell'\downarrow}^\dagger \widehat{c}_{\ell\uparrow} \right). \end{aligned}$$

For Hamilton operators with a bipartite hopping, the first term in Equation (2.137) simplifies since $\epsilon_{\ell\ell'} = -1$ for lattice sites that are connected via hopping. If the irreducible tensor operator with interchanged values for ℓ and ℓ' is added, the result is a spin-independent usual hopping term between the lattice sites ℓ and ℓ' . Thus, $SU(2)_{\text{charge}}$ might be a symmetry for Hamilton operators with bipartite hopping. A crucial ingredient for this, however, was introducing the staggered prefactor $\epsilon_{\ell} = \pm 1$. Although the $\mathfrak{su}(2)$ algebra would also be compatible with generators $\widehat{J}_{C'}$ without the sign factor, the usual hopping term could not be constructed with this choice of generators. Therefore, the usual definition of charge-pseudospin incorporates ϵ_{ℓ} in the x and y component.

Indeed, the two $SU(2)$ symmetries whose Lie algebras are generated by the operators in Equation (2.118) and Equation (2.131) do not interfere with each other and can be present at the same time, because their generators mutually commute:

$$\left[\widehat{J}_S^{(+)}, \widehat{J}_C^{(+)} \right] = \left[\widehat{J}_S^{(+)}, \widehat{J}_C^{(-)} \right] = \left[\widehat{J}_S^{(+)}, \widehat{J}_C^{(z)} \right] = \left[\widehat{J}_S^{(z)}, \widehat{J}_C^{(+)} \right] = \left[\widehat{J}_S^{(z)}, \widehat{J}_C^{(z)} \right] = 0. \quad (2.137)$$

Therefore, a system with an $SU(2)_{\text{spin}}$ symmetry and an $SU(2)_{\text{charge}}$ symmetry is also symmetric under the product $SU(2)_{\text{spin}} \otimes SU(2)_{\text{charge}}$, which is almost $SO(4)$ (the Lie algebras are isomorphic, i. e., $\mathfrak{su}(2) \oplus \mathfrak{su}(2) \cong \mathfrak{so}(4)$). In the presence of both symmetries, the degeneracies that appeared for the physical basis states are lifted: the doubly-degenerate spin singlet states $|0\rangle$ and $\epsilon_{\ell} |\uparrow\downarrow\rangle$ are components of the pseudospin doublet, and the doubly-degenerate pseudospin singlet states $|\uparrow\rangle$ and $|\downarrow\rangle$ constitute a spin doublet. For all states, the index that labels the irreducible representation is just the concatenations of the corresponding spin and pseudospin quantum number, and analogously, the index that counts the states within an irreducible representation is just the concatenation of the projection quantum numbers. With this, the local electronic Hilbert space can be written in terms of symmetry-adapted states:

$$\begin{aligned} |0\rangle &= |(0, \frac{1}{2}), 1, (0, -\frac{1}{2})\rangle, \\ |\uparrow\rangle &= |(\frac{1}{2}, 0), 1, (+\frac{1}{2}, 0)\rangle, \\ |\downarrow\rangle &= |(\frac{1}{2}, 0), 1, (-\frac{1}{2}, 0)\rangle, \\ \epsilon_{\ell} |\uparrow\downarrow\rangle &= |(0, \frac{1}{2}), 1, (0, +\frac{1}{2})\rangle. \end{aligned} \quad (2.138)$$

A set of operators now is an irreducible tensor operator of rank (r_S, r_C) , if the commutation relations with the generators of the spin symmetry correspond to an irreducible tensor operator of rank r_S , and the commutation relations with the generators of the charge symmetry correspond to an irreducible tensor operator of rank r_C . The previously defined local spin and pseudospin operators are irreducible tensor operators of rank $(1, 0)$ and $(0, 1)$, respectively. The adapted version of the Wigner–Eckart theorem reads

$$\begin{aligned} &\langle (j'_S, j'_C), \alpha', (m'_S, m'_C) | \widehat{T}_{n_S, n_C}^{[k_S, k_C]} | (j_S, j_C), \alpha, (m_S, m_C) \rangle \\ &= \Gamma_{m_S n_S \rightarrow m'_S}^{j_S k_S} \Gamma_{m_C n_C \rightarrow m'_C}^{j_C k_C} \langle (j'_S, j'_C), \alpha' | \widehat{T}^{[k_S, k_C]} | (j_S, j_C), \alpha \rangle. \end{aligned} \quad (2.139)$$

Electronic creators and annihilators can be combined into an irreducible tensor operator of rank $(\frac{1}{2}, \frac{1}{2})$:

$$\widehat{\psi}_{\ell}^{[\frac{1}{2}, \frac{1}{2}]} = \begin{pmatrix} (\widehat{\psi}_{\ell})_{+\frac{1}{2}, +\frac{1}{2}}^{[\frac{1}{2}, \frac{1}{2}]} \\ (\widehat{\psi}_{\ell})_{+\frac{1}{2}, -\frac{1}{2}}^{[\frac{1}{2}, \frac{1}{2}]} \\ (\widehat{\psi}_{\ell})_{-\frac{1}{2}, +\frac{1}{2}}^{[\frac{1}{2}, \frac{1}{2}]} \\ (\widehat{\psi}_{\ell})_{-\frac{1}{2}, -\frac{1}{2}}^{[\frac{1}{2}, \frac{1}{2}]} \end{pmatrix} = \begin{pmatrix} \epsilon_{\ell} \widehat{c}_{\ell\uparrow}^{\dagger} \\ \widehat{c}_{\ell\downarrow} \\ \epsilon_{\ell} \widehat{c}_{\ell\downarrow}^{\dagger} \\ -\widehat{c}_{\ell\uparrow} \end{pmatrix}, \quad (2.140)$$

with

$$\begin{aligned} \left[\widehat{J}_S^{(\pm)}, (\widehat{\psi}_\ell)_{m_S, m_C}^{[1/2, 1/2]} \right] &= \frac{\sqrt{(1 \mp 2m_S)(3 \pm 2m_S)}}{2} (\widehat{\psi}_\ell)_{m_S \pm 1, m_C}^{[1/2, 1/2]}, & \left[\widehat{J}_S^{(z)}, (\widehat{\psi}_\ell)_{m_S, m_C}^{[1/2, 1/2]} \right] &= m_S (\widehat{\psi}_\ell)_{m_S, m_C}^{[1/2, 1/2]}, \\ \left[\widehat{J}_C^{(\pm)}, (\widehat{\psi}_\ell)_{m_S, m_C}^{[1/2, 1/2]} \right] &= \frac{\sqrt{(1 \mp 2m_C)(3 \pm 2m_C)}}{2} (\widehat{\psi}_\ell)_{m_S, m_C \pm 1}^{[1/2, 1/2]}, & \left[\widehat{J}_C^{(z)}, (\widehat{\psi}_\ell)_{m_S, m_C}^{[1/2, 1/2]} \right] &= m_C (\widehat{\psi}_\ell)_{m_S, m_C}^{[1/2, 1/2]}. \end{aligned} \quad (2.141)$$

With this irreducible tensor operator, one can construct this scalar operator for hopping:

$$\begin{aligned} \left((\widehat{\psi}_\ell)^{[1/2, 1/2]} \star (\widehat{\psi}_{\ell'})^{[1/2, 1/2]} \right)^{[0, 0]} &= \Gamma_{+\frac{1}{2} - \frac{1}{2} \rightarrow 0}^{\frac{1}{2} \frac{1}{2} \rightarrow 0} \Gamma_{+\frac{1}{2} - \frac{1}{2} \rightarrow 0}^{\frac{1}{2} \frac{1}{2} \rightarrow 0} (\widehat{\psi}_\ell)_{+\frac{1}{2}, +\frac{1}{2}}^{[1/2, 1/2]} (\widehat{\psi}_{\ell'})_{-\frac{1}{2}, -\frac{1}{2}}^{[1/2, 1/2]} + \Gamma_{+\frac{1}{2} - \frac{1}{2} \rightarrow 0}^{\frac{1}{2} \frac{1}{2} \rightarrow 0} \Gamma_{-\frac{1}{2} + \frac{1}{2} \rightarrow 0}^{\frac{1}{2} \frac{1}{2} \rightarrow 0} (\widehat{\psi}_\ell)_{+\frac{1}{2}, -\frac{1}{2}}^{[1/2, 1/2]} (\widehat{\psi}_{\ell'})_{-\frac{1}{2}, +\frac{1}{2}}^{[1/2, 1/2]} \\ &\quad + \Gamma_{-\frac{1}{2} + \frac{1}{2} \rightarrow 0}^{\frac{1}{2} \frac{1}{2} \rightarrow 0} \Gamma_{+\frac{1}{2} - \frac{1}{2} \rightarrow 0}^{\frac{1}{2} \frac{1}{2} \rightarrow 0} (\widehat{\psi}_\ell)_{-\frac{1}{2}, +\frac{1}{2}}^{[1/2, 1/2]} (\widehat{\psi}_{\ell'})_{+\frac{1}{2}, -\frac{1}{2}}^{[1/2, 1/2]} + \Gamma_{-\frac{1}{2} + \frac{1}{2} \rightarrow 0}^{\frac{1}{2} \frac{1}{2} \rightarrow 0} \Gamma_{-\frac{1}{2} + \frac{1}{2} \rightarrow 0}^{\frac{1}{2} \frac{1}{2} \rightarrow 0} (\widehat{\psi}_\ell)_{-\frac{1}{2}, -\frac{1}{2}}^{[1/2, 1/2]} (\widehat{\psi}_{\ell'})_{+\frac{1}{2}, +\frac{1}{2}}^{[1/2, 1/2]} \\ &= -\frac{\epsilon_\ell}{2} \widehat{c}_{\ell\uparrow}^\dagger \widehat{c}_{\ell'\uparrow} - \frac{\epsilon_{\ell'}}{2} \widehat{c}_{\ell\downarrow} \widehat{c}_{\ell'\downarrow}^\dagger - \frac{\epsilon_\ell}{2} \widehat{c}_{\ell\downarrow}^\dagger \widehat{c}_{\ell'\downarrow} - \frac{\epsilon_{\ell'}}{2} \widehat{c}_{\ell\uparrow} \widehat{c}_{\ell'\uparrow}^\dagger \\ &= \frac{\epsilon_{\ell'}}{2} \left(-\epsilon_\ell \epsilon_{\ell'} \widehat{c}_{\ell\uparrow}^\dagger \widehat{c}_{\ell'\uparrow} + \widehat{c}_{\ell'\uparrow}^\dagger \widehat{c}_{\ell\uparrow} - \epsilon_\ell \epsilon_{\ell'} \widehat{c}_{\ell\downarrow}^\dagger \widehat{c}_{\ell'\downarrow} + \widehat{c}_{\ell'\downarrow}^\dagger \widehat{c}_{\ell\downarrow} - 2\delta_{\ell\ell'} \right). \end{aligned} \quad (2.142)$$

For ℓ and ℓ' from different sublattices this yields the usual hopping term:

$$\left((\widehat{\psi}_\ell)^{[1/2, 1/2]} \star (\widehat{\psi}_{\ell'})^{[1/2, 1/2]} \right)^{[0, 0]} = \frac{\epsilon_{\ell'}}{2} \left(\widehat{c}_{\ell\uparrow}^\dagger \widehat{c}_{\ell'\uparrow} + \widehat{c}_{\ell'\uparrow}^\dagger \widehat{c}_{\ell\uparrow} + \widehat{c}_{\ell\downarrow}^\dagger \widehat{c}_{\ell'\downarrow} + \widehat{c}_{\ell'\downarrow}^\dagger \widehat{c}_{\ell\downarrow} \right). \quad (2.143)$$

The reduced matrix elements of this irreducible tensor operator are given by

$$\begin{aligned} \langle\langle (1/2, 0), 1 \mid (\widehat{\psi}_\ell)^{[1/2, 1/2]} \mid (0, 1/2), 1 \rangle\rangle &= \frac{1}{\Gamma_{0+\frac{1}{2} \rightarrow +\frac{1}{2}}^{\frac{1}{2} \frac{1}{2} \rightarrow \frac{1}{2}} \Gamma_{+\frac{1}{2} - \frac{1}{2} \rightarrow 0}^{\frac{1}{2} \frac{1}{2} \rightarrow 0}} \langle\langle (1/2, 0), 1, (+1/2, 0) \mid (\widehat{\psi}_\ell)_{+\frac{1}{2}, -\frac{1}{2}}^{[1/2, 1/2]} \mid (0, 1/2), 1, (0, +1/2) \rangle\rangle \\ &= \sqrt{2} \langle\uparrow \mid \widehat{c}_{\ell\downarrow} \mid \uparrow\rangle = -\sqrt{2} \epsilon_\ell, \\ \langle\langle (0, 1/2), 1 \mid (\widehat{\psi}_\ell)^{[1/2, 1/2]} \mid (1/2, 0), 1 \rangle\rangle &= \frac{1}{\Gamma_{-\frac{1}{2} + \frac{1}{2} \rightarrow 0}^{\frac{1}{2} \frac{1}{2} \rightarrow 0} \Gamma_{0+\frac{1}{2} \rightarrow +\frac{1}{2}}^{\frac{1}{2} \frac{1}{2} \rightarrow \frac{1}{2}}} \langle\langle (0, 1/2), 1(0, +1/2) \mid (\widehat{\psi}_\ell)_{+\frac{1}{2}, +\frac{1}{2}}^{[1/2, 1/2]} \mid (1/2, 0), 1, (-1/2, 0) \rangle\rangle \\ &= -\sqrt{2} \langle\uparrow \downarrow \mid \epsilon_\ell \cdot \epsilon_\ell \widehat{c}_{\ell\uparrow}^\dagger \mid \downarrow\rangle = -\sqrt{2}. \end{aligned} \quad (2.144)$$

The other two reduced matrix elements vanish due to symmetry.

2.4 – Construction & Compression of Matrix Product Operators

Construction of matrix product operators

In Section 2.1, the existence of an MPO representation for operators was discussed. However, it was not clear how to find this representation without evaluating $\dim(\mathcal{H})^2$ matrix elements for each operator. In the next part, an efficient construction procedure is presented. For this, it is advantageous to shift the perspective on the MPO tensors a little bit. Instead of tensors of order 4, they are understood as matrices of operators which act on the local Hilbert spaces by setting

$$\widehat{W}(\ell)_{k_{\ell-1} k_\ell} = \sum_{n_\ell, m_\ell} W(\ell)_{k_{\ell-1} m_\ell}^{k_\ell n_\ell} |m_\ell\rangle \langle n_\ell|. \quad (2.145)$$

Later, the construction procedure is generalized to systems with symmetries. In the case of a U(1) symmetry, the selection rules for the quantum number part of the indices dictate that only terms with $k_{\ell-1} + m_\ell = k_\ell + n_\ell$ contribute, thus leading to an irreducible tensor operator (with respect to the U(1) symmetry) of rank $t_\ell =$

$k_\ell - k_{\ell-1}$. In the case of an SU(2) symmetry, the matrix entry is a weighted sum of components of irreducible tensor operators (with respect to the SU(2) symmetry, by comparison with Equation (2.75)) with different ranks:

$$\begin{aligned}
 \widehat{W}(\ell)_{(\mathbf{k}_{\ell-1} \mathbf{k}_{\ell-1}^{(z)}) (\mathbf{k}_\ell \mathbf{k}_\ell^{(z)})} &= \sum_{\mathbf{n}_\ell, \mathbf{n}_\ell^{(z)}, \mathbf{m}_\ell, \mathbf{m}_\ell^{(z)}} W(\ell)_{\mathbf{k}_{\ell-1} \mathbf{k}_{\ell-1}^{(z)} \mathbf{m}_\ell \mathbf{m}_\ell^{(z)}}^{\mathbf{k}_\ell \mathbf{k}_\ell^{(z)} \mathbf{n}_\ell \mathbf{n}_\ell^{(z)}} |\mathbf{m}_\ell, \mathbf{m}_\ell^{(z)}\rangle \langle \mathbf{n}_\ell, \mathbf{n}_\ell^{(z)}| \\
 &= \sum_{\mathbf{t}_\ell, \mathbf{t}_\ell^{(z)}} \Gamma_{\mathbf{k}_{\ell-1} \mathbf{k}_{\ell-1}^{(z)} \mathbf{t}_\ell \mathbf{t}_\ell^{(z)} \rightarrow \mathbf{k}_\ell \mathbf{k}_\ell^{(z)}} \sum_{\mathbf{n}_\ell, \mathbf{m}_\ell} \overline{W}^{[\mathbf{t}_\ell]}(\ell)_{\mathbf{k}_{\ell-1} \mathbf{m}_\ell}^{\mathbf{k}_\ell \mathbf{n}_\ell} \sum_{\mathbf{n}_\ell^{(z)}, \mathbf{m}_\ell^{(z)}} \Gamma_{\mathbf{n}_\ell \mathbf{t}_\ell \rightarrow \mathbf{m}_\ell}^{\mathbf{n}_\ell^{(z)} \mathbf{t}_\ell^{(z)} \rightarrow \mathbf{m}_\ell^{(z)}} |\mathbf{m}_\ell, \mathbf{m}_\ell^{(z)}\rangle \langle \mathbf{n}_\ell, \mathbf{n}_\ell^{(z)}| \\
 &= \sum_{\mathbf{t}_\ell, \mathbf{t}_\ell^{(z)}} \Gamma_{\mathbf{k}_{\ell-1} \mathbf{k}_{\ell-1}^{(z)} \mathbf{t}_\ell \mathbf{t}_\ell^{(z)} \rightarrow \mathbf{k}_\ell \mathbf{k}_\ell^{(z)}} \widehat{W}_{\mathbf{t}_\ell^{(z)}}^{[\mathbf{t}_\ell]}(\ell)_{\mathbf{k}_{\ell-1} \mathbf{k}_\ell}.
 \end{aligned} \tag{2.146}$$

Indeed, for a non-Abelian symmetry it is by no means excluded that two quantum numbers $k_{\ell-1}$ and k_ℓ are connected via the triangle rule by more than one quantum number t_ℓ , e. g., for angular momenta $k_{\ell-1} = k_\ell = 1$, irreducible tensor operators of rank $t_\ell \in \{0, 1, 2\}$ can mediate between these quantum numbers.

The construction procedure for MPOs relies on iterative addition of terms with a certain range. An arbitrary operator on the Hilbert space (Equation (2.98)) takes the form

$$\widehat{O} = \sum_{x=1}^X \widehat{O}_x, \quad \text{with} \quad \widehat{O}_x = \widehat{O}(1)_x \otimes \widehat{O}(2)_x \otimes \cdots \otimes \widehat{O}(L)_x. \tag{2.147}$$

A typical summand \widehat{O}_x acts non-trivially only on some local Hilbert spaces. The range of a summand \widehat{O}_x is the distance between the first and the last non-trivial local operator plus one, e. g., for an anisotropic spin coupling, $\widehat{S}_2^{(z)} \widehat{S}_4^{(z)} = \text{id} \otimes \widehat{S}_2^{(z)} \otimes \text{id} \otimes \widehat{S}_4^{(z)} \otimes \text{id} \otimes \cdots \otimes \text{id}$, the range is 3. Often, but not always, the transfer operators in between the first and last non-trivial operator are simply identity operators or – in the case of fermionic creators and annihilators – sign operators. Bearing in mind the string of sign operators that accompany creators or annihilators and the fact that sign operators square to identity, a typical hopping term contains sign operators only at the sites between the first and last site.

The starting point for MPO construction are uniform \widehat{W} matrices with two identity operators on the diagonal:

$$\widehat{W}(\ell) = \begin{pmatrix} \text{id} & 0 \\ 0 & \text{id} \end{pmatrix}. \tag{2.148}$$

These identity operators are used as a skeleton for the MPO – if one wants to add an operator of range r that acts on the local Hilbert spaces ℓ to $\ell + r$, with a left and right trivial continuation on the local Hilbert spaces 1 to $\ell - 1$ and $\ell + r + 1$ to L , the upper left identities function as left trivial identity operators and the lower right identities function as right trivial identity operators. First, the MPO bond dimensions μ_ℓ to $\mu_{\ell+r-1}$ are incremented by one, and the new entries in the MPO matrices are initialized as zero operators. Second, the local operators of the term are inserted: the first operator is placed in the first row of $\widehat{W}(\ell)$ in the new column. The last operator is placed in the second column of $\widehat{W}(\ell+r)$ in the new row. The transfer operators in between are added in the corresponding new row and column. Scalar prefactors can be distributed over the entries arbitrarily. After the last term is added, the second row of $\widehat{W}(1)$ and the first column of $\widehat{W}(L)$ are deleted.

For example, a (spinless) fermionic system with three sites is considered, with a next-nearest-neighbor hopping Hamilton operator $\widehat{H} = -t\widehat{c}_1^\dagger \widehat{s}_1 \widehat{c}_2 + t\widehat{c}_1 \widehat{s}_1 \widehat{c}_2^\dagger - t'\widehat{c}_1^\dagger \widehat{s}_1 \widehat{s}_2 \widehat{c}_3 + t'\widehat{c}_1 \widehat{s}_1 \widehat{s}_2 \widehat{c}_3^\dagger - t\widehat{c}_2^\dagger \widehat{s}_2 \widehat{c}_3 + t\widehat{c}_2 \widehat{s}_2 \widehat{c}_3^\dagger$. Iteratively

adding these terms from left to right results in this MPO representation:

$$\widehat{\mathbf{W}}(1) = \begin{pmatrix} \text{id} & 0 & -t\widehat{c}_1^\dagger\widehat{s}_1 & t\widehat{c}_1\widehat{s}_1 & -t'\widehat{c}_1^\dagger\widehat{s}_1 & t'\widehat{c}_1\widehat{s}_1 \end{pmatrix},$$

$$\widehat{\mathbf{W}}(2) = \begin{pmatrix} \text{id} & 0 & 0 & 0 & -t\widehat{c}_2^\dagger\widehat{s}_2 & t\widehat{c}_2\widehat{s}_2 \\ 0 & \text{id} & 0 & 0 & 0 & 0 \\ 0 & \widehat{c}_2 & 0 & 0 & 0 & 0 \\ 0 & \widehat{c}_2^\dagger & 0 & 0 & 0 & 0 \\ 0 & 0 & \widehat{s}_2 & 0 & 0 & 0 \\ 0 & 0 & 0 & \widehat{s}_2 & 0 & 0 \end{pmatrix}, \quad \widehat{\mathbf{W}}(3) = \begin{pmatrix} 0 \\ \text{id} \\ \widehat{c}_3 \\ \widehat{c}_3^\dagger \\ \widehat{c}_3 \\ \widehat{c}_3^\dagger \end{pmatrix}, \quad (2.149)$$

and indeed, $\widehat{\mathbf{W}}(1)\widehat{\mathbf{W}}(2)\widehat{\mathbf{W}}(3) = \widehat{H}$. This is not an optimal MPO representation yet, which means that, without loss of information, another choice of matrices provides a smaller bond dimension. Later in this section, a lossless compression algorithm will be presented that optimizes the MPO representation.

In the case of symmetry-induced quantum numbers, the construction algorithm experiences small adaptations. First of all, permissible operators are components of irreducible tensor operators of a certain rank. Any summand from a decomposition as in Equation (2.98) has to have matching quantum numbers r and $r^{(z)}$. If the operator has a non-trivial quantum number $r \neq 0$, then the “skeleton identities” are placed in different quantum number blocks, i. e., the one connecting to the left is located in the trivial block $k_{\ell-1} = k_\ell = 0$ and the one connecting to the right is located in the target quantum number block $k_{\ell-1} = k_\ell = r$. For scalar operators such as the Hamilton operator, they are both placed in the trivial block by using the degeneracy indices $\gamma_{\ell-1} = \gamma_\ell = 1$ for the left and $\gamma_{\ell-1} = \gamma_\ell = 2$ for the right identity.

Moreover, for each summand there exists a sequence of irreducible representation quantum numbers ($k_0 = 0, k_1, \dots, k_L = r$) which specify the quantum number blocks in which the local irreducible tensor operators $\widehat{W}_{t_\ell^{(z)}}^{[t_\ell]}(\ell)_{k_{\ell-1}k_\ell}$ are placed. The process of adding a term to the MPO matrices is quite obvious: if the corresponding MPO bond quantum numbers do not already exist, they are appended. Afterwards, for each corresponding quantum number, the multiplicity is increased by one, so that the local irreducible tensor operator and its Clebsch–Gordan coefficient can be added at the right position. The first operator is located in the same row as the left identity operator and the last operator is located in the same column as the right identity operator. For example, a system of $L = 3$ quantum spins may be considered, with a Heisenberg Hamilton operator $\widehat{H} = -\sqrt{3}J_{12} \left((\widehat{\mathcal{S}}_1)^{[1]} \star (\widehat{\mathcal{S}}_2)^{[1]} \right)^{[0]} - \sqrt{3}J_{13} \left((\widehat{\mathcal{S}}_1)^{[1]} \star (\widehat{\mathcal{S}}_3)^{[1]} \right)^{[0]} - \sqrt{3}J_{23} \left((\widehat{\mathcal{S}}_2)^{[1]} \star (\widehat{\mathcal{S}}_3)^{[1]} \right)^{[0]}$ that couples the spins via nearest-neighbor exchange couplings J_{12} , J_{23} and a next-nearest-neighbor exchange coupling J_{13} (for display reasons, the Clebsch–Gordan coefficients $\Gamma_{k_{\ell-1}^{(z)} t_\ell^{(z)} \rightarrow k_\ell^{(z)}}^{k_{\ell-1} t_\ell \rightarrow k_\ell}$ are omitted and have to be multiplied coefficient-wise):

$$\left(\begin{array}{c|ccc|c} \widehat{\mathbf{W}}(1)/\Gamma & k_1 = 0, k_1^{(z)} = 0 & k_1 = 1, k_1^{(z)} = +1 & k_1 = 1, k_1^{(z)} = 0 & k_1 = 1, k_1^{(z)} = -1 \\ \hline k_0 = 0, k_0^{(z)} = 0 & \text{id} & 0 & (\widehat{S}_1)_{+1}^{[1]} & (\widehat{S}_1)_{+1}^{[1]} & (\widehat{S}_1)_0^{[1]} & (\widehat{S}_1)_0^{[1]} & (\widehat{S}_1)_{-1}^{[1]} & (\widehat{S}_1)_{-1}^{[1]} \end{array} \right),$$

$$\left(\begin{array}{c|cc|cc|cc|c} \widehat{\mathbf{W}}(2)/\Gamma & k_2 = 0, k_2^{(z)} = 0 & k_2 = 1, k_2^{(z)} = +1 & k_2 = 1, k_2^{(z)} = 0 & k_2 = 1, k_2^{(z)} = -1 \\ \hline k_1 = 0, k_1^{(z)} = 0 & \text{id} & 0 & 0 & (\widehat{S}_2)_{+1}^{[1]} & 0 & (\widehat{S}_2)_0^{[1]} & 0 & (\widehat{S}_2)_{-1}^{[1]} \\ \hline k_1 = 1, k_1^{(z)} = +1 & 0 & -\sqrt{3}J_{12}(\widehat{S}_2)_{-1}^{[1]} & 0 & 0 & 0 & 0 & 0 & 0 \\ \hline k_1 = 1, k_1^{(z)} = 0 & 0 & -\sqrt{3}J_{12}(\widehat{S}_2)_0^{[1]} & 0 & 0 & 0 & 0 & 0 & 0 \\ \hline k_1 = 1, k_1^{(z)} = -1 & 0 & -\sqrt{3}J_{12}(\widehat{S}_2)_{+1}^{[1]} & 0 & 0 & 0 & 0 & 0 & 0 \end{array} \right),$$

$$\left(\begin{array}{c|c} \widehat{\mathbf{W}}(3)/\Gamma & k_3 = 0, k_3^{(z)} = 0 \\ \hline k_2 = 0, k_2^{(z)} = 0 & 0 \\ \hline k_2 = 1, k_2^{(z)} = +1 & -\sqrt{3}J_{13}(\widehat{S}_3)_{-1}^{[1]} \\ \hline k_2 = 1, k_2^{(z)} = 0 & -\sqrt{3}J_{23}(\widehat{S}_3)_{-1}^{[1]} \\ \hline k_2 = 1, k_2^{(z)} = -1 & -\sqrt{3}J_{13}(\widehat{S}_3)_0^{[1]} \\ \hline & -\sqrt{3}J_{23}(\widehat{S}_3)_0^{[1]} \\ \hline & -\sqrt{3}J_{13}(\widehat{S}_3)_{+1}^{[1]} \\ \hline & -\sqrt{3}J_{23}(\widehat{S}_3)_{+1}^{[1]} \end{array} \right). \tag{2.150}$$

Compression of matrix product operators

For many operators used to compute observables, small bond dimensions are sufficient. Hopping correlators such as $\widehat{c}_{\ell\sigma}^\dagger \widehat{c}_{\ell'\sigma'}$ can be represented by an MPO of bond dimension 1, and even an observable such as the total spin projection, which acts on all local Hilbert spaces non-trivially, needs a bond dimension of only 2. However, Hamilton operators may need a larger bond dimension, in particular if they must encode interactions between non-adjacent sites. From Equation (2.149) and Equation (2.150) one can anticipate that the MPO construction algorithm does not generally lead to an optimal MPO representation of an operator. Moreover, algebraic operations on MPOs such as addition or multiplication can result in MPOs with high bond dimensions, whilst there are other MPO representations that describe the same operator.

The simplest approach to compress the MPO tensors is doing the same thing as in the case of an MPS, i. e., perform a singular value decomposition of the MPO tensors and discard the lowest singular values in order to reduce the bond dimension. More precisely, one MPO tensor after the other, the fourth order tensor is reshaped into a tensor of second order by combining both physical indices and the incoming MPO bond index into a multi-index with $\mu_{\ell-1}d_\ell^2$ possible values. The emerging matrix is subject to a numerical singular value decomposition. The diagonal matrix of singular values in the middle is truncated, and the unitary matrices on the left and on the right are cut accordingly. The first unitary matrix is used as the new local MPO tensor, and the diagonal matrix and the second unitary matrix are multiplied onto the next local MPO tensor, where the procedure is repeated.

While this SVD compression for MPOs helps in reducing the bond dimension, it comes with some caveats: since in contrast to states, operators do not have to be normalized, for large systems large values can aggregate and are shifted through the sites, yielding matrix entries of tremendously different magnitudes. This makes the SVD prone to numerical instability and errors, as Hubig et al. demonstrated [75]. Even if the norm is distributed uniformly over the extent of the system, they encountered problems with the SVD compression when it is applied on operators that contain projectors. A more recent and promising approach by Parker et al. tries to bring the operator for a chosen bond into a special form in which it separates into a strictly left part, a strictly right part and a part that connects both parts [76]. The SVD is then performed only on the connecting part, which usually contains operators acting in the adjacency of the chosen bond. In doing so, they overcome the problem of coexistence of extensive and intensive singular values.

Another approach to compression of MPOs makes use of the fact that for typical Hamilton operators some local operators occur several times at a given site, leading to possibly redundant information. This redundancy can be eliminated, so that the bond dimension is reduced without losing information. If one takes a closer look at Equation (2.149), it is obvious that some rows and columns are linear dependent and another choice of MPO matrices can be found that yield the same operator:

$$\widehat{\mathbf{W}}(1) = \begin{pmatrix} \text{id} & \widehat{c}_1^\dagger \widehat{s}_1 & \widehat{c}_1 \widehat{s}_1 \end{pmatrix}, \quad \widehat{\mathbf{W}}(2) = \begin{pmatrix} 0 & -t\widehat{c}_2^\dagger \widehat{s}_2 & t\widehat{c}_2 \widehat{s}_2 \\ -t\widehat{c}_2 & -t'\widehat{s}_2 & 0 \\ t\widehat{c}_2^\dagger & 0 & t'\widehat{s}_2 \end{pmatrix}, \quad \widehat{\mathbf{W}}(3) = \begin{pmatrix} \text{id} \\ \widehat{c}_3 \\ \widehat{c}_3^\dagger \end{pmatrix}. \quad (2.151)$$

If there exists a column in the matrix $\widehat{\mathbf{W}}(\ell)$ that linearly depends on other columns in that matrix and can thus be expressed as a linear combination, then this column can be deleted and at the next site, the entries of the corresponding row can be distributed among other rows. More precisely, let $x \in \{1, \dots, \mu_\ell\}$ be a column of operators that can be written as a linear combination of other columns, i. e.,

$$\widehat{\mathbf{W}}(\ell)_{k_{\ell-1}, k_\ell=x} = \sum_{k_\ell}^{\neq x} \lambda_{k_\ell} \widehat{\mathbf{W}}(\ell)_{k_{\ell-1}, k_\ell} \quad \forall k_{\ell-1} \in \{1, \dots, \mu_{\ell-1}\}. \quad (2.152)$$

Then it follows

$$\begin{aligned} \left(\widehat{\mathbf{W}}(\ell) \cdot \widehat{\mathbf{W}}(\ell+1) \right)_{k_{\ell-1}, k_{\ell+1}} &= \sum_{k_\ell} \widehat{\mathbf{W}}(\ell)_{k_{\ell-1}, k_\ell} \widehat{\mathbf{W}}(\ell+1)_{k_\ell, k_{\ell+1}} \\ &= \sum_{k_\ell}^{\neq x} \widehat{\mathbf{W}}(\ell)_{k_{\ell-1}, k_\ell} \widehat{\mathbf{W}}(\ell+1)_{k_\ell, k_{\ell+1}} + \sum_{k_\ell}^{\neq x} \lambda_{k_\ell} \widehat{\mathbf{W}}(\ell)_{k_{\ell-1}, k_\ell} \widehat{\mathbf{W}}(\ell+1)_{x, k_{\ell+1}} \\ &= \sum_{k_\ell}^{\neq x} \widehat{\mathbf{W}}(\ell)_{k_{\ell-1}, k_\ell} \left(\widehat{\mathbf{W}}(\ell+1)_{k_\ell, k_{\ell+1}} + \lambda_{k_\ell} \widehat{\mathbf{W}}(\ell+1)_{x, k_{\ell+1}} \right). \end{aligned} \quad (2.153)$$

This means that the value $k_\ell = x$ can be erased, if the rows of the next MPO matrix are summed according to the linear combination coefficients λ_{k_ℓ} . In the special case of a zero column, the corresponding row at the next site does not enter at all and can be deleted without further adjustments. Moreover, this procedure of course also works for linear dependent rows, where the corresponding column at the previous site has to be redistributed. A similar “delinearisation” compression algorithm was proposed by Hubig et al. in the above mentioned publication, from which the algorithm used for this thesis was inspired.

On a technical level, in order to find linear dependent columns, a matrix $\mathbf{M} \in \text{Mat}(\mu_{\ell-1}d_\ell^2, \mu_\ell)$ is constructed with entries $M_{(k_{\ell-1}n_\ell m_\ell)k_\ell} = W(\ell)_{k_{\ell-1}m_\ell}^{k_\ell n_\ell}$. Then, one after another, the x -th column $\mathbf{v}(x)$ is cut from the matrix, and with the remaining matrix $\mathbf{M}(x)$ the linear equation $\mathbf{M}(x)\mathbf{y}(x) = \mathbf{v}(x)$ is investigated numerically using standard algorithms (in the specific case of the VMPS implementation used for this thesis, a Householder QR decomposition from the C++ library Eigen was used [77]). If there exists a solution vector $\mathbf{y}(x)$, then the components are the coefficients with which the x -th column can be represented by the other columns.

An efficient implementation of the compression algorithm takes advantage of the fact that an update to any bond, i. e., resolving linear dependencies either among the columns of the left matrix or among the rows of the right matrix of a MPO matrix bond, has no effect on bonds further away. However, by changing the rows of an MPO matrix, new linear dependencies among the columns can be generated and vice versa, so that the immediately adjacent bonds are affected by a local update. Therefore, in a highly parallelized algorithm, all even bonds can be treated at the same time. When all linear dependence are detected and resolved, in the next step all odd bonds are investigated. This procedure stops when all linear dependencies are removed.

It is important to note that this compression algorithm reduces the bond dimension without truncation or loss of information, but rather uses algebraic operations to find a better representation of the same operator. Thus, the compressed MPO yields exactly the same operator up to machine precision (small errors are introduced by solving the system of linear equations and by floating point arithmetic). If the physical system under consideration is subject to any symmetries that are exploited in the tensor network, this algorithm easily works for reduced MPO tensors with reduced matrix elements as entries because it does not mix entries from different irreducible representations and therefore respects the symmetry requirements.

In the next chapter, some physical applications are presented, for which an efficient MPO representation was crucial. Typically, the bond dimension of the Hamilton operator could be reduced by some amount, but the compression of the square of the Hamilton operator (needed for convergence checks during the sweep process, Equation (2.49)) was highly beneficial, leading to an MPO representation with a much smaller bond dimension. Hubig et al. found out that with their “delinearisation” they could achieve optimal or near-optimal MPO representations for most operators with an intermediate implementation complexity and computational cost.

3 – Applications of Compressed Matrix Product Operators

3.1 – The Antiferromagnetic $S = 1/2$ Heisenberg Model on the C_{60} Fullerene Geometry

Model and technical notes

The fullerene molecule C_{60} is a molecule consisting of 60 carbon atoms in a cage geometry of a truncated icosahedron – the shape of a football. The truncated icosahedron contains 20 hexagonal and 12 pentagonal faces. One carbon atom is located at each corner point. Thus, each carbon atom is part of two hexagons and one pentagon. After its discovery in the 1980s, the molecule C_{60} quickly became well-known for its chemical properties [78]. Perhaps the most interesting feature for physicists is the superconductivity of an A_3C_{60} lattice with alkali metals placed in between the fullerene molecules, which might imply a non-phononic mechanism [5].

The electron configuration of the carbon atoms in C_{60} can be roughly conceptualized as follows: each carbon atom contributes six electrons, two of which are tightly bound to the atom in the 1s orbital. The 2s orbital and the in-plane $2p_x$ and $2p_y$ atomic orbitals hybridize to form three equivalent orbitals (sp^2 hybridization), which overlap with their counterparts at the neighboring atoms and form one occupied binding and one unoccupied anti-binding molecular orbital. Thus, three electrons form covalent σ -bonds with the three neighboring carbon atoms. The out-of-plane $2p_z$ orbitals also overlap, yielding molecular orbitals for π -bonds. These are the least strongly bound electrons for which an effective theory of itinerant electrons can be established in terms of the phenomenologically simple Hubbard model, while the electrons in sp^2 orbitals are assumed to form a static valence background:

$$\hat{H} = \sum_{i,j,\sigma} t_{ij} \hat{c}_{i\sigma}^\dagger \hat{c}_{j\sigma} + U \sum_i \hat{c}_{i\uparrow}^\dagger \hat{c}_{i\uparrow} \hat{c}_{i\downarrow}^\dagger \hat{c}_{i\downarrow}. \quad (3.1)$$

This tight-binding model, in which electrons can occupy localized Wannier orbitals in the vicinity of each atom, describes the hopping of an electron from a site i to a site j by a tunneling amplitude t_{ij} , and an on-site Coulomb repulsion U which causes electrons to avoid double occupancies at the same site. The rapid decrease in the overlap between atomic orbitals for longer distances leads to the nearest-neighbor approximation, in which only tunneling to the nearest sites is modelled explicitly. C_{60} has two different types of nearest-neighbor bonds: common edges of two hexagons and common edges of one hexagon and one pentagon. Although these bonds have slightly different lengths and orbital overlaps, the tunneling amplitudes are assumed to be uniform. Since each carbon atom contributes one electron, the model is considered at half-filling with $N = 60$ electrons.

However, the Hubbard model on the C_{60} geometry is still a hard problem. Therefore, a further simplification is made concerning the Coulomb repulsion: for strong U (as compared to tunneling amplitude t), the energetic cost of creating a double occupancy is much higher than the amount of energy gained by further delocalizing of electrons to different sites. This means that at half-filling all sites are singly occupied, freezing out the local electronic basis states $|0\rangle$ and $|\uparrow\downarrow\rangle$ and leaving only the basis states $|\uparrow\rangle$ and $|\downarrow\rangle$ of a spin of length $S = 1/2$. However, a residual interaction comes from a super-exchange mechanism that describes the virtual back-and-forth tunneling of an electron. This interaction couples the remaining spin degrees of freedom in an antiferromagnetic fashion, i. e., after projecting out the double occupancies, the Hubbard model is effectively described by the antiferromagnetic Heisenberg model in the low-energy sector:

$$\hat{H} = J \sum_{\langle i,j \rangle} \hat{\mathbf{S}}_i \hat{\mathbf{S}}_j. \quad (3.2)$$

Here $\langle i,j \rangle$ denotes nearest neighbors. The spin exchange interaction is given by $J = 4t^2/U$. Actually, C_{60} is in the intermediate- U regime in which this approximation is questionable (with estimated values of $t \sim 2\text{--}3\text{ eV}$

and $U \sim 9$ eV). Nevertheless, one can expect this model to catch essential features of the physics from the fact that a Hartree–Fock treatment of C_{60} shows a magnetically ordered phase for $U/t > 2.6$ [79]. Moreover, the non-bipartite geometry of C_{60} including pentagon faces that cannot accommodate a staggered spin configuration leads to potentially interesting physics on its own, being related to spin frustration.

The Heisenberg model of Equation (3.2) on the C_{60} geometry is investigated using the VMPS technique. This method is a reasonable choice because of the limited number of carbon atoms that have to be taken into account. The invariance of the model under rotations in spin space can be exploited by using the $SU(2)$ -symmetry-adapted VMPS code. C_{60} also has the spatial symmetry I_h , i. e., the icosahedral group with 120 elements whose action maps carbon atoms to equivalent carbon atoms at other sites. This symmetry is not exploited explicitly but is used as an additional convergence check for the calculations.

Since the fullerene geometry is 2D-like with three nearest neighbors per site, the numbering of the sites becomes non-trivial. Sites which are close to each other should also be close in the VMPS site numbering. One has to keep the average as well as the maximum distance of adjacent carbon atoms small. The Schlegel graph, which is a two-dimensional projection of a 3D-polyhedron with correct topological properties of neighborhood, helps to choose such a sensible numbering. The numbering chosen for the following calculations is shown in Figure 19, it is a spiral from outside to inside on the Schlegel graph.

Using this mapping to a linear chain, the efficient MPO construction algorithm yields an MPO with a maximum bond dimension $\mu = 38$, which can be reduced to $\mu = 35$ after compression. Other reasonable numberings lead to very similar MPO bond dimensions. The benefit is larger for the square of the Hamilton operator, because by multiplying two operators more linear dependencies can be introduced. This operator is essential in order to calculate the energy deviation of Equation (2.49) and thus to check the convergence of the calculation. The compression algorithm reduces the bond dimension of \widehat{H}^2 from $\mu = 1444$ to $\mu = 564$. Since the MPO bond dimension enters the operational effort for the full contraction up to quadratically, this speeds up the convergence calculations by roughly a factor of 4. However, the computational time is not the only relevant measure: for random enumerations of the sites without any effort to encode the spatial adjacency, the groundstate algorithm exhibits a much worse convergence behavior, being unable to restore the correct icosahedral symmetry of the correlation functions.

The groundstate calculations are quite costly. While only up to ten different irreducible representations of the spin symmetry are required for the matrix product state of the groundstate, each of these invariant subspaces reaches dimensions (due to the multiplicity of the irreducible representation) of several thousands. Therefore, the calculations take several days and require more than 100 gigabytes of RAM.

Results

With the VMPS method the energetically lowest states in the sectors of total-spin singlet and triplet as well as the lowest excited singlet state were obtained. The results are summarized in Table 1. An $SU(2)$ -adapted bond dimension (i. e., the sum of the multiplicities of all required irreducible representations, not weighted with the symmetry-induced dimension $2j + 1$ of the subspaces – the plain bond dimension needed for the same MPS representation without exploiting the symmetry is thus larger) limit of 10 000 is sufficient to represent the groundstates quite faithfully, with the largest multiplicity reaching 3 966.

The groundstate of the Heisenberg model on the fullerene geometry is indeed a spin singlet. Due to non-bipartiteness, this could not be deduced from Marshall’s theorem [80]. The groundstate energy per site is $E_0/L = -0.51886(1)$ and comes close to that of the 2D hexagonal lattice with $E_0/L \approx -0.55$ (all energies are given in units of the exchange coupling $J = 1$). The first excited state is a triplet, and at least one excited spin-singlet state lies in the energy range from this triplet state to the lowest quintet state.

To make a statement about spin correlation functions $\langle \widehat{S}_i \widehat{S}_j \rangle$, one can specify the positions i and j of the carbon atoms by the shortest path connecting both sites, as can be seen in Figure 18. For nearest neighbors

| Spin S | Energy E | Bond dimension $\chi_{\text{SU}(2)}$ | Deviance $\Delta E^2/L$ | Gap $E - E_0$ | GS overlap $ \langle \Psi_0 \Psi \rangle ^2$ |
|----------|------------|--------------------------------------|-------------------------|---------------|--|
| 0 | -31.131(7) | 10 000 | $8 \cdot 10^{-5}$ | - | - |
| 1 | -30.775(6) | 10 000 | $1.9 \cdot 10^{-4}$ | 0.356(0) | 0 |
| 0 | -30.440(9) | 10 000 | $1.6 \cdot 10^{-4}$ | 0.690(8) | $\sim 10^{-8}$ |

Table 1: VMPS results for the energetically lowest eigenstates of the Heisenberg model on the C_{60} geometry. $J = 1$ fixes the energy scale.

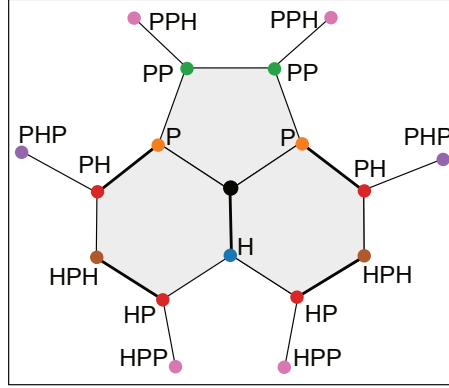


Figure 18: Visualization of the neighborhood of any site (black) in the C_{60} fullerene geometry. Points with the same color refer to equivalent lattice sites in the sense that they are connected by the same sequence of H and P bonds. Figure taken from [CP1].

with a distance of $d = 1$, there are two inequivalent types of bonds that can connect two sites: either they are connected by a common edge of two hexagons (“H bond”) or by a common edge of a hexagon and a pentagon (“P bond”). For next-nearest neighbors, one can either take the PP or the HP route (which is equivalent to PH), but HH does not exist because there is no vertex at which three hexagons meet. The corresponding values for the spin correlation function up to $d = 4$ are shown on the Schlegel graph in Figure 19 and as a histogram in Figure 20. In a perfectly converged groundstate that respects the icosahedral symmetry I_h , all equivalent tuples (i, j) would have the same correlation function $\langle \hat{S}_i \hat{S}_j \rangle$. Here, with a binsize of 0.003, the width of the distribution for equivalent tuples is another measure of the convergence of the MPS. The average value and the standard deviation are depicted in the legend of Figure 20.

The $d = 1$ H bonds show the strongest antiferromagnetic correlation. This seems quite natural, since hexagons per se are bipartite and a relatively strong correlation can effectively lower the energy. It comes remarkably close to the nearest-neighbor spin correlation function in the $L = 6$ antiferromagnetic Heisenberg ring. The antiferromagnetic spin correlation is less pronounced for the P bonds, since pentagons yield a frustrated geometry. This trend continues: sites which are connected by paths with alternating H and P bonds have the strongest correlation. Up to $d = 4$, the correlation function is strictly staggered, as expected for antiferromagnetically coupled spins. For $d > 4$ (not shown here), the spin correlation functions acquire mixed signs. An exponential fit of the decay of the correlation function with distance gives a correlation length of $\xi \approx 1.4$, implying that the spins are not strongly coupled over the entire molecule (with a maximum distance of $d = 9$). Thus, the pentagons seem to cause disorder.

The energetically lowest triplet state has an energy gap of $\Delta_S = E_0(S = 1) - E_0(S = 0) \approx 0.356$ to the groundstate. Its spin correlation function and its local spin expectation value $\langle \hat{S}_i \rangle$ are shown in Figure 21. The $SU(2)$ -symmetric VMPS implementation provides access to reduced matrix elements $\langle \psi^{[1]} | | \hat{S}_{\text{tot}}^{[1]} | | \psi^{[1]} \rangle$ in order to compute local magnetic moments without specifying any spatial direction. One can see that the local magnetic moment is localized on a ring consisting of 20 carbon atoms cycling around the molecule once, indicated by small arrows. This state is symmetry-broken in that sense that with the chosen site numbering,

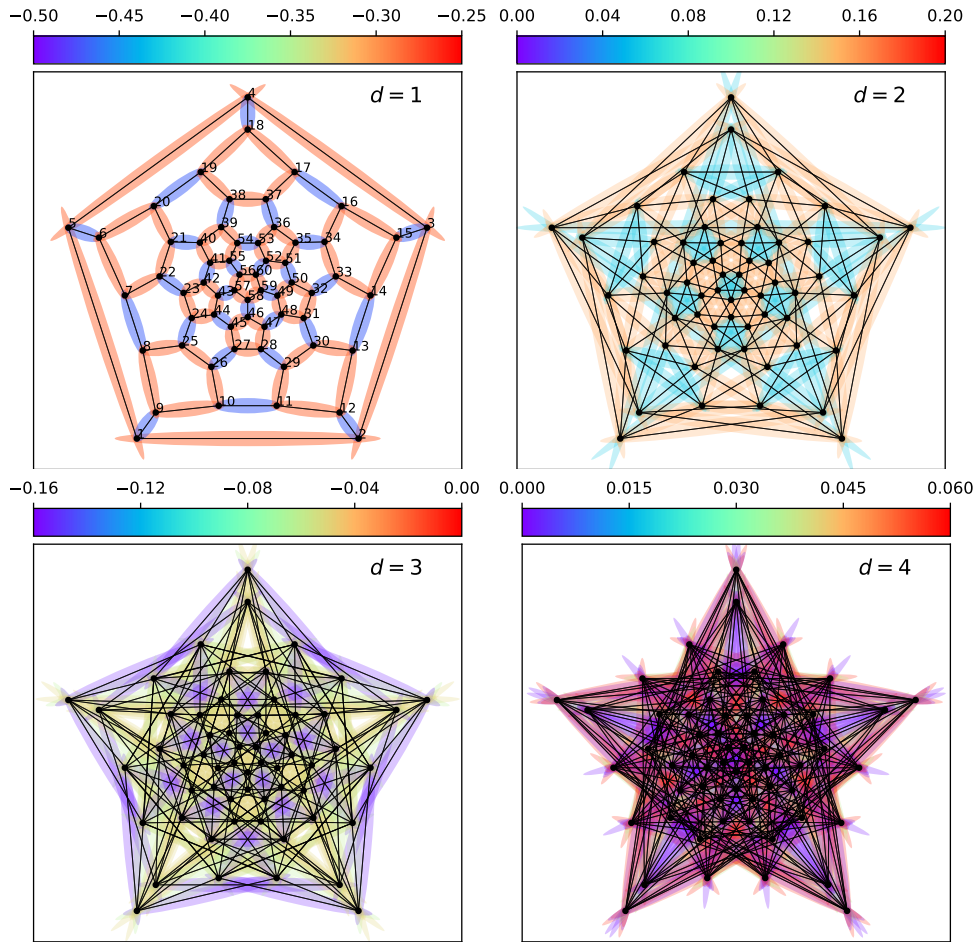


Figure 19: Spin-spin correlation function $\langle \hat{S}_i \hat{S}_j \rangle$ in the groundstate of the antiferromagnetic Heisenberg model on the fullerene geometry for spatial distances $d = 1, 2, 3, 4$ between the carbon atoms. In the upper left image, the numbering of the lattice sites can be seen. Figure taken from [CP1].

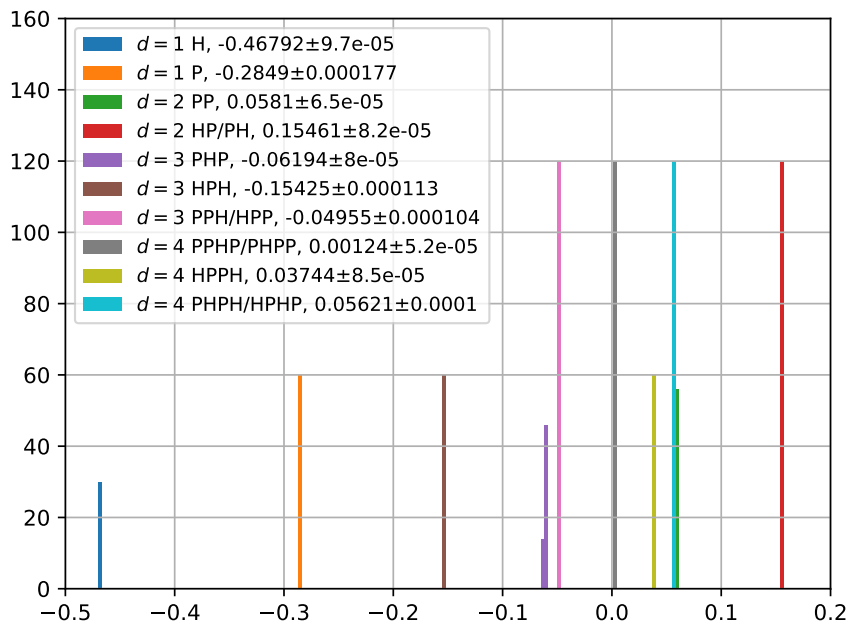


Figure 20: Histogram of the spin correlation function for different paths connecting the two spin sites. Figure taken from [CP1].

the VMPS technique always arrives at this configuration which selects a distinguished spatial orientation of the ring. Of course one can assume that due to the presence of the I_h symmetry, this state is part of an invariant subspace that also contains analogous states with other orientations of the excess spin ring. Since the smallest non-trivial irreducible representations of the icosahedral group are three-dimensional [81] and the triplet representation of $SU(2)$ is three-dimensional as well, it can be deduced that this lowest triplet state is at least nine-fold degenerate.

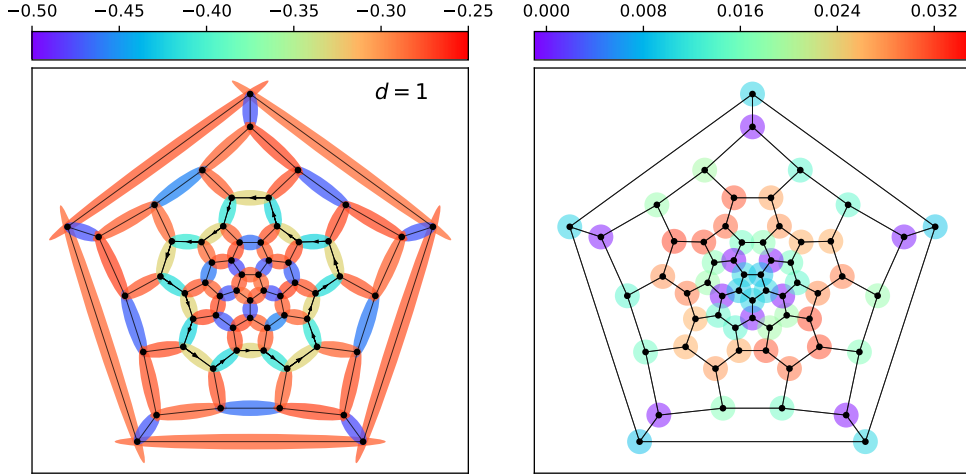


Figure 21: Nearest-neighbor spin correlation function and local spin expectation value for the groundstate of the antiferromagnetic Heisenberg model on the C_{60} fullerene geometry in the triplet sector. Figure taken from [CP1].

The first excited singlet state can be obtained by modifying the Hamilton operator $\hat{H}' = \hat{H} + E_{\text{pen}} |\Psi_0\rangle\langle\Psi_0|$ with a sufficiently strong energy penalty E_{pen} that projects out the former groundstate, so that the first excited state now becomes the groundstate. Formally, it would be possible to take the projector $|\Psi_0\rangle\langle\Psi_0|$ as an MPO and add it to the Hamilton operator. However, this is practically unfeasible because this MPO would have a bond dimension that equals the square of the MPS bond dimension. Nevertheless, it is possible to perform this projection on the fly in the local optimization process, for example with a modified Lanczos solver [49]. The energy of the first excited singlet lies significantly above the lowest triplet state, which is not typical for frustrated spin systems, as geometrical frustration in antiferromagnets usually comes along with various configurations to align the spins which are very close in energy. The spin correlation also shows a ring of altered values similar to the case of the triplet state, again indicating degeneracy of this state.

All in all, the antiferromagnetic Heisenberg model on the C_{60} fullerene geometry is very suitable to be analyzed within the VMPS framework. The correlation functions decay quickly, so that the molecule is not correlated across its whole extent. The hexagon faces in between the geometrically frustrating pentagon faces mitigate the spin frustration: the spins are highly correlated along bonds between two hexagons, while the spin correlations along the bonds between a hexagon and a pentagon are weaker as compared to an isolated $L = 5$ Heisenberg ring, meaning that the environment provides a way for the spins on the pentagon to disregard their neighbors in the same pentagon. Beyond what is rephrased here, in the publication [CP1] thermodynamic properties such as the temperature-dependent specific heat and spin susceptibility were investigated.

3.2 – Magnetic Properties of a Capped Kagome Molecule with 60 Quantum Spins

Model and technical notes

Building upon the study of the antiferromagnetic Heisenberg model on the C_{60} fullerene geometry, the same model is studied with another cage-like geometry, namely a molecular structure called *sodalite cage* in chemistry [82]. This geometry resembles a cage-like version of the capped kagome lattice. It can be conceptualized as follows: starting from a regular octahedron, the first step is a truncation, i. e., chopping off a pyramid at each of the six corners (leaving a polyhedron with eight regular hexagons and six squares), followed by a rectification step, in which all corners are again cut off. The resulting rectified, truncated octahedron is a polyhedron with 24 triangles, eight hexagons and six squares. This geometry, which is shown in Figure 22, already has two inequivalent types of vertices: vertices at which two hexagons and two triangles meet (green) and vertices at which one square, one hexagon and two triangles meet (blue). These vertices pose the inner layer of the sodalite cage geometry. Additionally, above each triangle another vertex is placed (red), serving as an outer layer of the molecule. Green vertices have six direct neighbors (four blue and two red vertices), blue vertices have six direct neighbors (two green, two blue and two red vertices), and red vertices have three direct neighbors (one green and two blue vertices) – thus, there are four inequivalent bond types: red-green, red-blue, green-blue and blue-blue. The axes piercing the centers of two opposite hexagons are C_3 symmetry axes, and the axes through opposite squares have a C_4 symmetry. Overall, this geometry has the full octahedral symmetry O_h with 48 group elements.

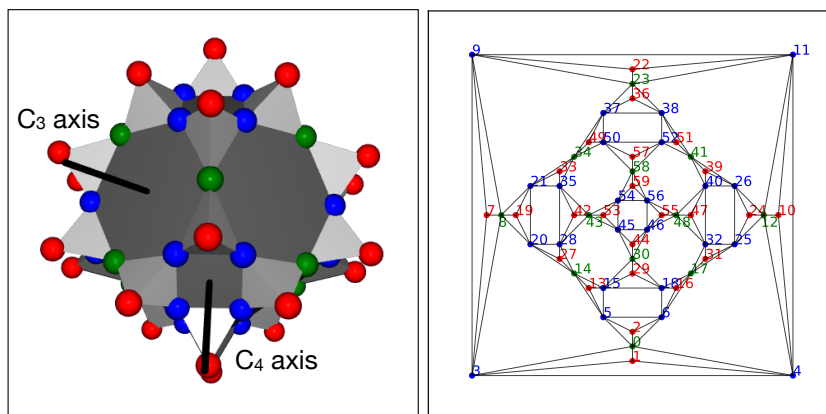


Figure 22: Left: Visualization of the sodalite cage geometry with different types of vertices. Right: Schlegel graph projection onto the plane with the chosen site enumeration. Figure taken from [CP2].

Experimental realizations of this molecular structure feature elements from the lanthanides such as gadolinium with a spin of $S = 7/2$ [83]. Despite not being synthesized (yet), for our publication [CP2] we focus on the case of $S = 1/2$, because the relatively large spin of Gd atoms leads to physics governed by the classical Heisenberg model. With spin frustration effects and quantum fluctuations in mind, the $S = 1/2$ case constitutes the extreme quantum limit of the model of interacting spins. Although the different bond types do not have exactly the same nearest-neighbor distances, it may be assumed as a simplification that all antiferromagnetic exchange couplings are the same, with $J = 1$ again fixing the energy scale. One thus arrives again at the antiferromagnetic Heisenberg model on the sodalite cage geometry:

$$\hat{H} = J \sum_{\langle i,j \rangle} \hat{S}_i \hat{S}_j. \quad (3.3)$$

In order to employ the VMPS algorithm, the vertices of the sodalite cage geometry have to be mapped onto a linear chain. This is achieved by compressing the graph of exchange couplings $J_{ij} \in \{0, 1\}$ by the Cuthill-

McKee algorithm [84], the resulting site numbering is shown in the right part of Figure 22. With the efficient MPO construction and compression, one can map this 2D geometry onto a 1D chain, arriving at an exact MPO representation of the Hamilton operator with bond dimension 23. As in the case of C_{60} , the $SU(2)$ symmetry of spin rotations is used explicitly in the implementation, whilst the spatial octahedral symmetry is rather used as an additional convergence check on top of the energy deviance from Equation (2.49).

Results

The groundstate of the antiferromagnetic $S = 1/2$ Heisenberg model on the sodalite cage geometry is calculated using the VMPS technique with an $SU(2)$ -adapted bond dimension of $\chi_{SU(2)} = 7000$, which would correspond to a higher bond dimension if the $SU(2)$ symmetry would not be used. The groundstate turns out to be a total-spin singlet. The nearest-neighbor spin correlation function $\langle \hat{S}_i \hat{S}_j \rangle$ in the groundstate as obtained from VMPS is shown in the left part of Figure 23.

There are two striking features about the spatial distribution of the spin correlation. First, the obtained groundstate is not symmetric with respect to the action of O_h . The rotational invariance of the formerly intact C_3 axes is completely broken, and the symmetry of two of the three C_4 axes is reduced to C_2 . Since the Hamilton operator is invariant under the action of O_h , this indicates that the found groundstate is part of an irreducible representation of O_h with non-trivial dimension and thus the existence of more energetically degenerate groundstates. Second, the molecule can be split into three regions in such a way that the spin correlations of bonds crossing the borders between these regions are very small. Two of these regions are environments of the poles at which the intact symmetry axis pierces (16 sites each), and the third region is a belt around the equator of the molecule (28 sites). The total spin of each regions is quite small, $\langle \hat{S}_{\text{region}}^2 \rangle \ll 1$.

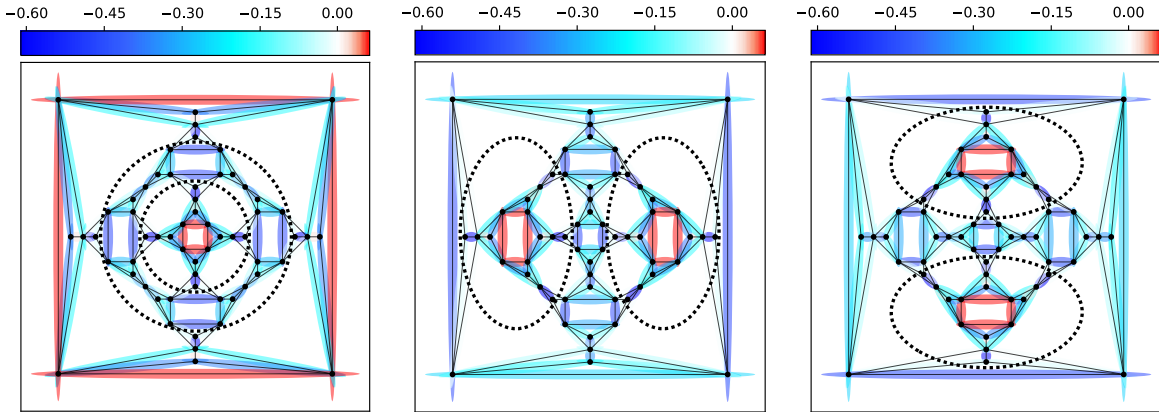


Figure 23: Nearest-neighbor spin correlation function $\langle \hat{S}_i \hat{S}_j \rangle$ in the groundstate of the antiferromagnetic Heisenberg model on the sodalite cage geometry. The left image shows the plain groundstate the VMPS method finds, the other two are targeted by assuming a nearby initial state. The dotted lines indicate where the correlation functions are so weak that the molecule splits into three almost decoupled parts. Figure taken from [CP2].

It is not surprising that the VMPS algorithm always converges to the same symmetry-broken groundstate, because the site numbering introduces a bias to the groundstate algorithm that favors a specific entanglement distribution over others. Nevertheless, one can try to find the other groundstates, but the simple energy penalty approach fails due to the decoupling of the three molecule parts: the entanglement structure of other groundstates is so different that one needs a global rearrangement of all spins. When VMPS is applied for the modified Hamilton operator $\hat{H}' = \hat{H} + E_{\text{pen}} |\Psi_0\rangle\langle\Psi_0|$, it gets stuck in an excited state slightly above the groundstate energy rather than finding another state from the groundstate multiplet. However, one can also rotate the groundstate $|\Psi_0\rangle$ manually. From the fact that in $|\Psi_0\rangle$ one of the three C_3 axes through opposite hexagons is selected, one may assume the existence of two other groundstates with the other two choices. A

rotation of $\frac{\pi}{2}$ about any C_4 axis maps a C_3 axis on another one. The mapping of sites can be written in terms of 45 transpositions, so that certain sequences of the spin- $1/2$ transposition operator

$$\widehat{P}_{ij} = 2\widehat{S}_i\widehat{S}_j + \frac{1}{2} \quad \text{with} \quad \widehat{P}_{12}|\sigma_1, \sigma_2\rangle = |\sigma_2, \sigma_1\rangle \quad (3.4)$$

can be applied onto the groundstate to find the rotated groundstate. Of course, an analytically exact application of these operators strongly increases the MPS bond dimension even though the MPOs have a small bond dimension of 2. Since intermediate (lossy) compression is necessary, the resulting MPS is not an eigenstate of the Hamilton operator anymore. However, these results turn out to be excellent candidates as the starting points of VMPS investigations of the groundstate, and within a limited number of sweeps, the two other groundstates presented in Figure 23 can be found, yielding a groundstate multiplet ($|\Psi_{0,1}\rangle, |\Psi_{0,2}\rangle, |\Psi_{0,3}\rangle$). The three obtained normalized states have an overlap smaller than 10^{-5} and coincide in energy in the first four digits, with $E_0/L \approx -0.4317$.

The symmetry breaking in finite systems has to be taken with the usual caveat: for finite systems, the barrier in free energy between these N -fold degenerate groundstates is finite and has non-zero tunneling probability, so that the thermalized state is described by a normalized projector on the groundstate multiplet:

$$\widehat{\rho} = \frac{1}{N} \sum_{n=1}^N |\Psi_{0,n}\rangle\langle\Psi_{0,n}|. \quad (3.5)$$

Here it becomes apparent that the explicit choice of an orthonormal basis in the groundstate manifold is irrelevant. When this density operator is used to calculate expectation values, the symmetry is restored, although the individual states that make up the density operator exhibit lower symmetry than the Hamilton operator. In the present case of the spin correlation function this gives

$$\overline{\langle\widehat{S}_i\widehat{S}_j\rangle} = \text{tr}(\widehat{\rho}\widehat{S}_i\widehat{S}_j) = \frac{1}{3} \left(\langle\Psi_{0,1}|\widehat{S}_i\widehat{S}_j|\Psi_{0,1}\rangle + \langle\Psi_{0,2}|\widehat{S}_i\widehat{S}_j|\Psi_{0,2}\rangle + \langle\Psi_{0,3}|\widehat{S}_i\widehat{S}_j|\Psi_{0,3}\rangle \right). \quad (3.6)$$

Indeed, when averaged over the three groundstates, the spin correlation function is quite close for all bonds of a given type. The spin correlation function and their standard deviation for the four bond types are summarized in Table 2 and visualized in Figure 24. The red-green bonds exhibit the strongest antiferromagnetic correlation.

The frustration introduced by the triangles with vertices red-blue-green is alleviated by putting a fairly strong antiferromagnetic correlation into the bond between the spins at the red and green vertex, at the cost of a low correlation between the green and blue vertex. Thus, the edges of the hexagons are weakly correlated although hexagons would allow for a staggered spin distribution. The triangles with one red and two blue vertices have a weaker correlation between the inner and outer layer of the molecule, leading to a stronger antiferromagnetic correlation along the edges of the squares.

The fact that the groundstate is a degenerate spin-singlet state can be related to the frustration. It is loosely reminiscent of a valence-bond solid state, i. e., a state with broken translational invariance in which each spin is paired with another one to form a maximally entangled singlet state, so that these spin-pair singlets then cover the system. However, in the present case, the singlets are only approximate and contain many spins.

In the presence of an external magnetic field with $\widehat{H}_B = -B\widehat{S}_{\text{tot}}^{(z)}$, states with non-zero magnetizations $M = \langle\widehat{S}_{\text{tot}}^{(z)}\rangle$ become the groundstates. The magnetic field explicitly breaks the $SU(2)$ symmetry of spin rotations down to a $U(1)$ symmetry around the z axis, but in order to find the groundstate for a given magnetic field, it is sufficient to just find the groundstates of the $SU(2)$ -symmetric antiferromagnetic Heisenberg model (without magnetic field) for all possible total spin quantum numbers from $S = 0$ to $S = 30$ by targeting them in VMPS, and add the field-induced Zeeman-splitting of the multiplet energies only later. This means that the energy of

| Bond type | $\overline{\langle \widehat{S}_i \widehat{S}_j \rangle}$ |
|------------|--|
| red-green | -0.3241 ± 0.0094 |
| red-blue | -0.1804 ± 0.0060 |
| green-blue | -0.0798 ± 0.0029 |
| blue-blue | -0.2345 ± 0.0073 |

Table 2: Nearest-neighbor spin correlation function averaged over the groundstate multiplet. The standard deviation determines the width of the distribution of the correlation function over all equivalent bonds and is thus a measure for the convergence of the VMPS result.

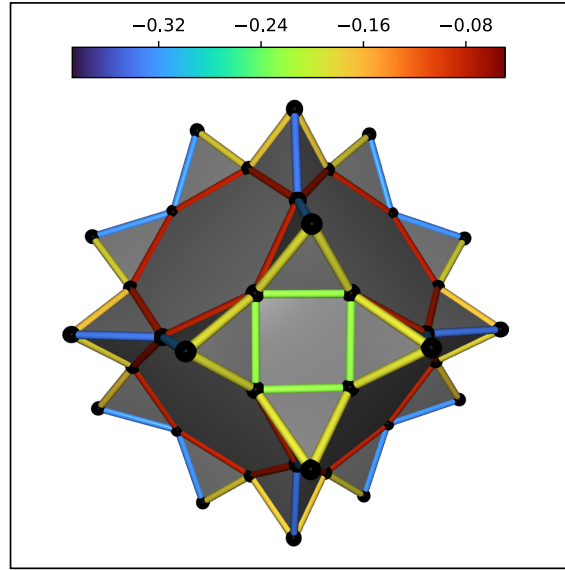


Figure 24: Nearest-neighbor spin correlation function averaged over the groundstate multiplet. Figure taken from [CP2].

the energetically lowest state with magnetization M is given by

$$E_M(B) = E_0(S = M) - BM. \quad (3.7)$$

The magnetization curve answers the question which magnetization the groundstate has for a given external magnetic field strength B . It is presented in Figure 25. Starting from the limit of high magnetic fields, in which the fully polarized state $|\Psi_{\text{FM}}\rangle = |\uparrow, \dots, \uparrow\rangle$ with $M = M_{\text{max}} = 30$ is the groundstate, the magnetization jumps to the value $M = 24$ exactly at $B = 4J$. This effect can be understood as an effect of localized magnons. These are spin excitations on top of the fully polarized state that decrement the spin quantum number. Usually, these excitations would propagate through the entire system, but under certain circumstances, destructive interference leads to a confinement of these excitations to a localized domain. In Appendix A.6 it is shown that for the sodalite cage geometry, there are 14 domains that are capable of hosting a localized magnon. This is a special feature that can be attributed to the mixture of bipartite and non-bipartite faces in the geometry. These 14 domains are the eight hexagons and the six squares of the sodalite cage. The energy of such a localized magnon is given by $\Delta E_{\text{magnon}} = B - 4J$. Since the squares have no overlapping sites, each square can host a magnon. It can be verified by VMPS calculations that the states with $N_{\text{magnon}} = 1, \dots, 6$ on top of $|\Psi_{\text{FM}}\rangle$ are not just eigenstates of the Hamilton operator but indeed constitute the groundstates in their respective magnetization subspace.

As soon as the magnetic field falls below the value of $B = 4J$, all six localized magnons become energetically favorable, thus leading to a magnetization jump from $M = 30$ to $M = 30 - 6 = 24$. At the exact value of $B = 4J$, all states with $N_{\text{magnon}} = 0, \dots, 6$ are degenerate. The total groundstate degeneracy sums up to 182, because for each magnon number there are several ways to distribute the magnons over the sodalite cage. The existence of a magnetization plateau is a general side effect of a magnetization jump, both being related to a gapped spin excitation [85,86]. The localized magnons explain the magnetization plateau at $\frac{4}{5}$ of the saturation magnetization. The other visible plateaus at $\frac{3}{5}$ and $\frac{1}{5}$ can also be traced back to approximately localized spin excitations. Details can be found in [CP2].

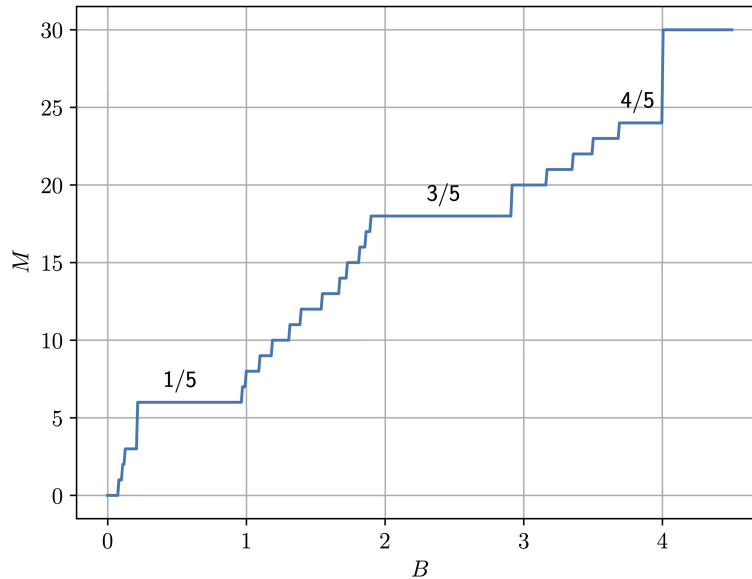


Figure 25: Magnetization curve of the antiferromagnetic Heisenberg model on the sodalite cage geometry, which tells what magnetization the groundstate exhibits for a given external magnetic field strength B in units of J . Figure taken from [CP1], edited.

3.3 – Matrix-Product-State Approach to the Generalized Nuclear-Pairing Hamiltonian

Model and technical notes

Besides electrons, atoms contain protons and neutrons which are particles with spin $S = 1/2$. The atomic nuclei thus represent systems of interacting fermions. For electrons, the dominant interaction is the electromagnetic Coulomb interaction. For nucleons, however, the strong interaction plays a crucial role. The fundamental strong interaction is mediated by gluons between quarks which carry a color charge. Protons and neutrons are bound states of three quarks with a neutral total color charge. A residual strong force between these nucleons causes an attraction that at short distances outweighs the Coulomb repulsion between protons.

In order to study the properties of atomic nuclei, the first-level approach is an effective single-particle theory in which the nucleons are subject to a mean-field potential caused by the other nucleons. An empirically well-established potential for this is the spherically-symmetric Woods-Saxon potential [87]. It describes a nearly constant potential within the nucleus to confine nucleons within the nuclear radius, and a diffuse boundary at the edge. This simple approach of two Fermi seas (one per species, protons and neutrons) of non-interacting fermions already explains the appearance of the so-called *magic numbers*, which explain the stability of certain isotopes. The solution of the stationary Schrödinger equation with this effective potential and a spin-orbit coupling yields

discrete orbitals $n[l]_j$, where n is the main quantum number, l is the (orbital) angular momentum quantum number and j is the total angular momentum that also includes the spin $S = 1/2$ and therefore is a half-integer number. Unlike for the Coulomb potential for electrons in atoms, the constraint $l \in \{0, \dots, n-1\}$ does not hold.

A shell is an orbital or a sequence of orbitals very close in energy. Whenever such a shell is completely filled, the corresponding nucleus tends to be more stable. The total nucleon numbers that finish a consecutively filled shell give rise to the magic numbers. In particular, since both nucleon species are independent of each other, certain nuclei have a magic number of protons and a magic number of neutrons at the same time.

For a more realistic description, the interactions between the nucleons cannot be neglected anymore. If the proton number is a magic number, one can again disregard the interaction between the different species, but should include the interaction between neutrons to arrive at an effective neutron-only theory (and vice versa). The most relevant interaction results in the formation of singlet pairs [88], i. e., coupling of two nucleons within the same orbital with total angular momentum j to a singlet. In condensed-matter language, this interaction can be modelled as an attractive pair-hopping term. Subsuming the main quantum number and the orbital angular momentum quantum number into a multi-index $\alpha = (n, l)$, nucleon-creation operators $\hat{c}_{j\alpha m}^\dagger$ can be introduced, which create a nucleon in the $n[l]_j$ orbital with spin projection m . With this, the singlet-pair creation operators are given by

$$\begin{aligned} \hat{p}_{j\alpha}^\dagger &= \sum_{m=-j}^j \Gamma_{m-m \rightarrow 0}^{j \ j} \hat{c}_{j\alpha m}^\dagger \hat{c}_{j\alpha, -m}^\dagger = \sum_{m=-j}^j \frac{(-1)^{j-m}}{\sqrt{2j+1}} \hat{c}_{j\alpha m}^\dagger \hat{c}_{j\alpha, -m}^\dagger \\ &= \frac{2}{\sqrt{2j+1}} \sum_{m>0} (-1)^{j-m} \hat{c}_{j\alpha m}^\dagger \hat{c}_{j\alpha, -m}^\dagger. \end{aligned} \quad (3.8)$$

The model Hamilton operator with attractive pair hopping $G_{j\alpha, j'\alpha'} \geq 0$ takes the following form:

$$\begin{aligned} \hat{H} &= \sum_{j,\alpha} \varepsilon_{j\alpha} \hat{n}_{j\alpha} - \sum_{j,\alpha, j',\alpha'} \frac{\sqrt{(2j+1)(2j'+1)} G_{j\alpha, j'\alpha'}}{4} \hat{p}_{j\alpha}^\dagger \hat{p}_{j'\alpha'} \\ &= \sum_{j,\alpha} \varepsilon_{j\alpha} \sum_{m>0} \left(\hat{c}_{j\alpha m}^\dagger \hat{c}_{j\alpha m} + \hat{c}_{j\alpha, -m}^\dagger \hat{c}_{j\alpha, -m} \right) \\ &\quad - \sum_{j,\alpha, j',\alpha'} G_{j\alpha, j'\alpha'} \sum_{m>0} (-1)^{j-m} \hat{c}_{j\alpha m}^\dagger \hat{c}_{j\alpha, -m}^\dagger \sum_{m'>0} (-1)^{j'-m'} \hat{c}_{j'\alpha', -m'} \hat{c}_{j'\alpha' m'}. \end{aligned} \quad (3.9)$$

Due to the short range of the nuclear force, one may assume a delta-like interaction as an approximation. With the coupled-angular-momentum states

$$|J(j, j'), (\alpha, \alpha'), M\rangle = \sum_{m, m'} \Gamma_{m m' \rightarrow M}^{j \ j' \rightarrow J} \hat{c}_{j\alpha m}^\dagger \hat{c}_{j'\alpha' m'}^\dagger |\text{vac}\rangle, \quad (3.10)$$

the coupling constants for singlet coupling can be calculated from

$$G_{j\alpha, j'\alpha'} = V_0 \langle 0(j, j), (\alpha, \alpha), 0 | \delta^{(3)}(\hat{\mathbf{r}}_1 - \hat{\mathbf{r}}_2) | 0(j', j'), (\alpha', \alpha'), 0 \rangle, \quad (3.11)$$

where a free parameter V_0 appears. The explicit values for the orbital energies $\varepsilon_{j\alpha}$ of a chosen nucleus are obtained by solving the single-particle problem of nucleons in the Woods-Saxon potential using a Seminole parametrization [89]. The value for the interaction strength V_0 (Equation (3.11)) is fitted to match experimental data. This will be discussed in more detail later.

The Hamilton operator from Equation (3.9) can be rewritten in terms of pseudospin operators as defined in Section 2.3:

$$\begin{aligned}
 \widehat{C}_{j\alpha}^{(+)} &= \sum_{m>0} (-1)^{j-m} \widehat{c}_{j\alpha m}^\dagger \widehat{c}_{j\alpha, -m}^\dagger = \frac{\sqrt{2j+1}}{2} \widehat{p}_{j\alpha}, \\
 \widehat{C}_{j\alpha}^{(-)} &= \sum_{m>0} (-1)^{j-m} \widehat{c}_{j\alpha, -m} \widehat{c}_{j\alpha m} = \frac{\sqrt{2j+1}}{2} \widehat{p}_{j\alpha}^\dagger, \\
 \widehat{C}_{j\alpha}^{(z)} &= \frac{1}{2} \sum_{m>0} \left(\widehat{c}_{j\alpha m}^\dagger \widehat{c}_{j\alpha m} + \widehat{c}_{j\alpha, -m}^\dagger \widehat{c}_{j\alpha, -m} - 1 \right) = \frac{1}{2} \widehat{n}_{j\alpha} - \frac{2j+1}{4}, \\
 \Rightarrow \widehat{H} &= \sum_{j,\alpha} \varepsilon_{j\alpha} \left(2\widehat{C}_{j\alpha}^{(z)} + \frac{2j+1}{2} \right) - \sum_{j,\alpha,j',\alpha'} G_{j\alpha,j'\alpha'} \widehat{C}_{j\alpha}^{(+)} \widehat{C}_{j'\alpha'}^{(-)}. \tag{3.12}
 \end{aligned}$$

In order to compute the groundstate of this Hamilton operator within the VMPS framework, a decomposition of the Hilbert space into local Hilbert spaces and, subsequently, a mapping to a linear chain of sites has to be performed. A natural way is to subsume the time-conjugated partner orbitals with the same n , l and j quantum numbers and opposing m quantum numbers into each local Hilbert space:

$$\mathcal{H}_{\text{loc}}(j, \alpha, m > 0) = \left\{ |\downarrow\rangle = |\text{vac}\rangle, |\downarrow\rangle = \widehat{c}_{j\alpha, -m}^\dagger |\text{vac}\rangle, |\uparrow\rangle = \widehat{c}_{j\alpha m}^\dagger |\text{vac}\rangle, |\uparrow\rangle = (-1)^{j-m} \widehat{c}_{j\alpha m}^\dagger \widehat{c}_{j\alpha, -m}^\dagger |\text{vac}\rangle \right\}. \tag{3.13}$$

The single-line arrows refer to the projection of total angular momentum, while the double-line arrows indicate the charge-pseudospin projection. The chosen mapping to a one-dimensional chain requires $\frac{2j+1}{2}$ sites for each orbital (j, α) , yielding a system size of

$$L = \sum_{(j,\alpha)}^{\text{relevant orbitals}} \frac{2j+1}{2}. \tag{3.14}$$

Obviously, the Hamilton operator is not $\text{SU}(2)_{\text{charge}}$ -symmetric, but it commutes with $\widehat{C}_{\text{tot}}^{(z)}$, which implies particle number conservation. A special feature of the singlet pair-hopping term is that it commutes with the local spin operator $\widehat{S}_{j\alpha m}^{(z)} = \frac{1}{2} \left(\widehat{c}_{j\alpha m}^\dagger \widehat{c}_{j\alpha m} - \widehat{c}_{j\alpha, -m}^\dagger \widehat{c}_{j\alpha, -m} \right)$. The term “spin” may be misleading here, because this operator actually measures the z component of the total angular momentum (up to a factor). However, as it is constructed analogous to the usual local spin operator in condensed matter and thus obeys the same commutation relations regarding the charge-pseudospins as in Section 2.3, it is called a spin here to make connection to the previous chapter. This local $\text{U}(1)_{\text{spin}}$ symmetry promotes the spin projections at each site to conserved quantities.

The local basis states $|\uparrow\rangle$ and $|\downarrow\rangle$ block their respective sites from achieving an energy optimization due to singlet pairing. For an even number of nucleons, it is possible that at each site there is an even number of nucleons, so that one can simply ignore the spin-polarized, odd-nucleon number states $|\uparrow\rangle$ and $|\downarrow\rangle$ and work only with the pseudospin states $|\uparrow\rangle$ and $|\downarrow\rangle$. This reduces the complexity of the problem from a Hubbard-like local Hilbert space to a Heisenberg-like local Hilbert space with only two basis states. The model from Equation (3.12) can be interpreted as an anisotropic charge-pseudospin Heisenberg model, which is subject to an external field in z direction. If, however, the nucleon number is odd, it is inevitable that at least one orbital is filled with exactly one nucleon and is thus blocked from singlet pairing. To take care of this circumstance, the *seniority scheme* is employed, in which for each orbital $n[l]_j$ an independent groundstate calculation with the constraint of an odd filling in the corresponding orbital is performed, and the lowest obtained energy marks the groundstate. In VMPS it is not a problem at all to have various different local Hilbert spaces. Therefore,

when applying the seniority scheme, the sites belonging to the chosen orbital are treated as Hubbard-like sites, whereas for all other sites the restriction to pseudospin-polarized states can be made. Nevertheless, the odd particle numbers sometimes cause problems as the VMPS algorithm gets stuck in an excited state due to the absence of a hopping term that lets a single nucleon change its orbital. Therefore, an initial guess for the state is used which takes the groundstate of the previous even nucleon number state and adds another nucleon to that orbital:

$$|\Psi_{\text{initial}}(N)\rangle = \sum_{m>0} \hat{c}_{j\alpha m}^\dagger |\Psi_0(N-1)\rangle \quad \text{for odd } N. \quad (3.15)$$

Results

The first nuclei that are investigated are isotopes of tin (Sn) with a fixed proton number of 50. Since 50 is a magic number for nucleons, the protons can be assumed to decouple from the neutron system. Moreover, the first 50 neutrons are also expected to fill the energetically lowest shells and to be unaffected by other neutrons. Therefore, 50 protons and 50 neutrons make up an inert core. Valence neutrons fill the orbitals $1g_{7/2}$, $2d_{5/2}$, $2d_{3/2}$, $3s_{1/2}$ and $1h_{11/2}$. The VMPS setup for $L = 16$ sites is sketched in Figure 26.

The MPO representation of the Hamilton operator can be constructed and compressed quite efficiently, most likely due to the m -independent coupling constants $G_{j\alpha, j'\alpha'}$. The MPO bond dimension can be reduced to $\mu = 8$. The MPS bond dimension is highest around half-filling, $N = 16$ (corresponding to 66 neutrons in total), but still is of the order of $\chi \approx 50$, which is easy to handle. Indeed, the groundstate calculations take less than one second on a standard computer and the results are the same as one gets from an exact diagonalization approach up to an error of $\mathcal{O}(10^{-10})$ [90], if the input parameters $\varepsilon_{j\alpha}$ and $G_{j\alpha, j'\alpha'}$ are the same.

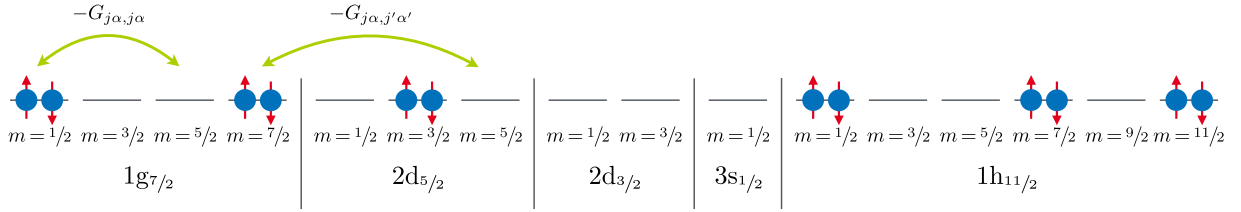


Figure 26: Visualization of the mapping to a linear chain of relevant orbitals for Sn with intra-shell pairing $-G_{j\alpha, j\alpha}$ and inter-shell pairing $-G_{j\alpha, j'\alpha'}$. The five orbitals require $L = 16$ sites in VMPS.

Encouraged by this accessibility, more orbitals are added to the setup in order to lessen the restrictions on the neutron configuration space, namely the orbitals $2f_{7/2}$, $3p_{3/2}$, $3p_{1/2}$, $1h_{9/2}$ and $2f_{5/2}$. The way to fix the free parameter V_0 (interaction strength) is by comparison with experimental data for the staggered even-odd mass difference:

$$\Delta_S^{(3)}(N) = (-1)^{N+N_{\text{core}}} \left(\frac{E_0(N+1) + E_0(N-1)}{2} - E_0(N) \right). \quad (3.16)$$

This quantity describes the imbalance in adding nucleons due to the desired singlet formation. The groundstate calculations in VMPS for all possible N in the range from 0 to 50 were performed for various values of V_0 to find the interaction strength which optimally reproduces the experimentally measured staggered even-odd mass difference. The acquired data points for the optimal $V_0 = 300 \text{ MeV fm}^3$ can be seen in Figure 27. For small N , both VMPS and ED struggle to match the experimental data well, probably indicating that the model Hamilton operator is not well-suited for the situation of sparsely filled valence shells. Around half-filling (purple shaded area), the ED approach cannot reproduce the experimental data, but the VMPS approach with more orbitals taken into account can do this. This means that the additionally added orbitals participate in the singlet pairing around half-filling. Lastly and not surprisingly, both numerical methods are able to resolve the magic number

$N + N_{\text{core}} = 82$ (grey shaded area) which corresponds to a stable neutron configuration.

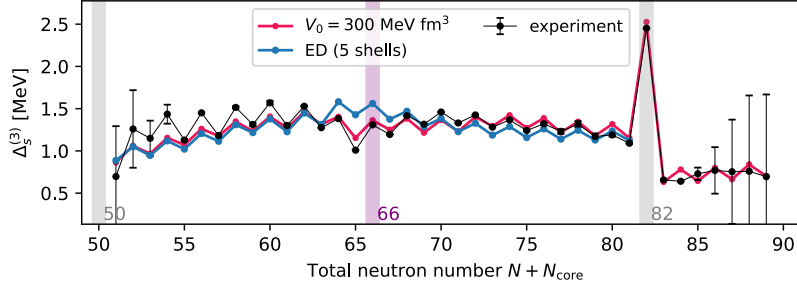


Figure 27: Staggered even-odd mass difference for Sn. For $V_0 = 300 \text{ MeV fm}^3$ the best agreement between experimental data and VMPS results was achieved. Figure taken from [CP4], edited.

However, the isotopes of tin are computationally not very challenging. The logical next step is the study of the lead (Pb) nucleus with the magic proton number 82. Once more, 82 neutrons and 82 protons create an inert core of the nucleus. For the valence neutrons, a large amount of shells is added to the VMPS variational space: $2f_{7/2}, 1h_{9/2}, 1i_{13/2}, 3p_{3/2}, 2f_{5/2}, 3p_{1/2}, 2g_{9/2}, 1i_{11/2}, 1j_{15/2}, 3d_{5/2}, 4s_{1/2}, 2g_{7/2}, 2d_{3/2}$. These orbitals can accommodate the magic numbers $N = 126$ (first six orbitals filled) and $N = 184$ (all 13 orbitals filled) of neutrons.

For VMPS, one needs $L = 51$ sites and an MPO bond dimension of $\mu = 16$. The MPS for the groundstate has a bond dimension of $\chi \lesssim 300$ and the algorithm takes some minutes on a standard computer to arrive at a converged result with $\Delta E^2/N \lesssim 10^{-9} \text{ MeV}^2$, indicating good convergence. The results for the staggered even-odd mass differences are shown in Figure 28. It is clearly visible that the interaction smears out the single-particle effect of sub-shell closings which are quite pronounced in the $V_0 = 0$ data. $V_0 = 250 \text{ MeV fm}^3$ leads to good agreement between VMPS simulations and experimental data.

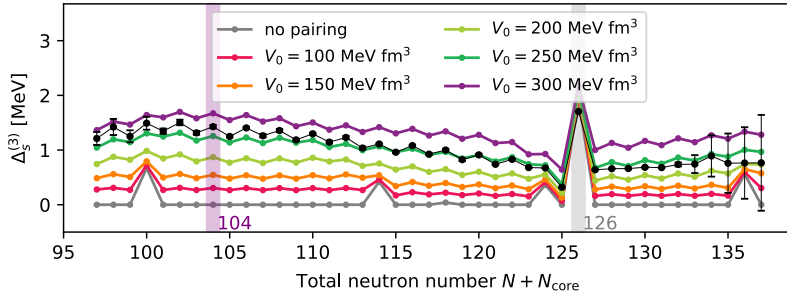


Figure 28: Staggered even-odd mass difference for Pb for various interaction strengths V_0 , and comparison to experimental data (black line, [91]). Figure taken from [CP4], edited.

Arguably more interesting than the particular values of $\Delta_S^{(3)}(N)$ is the fact that the VMPS method performs quite well for this problem from the realm of nuclear physics, at least from a condensed-matter perspective. It can handle more orbitals than exact diagonalization and yields better results than mean-field BCS for nuclear pairing (not shown here, but in the publication [CP4]). In contrast to Quantum Monte Carlo it does not suffer from the sign problem. The reason why VMPS works is the entanglement structure of nuclear-pairing problems. Figure 29 shows the entanglement entropy from Equation (2.16) calculated for different bipartitions of the orbitals along the chain.

As the orbitals are sorted in ascending order with respect to their single-particle energy levels, the bipartitions for which the entanglement is investigated cut the system into a part with low-energy orbitals and another part with high-energy orbitals. The grey dashed lines indicate those sites where the orbital changes. The overall values of the entanglement entropy are quite small, and the entanglement distribution along the chain has a dome profile, meaning that entanglement is built up and then decreases again. The doubly-magic ^{208}Pb has the lowest entanglement. Nevertheless, it is clearly visible that the different orbitals are entangled.

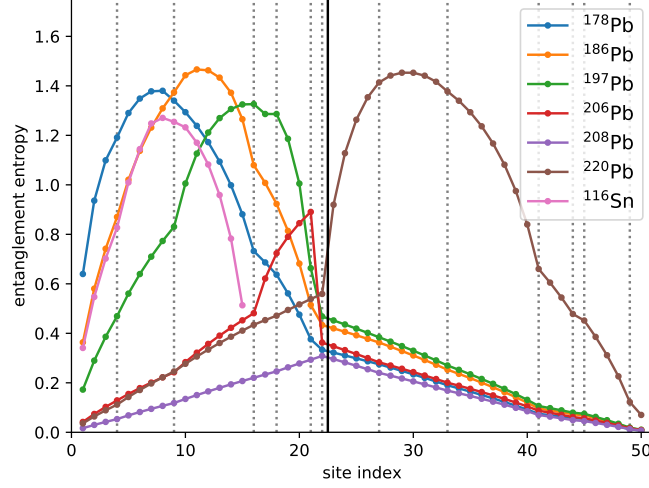


Figure 29: Entanglement entropy in the groundstate of various lead and tin isotopes along the chain of orbitals. Dotted grey lines indicate the fillings that correspond to the possible closure of an orbital. Figure taken from [CP4].

If the orbitals would be filled one after another as implied by the single-particle picture, there would not be entanglement at all in fully occupied orbitals. Nevertheless, one can observe a decisive behavior between sites 22 and 23 (black line), where the first six orbitals constitute the left part and the latter seven orbitals constitute the right part of the system. The decrease in entanglement can be attributed to the closure of a shell, yielding the magic number $N = 126$.

This regime of weakly entangled yet interacting systems is not a big challenge for tensor-network methods like VMPS. The entanglement entropy depends on the choice of local Hilbert spaces, which here stem from the single-particle solution with the Woods-Saxon potential. From the VMPS perspective, the Woods-Saxon potential seems to be a very good starting point that promises low entanglement.

Of course, the Hamilton operator from Equation (3.9) is still an idealized and simplified model for the true physics in atomic nuclei. A straightforward next step would be to allow nucleon pairs with total angular momentum other than zero to couple:

$$\hat{H} = \sum_{j,\alpha,m} \varepsilon_{j\alpha} \hat{c}_{j\alpha m}^\dagger \hat{c}_{j\alpha m} - \frac{1}{4} \sum_{J,M} \sum_{j,\alpha,j',\alpha'} G_{j\alpha,j'\alpha'}^{(J)} \left(\sum_m \Gamma_{m,M-m \rightarrow M}^{j \quad j \rightarrow J} \hat{c}_{j\alpha m}^\dagger \hat{c}_{j\alpha, M-m}^\dagger \right) \left(\sum_{m'} \Gamma_{m',M-m' \rightarrow M}^{j' \quad j' \rightarrow J} \hat{c}_{j'\alpha', M-m'} \hat{c}_{j'\alpha' m'} \right). \quad (3.17)$$

The non-singlet coupling breaks the pathological local spin conservation. The computations become more involved and the MPO compression is essential, but there are no fundamental problems. In the publication [CP4] this attempt is pursued, details can be found there. Moreover, the standard energy-penalty trick was used to calculate up to 100 excited states of ^{208}Pb and obtain the two-neutron-removal spectral function from it.

4 – Kondo Screening and Indirect Magnetic Exchange through a Conventional Superconductor

4.1 – Model & Charge Pseudospins

Hamilton operator

The Doniach phase diagram [92] shows the competition between two different magnetic interactions in systems with magnetic moments of adatoms or magnetic impurities which are coupled to an electronic host system: the antiferromagnetic local exchange coupling between local magnetic moments with the local spin moments in the host system, and the non-local magnetic interaction between the magnetic moments mediated by the electron system. The latter is an indirect coupling of the RKKY-type [19–21, 93]. It is accessible by perturbative means in the strength of the exchange coupling J/t and yields an effective exchange interaction $J_{\text{RKKY}} \propto J^2$ that couples the magnetic moments. The former, however, results in a screening process of the magnetic moments by the electrons and is a manifestation of the Kondo effect [18, 94, 95]. The Kondo effect is intrinsically non-perturbative and governed by a characteristic energy scale, the Kondo temperature $T_K \propto e^{-1/J}$. A well-suited platform for the investigation of this competition are Kondo models, in which the magnetic moments are treated as quantum spins which are either located at each site of the electronic host lattice (Kondo lattice model), or are dilutely placed at only some sites of the lattice (Kondo impurity model). The importance of treating the magnetic adatoms as quantum spins instead of classical entities was recently pointed out [96].

The competition between Kondo and RKKY physics changes fundamentally if the electronic system is gapped instead of being metallic: by introducing a gap δ , a third energy scale comes into play. The energy gap to some extent regularizes the single-impurity Kondo effect by cutting off low-energy excitations needed for the mesoscopically large Kondo cloud [97–101]. For insulating host systems, also the indirect RKKY exchange is altered, because the tunnel effect hinders communication between the impurities [22, 102]. The interplay between RKKY, Kondo and a finite-size gap has been investigated in [103] and [104]. Whether or not the impurities are Kondo-screened or RKKY-coupled is strongly influenced by the fermion parity and the specific geometry of the system. Moreover, there is a reentrant behavior for small exchange couplings and finite-size gaps, i. e., first the finite-size Kondo effect dominates, then the RKKY indirect coupling, and afterwards the bulk Kondo effect.

An interesting generalization of this problem concerns the influence of the mechanism that underlies the opening of a gap. In [CP5], the question is raised how RKKY and Kondo physics compete in the presence of conventional superconductivity. To this end, the electronic host system is modelled as a BCS-like s-wave superconductor [105, 106]. The Hamilton operator takes the following form:

$$\hat{H} = -t \sum_{i=1}^L \left(\hat{c}_{i\uparrow}^\dagger \hat{c}_{i+1,\uparrow} + \hat{c}_{i\downarrow}^\dagger \hat{c}_{i+1,\downarrow} + \hat{c}_{i+1,\uparrow}^\dagger \hat{c}_{i\uparrow} + \hat{c}_{i+1,\downarrow}^\dagger \hat{c}_{i\downarrow} \right) + \sum_{i=1}^L \left(\Delta \hat{c}_{i\uparrow}^\dagger \hat{c}_{i\downarrow}^\dagger + \Delta^* \hat{c}_{i\downarrow} \hat{c}_{i\uparrow} \right) + J \sum_{m=1}^M \hat{\mathbf{S}}_m \hat{\mathbf{s}}_{i_m}. \quad (4.1)$$

Here, the term proportional to t represents spin-independent nearest-neighbor hopping of electrons in the host, which is taken to be a linear chain of L lattice sites. The term proportional to $J > 0$ represents the antiferromagnetic exchange coupling of the quantum spin-1/2 impurities $\hat{\mathbf{S}}_m$ and the magnetic moments of the electrons $\hat{\mathbf{s}}_i = \frac{1}{2} \sum_{\sigma,\sigma'} \boldsymbol{\sigma}_{\sigma\sigma'} \hat{c}_{i\sigma}^\dagger \hat{c}_{i\sigma'}$ with M impurities located at the impurity sites i_1, \dots, i_M . The terms that contain either two electron creators or annihilators represent the pairing of electrons leading to s-wave superconductivity. In the absence of an exchange interaction, the system is readily solvable by exact diagonalization, because all contributions are quadratic in the fermionic operators, thus implying single-particle physics. In this single-particle regime, the energy spectrum is gapped by the superconducting pairing strength, i. e., $E_{\text{gap}} = 2|\Delta|$

(indeed, for open chains with an even number of lattice sites, there is a small correction of the order of $1/L^2$).

A similar problem was investigated by Yao et al. [107]. For their computational treatment of the problem they have employed the Numerical Renormalization Group technique [108] and model an RKKY coupling of the impurities explicitly, i. e., by an additional term in the Hamilton operator. In this work, however, the indirect magnetic exchange occurs as an emergent phenomenon produced by the collective behavior of electrons. In particular, it is analyzed how the geometry crucially impacts the emergent indirect magnetic exchange and how this can be changed by microscopic control of the system. Žitko et al. also studied the effect of magnetic anisotropy in this model [109].

Experimental realizations of small magnetic structures on superconducting host systems have received quite some attention in recent years [110–113], as the Yu–Shiba–Rusinov [114–116] states, which form a sub-band in the superconducting gap, were proposed as a platform for Majorana physics [117].

Symmetries of the model

The Hamilton operator of Equation (4.1) underlies certain symmetries that influence the physical behavior. Most strikingly, the pairing terms break the U(1) symmetry that leads to particle number conservation. Nevertheless, with the help of the charge pseudospin operators of Equation (2.131),

$$\begin{aligned} \hat{\eta}_i^{(x)} &= \frac{\epsilon_i}{2} \left(\hat{c}_{i\uparrow}^\dagger \hat{c}_{i\downarrow}^\dagger + \hat{c}_{i\downarrow} \hat{c}_{i\uparrow} \right) & \Rightarrow \hat{\eta}_i^{(+)} &= \hat{\eta}_i^{(x)} + i\hat{\eta}_i^{(y)} = \epsilon_i \hat{c}_{i\uparrow}^\dagger \hat{c}_{i\downarrow}^\dagger, \\ \hat{\eta}_i^{(y)} &= \frac{\epsilon_i}{2i} \left(\hat{c}_{i\uparrow}^\dagger \hat{c}_{i\downarrow}^\dagger - \hat{c}_{i\downarrow} \hat{c}_{i\uparrow} \right) & \Rightarrow \hat{\eta}_i^{(-)} &= \hat{\eta}_i^{(x)} - i\hat{\eta}_i^{(y)} = \epsilon_i \hat{c}_{i\downarrow} \hat{c}_{i\uparrow}, \\ \hat{\eta}_i^{(z)} &= \frac{1}{2} \left(\hat{c}_{i\uparrow}^\dagger \hat{c}_{i\uparrow} + \hat{c}_{i\downarrow}^\dagger \hat{c}_{i\downarrow} - 1 \right), \end{aligned} \quad (4.2)$$

the local superconductivity part can be rewritten as

$$\Delta \hat{c}_{i\uparrow}^\dagger \hat{c}_{i\downarrow}^\dagger + \Delta^* \hat{c}_{i\downarrow} \hat{c}_{i\uparrow} = |\Delta| e^{i\varphi} \cdot \epsilon_i \hat{\eta}_i^{(+)} + |\Delta| e^{-i\varphi} \cdot \epsilon_i \hat{\eta}_i^{(-)} = 2\epsilon_i |\Delta| \left(\cos(\varphi) \hat{\eta}_i^{(x)} - \sin(\varphi) \hat{\eta}_i^{(y)} \right), \quad (4.3)$$

where φ is the phase of the pairing strength Δ . By employing a unitary phase transformation of all creators and annihilators, $\hat{c}_{i\sigma} \rightarrow e^{-i\varphi/2} \hat{c}_{i\sigma}$, one can find a representation of the Hamilton operator in which the pairing strength is real and positive. In this case, the local superconductivity pairing part simply reads $2|\Delta| \epsilon_i \hat{\eta}_i^{(x)}$.

As explained in Section 2.3, where spin and pseudospin operators and their mutual relationship were examined, spin and pseudospin operators both obey the $\mathfrak{su}(2)$ commutation relations. They are compatible in the sense that spin and pseudospin operators commute. Furthermore, the spin-independent hopping term on a bipartite hopping graph is an irreducible tensor operator of rank 0 with respect to both the $SU(2)_{\text{spin}}$ and $SU(2)_{\text{charge}}$. The same holds true for the exchange-interaction term for the spins. The pairing term commutes with all generators of the spin, but it selects a distinct axis of the pseudospin – namely, for real-valued pairing strength, the x direction stands out as the BCS pairing term translates into a staggered external field in x direction coupling to the local pseudospin, i. e., $\mathbf{B}_{\eta,i} = 2|\Delta| \epsilon_i \mathbf{e}_x$. Therefore, the $SU(2)_{\text{charge}}$ is broken down to a $U(1)_{\text{charge}}$. However, the remaining unbroken generator $\hat{\eta}_{\text{tot}}^{(x)} = \sum_i \hat{\eta}_i^{(x)}$ is not the usual one that implies particle number conservation – that would be $\hat{\eta}_{\text{tot}}^{(z)}$. A rotation around the y axis by $\frac{\pi}{2}$, i. e., a unitary transformation embodied by $\hat{U} = \exp\left(\frac{i\pi}{2} \hat{\eta}_{\text{tot}}^{(y)}\right)$, twists the superconductivity part into a particle-number-conserving term with a staggered on-site potential while leaving all other terms invariant.

From this $SU(2)_{\text{spin}} \otimes U(1)_{\text{charge}}$ symmetry, the system's eigenstates can be characterized by their total spin quantum number S_{tot} and the x component of their total pseudospin, referred to as pseudocharge $Q_\eta = \langle \hat{\eta}_{\text{tot}}^{(x)} \rangle$, given by the eigenvalue of $\hat{\eta}_{\text{tot}}^{(x)}$. The impurities do not contribute to the determination of the pseudocharge. As explained in Section 2.3, the local electronic Hilbert space contains a doublet of spin and singlet of pseudospin (states $|\uparrow\rangle$ and $|\downarrow\rangle$), which is required for the build-up of magnetic correlations, and a singlet of spin and doublet of pseudospin (states $|0\rangle$ and $|\uparrow\downarrow\rangle$), which is favored by the BCS pairing terms. In that sense, the

conventional superconductivity not only introduces a gap to the system, but it also competes with magnetic order. In a product state, each lattice site contributes either $\pm 1/2$ to the total spin quantum number or to the pseudocharge, so that the total quantum numbers are either integer or half-integer. For spin- $1/2$ impurities, there is a relation between the total spin and the pseudocharge depending on the number of sites: for a system with even $L + M$, the pseudocharge is integer if and only if the total spin is integer. For odd $L + M$, the opposite holds, and either the pseudocharge or the total spin is half-integer. Due to the staggered external pseudospin field $2\Delta\epsilon_i$, the pseudospins have the tendency to align “antiferromagnetically”, typically leading to small values of the pseudocharge in the groundstate.

The fermion-parity operator can be represented via pseudospin operators as

$$\hat{\Pi} = (-1)^{\sum_i (\hat{n}_{i\uparrow} + \hat{n}_{i\downarrow})} = \exp\left(i\pi \sum_i \left(2\hat{\eta}_i^{(z)} + 1\right)\right) = (-1)^L \exp\left(2\pi i \hat{\eta}_{\text{tot}}^{(z)}\right). \quad (4.4)$$

Apparently, this operator commutes with all parts of the Hamilton operator, guaranteeing that the fermion parity Π is a good quantum number. For a mirror-symmetric placement of the impurity spins, spatial parity is also a symmetry of the system. For even system sizes L , however, the spatial parity operator for the host system $\sum_{i\sigma} \hat{c}_{i\sigma}^\dagger \hat{c}_{L+1-i,\sigma}$ does not commute with the charge pseudospin $\hat{\eta}_{\text{tot}}^{(x)}$, so that the pseudocharge and the spatial parity cannot be exploited as good quantum numbers simultaneously.

4.2 – VMPS Results

Single impurity

First of all, the $M = 1$ model was investigated. For $L = 1$, the model is easily solved analytically: if $|\Delta| > \frac{3J}{4}$, the groundstate takes the form $|\Phi_{0,\sigma}\rangle = \sqrt{\frac{1}{2}} (|0\rangle - e^{i\varphi} |\uparrow\downarrow\rangle) \otimes |\sigma\rangle$ with a decoupled impurity spin $|\sigma\rangle$ producing a spin doublet with energy $E_0 = -|\Delta|$. If $|\Delta| < \frac{3J}{4}$, the groundstate is given by a spin singlet in which the impurity spin is screened by the local magnetic moment of the electrons, i. e., $|\Psi_0\rangle = \sqrt{\frac{1}{2}} (|\uparrow\rangle \otimes |\downarrow\rangle - |\downarrow\rangle \otimes |\uparrow\rangle)$ with $E_0 = -\frac{3J}{4}$. Therefore, a quantum phase transition from a superconducting BCS phase to a magnetically ordered Kondo phase occurs at $\Delta_c = \frac{3J}{4}$. The phase transition manifests itself in the local spin correlation function $\langle \hat{S}_1 \hat{s}_{i_1} \rangle$ between the impurity and the electronic spin. For $|\Delta| < \Delta_c$, this correlation function takes the spin-singlet value $-\frac{3}{4}$, whilst for $|\Delta| > \Delta_c$, it vanishes.

For larger L , a competition between these local ordering mechanisms and the nonlocal hopping can be expected. The total energy is balanced between its contributions

$$\begin{aligned} \text{exchange energy:} & \quad J \langle \hat{S}_1 \hat{s}_{i_1} \rangle, \\ \text{superconducting pairing energy:} & \quad |\Delta| \sum_{i=1}^L \left(e^{i\varphi} \langle \hat{c}_{i\uparrow}^\dagger \hat{c}_{i\downarrow}^\dagger \rangle + e^{-i\varphi} \langle \hat{c}_{i\downarrow} \hat{c}_{i\uparrow} \rangle \right), \\ \text{delocalization energy:} & \quad -t \sum_{i=1}^{L-1} \sum_{\sigma} \left(\langle \hat{c}_{i\sigma}^\dagger \hat{c}_{i+1,\sigma} \rangle + \langle \hat{c}_{i+1,\sigma} \hat{c}_{i\sigma} \rangle \right). \end{aligned} \quad (4.5)$$

An extended host system of $L = 81$ electron sites is studied by employing the symmetry-adapted VMPS method for the $SU(2)_{\text{spin}}$ symmetry. The impurity is placed in the center of the system, with 40 lattice sites to the left and right. All presented VMPS results in the remainder of this chapter are well-converged to $\Delta E^2/L \leq 10^{-9} t^2$. For large values of J and $|\Delta|$, the physics will be the same as in the $L = 1$ model, because these energy contributions act locally. For J and $|\Delta|$ comparable to the hopping t , substantial deviations from the single-site model arise. This can be observed in Figure 30, where the total spin quantum number of the

groundstate is shown for a range of parameters J and $|\Delta|$. While still being numerically accessible by VMPS with runtimes of several hours, this model is large enough to accommodate long-wavelength correlations without the interference of finite-size effects for $J, |\Delta| \gtrsim 0.1 t$. For smaller parameters, the computation time grows, but also the universality of the physics breaks down, because the extent of correlations reaches the system's boundaries and is reflected from there [118]. Therefore, the following calculations are restricted to $J, |\Delta| \geq 0.1 t$. The points in the phase diagram where no computations were performed are marked in dark gray.

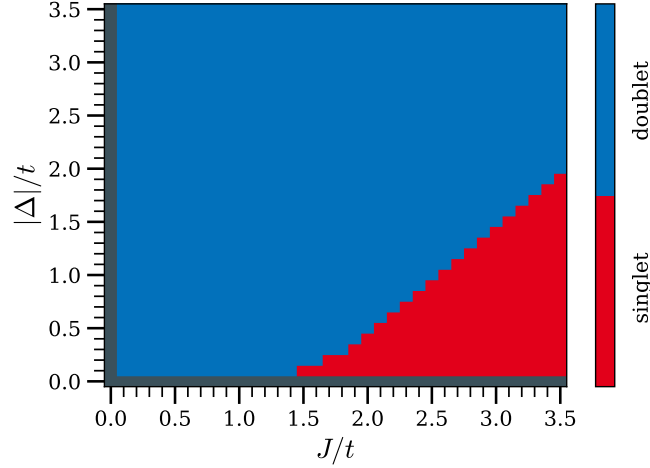


Figure 30: Groundstate phase diagram for a single impurity spin located at site $i_1 = 41$ of a chain of $L = 81$ sites. Figure taken from [CP5], edited.

The linear behavior of the phase-transition line can be seen for larger parameters, whereas for smaller parameters, it tends to bend into a sub-linear shape. Overall, the doublet phase extends beyond the former phase boundary into the regime of the singlet phase. The impurity in the singlet phase is Kondo-screened by an extended Kondo cloud (with the overall caveat that in this finite-size Kondo effect the long-wavelength/low-energy contributions are cut), which means that the local spin correlation function does not take the value $-\frac{3}{4}$ as the surrounding electrons participate in the screening of the impurity. From Figure 31 it is obvious that the spin-doublet phase is not a pure BCS state but gradually builds up magnetic correlations between the impurity and the host system for $J \gtrsim \frac{4|\Delta|}{3}$ before it jumps to its saturation value in the singlet phase. This effect is stronger for smaller pairing strength. An extended discussion of the $|\Delta| \rightarrow 0$ limit is given in Section 4.4.

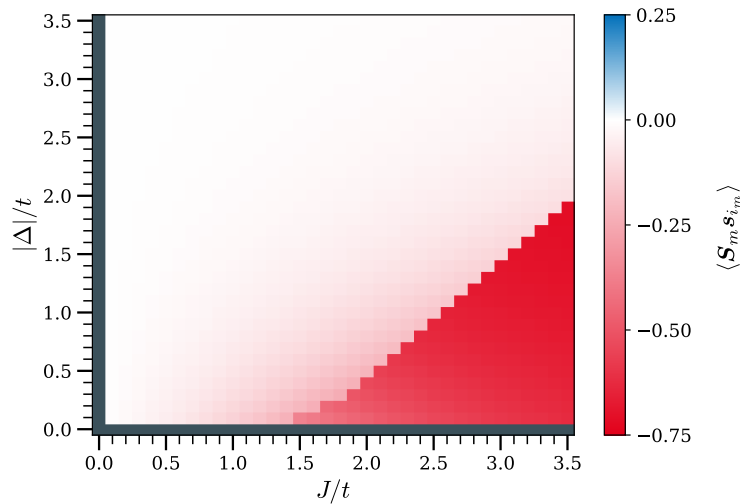


Figure 31: Local spin correlations for a single impurity spin located at site $i_1 = 41$ of a chain of $L = 81$ sites.

Two impurities

After getting an idea what happens for a single impurity, the necessary step towards the Kondo-vs.-RKKY competition is the inclusion of a second impurity. Figure 32 shows the groundstate total spin for a system with $L = 82$ sites and $M = 2$ impurities located directly next to each other at the sites $i_1 = 41$ and $i_2 = 42$.

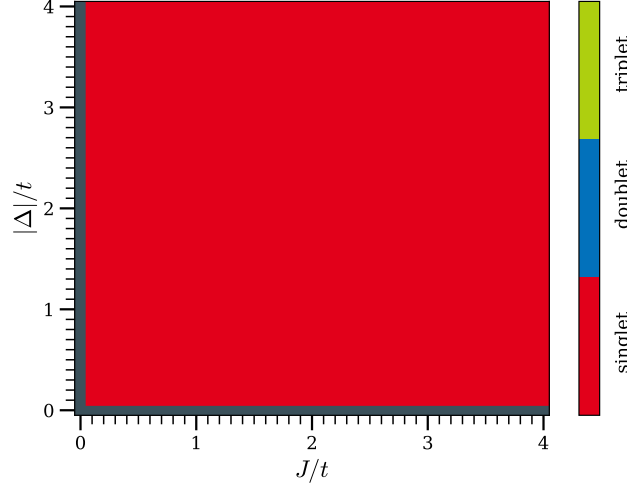


Figure 32: Groundstate phase diagram for a model with two impurities located at sites $i_1 = 41$ and $i_2 = 42$ of a chain of $L = 82$ sites.

Apparently, the groundstate phase diagram is featureless with $S_{\text{tot}} = 0$ in the entire parameter range. However, with a closer look at the impurity spin correlation function $\langle \hat{S}_1 \hat{S}_2 \rangle$ in Figure 33, one can identify a crossover from a regime where the impurities form a spin singlet to a state where the impurity spins are uncorrelated. In the limit $J \rightarrow 0$, the correlation function reaches its extreme value of $-\frac{3}{4}$. Since a spin singlet is inert and decouples from its environment, the host system takes its groundstate as if the impurities were absent, meaning a BCS-like spin-singlet groundstate (in the next subsection, a more detailed view on the BCS groundstate is provided). The impurity spins only experience a very weak emergent indirect exchange coupling through the BCS singlet which favors their antiferromagnetic alignment over a ferromagnetic one. The standard RKKY theory for metals predicts an antiferromagnetic indirect exchange coupling for nearest-neighboring sites, and in the next subsection it will be discussed that this also holds true for a BCS superconductor.

For stronger J , the impurity spins start to decouple as they build up more and more antiferromagnetic correlation with the electrons in the host, leading to a screening of the impurity spins. In the limit $J \rightarrow \infty$, the impurity spins are completely decoupled and form local Kondo singlets with their respective host sites. The fact that there is no phase transition can be related to the quantum numbers in the extreme limits of these regimes: the BCS state for $|\Delta| \gg J$ is a spin singlet. This fact is not altered by the RKKY singlet that comes on top. The pseudocharge is zero due to the staggered pseudospin field. In the opposite limit $J \gg |\Delta|$, however, the quantum numbers are indeed the same: the local Kondo singlets cut the host into two parts, which by themselves form BCS singlets, giving a total spin of zero and a pseudocharge of zero, because both sites that are singly occupied to form local Kondo singlets originate from inequivalent sublattices, and the rest aligns in a staggered fashion.

Since both extreme points of the phase diagram belong to the same symmetry sector, phase transitions caused by level crossings are much less likely [119] and the prototypical setting is a continuous crossover.

In the case of an even impurity distance, the situation becomes more complex and the phase diagram richer. For $d = 2$, the groundstate phase diagram presented in Figure 34 shows the occurrence of phases with $S_{\text{tot}} = 1/2$ and $S_{\text{tot}} = 1$, which separate two spin-singlet phases from each other. These four phases, whose prototypical states are conceptualized in Figure 37, are discussed in the following:

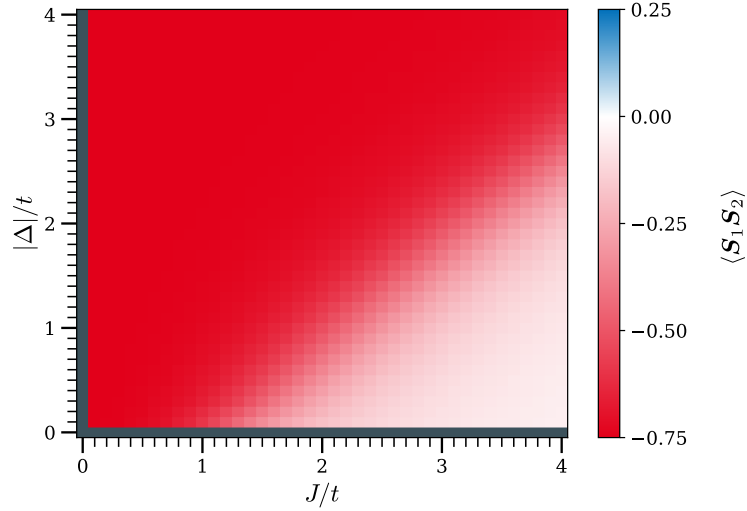


Figure 33: Impurity spin correlations for a model with two impurities located at sites $i_1 = 41$ and $i_2 = 42$ of a chain of $L = 82$ sites. Figure taken from [CP5], edited.

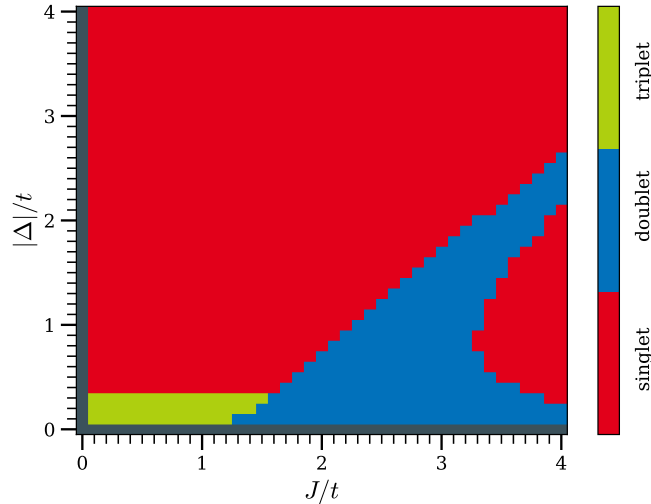


Figure 34: Groundstate phase diagram for a model with two impurities located at sites $i_1 = 41$ and $i_2 = 43$ of a chain of $L = 83$ sites. Figure taken from [CP5], edited.

- RKKY triplet:

For weak exchange couplings J and pairing strength $|\Delta|$, the groundstate is a spin-triplet state. This corresponds to the green color in Figure 34. In this case, the electronic host system forms a BCS singlet and both impurities are subject to an emergent ferromagnetic RKKY coupling which causes the impurity spins to align, giving a spin triplet. Since the one-particle gap in the electronic host $2|\Delta|$ is small in this case, the standard RKKY result of a ferromagnetic coupling for even distances is recovered, because the effective coupling is related to the static spin susceptibility via $J_{\text{RKKY}} = -J^2 \chi_{i_1 i_2}(\omega = 0)$, and this susceptibility is positive for a metallic system and even distances. This interpretation is supported by Figure 35, which shows an almost perfect ferromagnetic coupling $\langle \hat{S}_1 \hat{S}_2 \rangle \approx \frac{1}{4}$, with only small deviations in the vicinity of the phase boundary to the doublet phase. The decoupled electronic system in the BCS groundstate acquires a pseudocharge of $Q_\eta = +\frac{1}{2}$ because, if the first site is assigned a plus sign, the number of $\epsilon_i = +1$ sites exceeds the number of $\epsilon_i = -1$ sites by one.

- RKKY singlet:

If the pairing strength is increased beyond a certain value $\Delta_{\text{AFM}} \approx 0.35t$, the total spin of the system's groundstate suddenly changes to $S_{\text{tot}} = 0$. Figure 35 shows that the impurity spin correlation is drastically altered from ferromagnetic to antiferromagnetic. Therefore, the change of the total spin can be attributed to the impurities aligning differently and thus the emergent RKKY coupling must have undergone a sign change. In Section 4.3 it will be shown that this sign change can be understood perturbatively within second-order perturbation theory in the exchange coupling J .

The RKKY-singlet phase extends to arbitrarily large $|\Delta|$. For stronger J , its lower phase boundary becomes a straight line, yielding a linear scaling of the critical $\Delta_c(J)$, which describes the transition line between the RKKY-singlet phase and the phase with total spin $S_{\text{tot}} = 1/2$. In the limit of $J \rightarrow \infty$, the phase transition asymptotically takes place at $\Delta_c(J) = \frac{3J}{4}$, as the physics becomes more and more local, so that the non-local hopping contributions can be neglected as $\frac{t}{J} \rightarrow 0$. As is the case in the $M = 1$ model, weak local Kondo correlations $\langle \hat{\mathbf{S}}_m \hat{\mathbf{s}}_{i_m} \rangle$ build up for $|\Delta| \gtrsim \Delta_c$, as can be seen in Figure 36. Indeed, the phase-transition line in this model is quantitatively very close to the phase-transition line in the single-impurity model.

The electronic state does not change very much compared to the RKKY-triplet phase (apart from the fact that the next-nearest neighbor indirect exchange coupling mediated through the electronic host changes its sign), so that the pseudocharge is still $Q_\eta = +1/2$.

- Local Kondo singlet:

For any finite $|\Delta| > 0$ and for sufficiently strong J , the groundstate becomes a spin-singlet state again. This can be understood as the individual screening of both impurities by the electrons at their respective host sites. Figure 35 and Figure 36 support this interpretation: they show that the impurity spin correlation function vanishes, $\langle \hat{\mathbf{S}}_1 \hat{\mathbf{S}}_2 \rangle = 0$, while the local spin correlation takes its extremal antiferromagnetic value $\langle \hat{\mathbf{S}}_m \hat{\mathbf{s}}_{i_m} \rangle = -\frac{3}{4}$. The local Kondo singlets cut the host system into three parts: the sites $i = 1, \dots, i_1 - 1$, the central site $i = i_1 + 1$ and the sites $i = i_2 + 1, \dots, L$. Each of these parts can be in a BCS-like groundstate on their own. For $L = 83$, as chosen for the VMPS calculations, the left and right part have $Q_{\eta,\text{left}} = Q_{\eta,\text{right}} = 0$ and the central site has $Q_{\eta,\text{center}} = -1/2$. The corresponding total $Q_\eta = -1/2$, which is different from the case of the RKKY singlet, is readily explained by the fact that the local Kondo singlets take out two sites with $\epsilon_i = +1$ from the electronic host. The fact that the pseudocharge differs from the RKKY-singlet pseudocharge is inherently local and does not change for another L : for an analogous setup with $L = 85$, one would find $Q_{\eta,\text{left}} = Q_{\eta,\text{right}} = Q_{\eta,\text{center}} = +1/2$, with $Q_\eta = +3/2$.

- Partial Kondo screening:

The remaining spin-doublet phase is probably the most exotic phase and can be understood as a compromise between the two singlet phases. For strong J and $|\Delta|$, only one of the impurities is screened, while the other remains free. Due to spatial parity symmetry, the groundstate consists of a sum of two states in which the roles of the impurities are interchanged, yielding a bonding state. The antibonding state is an excited state. Deep in the partial-Kondo-screening phase, the σ component of the groundstate doublet can be conceptualized as a state of the following form:

$$|\text{PKS}\rangle = \frac{1}{\sqrt{2}} (|\text{BCS}\rangle_{i_1} \otimes |\text{LKS}\rangle_1 \otimes |\sigma\rangle_2 + |\text{BCS}\rangle_{i_2} \otimes |\text{LKS}\rangle_2 \otimes |\sigma\rangle_1), \quad (4.6)$$

where $|\text{BCS}\rangle_{\bar{i}}$ describes a BCS spin-singlet groundstate that extends over all electronic sites except for site i , $|\text{LKS}\rangle_m$ is a local Kondo singlet between the m -th impurity spin and the local magnetic moment at site

i_m , and $|\sigma\rangle_m$ stands for a decoupled m -th impurity spin. In this limit, where the non-local t defines the smallest energy scale, the correlation between the impurities vanishes, i. e., $\langle \text{PKS} | \widehat{\mathbf{S}}_1 \widehat{\mathbf{S}}_2 | \text{PKS} \rangle = 0$. This state also gives $\langle \text{PKS} | \widehat{\mathbf{S}}_m \widehat{\mathbf{s}}_{i_m} | \text{PKS} \rangle = -\frac{3}{8}$, matching the value of the local correlation function in Figure 36. As in both cases host sites with $\epsilon_i = +1$ are used to screen the spin, the pseudocharge is reduced to $Q_\eta = 0$. For weaker pairing strengths, however, one can observe severe deviations from the form of $|\text{PKS}\rangle$, as the correlation functions do not take the values predicted for the deep PKS limit. A possible interpretation for the underscreening is that both Kondo clouds extend over a few lattice sites, but since the impurity distance is so small, they overlap and interfere with each other, yielding a superposed Kondo cloud that screens a single quantum spin- $1/2$. This point will also be discussed in Section 4.4 in the context of the finite-size Kondo effect. Nevertheless, the entire phase is called partial-Kondo-screening phase for simplicity. For stronger parameters J and $|\Delta|$, one can assume the width of this phase to decrease, finally nestling up against the line with $|\Delta| = \frac{3J}{4}$.

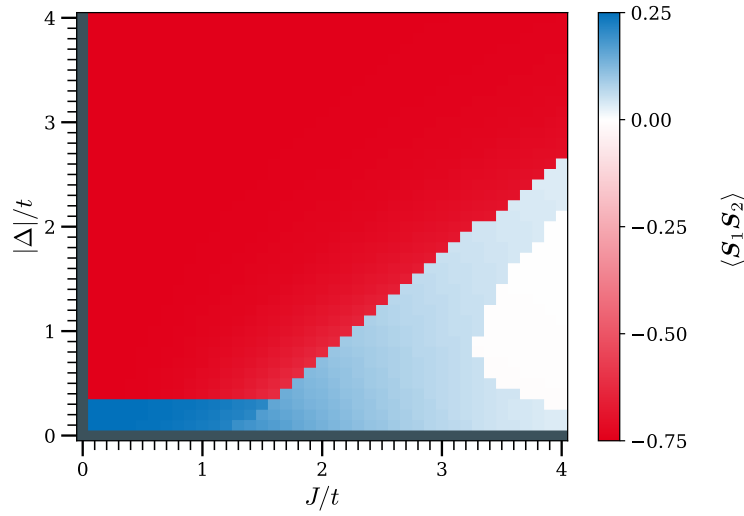


Figure 35: Impurity spin correlations for a model with two impurities located at sites $i_1 = 41$ and $i_2 = 43$ of a chain of $L = 83$ sites. Figure taken from [CP5], edited.

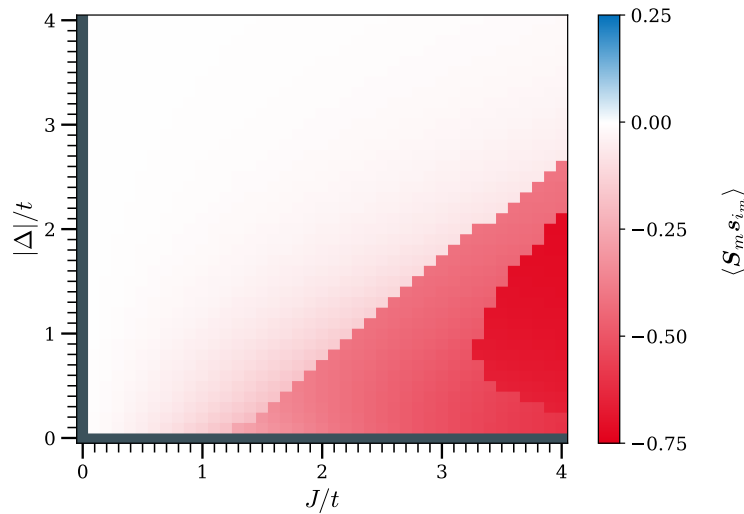


Figure 36: Local spin correlations for a model with two impurities located at sites $i_1 = 41$ and $i_2 = 43$ of a chain of $L = 83$ sites. Figure taken from [CP5], edited.

These four phases of the $d = 2$ phase diagram are similar to what Yao et al. found [107], but here, as the surrounding electronic environment is modelled explicitly, the strong impact of the impurity geometry becomes visible. The phase diagrams discussed here cannot be obtained by simply following the $I = 0$ axis of their publication (I is the explicit RKKY coupling). For $d = 1$, there are no distinct phases at all, but smooth crossovers between different regimes reminiscent of the RKKY-singlet phase and the local-Kondo-singlet phase. The spin-doublet phase is completely absent, which can be understood by considering that a state like $|\text{PKS}\rangle$ could not be the groundstate of the Hamilton operator because both impurities couple to electronic sites from different sublattices. Therefore, as one part of the linear combination removes an $\epsilon_i = +1$ site from the bulk and the other removes an $\epsilon_i = -1$ site, the state with partial Kondo screening cannot be an eigenstate of the unbroken pseudospin generator $\hat{\eta}_{\text{tot}}^{(x)}$.

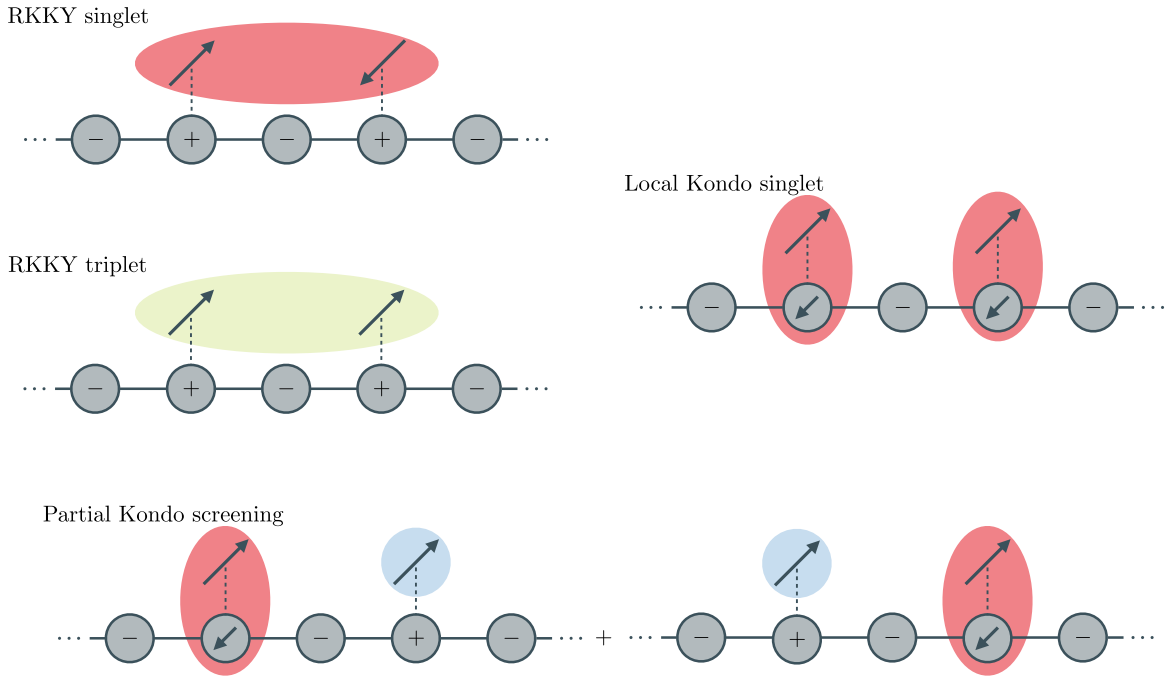


Figure 37: Sketches for the groundstates in the four different phases of the $d = 2$ model. The background shading symbolizes the coupled total spin of the corresponding part of the system (red: singlet, blue: doublet, green: triplet). The signs on the host sites refer to the sublattice sign $\epsilon_i = (-1)^{i-1}\epsilon_1$ and thus the staggered pseudospin field $\mathbf{B}_{\eta,i} = 2|\Delta|\epsilon_i\mathbf{e}_x$. The sketches apply in the following parameter regions: $0 < |\Delta| < \Delta_{\text{AFM}}$ and $J \rightarrow 0$ (RKKY triplet), $|\Delta| > \Delta_{\text{AFM}}$ and $J \rightarrow 0$ (RKKY singlet), $|\Delta| > 0$ and $J \rightarrow \infty$ (local Kondo singlet), $|\Delta| \rightarrow \infty$, $J \rightarrow \infty$ and $|\Delta| \lesssim \frac{3J}{4}$ (partial Kondo screening).

4.3 – Perturbation Theory in the Exchange Coupling

Groundstate of the BCS Hamilton operator

To develop an effective description of the physics at weak exchange coupling J , a perturbative approach is being pursued. To this end, the Hamilton operator from Equation (4.1) is split into the quadratic part of the host electrons,

$$\widehat{H}_0 = -t \sum_{i=1}^L \left(\widehat{c}_{i\uparrow}^\dagger \widehat{c}_{i+1,\uparrow} + \widehat{c}_{i\downarrow}^\dagger \widehat{c}_{i+1,\downarrow} + \widehat{c}_{i+1,\uparrow}^\dagger \widehat{c}_{i\uparrow} + \widehat{c}_{i+1,\downarrow}^\dagger \widehat{c}_{i\downarrow} \right) + \sum_{i=1}^L \left(\Delta \widehat{c}_{i\uparrow}^\dagger \widehat{c}_{i\downarrow}^\dagger + \Delta^* \widehat{c}_{i\downarrow} \widehat{c}_{i\uparrow} \right), \quad (4.7)$$

and the interacting part of the impurities coupling to the host,

$$\widehat{V} = J \sum_{m=1}^M \widehat{\mathbf{S}}_m \widehat{\mathbf{s}}_{i_m}. \quad (4.8)$$

In the case $J = 0$, the system is governed by the non-interacting Hamilton operator of the host \widehat{H}_0 . The impurity spins do not enter the calculation at all, yielding a highly degenerate spectrum of \widehat{H}_0 and the need to perform degenerate perturbation theory. However, the purely electronic host part has a non-degenerate groundstate, as will be shown in the following.

In order to determine the electronic groundstate, a Bogoliubov transformation is carried out, introducing new fermionic operators,

$$\begin{pmatrix} \widehat{f}_{i\uparrow} \\ \widehat{f}_{i\downarrow} \end{pmatrix} = \begin{pmatrix} e^{-i\varphi/2} \widehat{c}_{i\uparrow} \\ e^{i\varphi/2} \widehat{c}_{i\downarrow}^\dagger \end{pmatrix}, \quad \text{with } e^{i\varphi} = \frac{\Delta}{|\Delta|}, \quad (4.9)$$

which eventually leads to a particle-number-conserving Hamilton operator

$$\begin{aligned} \widehat{H}_0 &= -t \sum_{i=1}^L \left(\widehat{f}_{i\uparrow}^\dagger \widehat{f}_{i+1,\uparrow} + \widehat{f}_{i+1,\uparrow}^\dagger \widehat{f}_{i\uparrow} - \widehat{f}_{i\downarrow}^\dagger \widehat{f}_{i+1,\downarrow} - \widehat{f}_{i+1,\downarrow}^\dagger \widehat{f}_{i\downarrow} \right) + |\Delta| \sum_{i=1}^L \left(\widehat{f}_{i\uparrow}^\dagger \widehat{f}_{i\downarrow} + \widehat{f}_{i\downarrow}^\dagger \widehat{f}_{i\uparrow} \right) \\ &= \sum_{i,\sigma,i',\sigma'} h_{i\sigma,i'\sigma'} \widehat{f}_{i\sigma}^\dagger \widehat{f}_{i'\sigma'} = \widehat{\mathbf{f}}^\dagger \mathbf{h} \widehat{\mathbf{f}} \end{aligned} \quad (4.10)$$

with a vector of fermionic operators $\widehat{\mathbf{f}}$ and a Hamilton matrix \mathbf{h} with entries

$$h_{i\sigma,i'\sigma'} = \delta_{ii'}(1 - \delta_{\sigma\sigma'}) |\Delta| - (\delta_{i,i'+1} + \delta_{i+1,i'}) \delta_{\sigma\sigma'} \text{sgn}(\sigma)t, \quad \text{where } \text{sgn}(\uparrow) = +1, \text{sgn}(\downarrow) = -1. \quad (4.11)$$

This $2L \times 2L$ matrix can be diagonalized analytically. By introducing $k_n = \frac{\pi n}{L+1}$ for $1 \leq n \leq L$, which is reminiscent of a crystal momentum (but for this open system, this is not a strict analog), and by setting

$$\varepsilon_n = \sqrt{4t^2 \cos^2(k_n) + |\Delta|^2}, \quad (4.12)$$

the Hamilton matrix can be diagonalized with these coefficients:

$$v_{i\sigma}^{(n,\pm)} = \frac{(\delta_{\sigma\uparrow} \pm \delta_{\sigma\downarrow}) \sin(ik_n)}{\sqrt{L+1}} \cdot \sqrt{1 \mp \frac{2t \text{sgn}(\sigma) \cos(k_n)}{\varepsilon_n}}. \quad (4.13)$$

In fact, one finds:

$$\begin{aligned}
 \sum_{i',\sigma'} h_{i\sigma,i'\sigma'} v_{i'\sigma'}^{(n,\pm)} &= |\Delta| v_{i\sigma}^{(n,\pm)} - t \operatorname{sgn}(\sigma) \left(v_{i-1,\sigma}^{(n,\pm)} + v_{i+1,\sigma}^{(n,\pm)} \right) \\
 &= \sqrt{\varepsilon_n^2 - 4t^2 \cos^2(k_n)} \cdot \frac{(\delta_{\sigma\uparrow} \pm \delta_{\sigma\downarrow}) \sin(ik_n)}{\sqrt{L+1}} \cdot \sqrt{1 \mp \frac{2t \operatorname{sgn}(\sigma) \cos(k_n)}{\varepsilon_n}} \\
 &\quad - t \operatorname{sgn}(\sigma) \cdot \frac{\delta_{\sigma\uparrow} \pm \delta_{\sigma\downarrow}}{\sqrt{L+1}} \cdot \sqrt{1 \mp \frac{2t \operatorname{sgn}(\sigma) \cos(k_n)}{\varepsilon_n}} (\sin((i-1)k_n) + \sin((i+1)k_n)) \\
 &= \sqrt{(\varepsilon_n \mp 2t \operatorname{sgn}(\sigma) \cos(k_n))(\varepsilon_n \pm 2t \operatorname{sgn}(\sigma) \cos(k_n))} \cdot \frac{\pm(\delta_{\sigma\uparrow} \pm \delta_{\sigma\downarrow}) \sin(ik_n)}{\sqrt{L+1}} \cdot \sqrt{1 \pm \frac{2t \operatorname{sgn}(\sigma) \cos(k_n)}{\varepsilon_n}} \\
 &\quad - t \operatorname{sgn}(\sigma) \cdot \frac{\delta_{\sigma\uparrow} \pm \delta_{\sigma\downarrow}}{\sqrt{L+1}} \cdot \sqrt{1 \mp \frac{2t \operatorname{sgn}(\sigma) \cos(k_n)}{\varepsilon_n}} (2 \sin(ik_n) \cos(k_n) + 0 \cos(ik_n) \sin(k_n)) \\
 &= \frac{\delta_{\sigma\uparrow} \pm \delta_{\sigma\downarrow}}{\sqrt{L+1}} \cdot \sqrt{1 \mp \frac{2t \operatorname{sgn}(\sigma) \cos(k_n)}{\varepsilon_n}} (\pm \varepsilon_n + 2t \operatorname{sgn}(\sigma) \cos(k_n) - 2t \operatorname{sgn}(\sigma) \cos(k_n)) = \pm \varepsilon_n v_{i\sigma}^{(n,\pm)}. \quad (4.14)
 \end{aligned}$$

Since $v_{0,\sigma}^{(n,\pm)} \sim \sin(0) = 0$ and $v_{L+1,\sigma}^{(n,\pm)} \sim \sin((L+1)k_n) = \sin(n\pi) = 0$, the first line also holds for the leftmost and rightmost sites of the open chain. The eigenvalues of the Hamilton matrix are thus given by $\pm \varepsilon_n = \pm \sqrt{|\Delta|^2 + 4t^2 \cos^2(k_n)}$. Eigenvectors $\mathbf{v}^{(n,\pm)} = \left(v_{1\uparrow}^{(n,\pm)} \quad v_{1\downarrow}^{(n,\pm)} \quad \dots \quad v_{L\downarrow}^{(n,\pm)} \right)^T$ for different eigenvalues are orthonormal because \mathbf{h} is a real and symmetric matrix. However, since $\varepsilon_{L+1-n} = \sqrt{4t^2 \cos^2(k_{L+1-n}) + |\Delta|^2} = \sqrt{4t^2(-\cos(k_n))^2 + |\Delta|^2} = \varepsilon_n$, most of the eigenvalues are degenerate (except for $n = \frac{L+1}{2}$ in systems with odd sizes). For these eigenvectors, one can readily verify that they are orthonormal by employing the relation

$$\sum_{i=1}^L \sin\left(\frac{\pi in}{L+1}\right) \sin\left(\frac{\pi in'}{L+1}\right) = \frac{L+1}{2} (\delta_{(n-n') \bmod 2(L+1), 0} - \delta_{(n+n') \bmod 2(L+1), 0}). \quad (4.15)$$

The orthogonal matrix \mathbf{V} that is composed of the eigenvectors yields a transformation of the fermionic operators:

$$\widehat{H}_0 = \widehat{\mathbf{f}}^\dagger \mathbf{h} \widehat{\mathbf{f}} = \widehat{\mathbf{f}}^\dagger \mathbf{V} \mathbf{V}^T \mathbf{h} \mathbf{V} \mathbf{V}^T \widehat{\mathbf{f}} = \widehat{\mathbf{b}}^\dagger \boldsymbol{\varepsilon} \widehat{\mathbf{b}}. \quad (4.16)$$

These Bogoliubov quasiparticles can be expressed in terms of electronic creators and annihilators:

$$\widehat{b}_{n,\pm} = \sum_{i,\sigma} v_{i\sigma}^{(n,\pm)} \widehat{f}_{i\sigma} = \sum_i \left(v_{i\uparrow}^{(n,\pm)} e^{i\varphi/2} \widehat{c}_{i\uparrow} + v_{i\downarrow}^{(n,\pm)} e^{-i\varphi/2} \widehat{c}_{i\downarrow} \right), \quad (4.17)$$

and, vice versa,

$$\begin{aligned}
 \widehat{c}_{i\uparrow} &= e^{-i\varphi/2} \sum_{n=1}^L \left(v_{i\uparrow}^{(n,+)} \widehat{b}_{n,+} + v_{i\uparrow}^{(n,-)} \widehat{b}_{n,-} \right), \\
 \widehat{c}_{i\downarrow}^\dagger &= e^{i\varphi/2} \sum_{n=1}^L \left(v_{i\downarrow}^{(n,+)} \widehat{b}_{n,+} + v_{i\downarrow}^{(n,-)} \widehat{b}_{n,-} \right). \quad (4.18)
 \end{aligned}$$

The Hamilton operator takes a diagonal form in these Bogoliubov quasiparticles:

$$\widehat{H}_0 = \sum_{n=1}^L \varepsilon_n \left(\widehat{b}_{n,+}^\dagger \widehat{b}_{n,+} - \widehat{b}_{n,-}^\dagger \widehat{b}_{n,-} \right). \quad (4.19)$$

From this representation of the Hamilton operator, the groundstate can easily be read off: all modes with negative energies are occupied, whilst all modes with positive energies are unoccupied. More precisely, the vacuum of the Bogoliubov quasiparticles $|\text{vac}_b\rangle$ arises from the electron vacuum $|\text{vac}_c\rangle$ by filling all spin-down modes, i. e., $|\text{vac}_b\rangle = \hat{c}_{1\downarrow}^\dagger \cdots \hat{c}_{L\downarrow}^\dagger |\text{vac}_c\rangle$. The groundstate of the BCS Hamilton operator is then given by

$$|\Psi_0\rangle = \hat{b}_{1,-}^\dagger \cdots \hat{b}_{L,-}^\dagger |\text{vac}_b\rangle. \quad (4.20)$$

This state is non-degenerate as claimed above. A straightforward calculation (which can be found in Appendix A.7) shows that this groundstate is a spin singlet and has pseudocharge $Q_\eta = -\frac{1}{2} \cdot \epsilon_1$ for odd and $Q_\eta = 0$ for even system sizes L .

First-Order Perturbation Theory

For $J/t \ll 1$ and $J/\Delta \ll 1$, the coupling between the electronic system and the impurities can be treated as a small perturbation to the BCS Hamilton operator \hat{H}_0 . By means of an effective Hamilton operator that incorporates the low-energy physics of the perturbation order-by-order [120], the first-order correction is given by

$$\hat{H}_{\text{eff}}^{(1)} = \hat{P}_0 \hat{V} \hat{P}_0, \quad (4.21)$$

where \hat{P}_0 is the projector onto the groundstate subspace of the unperturbed Hamilton operator. Since the impurity spins do not contribute to the total energy in the $J = 0$ system, the groundstate space is 2^M -dimensional:

$$\hat{P}_0 = \sum_{\boldsymbol{\sigma}} |\Psi_0, \boldsymbol{\sigma}\rangle \langle \Psi_0, \boldsymbol{\sigma}|. \quad (4.22)$$

Here, $\boldsymbol{\sigma} = (\sigma_1, \dots, \sigma_M)$ describes the tuple of all impurity spin projections in the standard basis for quantum spins-1/2. With this follows:

$$\begin{aligned} \hat{H}_{\text{eff}}^{(1)} &= \frac{J}{2} \sum_{m, \boldsymbol{\sigma}, \boldsymbol{\sigma}'} |\Psi_0, \boldsymbol{\sigma}\rangle \langle \Psi_0, \boldsymbol{\sigma}| \hat{S}_m^{(+)} \hat{s}_{i_m}^{(-)} + \hat{S}_m^{(-)} \hat{s}_{i_m}^{(+)} + 2\hat{S}_m^{(z)} \hat{s}_{i_m}^{(z)} |\Psi_0, \boldsymbol{\sigma}'\rangle \langle \Psi_0, \boldsymbol{\sigma}'| \\ &= \frac{J}{2} \sum_{m, \boldsymbol{\sigma}, \boldsymbol{\sigma}'} |\Psi_0, \boldsymbol{\sigma}\rangle \langle \Psi_0, \boldsymbol{\sigma}'| \left(\langle \boldsymbol{\sigma}| \hat{S}_m^{(+)} |\boldsymbol{\sigma}'\rangle \langle \Psi_0| \hat{s}_{i_m}^{(-)} |\Psi_0\rangle + \langle \boldsymbol{\sigma}| \hat{S}_m^{(-)} |\boldsymbol{\sigma}'\rangle \langle \Psi_0| \hat{s}_{i_m}^{(+)} |\Psi_0\rangle \right. \\ &\quad \left. + 2 \langle \boldsymbol{\sigma}| \hat{S}_m^{(z)} |\boldsymbol{\sigma}'\rangle \langle \Psi_0| \hat{s}_{i_m}^{(z)} |\Psi_0\rangle \right). \end{aligned} \quad (4.23)$$

The fact that $|\Psi_0\rangle$ is a spin singlet implies that expectation values of arbitrary vector operators must vanish, e. g., $\langle \Psi_0| \hat{s}_i |\Psi_0\rangle = 0$. Thus, the first-order correction to the unperturbed Hamilton operator vanishes. This is independent of the system size L , as opposed to the case of a non-superconducting system [103], where there is an odd-even effect and the possibility of a linear Kondo term.

Second-Order Perturbation Theory

The second-order correction to the unperturbed Hamilton operator with respect to the unperturbed groundstate involves a projector P_N onto the subspace of the N -th excited state of \hat{H}_0 :

$$\hat{H}_{\text{eff}}^{(2)} = - \sum_N^{N \neq 0} \frac{\hat{P}_0 \hat{V} \hat{P}_N \hat{V} \hat{P}_0}{E_N - E_0}. \quad (4.24)$$

It can be seen from Equation (A.27) that the action of electron spin operators on the BCS groundstate yields contributions of the form $\hat{b}_{n,+}^\dagger \hat{b}_{n',-} |\Psi_0\rangle$ and $\hat{b}_{n,+}^\dagger \hat{b}_{n',+} |\Psi_0\rangle$ and $\hat{b}_{n,-} \hat{b}_{n',-} |\Psi_0\rangle$ only, i. e., states with two quasiparticle excitations above the groundstate. Their respective energies can be obtained easily:

$$\begin{aligned} \hat{H}_0 \hat{b}_{n,+}^\dagger \hat{b}_{n',-} |\Psi_0\rangle &= \left([\hat{H}_0, \hat{b}_{n,+}^\dagger] + \hat{b}_{n,+}^\dagger \hat{H}_0 \right) \hat{b}_{n',-} |\Psi_0\rangle = \varepsilon_n \hat{b}_{n,+}^\dagger \hat{b}_{n',-} |\Psi_0\rangle + \hat{b}_{n,+}^\dagger \left([\hat{H}_0, \hat{b}_{n',-}] + \hat{b}_{n',-} \hat{H}_0 \right) |\Psi_0\rangle \\ &= \varepsilon_n \hat{b}_{n,+}^\dagger \hat{b}_{n',-} |\Psi_0\rangle + \varepsilon_{n'} \hat{b}_{n,+}^\dagger \hat{b}_{n',-} |\Psi_0\rangle + \hat{b}_{n,+}^\dagger \hat{b}_{n',-} \hat{H}_0 |\Psi_0\rangle = (E_0 + \varepsilon_n + \varepsilon_{n'}) \hat{b}_{n,+}^\dagger \hat{b}_{n',-} |\Psi_0\rangle, \\ \hat{H}_0 \hat{b}_{n,+}^\dagger \hat{b}_{n',+} |\Psi_0\rangle &= (E_0 + \varepsilon_n + \varepsilon_{n'}) \hat{b}_{n,+}^\dagger \hat{b}_{n',+} |\Psi_0\rangle, \\ \hat{H}_0 \hat{b}_{n,-} \hat{b}_{n',-} |\Psi_0\rangle &= (E_0 + \varepsilon_n + \varepsilon_{n'}) \hat{b}_{n,-} \hat{b}_{n',-} |\Psi_0\rangle. \end{aligned} \quad (4.25)$$

Therefore, matrix elements of the perturbation \hat{V} including the BCS groundstate have to vanish unless the other state is of the above mentioned form. This simplifies the projector $\sum_N^{N \neq 0} \hat{P}_N$ that runs over all excited energy eigenspaces. Instead, one can restrict the sum to states with two quasiparticle excitations. The projectors on states with two creators and annihilators need to be rescaled to adjust for the double counting. The term is then given by:

$$\begin{aligned} \hat{H}_{\text{eff}}^{(2)} &= - \sum_{\sigma, \sigma'} \sum_{n, n'} \left(\frac{|\Psi_0, \sigma\rangle \langle \Psi_0, \sigma| \hat{V} \hat{b}_{n,+}^\dagger \hat{b}_{n',-} |\Psi_0, \sigma'\rangle \langle \Psi_0, \sigma'| \hat{b}_{n',-}^\dagger \hat{b}_{n,+} \hat{V} |\Psi_0, \sigma''\rangle \langle \Psi_0, \sigma''|}{E_0 + \varepsilon_n + \varepsilon_{n'} - E_0} \right. \\ &\quad + \frac{1}{2} \frac{|\Psi_0, \sigma\rangle \langle \Psi_0, \sigma| \hat{V} \hat{b}_{n,+}^\dagger \hat{b}_{n',+} |\Psi_0, \sigma'\rangle \langle \Psi_0, \sigma'| \hat{b}_{n',+} \hat{b}_{n,+} \hat{V} |\Psi_0, \sigma''\rangle \langle \Psi_0, \sigma''|}{E_0 + \varepsilon_n + \varepsilon_{n'} - E_0} \\ &\quad \left. + \frac{1}{2} \frac{|\Psi_0, \sigma\rangle \langle \Psi_0, \sigma| \hat{V} \hat{b}_{n',-} \hat{b}_{n,-} |\Psi_0, \sigma'\rangle \langle \Psi_0, \sigma'| \hat{b}_{n,-}^\dagger \hat{b}_{n',-}^\dagger \hat{V} |\Psi_0, \sigma''\rangle \langle \Psi_0, \sigma''|}{E_0 + \varepsilon_n + \varepsilon_{n'} - E_0} \right). \end{aligned} \quad (4.26)$$

Now, the matrix elements can be evaluated with the findings from Appendix A.7:

$$\begin{aligned} \langle \Psi_0, \sigma | \hat{b}_{n',-}^\dagger \hat{b}_{n,+} \hat{V} | \Psi_0, \sigma' \rangle &= \frac{J}{2} \sum_m \langle \Psi_0, \sigma | \hat{b}_{n',-}^\dagger \hat{b}_{n,+} \left(\hat{S}_m^{(+)} \hat{s}_{i_m}^{(-)} + \hat{S}_m^{(-)} \hat{s}_{i_m}^{(+)} + 2\hat{S}_m^{(z)} \hat{s}_{i_m}^{(z)} \right) | \Psi_0, \sigma' \rangle \\ &= \frac{J}{2} \sum_m 2 \langle \Psi_0 | \hat{b}_{n',-}^\dagger \hat{b}_{n,+} \hat{s}_{i_m}^{(z)} | \Psi_0 \rangle \langle \sigma | \hat{S}_m^{(z)} | \sigma' \rangle \\ &= \frac{J}{2} \sum_m \left(v_{i_m \uparrow}^{(n,+)} v_{i_m \uparrow}^{(n',-)} + v_{i_m \downarrow}^{(n,+)} v_{i_m \downarrow}^{(n',-)} \right) \langle \sigma | \hat{S}_m^{(z)} | \sigma' \rangle \\ &= \frac{J}{2} \sum_m \left(v_{i_m \uparrow}^{(n,-)} v_{i_m \downarrow}^{(n',-)} - v_{i_m \downarrow}^{(n,-)} v_{i_m \uparrow}^{(n',-)} \right) \langle \sigma | \hat{S}_m^{(z)} | \sigma' \rangle, \\ \langle \Psi_0, \sigma | \hat{b}_{n',+} \hat{b}_{n,+} \hat{V} | \Psi_0, \sigma' \rangle &= \frac{J}{2} \sum_m \langle \Psi_0 | \hat{b}_{n',+} \hat{b}_{n,+} \hat{s}_{i_m}^{(+)} | \Psi_0 \rangle \langle \sigma | \hat{S}_m^{(-)} | \sigma' \rangle \\ &= \frac{J}{2} \sum_m \left(v_{i_m \uparrow}^{(n,+)} v_{i_m \downarrow}^{(n',+)} - v_{i_m \downarrow}^{(n,+)} v_{i_m \uparrow}^{(n',+)} \right) \langle \sigma | \hat{S}_m^{(-)} | \sigma' \rangle \\ &= \frac{J}{2} \sum_m \left(v_{i_m \uparrow}^{(n,-)} v_{i_m \downarrow}^{(n',-)} - v_{i_m \downarrow}^{(n,-)} v_{i_m \uparrow}^{(n',-)} \right) \langle \sigma | \hat{S}_m^{(-)} | \sigma' \rangle, \\ \langle \Psi_0, \sigma | \hat{b}_{n,-} \hat{b}_{n',-} \hat{V} | \Psi_0, \sigma' \rangle &= \frac{J}{2} \sum_m \langle \Psi_0 | \hat{b}_{n,-} \hat{b}_{n',-} \hat{s}_{i_m}^{(-)} | \Psi_0 \rangle \langle \sigma | \hat{S}_m^{(+)} | \sigma' \rangle \\ &= \frac{J}{2} \sum_m \left(v_{i_m \uparrow}^{(n,-)} v_{i_m \downarrow}^{(n',-)} - v_{i_m \downarrow}^{(n,-)} v_{i_m \uparrow}^{(n',-)} \right) \langle \sigma | \hat{S}_m^{(+)} | \sigma' \rangle. \end{aligned} \quad (4.27)$$

From this one obtains:

$$\begin{aligned}
 \hat{H}_{\text{eff}}^{(2)} &= - \sum_{\sigma, \sigma', \sigma''} \sum_{n, n'} \sum_{m, m'} \frac{|\Psi_0, \sigma\rangle \langle \Psi_0, \sigma''|}{\varepsilon_n + \varepsilon_{n'}} \cdot \frac{J^2}{4} \left(v_{i_m \uparrow}^{(n, -)} v_{i_m \downarrow}^{(n', -)} - v_{i_m \downarrow}^{(n, -)} v_{i_m \uparrow}^{(n', -)} \right) \left(v_{i_{m'} \uparrow}^{(n, -)} v_{i_{m'} \downarrow}^{(n', -)} - v_{i_{m'} \downarrow}^{(n, -)} v_{i_{m'} \uparrow}^{(n', -)} \right) \\
 &\quad \left(\langle \sigma | \hat{S}_m^{(z)} | \sigma' \rangle \langle \sigma' | \hat{S}_{m'}^{(z)} | \sigma'' \rangle + \frac{1}{2} \langle \sigma | \hat{S}_m^{(+)} | \sigma' \rangle \langle \sigma' | \hat{S}_{m'}^{(-)} | \sigma'' \rangle + \langle \sigma | \hat{S}_m^{(-)} | \sigma' \rangle \langle \sigma' | \hat{S}_{m'}^{(+)} | \sigma'' \rangle \right) \\
 &= \sum_{m, m'} \sum_{n, n'} \frac{-J^2 \left(v_{i_m \uparrow}^{(n, -)} v_{i_m \downarrow}^{(n', -)} - v_{i_m \downarrow}^{(n, -)} v_{i_m \uparrow}^{(n', -)} \right) \left(v_{i_{m'} \uparrow}^{(n, -)} v_{i_{m'} \downarrow}^{(n', -)} - v_{i_{m'} \downarrow}^{(n, -)} v_{i_{m'} \uparrow}^{(n', -)} \right)}{4(\varepsilon_n + \varepsilon_{n'})} \hat{P}_0 \hat{S}_m \hat{S}_{m'} \hat{P}_0 \\
 &= \hat{P}_0 \sum_{m, m'} J_{\text{RKKY}}(i_m, i_{m'}) \hat{S}_m \hat{S}_{m'} \hat{P}_0. \tag{4.28}
 \end{aligned}$$

The second-order perturbation theory arrives at an effective Heisenberg model with an RKKY-type coupling between the impurity spins, given by:

$$J_{\text{RKKY}}(i, i') = - \frac{J^2}{4} \sum_{n, n'} \frac{\left(v_{i \uparrow}^{(n, -)} v_{i \downarrow}^{(n', -)} - v_{i \downarrow}^{(n, -)} v_{i \uparrow}^{(n', -)} \right) \left(v_{i' \uparrow}^{(n, -)} v_{i' \downarrow}^{(n', -)} - v_{i' \downarrow}^{(n, -)} v_{i' \uparrow}^{(n', -)} \right)}{\varepsilon_n + \varepsilon_{n'}}. \tag{4.29}$$

This can be brought into another form:

$$\begin{aligned}
 v_{i \uparrow}^{(n, -)} v_{i \downarrow}^{(n', -)} - v_{i \downarrow}^{(n, -)} v_{i \uparrow}^{(n', -)} &= \frac{\sin(ik_n) \sin(ik_{n'})}{L+1} \cdot \left(\sqrt{\left(1 - \frac{2t \cos(k_n)}{\varepsilon_n}\right) \left(1 + \frac{2t \cos(k_{n'})}{\varepsilon_{n'}}\right)} \right. \\
 &\quad \left. - \sqrt{\left(1 + \frac{2t \cos(k_n)}{\varepsilon_n}\right) \left(1 - \frac{2t \cos(k_{n'})}{\varepsilon_{n'}}\right)} \right), \\
 \Rightarrow \left(v_{i \uparrow}^{(n, -)} v_{i \downarrow}^{(n', -)} - v_{i \downarrow}^{(n, -)} v_{i \uparrow}^{(n', -)} \right) \left(v_{i' \uparrow}^{(n, -)} v_{i' \downarrow}^{(n', -)} - v_{i' \downarrow}^{(n, -)} v_{i' \uparrow}^{(n', -)} \right) \\
 &= \frac{\sin(ik_n) \sin(ik_{n'}) \sin(i'k_n) \sin(i'k_{n'})}{(L+1)^2} \left(2 - \frac{8t^2 \cos(k_n) \cos(k_{n'})}{\varepsilon_n \varepsilon_{n'}} - 2\sqrt{\frac{|\Delta|^2}{\varepsilon_n^2} \cdot \frac{|\Delta|^2}{\varepsilon_{n'}^2}} \right) \\
 &= \frac{2}{(L+1)^2} \cdot \sin(ik_n) \sin(ik_{n'}) \sin(i'k_n) \sin(i'k_{n'}) \cdot \frac{\varepsilon_n \varepsilon_{n'} - |\Delta|^2 - 4t^2 \cos(k_n) \cos(k_{n'})}{\varepsilon_n \varepsilon_{n'}}, \\
 \Rightarrow J_{\text{RKKY}}(i, i') &= \frac{-J^2}{2(L+1)^2} \sum_{n, n'} \sin(ik_n) \sin(ik_{n'}) \sin(i'k_n) \sin(i'k_{n'}) \cdot \frac{\varepsilon_n \varepsilon_{n'} - |\Delta|^2 - 4t^2 \cos(k_n) \cos(k_{n'})}{\varepsilon_n \varepsilon_{n'} (\varepsilon_n + \varepsilon_{n'})}. \tag{4.30}
 \end{aligned}$$

By inverting the summation order for n , i.e., $n \rightarrow L+1-n$, and using $\sin(ik_{L+1-n}) = (-1)^{i+1} \sin(ik_n)$, one can identify which terms contribute for odd or even distances $i - i'$:

$$\begin{aligned}
 J_{\text{RKKY}}^{(\text{even})}(i, i') &= \frac{-J^2}{2(L+1)^2} \sum_{n, n'} \sin(ik_n) \sin(ik_{n'}) \sin(i'k_n) \sin(i'k_{n'}) \cdot \frac{\varepsilon_n \varepsilon_{n'} - |\Delta|^2}{\varepsilon_n \varepsilon_{n'} (\varepsilon_n + \varepsilon_{n'})}, \\
 J_{\text{RKKY}}^{(\text{odd})}(i, i') &= \frac{J^2}{2(L+1)^2} \sum_{n, n'} \sin(ik_n) \sin(ik_{n'}) \sin(i'k_n) \sin(i'k_{n'}) \cdot \frac{4t^2 \cos(k_n) \cos(k_{n'})}{\varepsilon_n \varepsilon_{n'} (\varepsilon_n + \varepsilon_{n'})}. \tag{4.31}
 \end{aligned}$$

It is important to note here that Equation (4.28) contains independent sums over m and m' , so that for $m \neq m'$ two terms contribute to the coupling of \hat{S}_m and $\hat{S}_{m'}$. Since the RKKY coupling is symmetric under exchange

of the site indices, the effective RKKY coupling between the impurities is twice the value of $J_{\text{RKKY}}(i_m, i_{m'})$. For $m = m'$, however, no double counting appears.

Up to second order in J/t , the interaction between the impurities and the superconducting host maps onto an effective Heisenberg coupling between the impurities, whose interaction strength depends on the electronic structure of the BCS groundstate. A positive value of J_{RKKY} implies an effective antiferromagnetic coupling between the impurities, while a negative value describes a ferromagnetic coupling. Within the usual RKKY theory for metals, the coupling is found to be staggered between ferro- and antiferromagnetic, enveloped by a decrease with reciprocal distance [19–21]. Due to the presence of an energy gap $2|\Delta|$ in the BCS model, the indirect exchange coupling is more of the Bloembergen–Rowland-type [22] and can be expected as exponentially decreasing with the distance, i. e., $J_{\text{RKKY}}(i, i') \propto e^{-\alpha \cdot |\Delta| \cdot |i-i'|}$ for larger distances, since the tunnel barrier is of the size $|\Delta| \cdot |i - i'|$.

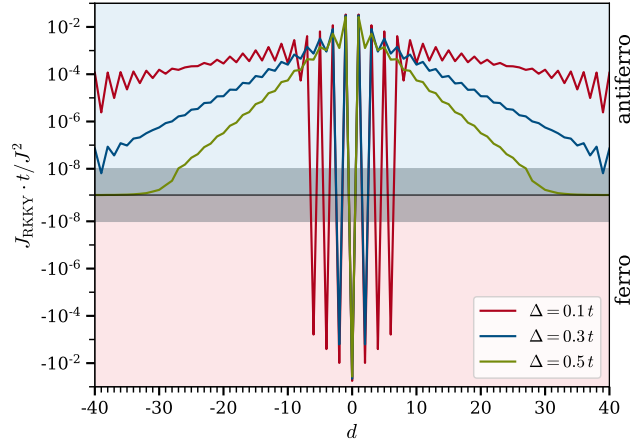


Figure 38: Site dependence of $(2 - \delta_{ii'})J_{\text{RKKY}}(i = 41, i' = 41 + d)$ in a system with $L = 81$ sites for various pairing strengths $|\Delta|$. Figure taken from [CP5], edited.

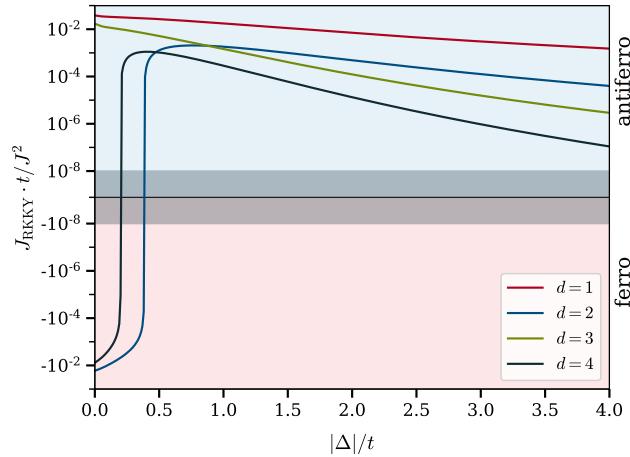


Figure 39: Pairing strength dependence of $2J_{\text{RKKY}}(i = 41, i' = 41 + d)$ in a system with $L = 81 + d$ sites for various distances $d = i' - i$. Figure taken from [CP5], edited.

In Figure 38 and Figure 39, this exponential decrease can be observed. The scale is logarithmic for larger positive and negative values, with a grey shaded area of linear scaling between -10^{-8} and 10^8 . In Figure 38 the spatial dependence of J_{RKKY} is shown for several values of $|\Delta|$ (the energy scale is fixed by $t = 1$). For the weakest pairing strength, an oscillatory behavior around the on-site term can be observed up to a distance of $d = \pm 6$. For larger distances, the formerly staggered exchange coupling stays antiferromagnetic, with a decaying

superimposed oscillation. These oscillations arise again in the vicinity of the system boundary, most likely as Friedel oscillations and thus a manifestation of finite-size effects. The fact that J_{RKKY} stops its sign-change behavior is an interesting deviation from the metallic RKKY theory. It can to some extent be explained by a sum rule which the exchange coupling has to obey and which can be proven with the help of Equation (4.15):

$$\begin{aligned} \sum_{i'=1}^L J_{\text{RKKY}}(i, i') &= \frac{-J^2}{2(L+1)^2} \sum_{n, n'} \sum_{i'=1}^L \sin(ik_n) \sin(ik_{n'}) \sin(i'k_n) \sin(i'k_{n'}) \cdot \frac{\varepsilon_n \varepsilon_{n'} - |\Delta|^2 - 4t^2 \cos(k_n) \cos(k_{n'})}{\varepsilon_n \varepsilon_{n'} (\varepsilon_n + \varepsilon_{n'})} \\ &= \frac{-J^2}{4(L+1)} \sum_n \sin^2(ik_n) \cdot \frac{\varepsilon_n^2 - |\Delta|^2 - 4t^2 \cos^2(k_n)}{2\varepsilon_n^3} = 0. \end{aligned} \quad (4.32)$$

The negative local contribution, which has the biggest absolute value, is not affected by the exponential suppression and has to be compensated by more and more positive but exponentially suppressed values for larger pairings strengths. Indeed, for $|\Delta| \rightarrow \infty$, the local part behaves as $J_{\text{RKKY}}(i, i) \rightarrow \frac{-J^2 t^2}{8|\Delta^3|}$ (for $i \neq 1, L$) and thus decreases only polynomially. Following this argument, one can expect the turning point between alternating coupling to purely antiferromagnetic exchange to shift towards smaller distances for increasing pairing strengths. For $|\Delta| = 0.5t$, the local contribution is the only ferromagnetic one and all other terms are positive.

Figure 39 provides another perspective on this situation: Here, the behavior of the fixed-distance RKKY coupling with varying pairing strength is shown. For $d = 1$ and $d = 3$, the impurities are located in different sublattices of the bipartite host system, such that standard RKKY theory predicts an antiferromagnetic coupling anyway. With increasing gap size, the coupling decreases exponentially, but always stays antiferromagnetic. Situations with even impurity distances appear to be more interesting because of the competition between mechanisms that produce ferromagnetic and antiferromagnetic effective exchange couplings. Indeed, for small pairing strengths, the $d = 2$ and $d = 4$ values start out as ferromagnetic, but with increasing gap size, they change their sign and become antiferromagnetic. The critical value of $|\Delta|$, at which the sign change takes place, is at $\Delta_c = 0.38t$ for $d = 1$. This is in perfect agreement with the critical value read off from the phase diagram in the previous section. For a larger distance, the critical pairing strength can be expected to be smaller, as explained above.

This perturbative effective Hamilton operator from Equation (4.28) can be expected to yield qualitatively good results for small to medium values of J/t , as long as the true groundstate stays close to the BCS groundstate. In order to check the validity of the effective RKKY description, the RKKY couplings can be compared with numerical data obtained by VMPS calculations. If the electronic part of the system is in a state close to the BCS groundstate, the system state takes the form $|\Psi_0\rangle \otimes |S, \sigma\rangle$, in which the host electrons and the impurity spins decouple and the impurity spins form either a singlet state or a triplet state. If one further assumes that those two states constitute the lowest states in their respective $\text{SU}(2)$ irreducible representation, an approximate formula for the effective and emergent RKKY coupling strength can be derived:

$$\begin{aligned} J_{\text{RKKY}}(i_m, i_{m'}) &= (\langle \Psi_0 | \otimes \langle S = 1, \sigma = 1 |) \hat{H}_{\text{eff}}^{(2)} (|\Psi_0\rangle \otimes |S = 1, \sigma = 1\rangle) \\ &\quad - (\langle \Psi_0 | \otimes \langle S = 0, \sigma = 0 |) \hat{H}_{\text{eff}}^{(2)} (|\Psi_0\rangle \otimes |S = 0, \sigma = 0\rangle) \\ &\approx (\langle \Psi_0 | \otimes \langle S = 1, \sigma = 1 |) (\hat{H}_0 + \hat{V}) (|\Psi_0\rangle \otimes |S = 1, \sigma = 1\rangle) \\ &\quad - (\langle \Psi_0 | \otimes \langle S = 0, \sigma = 0 |) (\hat{H}_0 + \hat{V}) (|\Psi_0\rangle \otimes |S = 0, \sigma = 0\rangle) \\ &= E_0(S = 1) - E_0(S = 0). \end{aligned} \quad (4.33)$$

Figure 40 shows a comparison between RKKY coupling strengths as obtained from second order perturbation theory as in Equation (4.30) and the numerical values $J_{\text{RKKY}}^{(\text{num.})} = E_0(S = 1) - E_0(S = 0)$ achieved by targeting the singlet and triplet sectors in the VMPS calculations. For smaller values of J/t , the agreement is excellent. Note that only with the help of a symmetry-adapted VMPS algorithm it is possible to determine the groundstate

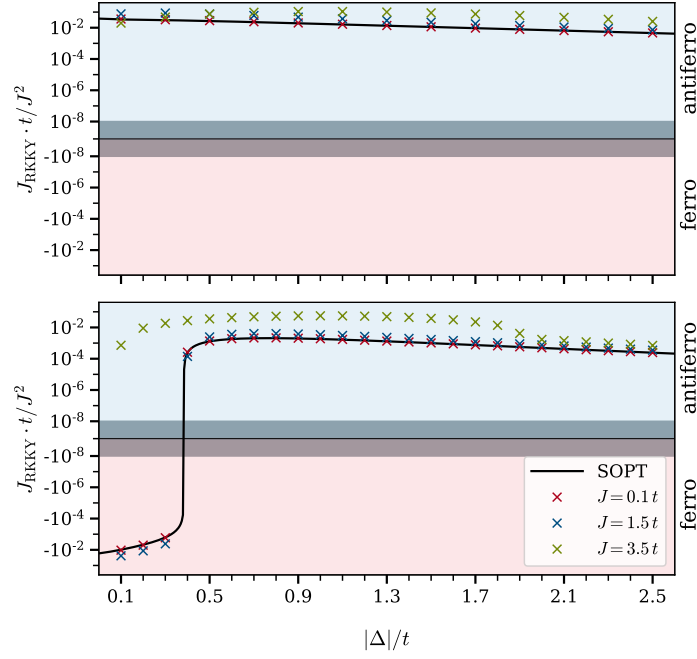


Figure 40: Pairing strength dependence of $J_{\text{RKKY}}(i = 41, i' = 41 + d)$ in a system with $L = 81 + d$ sites for impurity distance $d = 1$ (upper panel) and $d = 2$ (lower panel). The crosses mark the values of $J_{\text{RKKY}}^{(\text{num.})}$ as obtained from the corresponding VMPS calculations. Figure taken from [CP5], edited.

energies in such a precision that the energy difference can be extracted, as the energy difference is six orders of magnitude smaller than the absolute value of the energy. In particular, the critical pairing strength at which even-distance RKKY couplings switch from ferromagnetic to antiferromagnetic can be reproduced very well. For $J/t = 1.5$, small deviations are visible, but the overall trend still is in remarkable agreement, leading to the insight that even for intermediate values of J , the physics can be described by perturbation theory around the BCS groundstate. For even larger $J/t = 3.5$, the approximate formula from Equation (4.33) does not hold anymore, because the nature of the groundstate is qualitatively different and the system exhibits strong correlations between the electronic host system and the impurities.

4.4 – Discussion: Quantum Box, Thermodynamical Limit and Self-Consistency

Dependence on the system size

In Section 4.2 it was pointed out that the groundstates and the occurrence of different phases decisively depends on the local geometry of the system, i.e., on the geometry in the vicinity of the impurities. Therefore, the question arises how this local part of the system behaves on its own. A model with $L = 3$ sites and two impurities attached to the sites $i_1 = 1$ and $i_2 = 3$ can be solved by exact diagonalization. In Appendix A.8, some details are given, from which follows that the groundstate lies in either of the following three symmetry sectors with respect to the three present and mutually compatible symmetries $\text{SU}(2)_{\text{spin}}$, $\text{U}(1)_{\text{charge}}$ and Z_2 (parity with quantum numbers $P \in \{-, +\}$):

$$\begin{aligned}
 \mathcal{H}(S_{\text{tot}} = 0, Q_\eta = -1/2, P = -), \\
 \mathcal{H}(S_{\text{tot}} = 0, Q_\eta = +1/2, P = -), \\
 \mathcal{H}(S_{\text{tot}} = 1/2, Q_\eta = 0, P = +).
 \end{aligned} \tag{4.34}$$

In this $L = 3$ toy model, finite-size effects are expected to dominate the physical properties. First, the finite-size gap turns the indirect magnetic exchange to an antiferromagnetic value irrespective of the superconducting gap $2|\Delta|$, even for $|\Delta| \rightarrow 0$, and even if the distance between the impurities is even. Hence, there is no RKKY-triplet phase. The other phases, RKKY singlet, local Kondo singlet and partial Kondo screening, can already be found in the toy model, as shown in Figure 41.

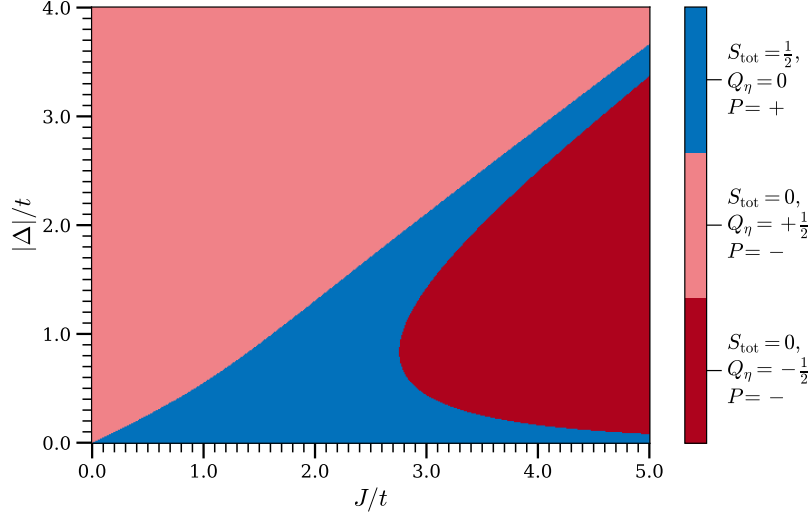


Figure 41: Groundstate phase diagram for a model with two impurities located at sites $i_1 = 1$ and $i_2 = 3$ of a chain of $L = 3$ sites. Figure taken from [CP5], edited.

The advantage of this very small model is that the $|\Delta| \rightarrow 0$ limit becomes accessible, which, in the VMPS treatment of larger systems, is computationally more and more expensive, because of the closing of the gap and the non-locality of the entanglement that builds up.

For $|\Delta| \gtrsim 0$, the BCS groundstate is likely the wrong reference state for the perturbation theory, and one should rather take the groundstate for $\Delta = 0$ as the starting point. For $\Delta = 0$, however, the symmetry of the system is different as the $SU(2)_{\text{charge}}$ is unbroken, and in particular, the number of particles is conserved. Hence, for a system at half-filling with an odd number of sites, the total spin has to be half-integer, and it is not surprising that the spin-doublet phase extends over the entire J axis for $\Delta = 0$. This brings the system into the realm of previously studied *Kondo-vs.-RKKY quantum box* physics [103]. Here, the perturbation theory for the exchange coupling is again regularized, but this time by the finite-size gap. The qualitatively different effective Hamilton operator up to second order in J/t takes the form

$$\hat{H}_{\text{eff}}^{(2)} = J_{\text{Kondo}} \left(\hat{\mathbf{S}}_1 + \hat{\mathbf{S}}_2 \right) \hat{\mathbf{s}}_F + 2J_{\text{RKKY}} \hat{\mathbf{S}}_1 \hat{\mathbf{S}}_2. \quad (4.35)$$

For $L = 3$ and $N = 3$ at half-filling, which is the *on-resonant* case with a spin-degenerate Fermi orbital $|\sigma\rangle_F$, a positive exchange coupling J_{Kondo} arises which couples the impurity spins and the magnetic moment of the singly occupied Fermi orbital. This finite-size Kondo exchange coupling is linear in J and thus, for sufficiently weak J , wins over $J_{\text{RKKY}} \propto J^2$. However, since both impurities couple to the same Fermi spin $\hat{\mathbf{s}}_F = \frac{1}{2} \sum_{\sigma, \sigma'} \boldsymbol{\sigma}_{\sigma\sigma'} \hat{c}_{F\sigma}^\dagger \hat{c}_{F\sigma'}$, which only provides a single screening channel, one impurity must remain unscreened, yielding a finite-size Kondo groundstate that resembles the form of the partial-Kondo-screening doublet (with $|\text{occ}\rangle$ describing the occupied levels below the Fermi orbital):

$$|\text{FSK}\rangle = \frac{1}{\sqrt{6}} |\text{occ}\rangle \otimes \left(\underbrace{(|\uparrow\rangle_F \otimes |\downarrow\rangle_1 \otimes |\sigma\rangle_2 - |\downarrow\rangle_F \otimes |\uparrow\rangle_1 \otimes |\sigma\rangle_2)}_{\text{Kondo singlet with first impurity}} + \underbrace{(|\uparrow\rangle_F \otimes |\sigma\rangle_1 \otimes |\downarrow\rangle_2 - |\downarrow\rangle_F \otimes |\sigma\rangle_1 \otimes |\uparrow\rangle_2)}_{\text{Kondo singlet with second impurity}} \right). \quad (4.36)$$

The main difference to the previously mentioned extreme PKS state is that both impurities are coupled to and screened by the same delocalized magnetic moment. Indeed, this leads to perfect ferromagnetic correlation between the impurities at $\Delta = 0$ and small J : $\langle \text{FSK} | \hat{S}_1 \hat{S}_2 | \text{FSK} \rangle = \frac{1}{4}$. This crossover in the spin-doublet phase to strong ferromagnetic coupling of the impurities can be seen in Figure 42 at $\Delta = 0$ and in the limit $J \rightarrow 0$.

For larger exchange couplings J , the groundstate gradually evolves into a state with local Kondo screening of the impurities. In Figure 43, the build-up of local antiferromagnetic correlations between the impurities and their respective host sites can be observed. For $J/t \rightarrow \infty$, the groundstate in the doublet phase consists of two locally screened Kondo singlets and a singly occupied lattice site $i = 2$ due to half-filling. Obviously, this state does not undergo a partial Kondo screening, as the doublet excess spin is located in the host system instead of an unscreened impurity.

If now $|\Delta|$ is switched on, the electronic configuration at the central site immediately changes from a spin doublet into the state $\frac{1}{\sqrt{2}}(|0\rangle - |\uparrow\downarrow\rangle)$, which is a spin singlet and an eigenstate of $\hat{\eta}_{\text{tot}}^{(x)}$. Hence, for strong exchange coupling, the spin-doublet phase becomes smaller and smaller and in the limit $J/t \rightarrow \infty$ only persists for $\Delta = 0$.

Overall, for $\Delta = 0$, there is a smooth crossover from a regime of finite-size Kondo physics with ferromagnetically coupled impurities to local Kondo singlets with uncorrelated impurities, without a discontinuous jump of the groundstate.

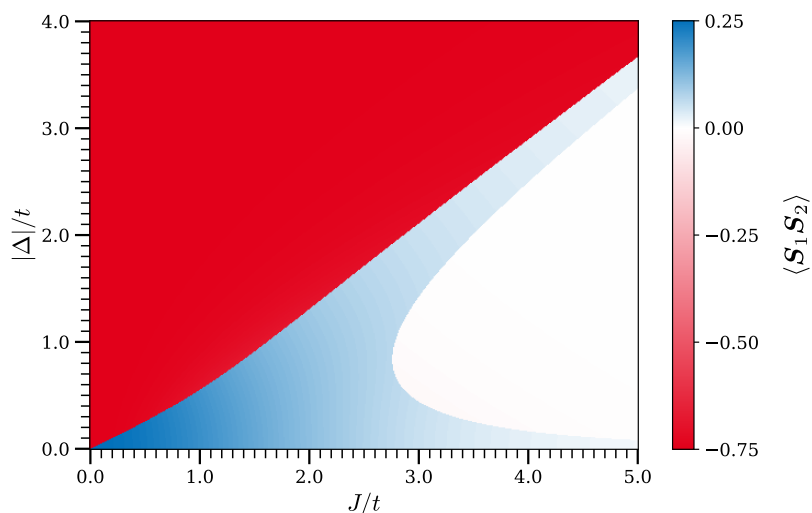


Figure 42: Impurity spin correlations for a model with two impurities located at sites $i_1 = 1$ and $i_2 = 3$ of a chain of $L = 3$ sites. Figure taken from [CP5], edited.

It is tempting to assume that for $\Delta = 0$ but larger systems, the doublet phase still extends over the entire J axis. With increasing L , the realm of the finite-size Kondo effect on the J axis shrinks and eventually vanishes in the thermodynamic limit. Hence, the small- J behavior is rather governed by the RKKY exchange between the impurities, which becomes ferromagnetic for sufficiently large systems and for impurity distance $d = 2$. For an odd number of host sites, the system without pairing terms has to have half-integer spin – however, in the RKKY region, the Fermi spin- $1/2$ is delocalized and completely smeared out over the extent of the system. In that sense, the fact that the system is a spin doublet (or quartet, depending on the total number of host sites) has no strong influence in the thermodynamic limit. The situation changes for increasing J , roughly when the bulk Kondo energy scale $T_K \propto e^{-1/J}$ exceeds the energy scales of finite-size Kondo and RKKY couplings. As explained above, the doublet excess spin is then localized at the central site of the host system between the now Kondo-screened impurities. This localized doublet can couple to the left and right host bulks by the inverse indirect magnetic exchange mechanism [121, 122], if the parts left and right to the impurities have non-

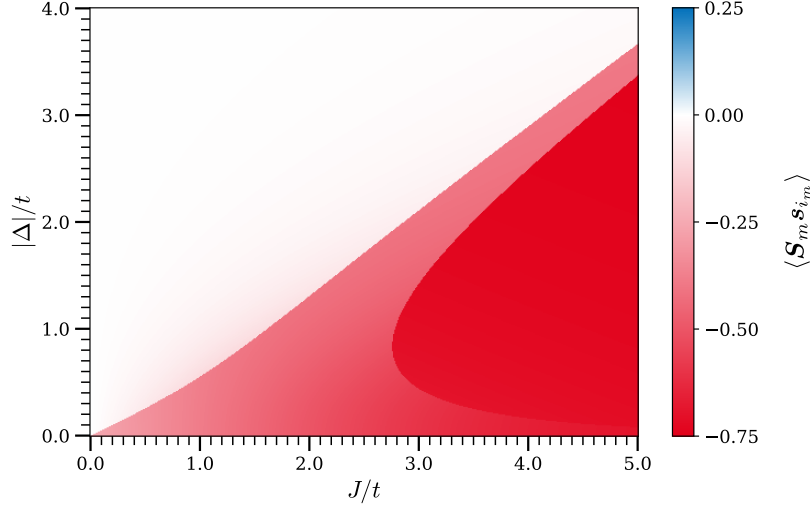


Figure 43: Local spin correlations for a model with two impurities located at sites $i_1 = 1$ and $i_2 = 3$ of a chain of $L = 3$ sites. Figure taken from [CP5], edited.

vanishing total spin, i. e., for $L = 4n + 1$, $n \in \mathbb{N}$. In this on-resonance scenario for the environmental host sites, this mechanism suggests that the three effective magnetic moments couple ferromagnetically, implying that the total spin quartet is slightly favored over the doublet for $\Delta = 0$ and $J \rightarrow \infty$. In this quartet state, two of the involved spins are thermodynamically irrelevant, as they are delocalized over the entire right and left bulk of the system.

For $L = 3$ and for weak parameters J and $|\Delta|$, the competition between the finite-size Kondo effect $\propto J$ (favoring the local electronic states $|\uparrow\rangle$ and $|\downarrow\rangle$) and the superconducting pairing $\propto |\Delta|$ (favoring $|0\rangle$ and $|\uparrow\downarrow\rangle$) creates a linear phase transition line. If the pairing wins, the electronic host changes its fermion parity from odd to even (which under the constraint of half-filling $\sum_{i=1}^3 \sum_{\sigma} \langle \hat{c}_{i\sigma}^\dagger \hat{c}_{i\sigma} \rangle = 3$ is only possible due to the partial breaking of the $SU(2)_{\text{charge}}$) and mediates an antiferromagnetic coupling of the Bloembergen–Rowland-type between the impurities, resulting in an RKKY singlet.

For larger systems, the weak- J and weak- $|\Delta|$ region is not dominated by the finite-size Kondo effect anymore, but by the indirect magnetic exchange between the impurities. Already very small pairing strengths are sufficient to drive the system from the PKS phase for $\Delta = 0$ into the RKKY phase. In contrast to the small model dominated by the finite-size gap, in the thermodynamic limit, the emergent even-distance J_{RKKY} is negative, yielding a ferromagnetic exchange coupling. When the pairing strength exceeds a certain value, the value for J_{RKKY} turns positive again, making the impurities align antiferromagnetically. As this sign flip of the emergent coupling can be understood by perturbation theory for weak J , there is a critical pairing strength $\Delta_{\text{AFM}} \approx 0.38 t$ which describes the phase transition line between RKKY singlet and RKKY triplet. In the region where perturbation theory applies, this critical pairing strength does not depend on J . All these assumptions for the thermodynamic limit are well in line with the VMPS results for the system with $L = 83$ sites from Figure 34, which comes close to the limit of $L \rightarrow \infty$ concerning the locality of the energy contributions proportional to J and $|\Delta|$.

Self-consistency

A central idea of the BCS theory of conventional superconductivity is that due to lattice distortions caused by electrons, other electrons are attracted to the location of the lattice distortion, yielding an attractive retarded contribution to the interaction among electrons [105, 106]. For a particular set of electrons (i. e., electrons in the vicinity of the Fermi edge, typically within an energy range of width of the Debye frequency ω_D), this can be modelled on a phenomenological level by an attractive- U Hubbard model:

$$\hat{H} = -t \sum_{\langle i,j \rangle, \sigma} \hat{c}_{i\sigma}^\dagger \hat{c}_{j\sigma} + U \sum_i \hat{c}_{i\uparrow}^\dagger \hat{c}_{i\downarrow}^\dagger \hat{c}_{i\downarrow} \hat{c}_{i\uparrow}, \quad (4.37)$$

with $U < 0$. This conceptually very reduced and simple model still is hard to solve due to the interaction term. While in principle the VMPS technique would be quite capable of finding groundstates for (at least one-dimensional) Hubbard models, a typical approach relies on the finding by Cooper which suggests that fermions subject to an attraction tend to create a bound state of two fermions [123]. This instability towards electron pairing provides another starting point for a perturbative treatment of the interaction, in which, for a mean-field decoupling of the quartic term, one should not neglect the terms with two fermionic creators or annihilators:

$$\begin{aligned} \hat{c}_{i\uparrow}^\dagger \hat{c}_{i\downarrow}^\dagger \hat{c}_{i\downarrow} \hat{c}_{i\uparrow} &\approx \underbrace{\langle \hat{c}_{i\uparrow}^\dagger \hat{c}_{i\uparrow} \rangle \langle \hat{c}_{i\downarrow}^\dagger \hat{c}_{i\downarrow} \rangle}_{\text{density-density interaction}} + \underbrace{\langle \hat{c}_{i\downarrow}^\dagger \hat{c}_{i\downarrow} \rangle \langle \hat{c}_{i\uparrow}^\dagger \hat{c}_{i\uparrow} \rangle - \langle \hat{c}_{i\uparrow}^\dagger \hat{c}_{i\downarrow} \rangle \langle \hat{c}_{i\downarrow} \hat{c}_{i\uparrow} \rangle}_{\text{magnetism}} + \underbrace{\langle \hat{c}_{i\uparrow}^\dagger \hat{c}_{i\downarrow} \rangle \langle \hat{c}_{i\downarrow} \hat{c}_{i\uparrow} \rangle + \langle \hat{c}_{i\downarrow} \hat{c}_{i\uparrow} \rangle \langle \hat{c}_{i\uparrow}^\dagger \hat{c}_{i\downarrow}^\dagger \rangle}_{\text{Cooper instability}} \\ &\quad - \underbrace{\langle \hat{c}_{i\uparrow}^\dagger \hat{c}_{i\uparrow} \rangle \langle \hat{c}_{i\downarrow}^\dagger \hat{c}_{i\downarrow} \rangle + \langle \hat{c}_{i\uparrow}^\dagger \hat{c}_{i\downarrow} \rangle \langle \hat{c}_{i\downarrow} \hat{c}_{i\uparrow} \rangle - \langle \hat{c}_{i\uparrow}^\dagger \hat{c}_{i\downarrow}^\dagger \rangle \langle \hat{c}_{i\downarrow} \hat{c}_{i\uparrow} \rangle}_{\text{avoid double counting}} \end{aligned} \quad (4.38)$$

When keeping the pairing terms, the $U(1)_{\text{charge}}$ symmetry of electron number conservation (which is always present for Hamilton operators containing only terms with the same number of creators and annihilators) is explicitly broken by the pair-creating and pair-annihilating processes:

$$\begin{aligned} \hat{H}_{\text{MF}} &= -t \sum_{\langle i,j \rangle, \sigma} \hat{c}_{i\sigma}^\dagger \hat{c}_{j\sigma} + U \sum_i \left(\langle \hat{c}_{i\uparrow}^\dagger \hat{c}_{i\downarrow}^\dagger \rangle \hat{c}_{i\downarrow} \hat{c}_{i\uparrow} + \langle \hat{c}_{i\downarrow} \hat{c}_{i\uparrow} \rangle \hat{c}_{i\uparrow}^\dagger \hat{c}_{i\downarrow}^\dagger - \langle \hat{c}_{i\uparrow}^\dagger \hat{c}_{i\downarrow}^\dagger \rangle \langle \hat{c}_{i\downarrow} \hat{c}_{i\uparrow} \rangle \right) \\ &= -t \sum_{\langle i,j \rangle, \sigma} \hat{c}_{i\sigma}^\dagger \hat{c}_{j\sigma} + \sum_i \left(\Delta_i^* \hat{c}_{i\downarrow} \hat{c}_{i\uparrow} + \Delta_i \hat{c}_{i\uparrow}^\dagger \hat{c}_{i\downarrow}^\dagger - \frac{|\Delta_i|^2}{U} \right) \quad \text{with } \Delta_i = U \langle \hat{c}_{i\downarrow} \hat{c}_{i\uparrow} \rangle. \end{aligned} \quad (4.39)$$

This means that the previous approach to include an ab-initio fixed and translationally invariant Δ as an external parameter could be improved by determining the value of the local pairing strengths self-consistently, i. e., by iteratively calculating the expectation values $\langle \Psi | \hat{c}_{i\downarrow} \hat{c}_{i\uparrow} | \Psi \rangle$ with a groundstate for some choice of parameters $\mathbf{\Delta} = (\Delta_1, \dots, \Delta_L)$, and using these to determine new parameters, until the results do not change anymore. The pairing strength is bounded by $|\Delta_i| \leq -\frac{U}{2}$, because $|\langle \hat{c}_{i\downarrow} \hat{c}_{i\uparrow} \rangle| \leq \frac{1}{2}$.

Another comment is in order: the usual mean-field decoupling is constructed in such a way that the grand-canonical potential is varied over the manifold of Hamilton operators quadratic in creators and annihilators. For the self-consistent solution, the grand-canonical potential becomes stationary. However, this finding relies on the use of Wick's theorem, which only applies for quadratic Hamilton operators. While the Hamilton operator from Equation (4.37) yields exactly the previously mentioned self-consistency relation $\Delta_i = U \langle \hat{c}_{i\downarrow} \hat{c}_{i\uparrow} \rangle$, the same is not obviously true in the case of an additional interaction that is not treated by a mean-field decoupling. Since the impurity-host exchange interaction $J\hat{S}_1\hat{s}_{i_1} + J\hat{S}_2\hat{s}_{i_2}$ remains, the used approach is somewhat tentative.

Due to its computational accessibility, this is done for the $L = 3$ toy model to see how a self-consistent BCS treatment of the conventional superconductivity changes the previous results. The first observation is that although they are in principle unconstrained, the self-consistent groundstate produces pairing strengths which all have the same complex phase (or shifted by π , thus giving a minus sign). Hence one can still assume that

Δ_i are real numbers. This is quite intuitive if the picture of an external pseudospin field is used:

$$\Delta_i \hat{c}_{i\uparrow}^\dagger \hat{c}_{i\downarrow}^\dagger + \Delta_i^* \hat{c}_{i\uparrow} \hat{c}_{i\downarrow} = U \epsilon_i^2 \langle \hat{\eta}_i^{(-)} \rangle \hat{\eta}_i^{(+)} + U \epsilon_i^2 \langle \hat{\eta}_i^{(+)} \rangle \hat{\eta}_i^{(-)} = 2U \left(\langle \hat{\eta}_i^{(x)} \rangle \hat{\eta}_i^{(x)} + \langle \hat{\eta}_i^{(y)} \rangle \hat{\eta}_i^{(y)} \right). \quad (4.40)$$

This pseudospin-field coupling $\mathbf{B}_{\eta,i} \hat{\eta}_i$ in the x - y plane yields a minimal energy if all pseudospin fields $\mathbf{B}_{\eta,i} = 2U \langle \hat{\eta}_i \rangle$ are aligned in the same (or opposite) direction, because all other contributions to the Hamilton operator are scalars with respect to the pseudospin and hence do not interfere with their alignment.

Choosing $\Delta_i \in \mathbb{R}$ without loss of generality, the phases of the three-site model are characterized by the two quantum numbers total spin S_{tot} and pseudocharge Q_η . The spatial parity is violated during the self-consistency, yielding a non-parity-symmetric Hamilton operator, which in turn does not give a parity-symmetric groundstate.

A second direct insight is that the sign of Q_η loses its meaning. What can already be assumed from the pseudospin-field picture becomes evident via a short calculation. Let $|\Psi\rangle$ be a self-consistent groundstate of the Hamilton operator $\hat{H}(\Delta)$ (which of course depends on the pairing strength parameters), i. e.,

$$\begin{aligned} \hat{H}_{\text{MF}}(\Delta) |\Psi\rangle &= E(\Delta) |\Psi\rangle, \\ \text{while also } \Delta_i &= U \epsilon_i \langle \Psi | \hat{\eta}_i^{(-)} | \Psi \rangle. \end{aligned} \quad (4.41)$$

Then, the action of $\hat{R} = \exp\left(i\pi \hat{\eta}_{\text{tot}}^{(z)}\right)$ gives another state $|\Phi\rangle = \hat{R} |\Psi\rangle$, which is also a solution of the self-consistency condition:

$$\begin{aligned} \tilde{\Delta}_i &= U \epsilon_i \langle \Phi | \hat{\eta}_i^{(-)} | \Phi \rangle = U \epsilon_i \langle \Psi | \hat{R}^\dagger \hat{\eta}_i^{(-)} \hat{R} | \Psi \rangle = U \epsilon_i \langle \Psi | -\hat{\eta}_i^{(-)} | \Psi \rangle = -\Delta_i, \\ \text{and } \hat{H}_{\text{MF}}(\tilde{\Delta}) |\Phi\rangle &= \hat{R} \hat{R}^\dagger \hat{H}(\tilde{\Delta}) \hat{R} |\Psi\rangle = \hat{R} \hat{H}(-\tilde{\Delta}) |\Psi\rangle = \hat{R} \hat{H}(\Delta) |\Psi\rangle = \hat{R} E(\Delta) |\Psi\rangle = E(\Delta) |\Phi\rangle. \end{aligned} \quad (4.42)$$

Therefore, if $|\Psi\rangle$ has pseudocharge Q_η , there is another solution of the self-consistency condition $\exp\left(i\pi \hat{\eta}_{\text{tot}}^{(z)}\right) |\Psi\rangle$ with the negative pseudocharge: $\langle \Psi | \exp\left(-i\pi \hat{\eta}_{\text{tot}}^{(z)}\right) \hat{\eta}_{\text{tot}}^{(x)} \exp\left(i\pi \hat{\eta}_{\text{tot}}^{(z)}\right) | \Psi \rangle = -Q_\eta$.

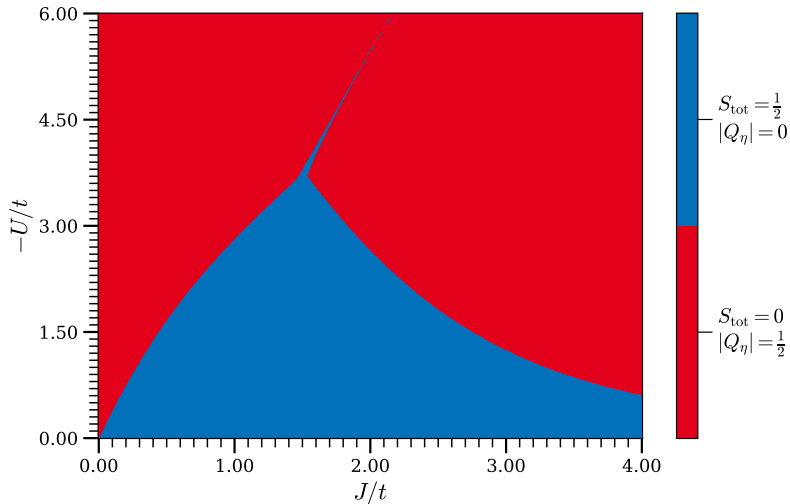


Figure 44: Phase diagram of the self-consistently determined groundstate for a model with two impurities located at sites $i_1 = 1$ and $i_2 = 3$ of a chain of $L = 3$ sites.

In Figure 44, only the absolute value of the calculated pseudocharge is shown. One finds general similarities between this phase diagram and the phase diagram in Figure 41. However, since the self-consistent pairing strengths are not translationally uniform, there is no one-to-one mapping between the former $|\Delta|$ axis and the $-U$ axis. The groundstate phase diagram has to be discussed in the context of the self-consistently determined

superconducting pairing strengths, which can be found in Figure 45. From there, it is obvious that a major part of the spin-doublet phase does not come with any conventional superconductivity, as all three pairing strengths vanish: $\Delta_1 = \Delta_2 = \Delta_3 = 0$. Since in the resulting Hamilton operator no pair-creating or pair-annihilating terms appear, the physics is the same as in the previous investigation of the $|\Delta| = 0$ model. In this case, the groundstate must have half-integer spin.

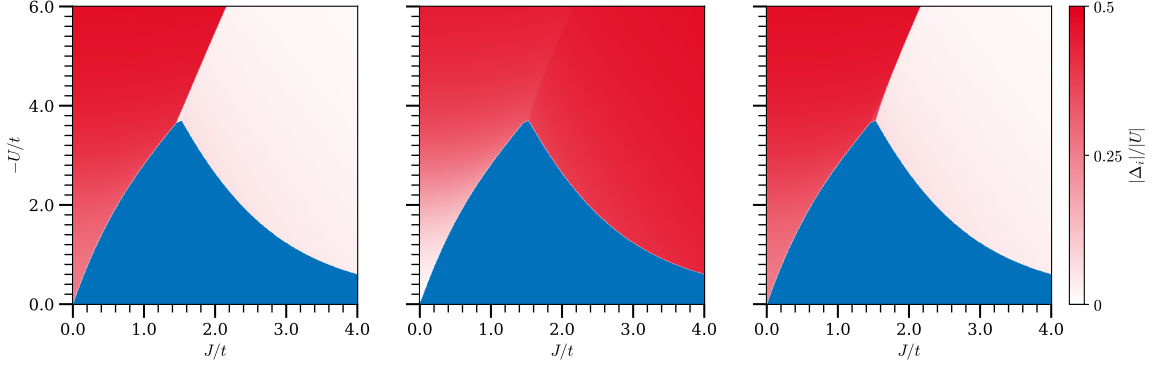


Figure 45: Pairing strengths for a model with two impurities located at sites $i_1 = 1$ and $i_2 = 3$ of a chain of $L = 3$ sites in the self-consistently determined groundstate. Δ_1 : left panel, Δ_2 : middle panel, Δ_3 : right panel. Values smaller than 10^{-4} are colorized in blue to differentiate trivial from non-trivial solutions.

More interesting are those parts of the phase diagram where a non-trivial superconducting solution could be obtained. Indeed, an RKKY-singlet and a local-Kondo-singlet phase could be found. The RKKY singlet again appears for weak exchange couplings J and all Hubbard interactions U . In this regime, the pairing strengths are pronounced, as the pseudospin is strongly polarized on all three sites. Only for small values of $-U$, small deviations from the maximum value are visible, in particular for the central site. This is in line with the expectations, as for weak interaction the hopping term gives the dominant energy scale, and the central site is the only site that has two neighbors. Indeed, from Figure 46 one can learn that the impurity spins are aligned antiferromagnetically with $\langle \hat{S}_1 \hat{S}_2 \rangle \approx -\frac{3}{4}$. Thus, this phase exhibits an impurity singlet on top of a superconducting host system.

The right part of the phase diagram is dominated by the local-Kondo-singlet phase. Because the sign of the pseudocharge has no meaning anymore as mentioned above, this phase is characterized by the same quantum numbers as the RKKY singlet. However, as can be seen in Figure 46, the impurity spin correlation vastly differs, with the impurity spin correlation function vanishing in this phase. The local Kondo screening needs spin polarization in the host system, which in turn reduces the pseudospin polarization. Accordingly, the pairing strengths at the impurity sites $i_1 = 1$ and $i_2 = 3$ are small compared to the central site, where $|\Delta_2| \approx -\frac{U}{2}$.

These two spin-singlet phases are separated by a thin spin-doublet phase. This doublet phase, which is connected to the trivial (at least from a superconductivity point of view) spin-doublet phase, allows for a non-trivial self-consistent solution. Figure 47 represents a zoom into the interesting parameter range for this non-trivial doublet. The phase only appears for a rather small parameter regime and shrinks with increasing $-U$, but its extension remains finite. Opposed to the RKKY and local Kondo singlet, which respect the spatial reflection symmetry ($\Delta_1 = \Delta_3$), the thin doublet phase realizes a spatial symmetry breaking. The first site shows a very small pairing strength, while the other two support pronounced pairing. The fact that it is always the first site which exhibits reduced pairing was achieved by introducing a biased initial configuration – of course, also the state with interchanged roles of first and last sites constitutes a solution of the self-consistency condition. By this breaking of reflection symmetry, the system realizes a partial Kondo screening: the first site is excluded from the superconductivity but is used to screen the first impurity, $\langle \hat{S}_1 \hat{s}_{i_1} \rangle \approx -\frac{3}{4}$. The third site does not screen the other impurity, $\langle \hat{S}_2 \hat{s}_{i_2} \rangle \approx 0$, so that this dangling impurity spin creates a spin doublet.

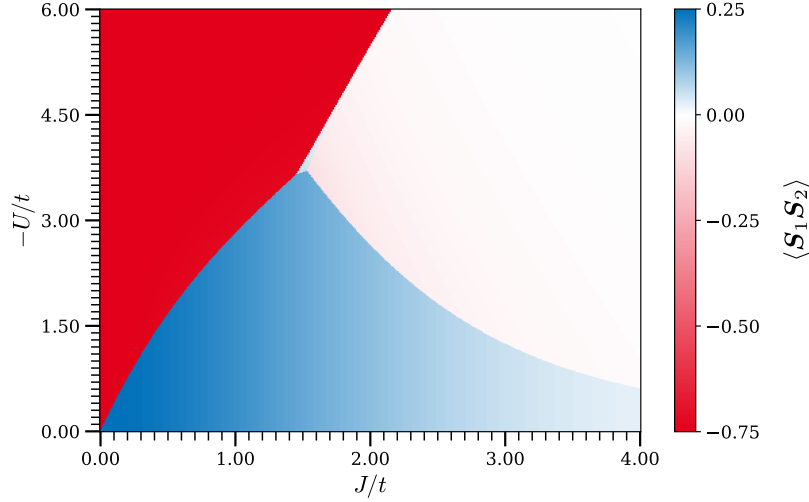


Figure 46: Impurity spin correlations for a model with two impurities located at sites $i_1 = 1$ and $i_2 = 3$ of a chain of $L = 3$ sites in the self-consistently determined groundstate. Figure taken from [CP5], edited.

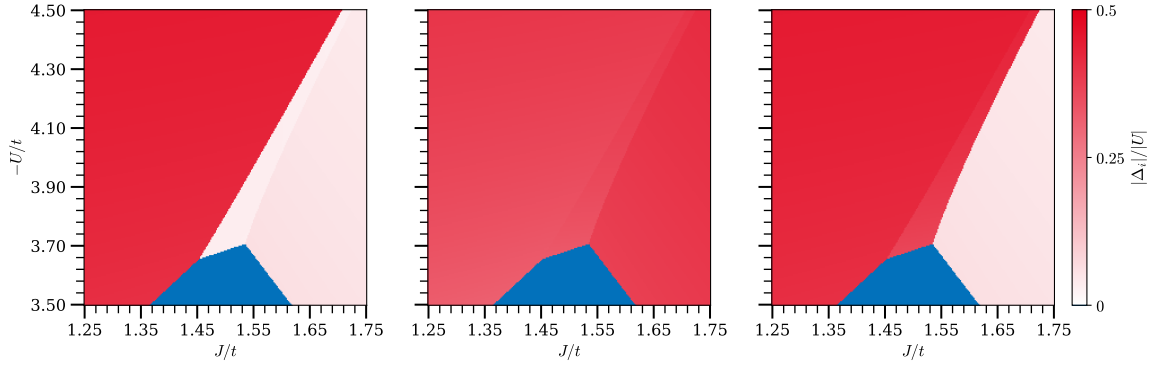


Figure 47: Pairing strengths for a model with two impurities located at sites $i_1 = 1$ and $i_2 = 3$ of a chain of $L = 3$ sites in the self-consistently determined groundstate. Δ_1 : left panel, Δ_2 : middle panel, Δ_3 : right panel. Values smaller than 10^{-4} are colorized in blue to differentiate trivial from non-trivial solutions. The angular shape of the phase boundaries is not a numerical artifact, but the true progression of the transition line, as the image is made up from $> 60\,000$ data points.

All in all, the topology of the phase diagram is the same as the topology of the non-self-consistent toy model, with an RKKY-singlet phase for weak J , a local-Kondo-singlet phase for strong J , and a spin-doublet phase in between. The only difference lies in the nature of the doublet phase, which is subdivided into two parts. In a large range of the parameters, in particular at smaller $-U$, the self-consistent solution is trivial with respect to the build-up of pairing correlations. Due to the absence of the fermionic pairing, the $\Delta = 0$ physics of the RKKY-vs.-Kondo quantum box is recovered. For larger $-U$, the spin doublet shows pairing correlations and realizes a spatial symmetry breaking to accommodate a partial-Kondo-screening phase. In the self-consistent approach, this phase has a smaller extension compared to the fixed- Δ approach, indicating that the partial Kondo screening is somewhat fragile and favored by the ad-hoc choice of a superconducting pairing. However, since the topology seems so similar and there are almost no qualitative differences, in the publication [CP5] the self-consistent approach was not extended to larger systems, where multiple VMPS calculations would have been needed for each data point.

5 – Conclusion

Summary

In this thesis, a symmetry-adapted matrix-product-state approach was applied to various problems in the context of quantum magnetism. To this end, the computational technique of *Variation of Matrix Product States* was reviewed in detail.

Matrix product states are certain factorizations of quantum states, which resemble simple product states but allow for the coefficients to be matrix-valued to encode entanglement. They provide a platform for a variational optimization of quantum states over a certain subset of the entire many-body Hilbert space, with the variational manifold given by all states which can be represented by a matrix product state of a certain maximum bond dimension. It can be shown that groundstates of non-critical Hamilton operators with short-range interactions obey an area-law for the entanglement, guaranteeing that the entanglement in groundstates of one-dimensional systems does not grow with the system size. In situations where the necessary bond dimension for a faithful representation is too large for feasible computations, a truncated matrix product state yields an approximation to the true state with matching entanglement structure.

The matrix-product-state ansatz introduces a mapping to a linear chain that is particularly suitable for computational algorithms. A well-established algorithm is used for groundstate search, which makes use of this linearity by carrying out local optimizations of the energy and sweeping through the matrix product state to approach the global minimum.

In the presence of symmetries the tensors in the VMPS approach factorize into one part that only depends on the quantum numbers labelling the irreducible representations, and another part that is completely determined by symmetry. The latter part of the tensor network can be contracted independently, offering a severe speed-up in calculation time and more precise results because mixtures of states from different irreducible representations can be avoided. A special focus of this work is on the handling of matrix product operators. Since a very precise matrix-product representation of the Hamilton operator is needed many times throughout a groundstate computation, it is highly beneficial to have a small yet exact matrix product operator at hand. The simultaneous appearance of intensive and extensive singular values impedes the naive compression algorithm for matrix product states that relies on singular value decomposition. Instead, the tensors are compressed analytically exact by detecting and eliminating redundant information.

The efficiently constructed and compressed matrix product operators are applied to a range of physical systems in Chapter 3, where VMPS results from a joint work with R. Rausch and M. Peschke are presented. These physical systems are (i) the fullerene molecule C_{60} [CP1], (ii) a similar cage-like molecule called *sodalite cage* [CP2], and (iii) atomic nuclei and the interaction among nucleons [CP4]. A fourth publication from this collaboration, which is concerned with ferrimagnetism on a sawtooth chain, was not considered in this thesis [CP3]. What the investigated models have in common is that the physical systems are not inherently one-dimensional, thus yielding non-local contributions in the Hamilton operator if a mapping to a linear chain of sites is introduced. In this case it is crucial to have compact MPO representations. In particular the squares of the Hamilton operators, which are needed for the determination of the energy variance and thus serve as a convergence check for the VMPS calculations, benefit significantly in the form of a reduced bond dimension.

The antiferromagnetic Heisenberg model with quantum spins- $1/2$ was studied on the C_{60} fullerene geometry as an approximate description of the itinerant electrons in the $2p_z$ orbitals. With the fullerene geometry containing pentagonal faces, this model exhibits quantum spin frustration as the spins cannot be aligned in a staggered way on rings with odd numbers of vertices. However, the frustration is lifted to some extent by hexagonal faces that are located between pentagonal faces. The main finding is that the spin correlations in the groundstate are fairly short-range, with a correlation distance of $\xi \approx 1.4$ in terms of inter-atom distances

with respect to an exponential fit of the spin correlation function. The absence of long-range correlations, which would require paths that contain edges of pentagons, lifts the geometrical frustration of the molecule. Instead, a lot of correlation is allocated on the nearest-neighbor bonds between two hexagons. The first excited spin-triplet state is overall nine-fold degenerate and distributes its excess spin on an equatorial ring of the molecule.

The sodalite-cage geometry, which is a similar ball-shaped molecule that has been experimentally synthesized using atoms with larger spin, is also studied for the antiferromagnetic $S = 1/2$ Heisenberg model. This can be thought of as the extreme quantum limit where frustration effects and quantum fluctuations are most pronounced. The matrix product representation of the Hamilton operator for the sodalite-cage geometry with its 60 sites has to be chosen very carefully in order not to arrive at high bond dimensions due to long-range magnetic exchange. Therefore, before the compression algorithm is applied, the adjacency graph of the geometry is transformed using the Cuthill-McKee algorithm. The obtained site-numbering has an adjacency graph of reduced bandwidth, so that after compression, the MPO bond dimension is feasible for calculations on computing clusters. The groundstate is found to be in a non-trivial irreducible representation of the octahedral symmetry of the molecule, indicating a spontaneous breaking of the spatial symmetry, which is only restored when considering the mixed state that contains the full multiplet of states. Moreover, the spin correlations in the groundstate separate the molecule into three parts: one belt around the equator and two regions around opposite poles. The spin correlations between these areas are quite weak, and each of these areas comes close to a spin singlet on its own.

The magnetization curve was calculated by targeting different quantum numbers of total spin, which is possible when the $SU(2)_{\text{spin}}$ symmetry of the model is incorporated in the VMPS code. It shows wide plateaus at special fractions of the saturation magnetization, which partially can be traced back to localized magnons. These spinful excitations can be confined to the squares or hexagons which are surrounded by triangles, as an analytical calculation shows.

The third publication in this context leaves the field of condensed matter and switches to nuclear physics, where the VMPS technique is applied to find groundstates of interacting nucleons. The protons and neutrons in atomic nuclei, and in particular the quarks they consist of, are subject to the strong interaction, mediated by gluons. On a less fundamental level, the interaction is accurately described as an attractive strong force between the nucleons which relies on the exchange of pions. This two-species fermionic problem can be brought into the form needed for the VMPS algorithms by mapping the different orbitals to the sites of a linear chain. The transition amplitudes between the orbitals are translated into hopping terms, the orbital energies are derived from the so-called Woods-Saxon potential, and the pion exchange is modelled by an attractive interaction term. The Woods-Saxon potential is an effective single-particle potential motivated phenomenologically, which already helps in understanding the stability of some lighter nuclei, i. e., the occurrence of magic numbers of protons and neutrons which describe nucleon numbers that are energetically favored and therefore stabilized. However, one needs to include interactions beyond the smeared-out mean-field-like Woods-Saxon potential in order to reach more realistic models. Motivated by the Cooper instability of conventional superconductivity, a simple yet non-trivial approach to the interaction is to consider fermion pairing, in which two time-conjugated nucleons form a singlet of spin, and these singlets couple to each other. This singlet-coupling model can be expanded by allowing for other spin quantum numbers to couple, e. g., triplet coupling.

The groundstates of the singlet-coupling model for tin and lead can be found quite easily by employing the VMPS method. The somewhat surprising reason for this is that even though the nucleus is a system of correlated fermions the entanglement inside the nucleus is rather low. Indeed, the entanglement entropy of the system can be used to trace back closures of energy shells or sub-shells which are related to magic numbers. For even nucleon numbers, the computations can be further simplified by reformulating the model in a pseudospin representation, yielding an anisotropic Heisenberg-like model in an external field – in terms of charge-pseudospins. The ladder operators of this charge-pseudospin correspond to pair-creation and pair-annihilation operators.

The more realistic model with couplings between general spin multiplets is much more involved and needs more computation time in order to obtain a converged groundstate. Nevertheless, the VMPS technique has proven capable of solving problems from nuclear physics while providing a new perspective on nucleon fillings and magic numbers in terms of entanglement.

In addition to the aforementioned topics, which are presented in an overview format, this thesis places a significant emphasis on the interplay between indirect magnetic exchange and local Kondo screening on a conventional superconductor, which describe two opposing coupling mechanisms for magnetic moments. To this end, a Kondo impurity model with two quantum spins- $1/2$ located at the center of a one-dimensional BCS superconductor is investigated using VMPS. Although the exchange interaction precludes the single-particle treatment of this problem, the presence of the superconducting gap in the electronic single-particle sector appears to facilitate the algorithm. In contrast to previous NRG studies, the indirect magnetic exchange between the impurities is not taken as an external parameter of the model, but it arises as an emergent interaction mediated by the superconducting host system. It thus depends strongly on the properties of the electrons and is susceptible to the system geometry in the vicinity of the impurities. The considered systems are sufficiently large to ensure that the impurities are essentially free from finite-size effects, which otherwise would affect the physical properties and break the universality of the results.

In the theoretical description once again the charge-pseudospins play a major role. Conventional superconductors are the prime examples in which the Cooper instability produces fermion pairing. In the BCS approach, however, the $U(1)$ symmetry describing particle number conservation is broken explicitly by a mean-field-like decoupling of an interaction term into pair-creation and pair-annihilation terms. This is in contrast to the previously mentioned nuclear-pairing problem, where a faithful description of the interaction was the focus, while here, the mechanism for superconductivity is not the primary object of interest. In terms of charge-pseudospins, the $SU(2)_{\text{charge}}$ is broken, but there is a somewhat subtle $U(1)_{\text{charge}}$ symmetry left. The symmetry axis is positioned in the x - y plane, depending on the complex phase of the pairing strength Δ . The existence of this residual symmetry implies the existence of a conserved pseudocharge which can be used to characterize eigenstates of the Hamilton operator. The superconductivity favors the polarization of pseudospins which hinders the spin polarization necessary for magnetic ordering.

For strong antiferromagnetic impurity-host coupling, each impurity spin is screened individually by the electronic host. In the extreme case, a local Kondo singlet is formed between each impurity and the local magnetic moment at its corresponding host site.

For a weak coupling of the impurities to the host system, the groundstate of the system is dominated by the electronic energy scales. Therefore, the host system takes its purely electronic groundstate and is only weakly entangled with the impurity spins. Depending on whether the emergent indirect magnetic exchange coupling between the impurities favors ferromagnetic or antiferromagnetic alignment, the impurity spins form a singlet or a triplet. For an odd distance between the impurities (in terms of electronic lattice sites), the standard RKKY theory for metals predicts an antiferromagnetic coupling, so that an RKKY singlet is obtained. For an even impurity distance, both impurities couple to sites from the same sublattice of the bipartite chain, and one expects a ferromagnetic exchange coupling and an RKKY triplet. It turns out, however, that this only holds for weak superconducting pairing strengths, while for stronger pairing strengths, one finds an RKKY singlet. This behavior can be explained by perturbation theory for weak impurity-host exchange. In second order, the effective Hamilton operator projects the electronic part to the BCS groundstate and yields an effective Heisenberg model for the impurity spins with a numerically accessible RKKY coupling. Due to the presence of a single-particle gap $2|\Delta|$ in the electronic host system, the indirect magnetic exchange drops off exponentially, and since there is a sum rule for all possible exchange couplings, distant couplings turn antiferromagnetic irrespective of the sublattice for increasing energy gap to compensate the strong ferromagnetic local contribution.

How the system evolves from one regime to the other again depends on the distance between the impurities. For an odd impurity distance, a smooth crossover between an RKKY singlet and a local Kondo singlet is ob-

tained. For an even distance, the groundstate phase diagram becomes richer: apart from the already mentioned RKKY-singlet to RKKY-triplet phase transition with increasing pairing strength, there also appears another phase that is a doublet of total spin and that, for sufficiently large pairing strengths, exhibits a partial Kondo screening, i. e., the screening of only one of the impurities whilst the other remains free, creating a doublet. This phase acts as an intermediate step between the RKKY-singlet phase and the local-Kondo-singlet phase. The occurrence of these four phases with local quantum phase transitions between them can be traced back to the quantum numbers which characterize the conceptualized extreme states. For odd distance, the RKKY singlet and the local Kondo singlet have the same quantum numbers, which allows for a smooth crossover. For an even distance, the pseudospin for the RKKY singlet and the local Kondo singlet is different, necessitating a change in the quantum number if the groundstate changes due to a level crossing. Moreover, the extreme partial-Kondo-screening state cannot be an eigenstate of the conserved pseudospin for an odd impurity distance, making such a phase impossible.

The same setup is also studied on a toy model with only three lattice sites and the impurities located at the left and right site. Here, the finite-size effects dominate, and the finite-size gap causes the indirect magnetic exchange obtained by second-order perturbation theory to be always antiferromagnetic. The advantage of this small model is its numerical accessibility, so that the interesting limit $\Delta \rightarrow 0$ can be investigated. In this limit, the finite-size Kondo effect emerges as the dominant phenomenon for weak coupling. A straight phase-transition line is produced by the competing linear-in- J finite-size Kondo effect and the linear-in- $|\Delta|$ superconductivity. This model is also studied with self-consistently adapted pairing strengths, which yields the same topology of the phase diagram with a somewhat shrunk partial-Kondo-screening phase.

Outlook

The broad variety of applications covered in this thesis underlines the versatility of the VMPS method, which can be applied to a plethora of physical problems. While it performs excellent for one-dimensional gapped systems with short-range interactions, it can also deal with several critical systems or mesoscopic systems in higher dimensions. The key towards employing VMPS in higher dimensions is the efficient handling of matrix product operators. If the mapping of local Hilbert spaces to a linear chain, i. e., the enumeration of sites, can be accomplished in a manner that aligns with the a priori unknown entanglement structure of the system – that is to say, the entanglement is predominantly local and does not grow too fast – then the system is well-suited for the VMPS ansatz. Symmetry-adapted and compressed matrix product operators facilitate the groundstate search, because smaller tensors have to be contracted in the local optimizations during sweeping. The entanglement, which is the decisive property for the success of VMPS, represents an observable that yields a distinct perspective on the classification of states of matter. For higher-dimensional systems in which matrix product states do not suffice, there exist more advanced tensor networks building upon the VMPS ansatz, such as *projected entangled pair states* (PEPS) or *multi-scale entanglement renormalization ansatz* (MERA) [68, 69], which are often a better choice for two-dimensional lattice problems.

On a physical level, it would be interesting to study the fullerene and sodalite-cage molecule in terms of the Hubbard model, i. e., by modelling itinerant electrons instead of localized magnetic moments within the Heisenberg model. As the local Hilbert space of the Hubbard model is doubled compared to that of the Heisenberg model, this needs substantially longer computation times, but it is not out of reach. It is known that lattices of fullerene molecules doped with alkali metals can exhibit superconductivity [7, 124], while also being prone to photoinduced high-temperature superconductivity [8]. A possible scenario could go into the direction to employ the VMPS method as a solver for a C_{60} block in a Cluster-Dynamical-Mean-Field calculation for these lattices. Regarding the nuclear-pairing problem, future research may aim to describe more realistic models, i. e., using more general Hamilton operators and taking into account, for example, spatial distortions like the Jahn–Teller effect [125].

The interaction of two magnetic impurities on a superconducting host and their magnetic coupling mechanisms are interesting and important on their own, because they serve as a building block for more complex structures. By employing the Lanczos transformation [126], single-impurity problems with rather general substrate geometries and dimensionalities can be mapped to an impurity coupled to a one-dimensional chain, which increases the relevance of a profound understanding of the physics in one-dimensional systems.

The fact that the emergent indirect magnetic exchange coupling can switch from ferromagnetism to antiferromagnetism depending on the superconducting gap paves the way for possible experimental applications: since the gap can be modified, e. g., by varying the temperature, the sign of exchange coupling and thus the spin alignment can be controlled experimentally. Moreover, other ways of opening a gap in the electronic system could also enable control over the magnetic coupling. As discussed in Chapter 4, the Semenoff-like insulator [127] with a staggered on-site potential is related to the BCS superconductor by a unitary transformation in pseudospin space and thus leads to the same physics as discussed above.

Open questions regarding the system under investigation are related to the weaknesses of the VMPS technique as a wavefunction-based method. One obtains the groundstate at zero temperature with an excellent precision, but the thermal state and the excitations remain unknown. While there are algorithms at hand for temperature dependence, such as the *Time-Evolving Block Decimation* for evolving the density operator in imaginary time from initially infinite temperature [60], there might be better choices than VMPS to answer these questions. It would be intriguing to see one-particle excitations such as the Yu–Shiba–Rusinov states in the energy gap [128], and how they participate in the Kondo-screening mechanisms at work [129]. Assuming that the critical temperature for BCS superconductivity lies below the Kondo temperature, how does the Kondo resonance evolve upon lowering the temperature, i. e., by opening the superconducting gap? What kind of influence do excitations have on the competition between Kondo screening and indirect magnetic exchange?

A natural next step is to add more impurities. The transition from the Kondo impurity model to the Kondo lattice model promises the appearance of heavy-fermion physics with flat bands [95, 130, 131], which would have a strong impact on the indirect magnetic exchange. Furthermore, the localized Yu–Shiba–Rusinov states that appear in the superconducting gap for a dilute impurity distribution turn into Yu–Shiba–Rusinov subgap bands for an increasing number of impurities. Such a subgap band is thought to be capable of hosting p-wave superconductivity, because superconducting features are imprinted on these states by the proximity effect [132]. Therefore, the low-energy effective model of a conventional s-wave superconductor with many quantum spins- $1/2$ on top could be described by a Kitaev chain [133] and thus be an interesting model in terms of Majorana physics, topological superconductivity, and topological quantum computing [112, 117, 134–137].

A – Appendix

A.1 – Hilbert Spaces of MPS and MPO Bond Indices

For the left-to-right constructed MPS Hilbert spaces from Equation (2.35),

$$\mathcal{H}_{\text{MPS}}(\ell) = \text{span}(|i_\ell\rangle \mid 1 \leq i_\ell \leq \chi_\ell) \quad \text{with} \quad |i_\ell\rangle = \sum_{n_\ell, i_{\ell-1}} A(\ell)_{i_{\ell-1} n_\ell}^{i_\ell} |i_{\ell-1}\rangle \otimes |n_\ell\rangle,$$

the states $|i_\ell\rangle$ form an ONB for $\mathcal{H}_{\text{MPS}}(\ell)$, if all MPS tensors $\mathbf{A}(1), \dots, \mathbf{A}(\ell)$ are left-normalized: $\langle j_0 | i_0 \rangle = \delta_{i_0 j_0}$ is obvious, because $\mathcal{H}_{\text{MPS}}(0)$ is one-dimensional. If the states $|i_{\ell-1}\rangle$ form an ONB of $\mathcal{H}_{\text{MPS}}(\ell-1)$, then:

$$\begin{aligned} \langle j_\ell | i_\ell \rangle &= \left(\sum_{m_\ell, j_{\ell-1}} A^\dagger(\ell)_{j_\ell}^{j_{\ell-1} m_\ell} \langle j_{\ell-1} | \otimes \langle m_\ell | \right) \left(\sum_{n_\ell, i_{\ell-1}} A(\ell)_{i_{\ell-1} n_\ell}^{i_\ell} |i_{\ell-1}\rangle \otimes |n_\ell\rangle \right) \\ &= \sum_{n_\ell, m_\ell, i_{\ell-1}, j_{\ell-1}} A^\dagger(\ell)_{j_\ell}^{j_{\ell-1} m_\ell} A(\ell)_{i_{\ell-1} n_\ell}^{i_\ell} \delta_{i_{\ell-1} j_{\ell-1}} \delta_{n_\ell m_\ell} = \sum_{n_\ell, i_{\ell-1}} A^\dagger(\ell)_{j_\ell}^{i_{\ell-1} n_\ell} A(\ell)_{i_{\ell-1} n_\ell}^{i_\ell} = \delta_{i_\ell j_\ell}. \end{aligned}$$

Although the states form an orthonormal basis for the MPS Hilbert space $\mathcal{H}_{\text{MPS}}(\ell)$, they are in general not a basis for $\mathcal{H}_{\text{loc}}(1) \otimes \dots \otimes \mathcal{H}_{\text{loc}}(\ell)$ of which $\mathcal{H}_{\text{MPS}}(\ell)$ is a subspace, because $\dim(\mathcal{H}_{\text{MPS}}(\ell)) = \chi_\ell \leq d_1 \dots d_\ell$.

For right-to-left constructed MPS Hilbert spaces (Equation (2.36)),

$$\widetilde{\mathcal{H}}_{\text{MPS}}(\ell) = \text{span}(\widetilde{|i_{\ell-1}\rangle} \mid 1 \leq i_{\ell-1} \leq \chi_{\ell-1}) \quad \text{with} \quad \widetilde{|i_{\ell-1}\rangle} = \sum_{n_\ell, i_\ell} A(\ell)_{i_{\ell-1} n_\ell}^{i_\ell} |n_\ell\rangle \otimes \widetilde{|i_\ell\rangle},$$

the reasoning is completely analogous: $\langle \widetilde{j_L} | \widetilde{i_L} \rangle = \delta_{i_L j_L}$ because $\dim(\widetilde{\mathcal{H}}_{\text{MPS}}(L+1)) = 1$, and for right-normalized $\mathbf{A}(\ell), \dots, \mathbf{A}(L)$:

$$\begin{aligned} \langle \widetilde{j_{\ell-1}} | \widetilde{i_{\ell-1}} \rangle &= \left(\sum_{m_\ell, j_\ell} A^\dagger(\ell)_{j_\ell}^{j_{\ell-1} m_\ell} \langle m_\ell | \otimes \langle j_\ell | \right) \left(\sum_{n_\ell, i_\ell} A(\ell)_{i_{\ell-1} n_\ell}^{i_\ell} |n_\ell\rangle \otimes \widetilde{|i_\ell\rangle} \right) \\ &= \sum_{n_\ell, m_\ell, i_\ell, j_\ell} A^\dagger(\ell)_{j_\ell}^{j_{\ell-1} m_\ell} A(\ell)_{i_{\ell-1} n_\ell}^{i_\ell} \delta_{i_\ell j_\ell} \delta_{n_\ell m_\ell} = \sum_{n_\ell, i_\ell} A^\dagger(\ell)_{j_\ell}^{i_{\ell-1} n_\ell} A(\ell)_{i_{\ell-1} n_\ell}^{i_\ell} = \delta_{i_{\ell-1} j_{\ell-1}}. \end{aligned}$$

If the MPS tensors are not left- or right-normalized, the states $|i_\ell\rangle$ and $\widetilde{|i_{\ell-1}\rangle}$ still form a basis for their respective Hilbert spaces as long as the MPS tensors are minimal in that sense that they do not encode redundant information, i. e., the matrices created from the MPS tensors by combining either the incoming MPS index and the physical index or the outgoing MPS index and the physical index into one index have full rank.

The same insights apply to the case of MPO bond indices and their respective Hilbert spaces. Normalization of the MPO tensors,

$$\begin{aligned} \text{Left-Normalization:} \quad & \sum_{n_\ell, m_\ell, k_{\ell-1}} W^\dagger(\ell)_{i_\ell n_\ell}^{k_{\ell-1} m_\ell} W(\ell)_{k_{\ell-1} m_\ell}^{k_\ell n_\ell} = \delta_{k_\ell i_\ell}, \\ \text{Right-Normalization:} \quad & \sum_{n_\ell, m_\ell, k_\ell} W^\dagger(\ell)_{k_\ell n_\ell}^{i_{\ell-1} m_\ell} W(\ell)_{k_{\ell-1} m_\ell}^{k_\ell n_\ell} = \delta_{k_{\ell-1} i_{\ell-1}}, \end{aligned} \tag{A.1}$$

can be achieved by the procedure detailed above for the case of MPS tensors by joining the two physical indices

n_ℓ and m_ℓ at every site. Then the states

$$|k_\ell\rangle = \sum_{n_\ell, m_\ell, k_{\ell-1}} W(\ell)_{k_{\ell-1} m_\ell}^{k_\ell n_\ell} |k_{\ell-1}\rangle \otimes |n_\ell\rangle \langle m_\ell| \quad \text{for } 1 \leq \ell \leq L \text{ and } |k_0\rangle = 1$$

$$\text{with } \mathcal{H}_{\text{MPO}}(\ell) = \text{span}(|k_\ell\rangle \mid 1 \leq k_\ell \leq \mu_\ell) \subseteq \mathcal{H}_{\text{loc}}(1) \otimes \mathcal{H}_{\text{loc}}^*(1) \otimes \cdots \mathcal{H}_{\text{loc}}(\ell) \otimes \mathcal{H}_{\text{loc}}^*(\ell)$$

$$|\widetilde{k_{\ell-1}}\rangle = \sum_{n_\ell, m_\ell, k_\ell} W(\ell)_{k_{\ell-1} m_\ell}^{k_\ell n_\ell} |n_\ell\rangle \langle m_\ell| \otimes |\widetilde{k_\ell}\rangle \quad \text{for } 1 \leq \ell \leq L \text{ and } |\widetilde{k_L}\rangle = 1$$

$$\text{with } \widetilde{\mathcal{H}}_{\text{MPO}}(\ell) = \text{span}\left(|\widetilde{k_{\ell-1}}\rangle \mid 1 \leq k_{\ell-1} \leq \mu_{\ell-1}\right) \subseteq \mathcal{H}_{\text{loc}}(\ell) \otimes \mathcal{H}_{\text{loc}}^*(\ell) \otimes \cdots \mathcal{H}_{\text{loc}}(L) \otimes \mathcal{H}_{\text{loc}}^*(L) \quad (\text{A.2})$$

form orthonormal basis sets for their respective MPO Hilbert spaces:

$$\langle l_\ell | k_\ell \rangle = \delta_{k_\ell l_\ell} \quad \text{if } \mathbf{W}(1), \dots, \mathbf{W}(\ell) \text{ left-normalized.}$$

$$\langle \widetilde{l_{\ell-1}} | \widetilde{k_{\ell-1}} \rangle = \delta_{k_{\ell-1} l_{\ell-1}} \quad \text{if } \mathbf{W}(L), \dots, \mathbf{W}(\ell) \text{ right-normalized.} \quad (\text{A.3})$$

A.2 – Minimizing the Frobenius Scalar Product

Let $\mathbf{D} \in \text{Mat}(n, m)$ be a diagonal matrix of rank $r \leq \min(m, n)$ with diagonal entries sorted in descending order, $d_1 \geq d_2 \geq \dots \geq d_r > 0$, and let $\mathbf{X} \in \text{Mat}(n, m)$ be a diagonal matrix of rank $k < r$ with diagonal entries sorted in descending order, $x_1 \geq x_2 \geq \dots \geq x_k > 0$. This type of matrices appear in singular value decompositions.

Claim: For arbitrary unitary matrices $\mathbf{U} \in \text{Mat}(n, n)$ and $\mathbf{V} \in \text{Mat}(m, m)$:

$$M(\mathbf{D}, \mathbf{X}) := \max_{\mathbf{U}, \mathbf{V}} \left(\text{Re} \left(\text{tr} \left(\mathbf{X}^\dagger \mathbf{U} \mathbf{D} \mathbf{V}^\dagger \right) \right) \right) = \text{tr} \left(\mathbf{X}^\dagger \mathbf{D} \right), \quad (\text{A.4})$$

where this maximum is achieved for $\mathbf{U} = \mathbf{1}_n$ and $\mathbf{V} = \mathbf{1}_m$.

Proof: The matrices \mathbf{D} and \mathbf{X} can be written as a product of smaller matrices:

$$\mathbf{D} = \begin{pmatrix} \mathbf{S} \\ \mathbf{0} \end{pmatrix} \begin{pmatrix} \mathbf{S} & \mathbf{0} \end{pmatrix} \quad \text{where } \mathbf{S} \in \text{Mat}(r, r), \quad S_{ij} = \begin{cases} \sqrt{d_i}, & i = j \\ 0, & \text{otherwise} \end{cases}$$

$$\mathbf{X} = \begin{pmatrix} \mathbf{T} \\ \mathbf{0} \end{pmatrix} \begin{pmatrix} \mathbf{T} & \mathbf{0} \end{pmatrix} \quad \text{where } \mathbf{T} \in \text{Mat}(r, r), \quad T_{ij} = \begin{cases} \sqrt{x_i}, & i = j \leq k \\ 0, & \text{otherwise} \end{cases}$$

With this:

$$\begin{aligned} M(\mathbf{D}, \mathbf{X}) &\leq \max_{\mathbf{U}, \mathbf{V}} \left(\left| \text{tr} \left(\begin{pmatrix} \mathbf{T} \\ \mathbf{0} \end{pmatrix} \begin{pmatrix} \mathbf{T} & \mathbf{0} \end{pmatrix} \mathbf{U} \begin{pmatrix} \mathbf{S} \\ \mathbf{0} \end{pmatrix} \begin{pmatrix} \mathbf{S} & \mathbf{0} \end{pmatrix} \mathbf{V}^\dagger \right) \right| \right) \\ &= \max_{\mathbf{U}, \mathbf{V}} \left(\left| \text{tr} \left(\begin{pmatrix} \mathbf{V} \begin{pmatrix} \mathbf{S} \\ \mathbf{0} \end{pmatrix} \end{pmatrix}^\dagger \begin{pmatrix} \mathbf{T} \\ \mathbf{0} \end{pmatrix} \begin{pmatrix} \mathbf{T} & \mathbf{0} \end{pmatrix} \mathbf{U} \begin{pmatrix} \mathbf{S} \\ \mathbf{0} \end{pmatrix} \right) \right| \right) \end{aligned}$$

Now the columns of $\mathbf{U} \begin{pmatrix} \mathbf{S} \\ \mathbf{0} \end{pmatrix}$ constitute r orthogonal vectors $\mathbf{a}_1, \dots, \mathbf{a}_r \in \mathbb{C}^n$:

$$\mathbf{a}_i = \left(\sqrt{d_i} U_{1i} \quad \dots \quad \sqrt{d_i} U_{ni} \right)^\top \quad \text{with} \quad \langle \mathbf{a}_i, \mathbf{a}_j \rangle = \sum_{l=1}^n (\mathbf{a}_i)_l^* (\mathbf{a}_j)_l = \sqrt{d_i d_j} \sum_{l=1}^n U_{li}^* U_{lj} = d_i \delta_{ij},$$

and the columns of $\mathbf{V} \begin{pmatrix} \mathbf{S} \\ \mathbf{0} \end{pmatrix}$ constitute r orthogonal vectors $\mathbf{b}_1, \dots, \mathbf{b}_r \in \mathbb{C}^m$:

$$\mathbf{b}_i = \left(\sqrt{d_i} V_{1i} \quad \dots \quad \sqrt{d_i} V_{mi} \right)^\top \quad \text{with} \quad \langle \mathbf{b}_i, \mathbf{b}_j \rangle = \sum_{l=1}^m (\mathbf{b}_i)_l^* (\mathbf{b}_j)_l = \sqrt{d_i d_j} \sum_{l=1}^m V_{li}^* V_{lj} = d_i \delta_{ij}.$$

Therefore:

$$M(\mathbf{D}, \mathbf{X}) \leq \max_{\mathbf{U}, \mathbf{V}} \left(\left| \sum_{i=1}^r \left\langle \begin{pmatrix} \mathbf{T} & \mathbf{0} \end{pmatrix} \mathbf{b}_i, \begin{pmatrix} \mathbf{T} & \mathbf{0} \end{pmatrix} \mathbf{a}_i \right\rangle \right| \right) \leq \max_{\mathbf{U}, \mathbf{V}} \left(\sum_{i=1}^r \left| \left\langle \begin{pmatrix} \mathbf{T} & \mathbf{0} \end{pmatrix} \mathbf{b}_i, \begin{pmatrix} \mathbf{T} & \mathbf{0} \end{pmatrix} \mathbf{a}_i \right\rangle \right| \right).$$

One should keep in mind that the two appearing zero matrices are of different dimensions, since $\mathbf{a}_i \in \mathbb{C}^n$ and $\mathbf{b}_i \in \mathbb{C}^m$. The Cauchy–Schwarz inequality states that the upper bound of each summand is reached when the vectors are parallel, so the maximum value of this expression is reached when \mathbf{U} and \mathbf{V} ensure that this condition is met. Since only the first k components of \mathbf{a}_i and \mathbf{b}_i contribute at all, the condition reads for all $1 \leq i \leq k$ and $1 \leq j \leq r$:

$$\begin{aligned} \left(\begin{pmatrix} \mathbf{T} & \mathbf{0} \end{pmatrix} \mathbf{b}_j \right)_i &= \sum_{l=1}^r T_{il} V_{lj} \sqrt{d_j} = T_{ii} \sqrt{d_j} V_{ij} \stackrel{!}{=} \lambda \left(\begin{pmatrix} \mathbf{T} & \mathbf{0} \end{pmatrix} \mathbf{a}_j \right)_i = \lambda \sum_{l=1}^r T_{il} U_{lj} \sqrt{d_j} = \lambda T_{ii} \sqrt{d_j} U_{ij}, \\ \Rightarrow V_{ij} &= \lambda U_{ij} \end{aligned}$$

The expression is at its maximum when the vectors have their maximum norm:

$$\left\| \begin{pmatrix} \mathbf{T} & \mathbf{0} \end{pmatrix} \mathbf{a}_j \right\|^2 = \sum_{i=1}^k |T_{ii} (\mathbf{a}_j)_i|^2 = \sum_{i=1}^k T_{ii}^2 |U_{ij}|^2 S_{jj}^2 = d_j \sum_{i=1}^k x_i |U_{ij}|^2 \quad \text{and} \quad \left\| \begin{pmatrix} \mathbf{T} & \mathbf{0} \end{pmatrix} \mathbf{b}_j \right\|^2 = d_j \sum_{i=1}^k x_i |V_{ij}|^2.$$

Only for $i \leq k$ and $j \leq r$ the coefficients U_{ij} and V_{ij} enter the expression, so there are several degrees of freedom which can be chosen without altering the expression. First, since the coefficients d_j and x_i are non-negative, $|U_{ij}|$ and $|V_{ij}|$ should be as large as possible, i. e., for each of the first k rows, the absolute value squares of the first r entries sum to 1, the rest of the row is zero. The first k rows span a subspace of \mathbb{C}^r (embedded in \mathbb{C}^n or \mathbb{C}^m respectively) and additional $r - k$ row vectors are needed to span \mathbb{C}^r . Without loss of generality, these row vectors can be chosen to be the rows $k + 1$ to r . Then \mathbf{U} and \mathbf{V} take on a block structure: the upper left $r \times r$ block and the lower right block (of size $(n - r) \times (n - r)$ or $(m - r) \times (m - r)$) are unitary matrices on their own. Now it follows for $1 \leq i \leq k$:

$$1 = \sum_{j=1}^m |V_{ij}|^2 = \sum_{j=1}^r |V_{ij}|^2 = \sum_{j=1}^r |\lambda|^2 |U_{ij}|^2 = |\lambda|^2 \sum_{j=1}^r |U_{ij}|^2 = |\lambda|^2.$$

λ is just a complex phase factor. Absorbing it into the global phase of the unitary matrix \mathbf{V} yields $U_{ij} = V_{ij}$ for $1 \leq i \leq k$, $1 \leq j \leq r$. Since all other entries do not contribute, without loss of generality $U_{ij} = V_{ij}$ can be chosen for $k + 1 \leq i \leq r$, $1 \leq j \leq r$. Let $\mathbf{W} \in \text{Mat}(r, r)$ be the unitary matrix of the upper left block, then the matrices \mathbf{U} and \mathbf{V} maximize the expression are of the form:

$$\mathbf{U} = \begin{pmatrix} \mathbf{W} & \mathbf{0} \\ \mathbf{0} & \mathbf{U}' \end{pmatrix} \quad \text{and} \quad \mathbf{V} = \begin{pmatrix} \mathbf{W} & \mathbf{0} \\ \mathbf{0} & \mathbf{V}' \end{pmatrix}.$$

With the orthonormal vectors $\mathbf{w}_1, \dots, \mathbf{w}_r \in \mathbb{C}^r$ from the columns of \mathbf{W} it follows $\begin{pmatrix} \mathbf{T} & \mathbf{0} \end{pmatrix} \mathbf{a}_i = \begin{pmatrix} \mathbf{T} & \mathbf{0} \end{pmatrix} \mathbf{b}_i = \sqrt{d_i} \mathbf{T} \mathbf{w}_i$.

$$M(\mathbf{D}, \mathbf{X}) \leq \max_{\substack{\mathbf{w}_1, \dots, \mathbf{w}_r \\ \text{ONB of } \mathbb{C}^r}} \sum_{i=1}^r \left| \left\langle \sqrt{d_i} \mathbf{T} \mathbf{w}_i, \sqrt{d_i} \mathbf{T} \mathbf{w}_i \right\rangle \right| = \max_{\substack{\mathbf{w}_1, \dots, \mathbf{w}_r \\ \text{ONB of } \mathbb{C}^r}} \sum_{i=1}^r d_i \langle \mathbf{w}_i, \mathbf{T}^2 \mathbf{w}_i \rangle. \quad (\text{A.5})$$

Claim: Let $\mathbf{X}, \mathbf{D} \in \text{Mat}(r, r)$ be diagonal matrices with entries sorted in descending order, i. e. $d_1 \geq d_2 \geq \dots \geq$

$d_r, x_1 \geq x_2 \geq \dots \geq x_r$. Then:

$$\max_{\substack{\mathbf{w}_1, \dots, \mathbf{w}_r \\ \text{ONB of } \mathbb{C}^r}} \sum_{i=1}^r d_i \langle \mathbf{w}_i, \mathbf{X} \mathbf{w}_i \rangle = \sum_{i=1}^r d_i x_i. \quad (\text{A.6})$$

Proof by induction: For $r = 1$ the equation is obvious: $d_1 \langle \mathbf{w}_1, \mathbf{X} \mathbf{w}_1 \rangle = d_1 \left(e^{-i\varphi} \right) \left(x_1 \right) \left(e^{i\varphi} \right) = d_1 x_1$.

Let the claim hold true for some $r \in \mathbb{N}$, and for all $r \times r$ matrices \mathbf{X} and \mathbf{D} that fulfill the condition stated above.

From this follows for $r + 1$:

$$\begin{aligned} & \max_{\substack{\mathbf{w}_1, \dots, \mathbf{w}_{r+1} \\ \text{ONB of } \mathbb{C}^{r+1}}} \sum_{i=1}^{r+1} d_i \langle \mathbf{w}_i, \mathbf{X} \mathbf{w}_i \rangle = \max_{\substack{\mathbf{w}_1, \dots, \mathbf{w}_{r+1} \\ \text{ONB of } \mathbb{C}^{r+1}}} \left(\sum_{i=1}^r d_i \langle \mathbf{w}_i, \mathbf{X} \mathbf{w}_i \rangle + d_{r+1} \left(\sum_{i=1}^{r+1} x_i - \sum_{i=1}^r \langle \mathbf{w}_i, \mathbf{X} \mathbf{w}_i \rangle \right) \right) \\ & \quad \text{where it was used that } \sum_{i=1}^{r+1} \langle \mathbf{w}_i, \mathbf{X} \mathbf{w}_i \rangle = \text{tr}(\mathbf{X}) = \sum_{i=1}^{r+1} x_i \text{ for any orthonormal basis vectors } \mathbf{w}_i \\ & = \max_{\substack{\mathbf{w}_1, \dots, \mathbf{w}_{r+1} \\ \text{ONB of } \mathbb{C}^{r+1}}} \left(\sum_{i=1}^r (d_i - d_{r+1}) \langle \mathbf{w}_i, \mathbf{X} \mathbf{w}_i \rangle + d_{r+1} \sum_{i=1}^{r+1} x_i \right) \\ & \quad \text{with } \mathbf{X}' \in \text{Mat}(r, r) \text{ defined by taking } \mathbf{X} \in \text{Mat}(r+1, r+1) \text{ and disregarding the last row and column} \\ & \quad \text{and } \mathbf{w}_i' \in \text{Mat}(C)^r \text{ by disregarding the last entry of } \mathbf{w}_i \\ & = \max_{\substack{\mathbf{w}_1, \dots, \mathbf{w}_{r+1} \\ \text{ONB of } \mathbb{C}^{r+1}}} \left(\sum_{i=1}^r (d_i - d_{r+1}) \left(\langle \mathbf{w}_i', \mathbf{X}' \mathbf{w}_i' \rangle + x_{r+1} |(\mathbf{w}_i)_{r+1}|^2 \right) + d_{r+1} \sum_{i=1}^{r+1} x_i \right) \\ & \quad \text{where } \langle \mathbf{w}_i', \mathbf{w}_i' \rangle + |(\mathbf{w}_i)_{r+1}|^2 = \langle \mathbf{w}_i, \mathbf{w}_i \rangle = 1 \text{ was used} \\ & = \max_{\substack{\mathbf{w}_1, \dots, \mathbf{w}_{r+1} \\ \text{ONB of } \mathbb{C}^{r+1}}} \left(\sum_{i=1}^r (d_i - d_{r+1}) \langle \mathbf{w}_i', (\mathbf{X}' - x_{r+1} \mathbf{1}_r) \mathbf{w}_i' \rangle \right) + x_{r+1} \sum_{i=1}^r (d_i - d_{r+1}) + d_{r+1} \sum_{i=1}^{r+1} x_i. \end{aligned}$$

$\mathbf{X}' - x_{r+1} \mathbf{1}_r$ is a semi-positive definite matrix and $d_i - d_{r+1} \geq 0$, so for the maximal value, all $\mathbf{w}_1', \dots, \mathbf{w}_r'$ are unit vectors such that $(\mathbf{w}_i)_{r+1} = 0$. This in turn means that $(\mathbf{w}_{r+1})_{r+1} = 1$, so that $\mathbf{w}_1', \dots, \mathbf{w}_r'$ form an orthonormal basis for \mathbb{C}^r . Then, since $\mathbf{X}' - x_{r+1} \mathbf{1}_r$ and $\mathbf{D}' - d_{r+1} \mathbf{1}_r$ fulfill the condition for their diagonal entries stated in the claim, so that the induction precondition can be used:

$$\begin{aligned} & = \max_{\substack{\mathbf{w}_1', \dots, \mathbf{w}_r' \\ \text{ONB of } \mathbb{C}^r}} \left(\sum_{i=1}^r (d_i - d_{r+1}) \langle \mathbf{w}_i', (\mathbf{X}' - x_{r+1} \mathbf{1}_r) \mathbf{w}_i' \rangle \right) + x_{r+1} \sum_{i=1}^r (d_i - d_{r+1}) + d_{r+1} \sum_{i=1}^{r+1} x_i \\ & = \sum_{i=1}^r (d_i - d_{r+1})(x_i - x_{r+1}) + x_{r+1} \sum_{i=1}^r (d_i - d_{r+1}) + d_{r+1} \sum_{i=1}^{r+1} x_i = \sum_{i=1}^r d_i x_i. \end{aligned}$$

If the now proven result of Equation (A.6) is used to evaluate the expression in Equation (A.5), this results in:

$$M(\mathbf{D}, \mathbf{X}) \leq \sum_{i=1}^r d_i x_i = \sum_{i=1}^k d_i x_i.$$

On the other hand, for $\mathbf{U} = \mathbf{1}_n$ and $\mathbf{V} = \mathbf{1}_m$ it follows:

$$M(\mathbf{D}, \mathbf{X}) \geq \text{Re} \left(\text{tr} \left(\mathbf{X}^\dagger \mathbf{1}_n \mathbf{D} \mathbf{1}_m \right) \right) = \text{Re} \left(\sum_{i=1}^r x_i d_i \right) = \sum_{i=1}^r d_i x_i,$$

and thus, the claim is proven.

A.3 – Properties of Clebsch–Gordan Coefficients

The Clebsch–Gordan coefficients introduced in Section 2.2 are subject to several symmetries and properties. Some of these, which are used in the thesis, are presented in the following.

The Clebsch–Gordan coefficients are coefficients of a unitary transformation of the tensor product basis $(|j_1, m_1; j_2, m_2\rangle \mid -j_1 \leq m_1 \leq j_1, -j_2 \leq m_2 \leq j_2)$ of two distinct angular momenta to a basis of coupled angular momenta $(|J(j_1, j_2), M\rangle \mid -J \leq M \leq J)$ (possible degeneracy quantum numbers are omitted here for simplicity, but their incorporation is straightforward, e. g., Equation (2.62)). They are chosen real and they vanish, unless the angular momenta fulfill the selection rules:

$$\Gamma_{m_1 m_2 \rightarrow M}^{j_1 j_2 \rightarrow J} = \langle j_1, m_1; j_2, m_2 | J(j_1, j_2), M \rangle = 0 \quad \text{unless } |j_1 - j_2| \leq J \leq j_1 + j_2$$

$$\text{and } m_1 + m_2 = M. \quad (\text{A.7})$$

They obey the following symmetry properties:

$$\Gamma_{m_1 m_2 \rightarrow M}^{j_1 j_2 \rightarrow J} = (-1)^{j_1 + j_2 - J} \Gamma_{-m_1 -m_2 \rightarrow -M}^{j_1 j_2 \rightarrow J} \quad (\text{Time reversal}),$$

$$= (-1)^{j_1 + j_2 - J} \Gamma_{m_2 m_1 \rightarrow M}^{j_2 j_1 \rightarrow J} \quad (\text{Coupling order inversion}),$$

$$= (-1)^{j_2 + m_2} \sqrt{\frac{2J + 1}{2j_1 + 1}} \Gamma_{-m_2 M \rightarrow m_1}^{j_2 J \rightarrow j_1} \quad (\text{Cyclic permutation}). \quad (\text{A.8})$$

From the fact the angular momentum quantum numbers as well as the projection quantum numbers are integer or half-integer numbers follow some rules for phase factors:

$$\Gamma_{m_1 m_2 \rightarrow m_3}^{j_1 j_2 \rightarrow j_3} = (-1)^{m_1 + m_2 - m_3} \Gamma_{m_1 m_2 \rightarrow m_3}^{j_1 j_2 \rightarrow j_3} \quad (m_1 + m_2 = m_3),$$

$$= (-1)^{4j_i} \Gamma_{m_1 m_2 \rightarrow m_3}^{j_1 j_2 \rightarrow j_3} = (-1)^{4m_i} \Gamma_{m_1 m_2 \rightarrow m_3}^{j_1 j_2 \rightarrow j_3} \quad (j_i, m_i \in 1/2\mathbb{Z}),$$

$$= (-1)^{2j_i + 2m_i} \Gamma_{m_1 m_2 \rightarrow m_3}^{j_1 j_2 \rightarrow j_3} \quad (m_i = j_i + z, z \in \mathbb{Z}),$$

$$= (-1)^{2j_1 + 2j_2 + 2j_3} \Gamma_{m_1 m_2 \rightarrow m_3}^{j_1 j_2 \rightarrow j_3} \quad (j_3 = j_1 + j_2 + z, z \in \mathbb{Z}). \quad (\text{A.9})$$

Moreover, these orthogonality relations can easily be proven:

$$\delta_{m_1 m'_1} \delta_{m_2 m'_2} = \langle j_1, m_1; j_2, m_2 | j_1, m'_1; j_2, m'_2 \rangle$$

$$= \sum_{J=|j_1-j_2|}^{j_1+j_2} \sum_{M=-J}^J \langle j_1, m_1; j_2, m_2 | J(j_1, j_2), M \rangle \langle J(j_1, j_2), M | j_1, m'_1; j_2, m'_2 \rangle$$

$$= \sum_{J=|j_1-j_2|}^{j_1+j_2} \sum_{M=-J}^J \Gamma_{m_1 m_2 \rightarrow M}^{j_1 j_2 \rightarrow J} \Gamma_{m'_1 m'_2 \rightarrow M}^{j_1 j_2 \rightarrow J} \quad (\text{A.10})$$

and

$$\delta_{JJ'} \delta_{MM'} = \langle J(j_1, j_2), M | J'(j_1, j_2), M' \rangle$$

$$= \sum_{m_1=-j_1}^{j_1} \sum_{m_2=-j_2}^{j_2} \langle J(j_1, j_2), M | j_1, m_1; j_2, m_2 \rangle \langle j_1, m_1; j_2, m_2 | J'(j_1, j_2), M' \rangle$$

$$= \sum_{m_1=-j_1}^{j_1} \sum_{m_2=-j_2}^{j_2} \Gamma_{m_1 m_2 \rightarrow M}^{j_1 j_2 \rightarrow J} \Gamma_{m_1 m_2 \rightarrow M'}^{j_1 j_2 \rightarrow J'}. \quad (\text{A.11})$$

Two important recursion relations can be obtained by application of $\widehat{J}^{(\pm)}$ in between the overlap:

$$\begin{aligned}
 \langle j_1, m_1; j_2, m_2 | \widehat{J}^{(\pm)} | J(j_1, j_2), M \rangle &= \sqrt{(J \mp M)(J \pm M + 1)} \langle j_1, m_1; j_2, m_2 | J(j_1, j_2), M \pm 1 \rangle \\
 &= \langle j_1, m_1; j_2, m_2 | \widehat{j}_1^{(\pm)} + \widehat{j}_2^{(\pm)} | J(j_1, j_2), M \rangle \\
 &= \sqrt{(j_1 \pm m_1)(j_1 \mp m_1 + 1)} \langle j_1, m_1 \mp 1; j_2, m_2 | J(j_1, j_2), M \rangle \\
 &\quad + \sqrt{(j_2 \pm m_2)(j_2 \mp m_2 + 1)} \langle j_1, m_1; j_2, m_2 \mp 1 | J(j_1, j_2), M \rangle \\
 \Rightarrow \sqrt{(J \mp M)(J \pm M + 1)} \Gamma_{m_1 m_2 \rightarrow M \pm 1}^{j_1 j_2 \rightarrow J} & \\
 &= \sqrt{(j_1 \pm m_1)(j_1 \mp m_1 + 1)} \Gamma_{m_1 \mp 1 m_2 \rightarrow M}^{j_1 j_2 \rightarrow J} + \sqrt{(j_2 \pm m_2)(j_2 \mp m_2 + 1)} \Gamma_{m_1 m_2 \mp 1 \rightarrow M}^{j_1 j_2 \rightarrow J}. \tag{A.12}
 \end{aligned}$$

Lastly, due to known behavior of angular momentum eigenstates under an SU(2) rotation g , the transformation behavior of Clebsch–Gordan coefficients can be derived:

$$\begin{aligned}
 \Gamma_{m_1 m_2 \rightarrow M}^{j_1 j_2 \rightarrow J} &= \langle j_1, m_1; j_2, m_2 | J(j_1, j_2), M \rangle = \langle j_1, m_1; j_2, m_2 | \widehat{U}_g^\dagger \widehat{U}_g | J(j_1, j_2), M \rangle \\
 &= \sum_{m'_1, m'_2, M'} \langle j_1, m'_1; j_2, m'_2 | \left(D_{m'_1 m_1}^{[j_1]} \right)^* \left(D_{m'_2 m_2}^{[j_2]} \right)^* D_{M' M}^{[J]} | J(j_1, j_2), M' \rangle \\
 &= \sum_{m'_1, m'_2, M'} \left(D_{m'_1 m_1}^{[j_1]} \right)^* \left(D_{m'_2 m_2}^{[j_2]} \right)^* D_{M' M}^{[J]} \Gamma_{m'_1 m'_2 \rightarrow M'}^{j_1 j_2 \rightarrow J} \\
 &= \sum_{m'_1, m'_2, M'} D_{m_1 m'_1}^{[j_1]} D_{m_2 m'_2}^{[j_2]} \left(D_{M M'}^{[J]} \right)^* \Gamma_{m'_1 m'_2 \rightarrow M'}^{j_1 j_2 \rightarrow J}. \tag{A.13}
 \end{aligned}$$

A.4 – Reduced Matrix Elements

In the following, some basic properties of reduced matrix elements are presented. These are useful for efficient computation of reduced matrix elements in a VMPS implementation because matrix elements for more complicated irreducible tensor operators can be obtained by manipulating reduced matrix elements of some basic irreducible tensor operators.

The reduced matrix elements of a product of two irreducible tensor operators $\widehat{\mathbf{R}}^{[k]}$ and $\widehat{\mathbf{S}}^{[k']}$ can be computed from the individual reduced matrix elements:

$$\begin{aligned}
\langle\langle j', \alpha' | \left(\widehat{\mathbf{R}}^{[k]} \star \widehat{\mathbf{S}}^{[k']} \right)^{[K]} | j, \alpha \rangle\rangle &= \langle\langle j', \alpha' | \left(\widehat{\mathbf{R}}^{[k]} \star \widehat{\mathbf{S}}^{[k']} \right)^{[K]} | j, \alpha \rangle\rangle \sum_{m, m', N} \frac{\Gamma_{mN \rightarrow m'}^{j K \rightarrow j'} \Gamma_{mN \rightarrow m'}^{j K \rightarrow j'}}{2j' + 1} \\
&= \sum_{\substack{m, m', \\ n, n', N}} \frac{\Gamma_{mN \rightarrow m'}^{j K \rightarrow j'} \Gamma_{nn' \rightarrow N}^{k k' \rightarrow K}}{2j' + 1} \langle j', \alpha', m' | \widehat{\mathbf{R}}_n^{[k]} \widehat{\mathbf{S}}_{n'}^{[k']} | j, \alpha, m \rangle \\
&= \sum_{j'', \alpha'', m''} \sum_{\substack{m, m', \\ n, n', N}} \frac{\Gamma_{mN \rightarrow m'}^{j K \rightarrow j'} \Gamma_{nn' \rightarrow N}^{k k' \rightarrow K}}{2j' + 1} \langle j', \alpha', m' | \widehat{\mathbf{R}}_n^{[k]} | j'', \alpha'', m'' \rangle \langle j'', \alpha'', m'' | \widehat{\mathbf{S}}_{n'}^{[k']} | j, \alpha, m \rangle \\
&= \sum_{j'', \alpha''} \langle\langle j', \alpha' | \widehat{\mathbf{R}}^{[k]} | j'', \alpha'' \rangle\rangle \langle\langle j'', \alpha'' | \widehat{\mathbf{S}}^{[k']} | j, \alpha \rangle\rangle \sum_{\substack{m, m', m'', \\ n, n', N}} \frac{\Gamma_{mN \rightarrow m'}^{j K \rightarrow j'} \Gamma_{nn' \rightarrow N}^{k k' \rightarrow K} \Gamma_{m''n \rightarrow m'}^{j'' k \rightarrow j'} \Gamma_{m''n' \rightarrow m''}^{j k' \rightarrow j''}}{2j' + 1}.
\end{aligned}$$

Concerning the Clebsch–Gordan part of the expression, one can use the identities from Appendix A.3 to rearrange the order of angular momenta:

$$\begin{aligned}
&\sum_{\substack{m, m', m'', \\ n, n', N}} \frac{\Gamma_{mN \rightarrow m'}^{j K \rightarrow j'} \Gamma_{nn' \rightarrow N}^{k k' \rightarrow K} \Gamma_{m''n \rightarrow m'}^{j'' k \rightarrow j'} \Gamma_{m''n' \rightarrow m''}^{j k' \rightarrow j''}}{2j' + 1} \\
&= \sum_{\substack{m, m', m'', \\ n, n', N}} \frac{(-1)^{K+N+k+n+k'+n'}}{2j' + 1} \sqrt{\frac{(2j' + 1)(2j' + 1)(2j'' + 1)}{(2j + 1)(2j'' + 1)(2j + 1)}} \Gamma_{-m'N \rightarrow -m}^{j' K \rightarrow j} \Gamma_{nn' \rightarrow N}^{k k' \rightarrow K} \Gamma_{-m'n \rightarrow -m''}^{j' k \rightarrow j''} \Gamma_{-m''n' \rightarrow -m}^{j'' k' \rightarrow j} \\
&= \sum_{\substack{m, m', m'', \\ n, n', N}} \frac{(-1)^{K+N+k+n+k'+n'}}{2j + 1} \Gamma_{m'N \rightarrow m}^{j' K \rightarrow j} \Gamma_{nn' \rightarrow N}^{k k' \rightarrow K} \Gamma_{m'n \rightarrow m''}^{j' k \rightarrow j''} \Gamma_{m''n' \rightarrow m}^{j'' k' \rightarrow j} \\
&= \frac{(-1)^{K+3k+3k'}}{2j + 1} \sum_{\substack{m, m', m'', \\ n, n', N}} \Gamma_{m'N \rightarrow m}^{j' K \rightarrow j} \Gamma_{nn' \rightarrow N}^{k k' \rightarrow K} \Gamma_{m'n \rightarrow m''}^{j' k \rightarrow j''} \Gamma_{m''n' \rightarrow m}^{j'' k' \rightarrow j}.
\end{aligned}$$

In the last step, a trivial factor $1 = (-1)^{N-n-n'} \cdot (-1)^{2K-2N} \cdot (-1)^{2k+2k'-2K}$ was introduced. Now sums over m', m'', n, n' and N can be performed, leading to a rescaled Wigner 6j-symbol:

$$\begin{aligned}
&= \frac{(-1)^{K+3k+3k'}}{2j+1} \sum_m (-1)^{j'+k+k'+j} \sqrt{(2j''+1)(2K+1)} \left\{ \begin{matrix} j' & k & j'' \\ k' & j & K \end{matrix} \right\} \\
&= (-1)^{K+j+j'} \sqrt{(2j''+1)(2K+1)} \left\{ \begin{matrix} j' & k & j'' \\ k' & j & K \end{matrix} \right\} = \left[\begin{matrix} j' & k & j'' \\ k' & j & K \end{matrix} \right],
\end{aligned}$$

where

$$\left[\begin{matrix} j_1 & j_2 & J_{12} \\ j_3 & J & J_{23} \end{matrix} \right] = (-1)^{j_1+J_{23}+J} \sqrt{(2J_{12}+1)(2J_{23}+1)} \left\{ \begin{matrix} j_1 & j_2 & J_{12} \\ j_3 & J & J_{23} \end{matrix} \right\}. \quad (\text{A.14})$$

Thus this identity holds:

$$\langle\langle j', \alpha' | \left(\widehat{\mathbf{R}}^{[k]} \star \widehat{\mathbf{S}}^{[k']} \right)^{[K]} | j, \alpha \rangle\rangle = \sum_{j'', \alpha''} \left[\begin{matrix} j' & k & j'' \\ k' & j & K \end{matrix} \right] \langle\langle j', \alpha' | \widehat{\mathbf{R}}^{[k]} | j'', \alpha'' \rangle\rangle \langle\langle j'', \alpha'' | \widehat{\mathbf{S}}^{[k']} | j, \alpha \rangle\rangle. \quad (\text{A.15})$$

If the system can be divided into a tensor product of two subsystems and each of the two irreducible tensor operators act trivially on one part of the system, the above expression can be extended even further. In a first step such a matrix element is calculated in the basis $(|J(j_1, j_2), M, (\alpha_1, \alpha_2)\rangle)$ of coupled angular momenta and concatenated degeneracies:

$$\begin{aligned}
& \langle\langle J'(j'_1, j'_2), (\alpha'_1, \alpha'_2) \parallel \left(\left(\widehat{\mathbf{R}}^{[k_1]} \otimes \text{id} \right) \star \left(\text{id} \otimes \widehat{\mathbf{S}}^{[k_2]} \right) \right)^{[K]} \parallel J(j_1, j_2), (\alpha_1, \alpha_2) \rangle\rangle \\
&= \sum_{\substack{M, M', \\ n_1, n_2, N}} \frac{\Gamma_{MN \rightarrow M'}^{JK \rightarrow J'} \Gamma_{n_1 n_2 \rightarrow N}^{k_1 k_2 \rightarrow K}}{2J' + 1} \langle J'(j'_1, j'_2), (\alpha'_1, \alpha'_2), M' \parallel \widehat{\mathbf{R}}_{n_1}^{[k_1]} \otimes \widehat{\mathbf{S}}_{n_2}^{[k_2]} \parallel J(j_1, j_2), (\alpha_1, \alpha_2), M \rangle \\
&= \sum_{\substack{m_1, m_2, M, \\ m'_1, m'_2, M', \\ n_1, n_2, N}} \frac{\Gamma_{MN \rightarrow M'}^{JK \rightarrow J'} \Gamma_{n_1 n_2 \rightarrow N}^{k_1 k_2 \rightarrow K}}{2J' + 1} \langle J'(j'_1, j'_2), (\alpha'_1, \alpha'_2), M' \parallel j'_1, \alpha'_1, m'_1; j'_2, \alpha'_2, m'_2 \rangle \\
&\quad \cdot \langle j'_1, \alpha'_1, m'_1; j'_2, \alpha'_2, m'_2 \parallel \widehat{\mathbf{R}}_{n_1}^{[k_1]} \otimes \widehat{\mathbf{S}}_{n_2}^{[k_2]} \parallel j_1, \alpha_1, m_1; j_2, \alpha_2, m_2 \rangle \langle j_1, \alpha_1, m_1; j_2, \alpha_2, m_2 \parallel J(j_1, j_2), (\alpha_1, \alpha_2), M \rangle \\
&= \sum_{\substack{m_1, m_2, M, \\ m'_1, m'_2, M', \\ n_1, n_2, N}} \frac{\Gamma_{MN \rightarrow M'}^{JK \rightarrow J'} \Gamma_{n_1 n_2 \rightarrow N}^{k_1 k_2 \rightarrow K} \Gamma_{m'_1 m'_2 \rightarrow M'}^{j'_1 j'_2 \rightarrow J'} \Gamma_{m_1 m_2 \rightarrow M}^{j_1 j_2 \rightarrow J}}{2J' + 1} \langle j'_1, \alpha'_1, m'_1 \parallel \widehat{\mathbf{R}}_{n_1}^{[k_1]} \parallel j_1, \alpha_1, m_1 \rangle \langle j'_2, \alpha'_2, m'_2 \parallel \widehat{\mathbf{S}}_{n_2}^{[k_2]} \parallel j_2, \alpha_2, m_2 \rangle \\
&= \sum_{\substack{m_1, m_2, M, \\ m'_1, m'_2, M', \\ n_1, n_2, N}} \frac{\Gamma_{MN \rightarrow M'}^{JK \rightarrow J'} \Gamma_{n_1 n_2 \rightarrow N}^{k_1 k_2 \rightarrow K} \Gamma_{m'_1 m'_2 \rightarrow M'}^{j'_1 j'_2 \rightarrow J'} \Gamma_{m_1 m_2 \rightarrow M}^{j_1 j_2 \rightarrow J} \Gamma_{m_1 n_1 \rightarrow m'_1}^{j_1 k_1 \rightarrow j'_1} \Gamma_{m_2 n_2 \rightarrow m'_2}^{j_2 k_2 \rightarrow j'_2}}{2J' + 1} \\
&\quad \cdot \langle j'_1, \alpha'_1 \parallel \widehat{\mathbf{R}}^{[k_1]} \parallel j_1, \alpha_1 \rangle \langle j'_2, \alpha'_2 \parallel \widehat{\mathbf{S}}^{[k_2]} \parallel j_2, \alpha_2 \rangle \\
&= \sum_{M'} \frac{\sqrt{(2j'_1 + 1)(2j'_2 + 1)(2K + 1)(2J + 1)}}{2J' + 1} \left\{ \begin{array}{ccc} j_1 & j_2 & J \\ k_1 & k_2 & K \\ j'_1 & j'_2 & J' \end{array} \right\} \langle\langle j'_1, \alpha'_1 \parallel \widehat{\mathbf{R}}^{[k_1]} \parallel j_1, \alpha_1 \rangle\rangle \langle\langle j'_2, \alpha'_2 \parallel \widehat{\mathbf{S}}^{[k_2]} \parallel j_2, \alpha_2 \rangle\rangle \\
&= \left[\begin{array}{ccc} j_1 & j_2 & J \\ k_1 & k_2 & K \\ j'_1 & j'_2 & J' \end{array} \right] \langle\langle j'_1, \alpha'_1 \parallel \widehat{\mathbf{R}}^{[k_1]} \parallel j_1, \alpha_1 \rangle\rangle \langle\langle j'_2, \alpha'_2 \parallel \widehat{\mathbf{S}}^{[k_2]} \parallel j_2, \alpha_2 \rangle\rangle,
\end{aligned}$$

with a rescaled Wigner 9j-symbol:

$$\left[\begin{array}{ccc} j_1 & j_2 & J_{12} \\ j_3 & j_4 & J_{34} \\ J_{13} & J_{24} & J \end{array} \right] = \sqrt{(2J_{12} + 1)(2J_{34} + 1)(2J_{13} + 1)(2J_{24} + 1)} \left\{ \begin{array}{ccc} j_1 & j_2 & J_{12} \\ j_3 & j_4 & J_{34} \\ J_{13} & J_{24} & J \end{array} \right\}. \quad (\text{A.16})$$

For an arbitrary basis of angular momentum eigenstates now follows:

$$\begin{aligned}
& \langle\langle J'(j'_1, j'_2), \mathcal{A}' | \left((\widehat{\mathbf{R}}^{[k_1]} \otimes \text{id}) \star (\text{id} \otimes \widehat{\mathbf{S}}^{[k_2]}) \right)^{[K]} | J(j_1, j_2), \mathcal{A} \rangle\rangle \\
&= \sum_{M, N, M'} \frac{\Gamma_{MN \rightarrow M'}^{J K \rightarrow J'}}{2J'+1} \langle J'(j'_1, j'_2), \mathcal{A}', M' | \left((\widehat{\mathbf{R}}^{[k_1]} \otimes \text{id}) \star (\text{id} \otimes \widehat{\mathbf{S}}^{[k_2]}) \right)^{[K]} | J(j_1, j_2), \mathcal{A}, M \rangle \\
&= \sum_{\substack{M, N, M', \\ \alpha_1, \alpha_2, \\ \alpha'_1, \alpha'_2}} \frac{\Gamma_{MN \rightarrow M'}^{J K \rightarrow J'}}{2J'+1} \langle J', \mathcal{A}' | j'_1, \alpha'_1; j'_2, \alpha'_2 \rangle \langle j_1, \alpha_1; j_2, \alpha_2 | J, \mathcal{A} \rangle \\
&\quad \cdot \langle J'(j'_1, j'_2), (\alpha'_1, \alpha'_2), M' | \left((\widehat{\mathbf{R}}^{[k_1]} \otimes \text{id}) \star (\text{id} \otimes \widehat{\mathbf{S}}^{[k_2]}) \right)^{[K]} | J(j_1, j_2), (\alpha_1, \alpha_2), M \rangle \\
&= \sum_{\substack{\alpha_1, \alpha_2, \\ \alpha'_1, \alpha'_2}} \langle J', \mathcal{A}' | j'_1, \alpha'_1; j'_2, \alpha'_2 \rangle \langle j_1, \alpha_1; j_2, \alpha_2 | J, \mathcal{A} \rangle \\
&\quad \cdot \langle J'(j'_1, j'_2), (\alpha'_1, \alpha'_2) | \left((\widehat{\mathbf{R}}^{[k_1]} \otimes \text{id}) \star (\text{id} \otimes \widehat{\mathbf{S}}^{[k_2]}) \right)^{[K]} | J(j_1, j_2), (\alpha_1, \alpha_2) \rangle \\
&= \sum_{\substack{\alpha_1, \alpha_2, \\ \alpha'_1, \alpha'_2}} \langle J', \mathcal{A}' | j'_1, \alpha'_1; j'_2, \alpha'_2 \rangle \langle j_1, \alpha_1; j_2, \alpha_2 | J, \mathcal{A} \rangle \\
&\quad \cdot \begin{bmatrix} j_1 & j_2 & J \\ k_1 & k_2 & K \\ j'_1 & j'_2 & J' \end{bmatrix} \langle j'_1, \alpha'_1 | \widehat{\mathbf{R}}^{[k_1]} | j_1, \alpha_1 \rangle \langle j'_2, \alpha'_2 | \widehat{\mathbf{S}}^{[k_2]} | j_2, \alpha_2 \rangle. \tag{A.17}
\end{aligned}$$

This means that additional reduced scalar products appear which incorporate the basis transformation.

Reduced matrix elements of adjoint irreducible tensor operators can be obtained easily:

$$\begin{aligned}
\langle\langle j', \alpha' | (\widehat{\mathbf{T}}^\dagger)^{[k]} | j, \alpha \rangle\rangle &= \sum_{m, n, m'} \frac{\Gamma_{mn \rightarrow m'}^{j k \rightarrow j'}}{2j'+1} \langle j', \alpha', m' | (\widehat{\mathbf{T}}^\dagger)_n^{[k]} | j, \alpha, m \rangle \\
&= \sum_{m, n, m'} \frac{\Gamma_{mn \rightarrow m'}^{j k \rightarrow j'}}{2j'+1} (-1)^{k-n} \langle j', \alpha', m' | (\widehat{\mathbf{T}}_{-n}^{[k]})^\dagger | j, \alpha, m \rangle \\
&= \sum_{m, n, m'} \frac{\Gamma_{mn \rightarrow m'}^{j k \rightarrow j'}}{2j'+1} (-1)^{k-n} \langle j, \alpha, m | \widehat{\mathbf{T}}_{-n}^{[k]} | j', \alpha', m' \rangle^* \\
&= \sum_{m, n, m'} \frac{(-1)^{j+k-j'}}{\sqrt{(2j+1)(2j'+1)}} \Gamma_{m'-n \rightarrow m}^{j' k \rightarrow j} \langle j, \alpha, m | \widehat{\mathbf{T}}_{-n}^{[k]} | j', \alpha', m' \rangle^* \\
&= \sum_{m, n, m'} \frac{(-1)^{j+k-j'}}{\sqrt{(2j+1)(2j'+1)}} \langle j, \alpha | \widehat{\mathbf{T}}^{[k]} | j', \alpha' \rangle^* \Gamma_{m'-n \rightarrow m}^{j' k \rightarrow j} \Gamma_{m'-n \rightarrow m}^{j' k \rightarrow j} \\
&= (-1)^{j+k-j'} \sqrt{\frac{2j+1}{2j'+1}} \langle j, \alpha | \widehat{\mathbf{T}}^{[k]} | j', \alpha' \rangle^*. \tag{A.18}
\end{aligned}$$

A.5 – Product of SU(2)-Symmetric Matrix Product Operators

Given two matrix product representations of irreducible tensor operators $\widehat{U}^{[r_1]}$ and $\widehat{V}^{[r_2]}$ with SU(2)-symmetric MPO tensors $U(\ell)$ and $V(\ell)$ respectively, one can find an SU(2)-symmetric matrix product representation of the product:

$$\begin{aligned} \widehat{W}_{\mathcal{R}^{(z)}}^{[R]} &= \sum_{\substack{r_1^{(z)}, r_2^{(z)} \\ r_1^{(z)}, r_2^{(z)}}} \Gamma_{r_1^{(z)}, r_2^{(z)}}^{r_1, r_2 \rightarrow R} \widehat{U}_{r_1^{(z)}, r_2^{(z)}}^{[r_1]} \widehat{V}_{r_1^{(z)}, r_2^{(z)}}^{[r_2]} \\ &= \sum_{\substack{r_1^{(z)}, r_2^{(z)} \\ r_1^{(z)}, r_2^{(z)}}} \Gamma_{r_1^{(z)}, r_2^{(z)}}^{r_1, r_2 \rightarrow R} \sum_{\substack{k_L^{(z)}=r_1^{(z)}, \\ l_L^{(z)}=r_2^{(z)}}} \sum_{\substack{\mathbf{k}_0, \dots, \mathbf{k}_L, \mathbf{m}_1, \dots, \mathbf{m}_L, \\ \mathbf{l}_0, \dots, \mathbf{l}_L, \mathbf{o}_1, \dots, \mathbf{o}_L, \\ \mathbf{k}_0^{(z)}, \dots, \mathbf{k}_L^{(z)}, \mathbf{n}_1, \dots, \mathbf{n}_L, \\ \mathbf{l}_0^{(z)}, \dots, \mathbf{l}_L^{(z)}, \mathbf{m}_1^{(z)}, \dots, \mathbf{m}_L^{(z)}, \\ \mathbf{o}_1^{(z)}, \dots, \mathbf{o}_L^{(z)}}} U(1)_{\mathbf{k}_0 \mathbf{k}_0^{(z)} \mathbf{o}_1 \mathbf{o}_1^{(z)}}^{\mathbf{k}_1 \mathbf{k}_1^{(z)}} V(1)_{\mathbf{l}_0 \mathbf{l}_0^{(z)} \mathbf{o}_1 \mathbf{o}_1^{(z)}}^{\mathbf{l}_1 \mathbf{l}_1^{(z)} \mathbf{n}_1 \mathbf{n}_1^{(z)}} \dots U(L)_{\mathbf{k}_{L-1} \mathbf{k}_{L-1}^{(z)} \mathbf{m}_L \mathbf{m}_L^{(z)}}^{\mathbf{k}_L \mathbf{k}_L^{(z)} \mathbf{o}_L \mathbf{o}_L^{(z)}} V(L)_{\mathbf{l}_{L-1} \mathbf{l}_{L-1}^{(z)} \mathbf{o}_L \mathbf{o}_L^{(z)}}^{\mathbf{l}_L \mathbf{l}_L^{(z)} \mathbf{n}_L \mathbf{n}_L^{(z)}} \\ &\quad \cdot |\mathbf{m}_1, \mathbf{m}_1^{(z)}; \dots; \mathbf{m}_L, \mathbf{m}_L^{(z)}\rangle \langle \mathbf{n}_1, \mathbf{n}_1^{(z)}; \dots; \mathbf{n}_L, \mathbf{n}_L^{(z)}|. \end{aligned}$$

The MPO bond bases with states $(|\mathbf{k}_\ell, \mathbf{k}_\ell^{(z)}\rangle)$ and $(|\mathbf{l}_\ell, \mathbf{l}_\ell^{(z)}\rangle)$ are fused to a new MPO bond basis $(|\mathbf{K}_\ell, \mathbf{K}_\ell^{(z)}\rangle)$ by taking the tensor product. Here, the degeneracy indices Γ_ℓ have to ensure that a state from the tensor product basis is made up of exactly two multiplets $(|(\bar{\mathbf{k}}_\ell, \bar{\gamma}_\ell), \mathbf{k}_\ell^{(z)}\rangle | -\bar{\mathbf{k}}_\ell \leq \mathbf{k}_\ell^{(z)} \leq \bar{\mathbf{k}}_\ell)$ and $(|(\bar{\mathbf{l}}_\ell, \bar{\lambda}_\ell), \mathbf{l}_\ell^{(z)}\rangle | -\bar{\mathbf{l}}_\ell \leq \mathbf{l}_\ell^{(z)} \leq \bar{\mathbf{l}}_\ell)$:

$$\begin{aligned} |(\mathbf{K}_\ell, \Gamma_\ell), \mathbf{K}_\ell^{(z)}\rangle &= \sum_{\substack{\mathbf{k}_\ell, \gamma_\ell, \mathbf{k}_\ell^{(z)}, \\ \mathbf{l}_\ell, \lambda_\ell, \mathbf{l}_\ell^{(z)}}} \langle (\mathbf{K}_\ell, \Gamma_\ell) | (\mathbf{k}_\ell, \gamma_\ell); (\mathbf{l}_\ell, \lambda_\ell) \rangle \Gamma_{\mathbf{k}_\ell^{(z)} \mathbf{l}_\ell^{(z)} \rightarrow \mathbf{K}_\ell^{(z)}}^{\mathbf{k}_\ell \mathbf{l}_\ell \rightarrow \mathbf{K}_\ell} \cdot |(\mathbf{k}_\ell, \gamma_\ell), \mathbf{k}_\ell^{(z)}\rangle \otimes |(\mathbf{l}_\ell, \lambda_\ell), \mathbf{l}_\ell^{(z)}\rangle \\ &= \sum_{\mathbf{k}_\ell^{(z)}, \mathbf{l}_\ell^{(z)}} \Gamma_{\mathbf{k}_\ell^{(z)} \mathbf{l}_\ell^{(z)} \rightarrow \mathbf{K}_\ell^{(z)}}^{\bar{\mathbf{k}}_\ell \bar{\mathbf{l}}_\ell \rightarrow \mathbf{K}_\ell} |(\bar{\mathbf{k}}_\ell, \bar{\gamma}_\ell), \mathbf{k}_\ell^{(z)}\rangle \otimes |(\bar{\mathbf{l}}_\ell, \bar{\lambda}_\ell), \mathbf{l}_\ell^{(z)}\rangle. \end{aligned}$$

The reduced matrix elements $\langle \langle \mathbf{K}_\ell | \mathbf{k}_\ell; \mathbf{l}_\ell \rangle \rangle$ are either 0 or 1 and function as selector for the correct states. With this, one finds a representation of unity:

$$\begin{aligned} 1 &= \sum_{\substack{\mathbf{k}'_\ell, \mathbf{l}'_\ell, \mathbf{K}_\ell, \mathbf{K}_\ell^{(z)} \\ \mathbf{k}_\ell^{(z)}, \mathbf{l}_\ell^{(z)}, \mathbf{K}_\ell}} \langle \mathbf{k}_\ell, \mathbf{K}_\ell^{(z)}; \mathbf{l}_\ell, \mathbf{l}_\ell^{(z)} | \mathbf{k}'_\ell, \mathbf{k}_\ell^{(z)}; \mathbf{l}'_\ell, \mathbf{l}_\ell^{(z)} \rangle = \sum_{\substack{\mathbf{k}'_\ell, \mathbf{l}'_\ell, \mathbf{K}_\ell, \\ \mathbf{k}_\ell^{(z)}, \mathbf{l}_\ell^{(z)}, \mathbf{K}_\ell}} \langle \mathbf{k}_\ell, \mathbf{K}_\ell^{(z)}; \mathbf{l}_\ell, \mathbf{l}_\ell^{(z)} | \mathbf{K}_\ell, \mathbf{K}_\ell^{(z)} \rangle \langle \mathbf{K}_\ell, \mathbf{K}_\ell^{(z)} | \mathbf{k}'_\ell, \mathbf{k}_\ell^{(z)}; \mathbf{l}'_\ell, \mathbf{l}_\ell^{(z)} \rangle \\ &= \sum_{\substack{\mathbf{k}'_\ell, \mathbf{l}'_\ell, \mathbf{K}_\ell, \\ \mathbf{k}_\ell^{(z)}, \mathbf{l}_\ell^{(z)}, \mathbf{K}_\ell}} \langle \mathbf{k}_\ell; \mathbf{l}_\ell | \mathbf{K}_\ell \rangle \langle \langle \mathbf{K}_\ell | \mathbf{k}'_\ell; \mathbf{l}'_\ell \rangle \rangle \Gamma_{\mathbf{k}_\ell^{(z)} \mathbf{l}_\ell^{(z)} \rightarrow \mathbf{K}_\ell^{(z)}}^{\mathbf{k}_\ell \mathbf{l}_\ell \rightarrow \mathbf{K}_\ell} \Gamma_{\mathbf{k}'_\ell^{(z)} \mathbf{l}'_\ell^{(z)} \rightarrow \mathbf{K}_\ell^{(z)}}^{\mathbf{k}'_\ell \mathbf{l}'_\ell \rightarrow \mathbf{K}_\ell}. \end{aligned}$$

Plugging this in for each bond leads to:

$$\begin{aligned}
\widehat{W}_{\mathcal{R}^{(z)}}^{[R]} &= \sum_{\substack{r_1^{(z)}, r_2^{(z)} \\ r_1^{(z)}, r_2^{(z)} \rightarrow \mathcal{R}^{(z)}}} \Gamma_{r_1^{(z)}, r_2^{(z)}}^{r_1, r_2 \rightarrow R} \sum_{\substack{\mathbf{k}_0, \dots, \mathbf{k}_L, \\ \mathbf{l}_0, \dots, \mathbf{l}_L, \\ \mathbf{k}_0^{(z)}, \dots, \mathbf{k}_L^{(z)}, \\ \mathbf{l}_0^{(z)}, \dots, \mathbf{l}_L^{(z)}}} \sum_{\substack{\mathbf{k}'_0, \dots, \mathbf{k}'_L, \\ \mathbf{l}'_0, \dots, \mathbf{l}'_L, \\ \mathbf{k}'_0^{(z)}, \dots, \mathbf{k}'_L^{(z)}, \\ \mathbf{l}'_0^{(z)}, \dots, \mathbf{l}'_L^{(z)}}} \sum_{\substack{\mathbf{n}_1, \dots, \mathbf{n}_L, \\ \mathbf{m}_1, \dots, \mathbf{m}_L, \\ \mathbf{o}_1, \dots, \mathbf{o}_L, \\ \mathbf{K}_0, \dots, \mathbf{K}_L, \\ \mathbf{K}_0^{(z)}, \dots, \mathbf{K}_L^{(z)}}} \sum_{\substack{\mathbf{n}_1, \dots, \mathbf{n}_L, \\ \mathbf{m}_1, \dots, \mathbf{m}_L, \\ \mathbf{o}_1, \dots, \mathbf{o}_L, \\ \mathbf{K}_0, \dots, \mathbf{K}_L, \\ \mathbf{K}_0^{(z)}, \dots, \mathbf{K}_L^{(z)}}} |\mathbf{m}_1, \mathbf{m}_1^{(z)}; \dots; \mathbf{m}_L, \mathbf{m}_L^{(z)}\rangle \langle \mathbf{n}_1, \mathbf{n}_1^{(z)}; \dots; \mathbf{n}_L, \mathbf{n}_L^{(z)} | \\
&\quad \cdots \langle \mathbf{K}_{\ell-1} \| \mathbf{k}'_{\ell-1}; \mathbf{l}'_{\ell-1} \rangle \Gamma_{\substack{\mathbf{k}'_{\ell-1}, \mathbf{l}'_{\ell-1} \rightarrow \mathbf{K}_{\ell-1} \\ \mathbf{k}'_{\ell-1}^{(z)}, \mathbf{l}'_{\ell-1}^{(z)} \rightarrow \mathbf{K}_{\ell-1}^{(z)}}} \mathbf{k}'_{\ell-1}, \mathbf{l}'_{\ell-1} \rightarrow \mathbf{K}_{\ell-1} U(\ell) \mathbf{k}_\ell \mathbf{k}_\ell^{(z)} \mathbf{o}_\ell \mathbf{o}_\ell^{(z)} \mathbf{k}'_{\ell-1}, \mathbf{l}'_{\ell-1} \rightarrow \mathbf{K}_{\ell-1} V(\ell) \mathbf{l}_\ell \mathbf{l}_\ell^{(z)} \mathbf{n}_\ell \mathbf{n}_\ell^{(z)} \mathbf{l}'_{\ell-1}, \mathbf{l}'_{\ell-1} \rightarrow \mathbf{K}_{\ell-1} \mathbf{o}_\ell \mathbf{o}_\ell^{(z)} \langle \mathbf{k}_\ell; \mathbf{l}_\ell \| \mathbf{K}_\ell \rangle \Gamma_{\substack{\mathbf{k}_\ell, \mathbf{l}_\ell \rightarrow \mathbf{K}_\ell \\ \mathbf{k}_\ell^{(z)}, \mathbf{l}_\ell^{(z)} \rightarrow \mathbf{K}_\ell^{(z)}}} \cdots \\
&= \sum_{\substack{r_1^{(z)}, r_2^{(z)} \\ r_1^{(z)}, r_2^{(z)} \rightarrow \mathcal{R}^{(z)}}} \Gamma_{r_1^{(z)}, r_2^{(z)}}^{r_1, r_2 \rightarrow R} \sum_{\substack{\mathbf{K}_0, \dots, \mathbf{K}_L, \\ \mathbf{K}_0^{(z)}, \dots, \mathbf{K}_L^{(z)}}} \sum_{\substack{\mathbf{n}_1, \dots, \mathbf{n}_L, \\ \mathbf{m}_1, \dots, \mathbf{m}_L, \\ \mathbf{n}_1^{(z)}, \dots, \mathbf{n}_L^{(z)}, \\ \mathbf{m}_1^{(z)}, \dots, \mathbf{m}_L^{(z)}}} |\mathbf{m}_1, \mathbf{m}_1^{(z)}; \dots; \mathbf{m}_L, \mathbf{m}_L^{(z)}\rangle \langle \mathbf{n}_1, \mathbf{n}_1^{(z)}; \dots; \mathbf{n}_L, \mathbf{n}_L^{(z)} | \\
&\quad \cdot \sum_{\substack{\mathbf{k}_0, \mathbf{l}_0, \\ \mathbf{k}_0^{(z)}, \mathbf{l}_0^{(z)}}} \langle \mathbf{k}_0; \mathbf{l}_0 \| \mathbf{K}_0 \rangle \Gamma_{\substack{\mathbf{k}_0, \mathbf{l}_0 \rightarrow \mathbf{K}_0 \\ \mathbf{k}_0^{(z)}, \mathbf{l}_0^{(z)} \rightarrow \mathbf{K}_0^{(z)}}} \\
&\quad \cdot \sum_{\substack{\mathbf{k}'_0, \mathbf{l}'_0, \\ \mathbf{k}_1, \mathbf{l}_1, \mathbf{o}_1, \\ \mathbf{k}'_0^{(z)}, \mathbf{l}'_0^{(z)}, \\ \mathbf{l}_1^{(z)}, \mathbf{l}_1^{(z)}, \mathbf{o}_1^{(z)}}} \langle \mathbf{K}_0 \| \mathbf{k}'_0; \mathbf{l}'_0 \rangle \Gamma_{\substack{\mathbf{k}'_0, \mathbf{l}'_0 \rightarrow \mathbf{K}_0 \\ \mathbf{k}'_0^{(z)}, \mathbf{l}'_0^{(z)} \rightarrow \mathbf{K}_0^{(z)}}} U(1) \mathbf{k}_1 \mathbf{k}_1^{(z)} \mathbf{o}_1 \mathbf{o}_1^{(z)} \mathbf{k}'_0, \mathbf{l}'_0 \rightarrow \mathbf{K}_0 V(1) \mathbf{l}_1 \mathbf{l}_1^{(z)} \mathbf{n}_1 \mathbf{n}_1^{(z)} \mathbf{l}'_0, \mathbf{l}'_0 \rightarrow \mathbf{K}_0 \mathbf{o}_1 \mathbf{o}_1^{(z)} \langle \mathbf{k}_1; \mathbf{l}_1 \| \mathbf{K}_1 \rangle \Gamma_{\substack{\mathbf{k}_1, \mathbf{l}_1 \rightarrow \mathbf{K}_1 \\ \mathbf{k}_1^{(z)}, \mathbf{l}_1^{(z)} \rightarrow \mathbf{K}_1^{(z)}}} \\
&\quad \vdots \\
&\quad \cdot \sum_{\substack{\mathbf{k}'_{\ell-1}, \mathbf{l}'_{\ell-1}, \\ \mathbf{k}_\ell, \mathbf{l}_\ell, \mathbf{o}_\ell, \\ \mathbf{k}'_{\ell-1}^{(z)}, \mathbf{l}'_{\ell-1}^{(z)}, \\ \mathbf{l}_\ell^{(z)}, \mathbf{l}_\ell^{(z)}, \mathbf{o}_\ell^{(z)}}} \langle \mathbf{K}_{\ell-1} \| \mathbf{k}'_{\ell-1}; \mathbf{l}'_{\ell-1} \rangle \Gamma_{\substack{\mathbf{k}'_{\ell-1}, \mathbf{l}'_{\ell-1} \rightarrow \mathbf{K}_{\ell-1} \\ \mathbf{k}'_{\ell-1}^{(z)}, \mathbf{l}'_{\ell-1}^{(z)} \rightarrow \mathbf{K}_{\ell-1}^{(z)}}} U(\ell) \mathbf{k}_\ell \mathbf{k}_\ell^{(z)} \mathbf{o}_\ell \mathbf{o}_\ell^{(z)} \mathbf{k}'_{\ell-1}, \mathbf{l}'_{\ell-1} \rightarrow \mathbf{K}_{\ell-1} V(\ell) \mathbf{l}_\ell \mathbf{l}_\ell^{(z)} \mathbf{n}_\ell \mathbf{n}_\ell^{(z)} \mathbf{l}'_{\ell-1}, \mathbf{l}'_{\ell-1} \rightarrow \mathbf{K}_{\ell-1} \mathbf{o}_\ell \mathbf{o}_\ell^{(z)} \langle \mathbf{k}_\ell; \mathbf{l}_\ell \| \mathbf{K}_\ell \rangle \Gamma_{\substack{\mathbf{k}_\ell, \mathbf{l}_\ell \rightarrow \mathbf{K}_\ell \\ \mathbf{k}_\ell^{(z)}, \mathbf{l}_\ell^{(z)} \rightarrow \mathbf{K}_\ell^{(z)}}} \\
&\quad \vdots \\
&\quad \cdot \sum_{\substack{\mathbf{k}'_{L-1}, \mathbf{l}'_{L-1}, \\ \mathbf{k}_L, \mathbf{l}_L, \mathbf{o}_L, \\ \mathbf{k}'_{L-1}^{(z)}, \mathbf{l}'_{L-1}^{(z)}, \\ \mathbf{l}_L^{(z)}, \mathbf{l}_L^{(z)}, \mathbf{o}_L^{(z)}}} \langle \mathbf{K}_{L-1} \| \mathbf{k}'_{L-1}; \mathbf{l}'_{L-1} \rangle \Gamma_{\substack{\mathbf{k}'_{L-1}, \mathbf{l}'_{L-1} \rightarrow \mathbf{K}_{L-1} \\ \mathbf{k}'_{L-1}^{(z)}, \mathbf{l}'_{L-1}^{(z)} \rightarrow \mathbf{K}_{L-1}^{(z)}}} U(L) \mathbf{k}_L \mathbf{k}_L^{(z)} \mathbf{o}_L \mathbf{o}_L^{(z)} \mathbf{k}'_{L-1}, \mathbf{l}'_{L-1} \rightarrow \mathbf{K}_{L-1} V(L) \mathbf{l}_L \mathbf{l}_L^{(z)} \mathbf{n}_L \mathbf{n}_L^{(z)} \mathbf{l}'_{L-1}, \mathbf{l}'_{L-1} \rightarrow \mathbf{K}_{L-1} \mathbf{o}_L \mathbf{o}_L^{(z)} \langle \mathbf{k}_L; \mathbf{l}_L \| \mathbf{K}_L \rangle \Gamma_{\substack{\mathbf{k}_L, \mathbf{l}_L \rightarrow \mathbf{K}_L \\ \mathbf{k}_L^{(z)}, \mathbf{l}_L^{(z)} \rightarrow \mathbf{K}_L^{(z)}}} \\
&\quad \cdot \sum_{\substack{\mathbf{k}'_L, \mathbf{l}'_L, \\ \mathbf{k}_L^{(z)}, \mathbf{l}_L^{(z)}}} \langle \mathbf{K}_L \| \mathbf{k}'_L; \mathbf{l}'_L \rangle \Gamma_{\substack{\mathbf{k}'_L, \mathbf{l}'_L \rightarrow \mathbf{K}_L \\ \mathbf{k}'_L^{(z)}, \mathbf{l}'_L^{(z)} \rightarrow \mathbf{K}_L^{(z)}}}.
\end{aligned}$$

Here the term

$$\sum_{\substack{\mathbf{k}_0, \mathbf{l}_0, \\ \mathbf{k}_0^{(z)}, \mathbf{l}_0^{(z)}}} \langle \mathbf{k}_0; \mathbf{l}_0 \| \mathbf{K}_0 \rangle \Gamma_{\substack{\mathbf{k}_0, \mathbf{l}_0 \rightarrow \mathbf{K}_0 \\ \mathbf{k}_0^{(z)}, \mathbf{l}_0^{(z)} \rightarrow \mathbf{K}_0^{(z)}}} = \langle (0, 1); (0, 1) \| \mathbf{K}_0 \rangle \Gamma_{00 \rightarrow \mathbf{K}_0}^{00 \rightarrow \mathbf{K}_0}$$

fixes the possible values of the composite MPO index $\mathbf{K}_0 = (0, 1)$, and thus $\mathbf{K}_0^{(z)} = 0$. The term

$$\sum_{r_1^{(z)}, r_2^{(z)}} \Gamma_{r_1^{(z)} r_2^{(z)} \rightarrow \mathcal{R}^{(z)}}^{r_1 r_2 \rightarrow R} \sum_{\substack{\mathbf{k}_L^{(z)} = r_1^{(z)}, \\ \mathbf{l}_L^{(z)} = r_2^{(z)}}} \langle\langle \mathbf{K}_L \| \mathbf{k}'_L; \mathbf{l}'_L \rangle\rangle \Gamma_{\mathbf{k}_L^{(z)} \mathbf{l}'_L \rightarrow \mathbf{K}_L}^{\mathbf{k}'_L \mathbf{l}'_L \rightarrow \mathbf{K}_L} = \langle\langle \mathbf{K}_L \| (r_1, 1); (r_2, 1) \rangle\rangle \sum_{r_1^{(z)}, r_2^{(z)}} \Gamma_{r_1^{(z)} r_2^{(z)} \rightarrow \mathcal{R}^{(z)}}^{r_1 r_2 \rightarrow R} \Gamma_{r_1^{(z)} r_2^{(z)} \rightarrow \mathbf{K}_L}^{r_1 r_2 \rightarrow \mathbf{K}_L}$$

enforces $\mathbf{K}_L = (R, 1)$ and $\mathbf{K}_L^{(z)} = R^{(z)}$. The multiplicity is trivial, because there is only one possibility in which a non-degenerate $\mathbf{k}_L = (r_1, 1)$ and $\mathbf{l}_L = (r_2, 1)$ can couple to a total angular momentum R . With this, the operator product can be written as:

$$\widehat{W}_{\mathcal{R}^{(z)}}^{[R]} = \sum_{\substack{\mathbf{K}_0, \dots, \mathbf{K}_L, \\ \mathbf{K}_0^{(z)}, \dots, \mathbf{K}_L^{(z)}}}^{\mathbf{K}_L^{(z)} = \mathcal{R}^{(z)}} \sum_{\substack{\mathbf{n}_1, \dots, \mathbf{n}_L, \\ \mathbf{m}_1, \dots, \mathbf{m}_L, \\ \mathbf{n}_1^{(z)}, \dots, \mathbf{n}_L^{(z)}, \\ \mathbf{m}_1^{(z)}, \dots, \mathbf{m}_L^{(z)}}} W(1)_{\mathbf{K}_0 \mathbf{K}_0^{(z)} \mathbf{m}_1 \mathbf{m}_1^{(z)}}^{\mathbf{K}_1 \mathbf{K}_1^{(z)} \mathbf{n}_1 \mathbf{n}_1^{(z)}} \cdots W(L)_{\mathbf{K}_{L-1} \mathbf{K}_{L-1}^{(z)} \mathbf{m}_L \mathbf{m}_L^{(z)}}^{\mathbf{K}_L \mathbf{K}_L^{(z)} \mathbf{n}_L \mathbf{n}_L^{(z)}} \cdot |\mathbf{m}_1, \mathbf{m}_1^{(z)}; \dots; \mathbf{m}_L, \mathbf{m}_L^{(z)}\rangle \langle \mathbf{n}_1, \mathbf{n}_1^{(z)}; \dots; \mathbf{n}_L, \mathbf{n}_L^{(z)} |,$$

where the occurring MPO tensors are given by:

$$\begin{aligned} & W(\ell)_{\mathbf{K}_{\ell-1} \mathbf{K}_{\ell-1}^{(z)} \mathbf{m}_{\ell} \mathbf{m}_{\ell}^{(z)}}^{\mathbf{K}_{\ell} \mathbf{K}_{\ell}^{(z)} \mathbf{n}_{\ell} \mathbf{n}_{\ell}^{(z)}} \\ &= \sum_{\substack{\mathbf{k}_{\ell-1}, \mathbf{l}_{\ell-1}, \\ \mathbf{k}_{\ell}, \mathbf{l}_{\ell}, \mathbf{o}_{\ell}}} \sum_{\substack{\mathbf{k}_{\ell-1}^{(z)}, \mathbf{l}_{\ell-1}^{(z)}, \\ \mathbf{k}_{\ell}^{(z)}, \mathbf{l}_{\ell}^{(z)}, \mathbf{o}_{\ell}^{(z)}}} U(\ell)_{\mathbf{k}_{\ell-1} \mathbf{k}_{\ell-1}^{(z)} \mathbf{m}_{\ell} \mathbf{m}_{\ell}^{(z)}}^{\mathbf{k}_{\ell} \mathbf{k}_{\ell}^{(z)} \mathbf{o}_{\ell} \mathbf{o}_{\ell}^{(z)}} V(\ell)_{\mathbf{l}_{\ell-1} \mathbf{l}_{\ell-1}^{(z)} \mathbf{o}_{\ell} \mathbf{o}_{\ell}^{(z)}}^{\mathbf{l}_{\ell} \mathbf{l}_{\ell}^{(z)} \mathbf{n}_{\ell} \mathbf{n}_{\ell}^{(z)}} \langle\langle \mathbf{K}_{\ell-1} \| \mathbf{k}_{\ell-1}; \mathbf{l}_{\ell-1} \rangle\rangle \langle\langle \mathbf{k}_{\ell}; \mathbf{l}_{\ell} \| \mathbf{K}_{\ell} \rangle\rangle \Gamma_{\mathbf{k}_{\ell-1} \mathbf{l}_{\ell-1} \rightarrow \mathbf{K}_{\ell-1}}^{\mathbf{k}_{\ell-1} \mathbf{l}_{\ell-1} \rightarrow \mathbf{K}_{\ell-1}} \Gamma_{\mathbf{k}_{\ell} \mathbf{l}_{\ell} \rightarrow \mathbf{K}_{\ell}}^{\mathbf{k}_{\ell} \mathbf{l}_{\ell} \rightarrow \mathbf{K}_{\ell}} \\ & \quad \text{Inserting } 1 = \sum_{\mathbf{K}_{\ell-1}^{(z)}, \mathbf{K}_{\ell}^{(z)}} \delta_{\mathbf{K}_{\ell-1}^{(z)} \mathbf{K}_{\ell-1}^{(z)}} \delta_{\mathbf{K}_{\ell}^{(z)} \mathbf{K}_{\ell}^{(z)}} = \sum_{\mathbf{T}_{\ell}, \mathbf{T}_{\ell}^{(z)}, \mathbf{K}_{\ell-1}^{(z)}, \mathbf{K}_{\ell}^{(z)}} \Gamma_{\mathbf{K}_{\ell-1} \mathbf{K}_{\ell} \rightarrow \mathbf{T}_{\ell}}^{\mathbf{K}_{\ell-1} \mathbf{K}_{\ell} \rightarrow \mathbf{T}_{\ell}} \Gamma_{\mathbf{K}_{\ell-1} \mathbf{K}_{\ell} \rightarrow \mathbf{T}_{\ell}^{(z)}}^{\mathbf{K}_{\ell-1} \mathbf{K}_{\ell} \rightarrow \mathbf{T}_{\ell}^{(z)}} \\ & \quad \text{and } 1 = \sum_{\mathbf{n}_{\ell}^{(z)}, \mathbf{m}_{\ell}^{\prime(z)}} \delta_{\mathbf{m}_{\ell}^{(z)} \mathbf{m}_{\ell}^{\prime(z)}} \delta_{\mathbf{n}_{\ell}^{(z)} \mathbf{n}_{\ell}^{\prime(z)}} = \sum_{\mathbf{T}_{\ell}^{\prime}, \mathbf{T}_{\ell}^{\prime(z)}, \mathbf{m}_{\ell}^{\prime(z)}, \mathbf{n}_{\ell}^{\prime(z)}} \Gamma_{\mathbf{m}_{\ell}^{(z)} \mathbf{n}_{\ell}^{(z)} \rightarrow \mathbf{T}_{\ell}^{\prime}}^{\mathbf{m}_{\ell} \mathbf{n}_{\ell} \rightarrow \mathbf{T}_{\ell}^{\prime}} \Gamma_{\mathbf{m}_{\ell}^{\prime(z)} \mathbf{n}_{\ell}^{\prime(z)} \rightarrow \mathbf{T}_{\ell}^{\prime(z)}}^{\mathbf{m}_{\ell} \mathbf{n}_{\ell} \rightarrow \mathbf{T}_{\ell}^{\prime(z)}} : \\ &= \sum_{\substack{\mathbf{k}_{\ell-1}, \mathbf{l}_{\ell-1}, \\ \mathbf{k}_{\ell}, \mathbf{l}_{\ell}, \mathbf{o}_{\ell}}} \sum_{\substack{\mathbf{k}_{\ell-1}^{(z)}, \mathbf{l}_{\ell-1}^{(z)}, \\ \mathbf{k}_{\ell}^{(z)}, \mathbf{l}_{\ell}^{(z)}, \mathbf{o}_{\ell}^{(z)}, \\ \mathbf{n}_{\ell}^{\prime(z)}, \mathbf{m}_{\ell}^{\prime(z)}, \\ \mathbf{K}_{\ell-1}^{(z)}, \mathbf{K}_{\ell}^{\prime(z)}}} U(\ell)_{\mathbf{k}_{\ell-1} \mathbf{k}_{\ell-1}^{(z)} \mathbf{m}_{\ell} \mathbf{m}_{\ell}^{\prime(z)}}^{\mathbf{k}_{\ell} \mathbf{k}_{\ell}^{(z)} \mathbf{o}_{\ell} \mathbf{o}_{\ell}^{(z)}} V(\ell)_{\mathbf{l}_{\ell-1} \mathbf{l}_{\ell-1}^{(z)} \mathbf{o}_{\ell} \mathbf{o}_{\ell}^{(z)}}^{\mathbf{l}_{\ell} \mathbf{l}_{\ell}^{(z)} \mathbf{n}_{\ell} \mathbf{n}_{\ell}^{\prime(z)}} \langle\langle \mathbf{K}_{\ell-1} \| \mathbf{k}_{\ell-1}; \mathbf{l}_{\ell-1} \rangle\rangle \langle\langle \mathbf{k}_{\ell}; \mathbf{l}_{\ell} \| \mathbf{K}_{\ell} \rangle\rangle \Gamma_{\mathbf{k}_{\ell-1} \mathbf{l}_{\ell-1} \rightarrow \mathbf{K}_{\ell-1}}^{\mathbf{k}_{\ell-1} \mathbf{l}_{\ell-1} \rightarrow \mathbf{K}_{\ell-1}} \Gamma_{\mathbf{k}_{\ell} \mathbf{l}_{\ell} \rightarrow \mathbf{K}_{\ell}}^{\mathbf{k}_{\ell} \mathbf{l}_{\ell} \rightarrow \mathbf{K}_{\ell}} \\ & \quad \cdot \sum_{\substack{\mathbf{T}_{\ell}, \mathbf{T}_{\ell}^{\prime}, \\ \mathbf{T}_{\ell}^{(z)}, \mathbf{T}_{\ell}^{\prime(z)}}} \frac{(2\mathbf{T}_{\ell} + 1)(2\mathbf{T}_{\ell}^{\prime} + 1)}{(2\mathbf{m}_{\ell} + 1)(2\mathbf{K}_{\ell} + 1)} \cdot \Gamma_{\mathbf{K}_{\ell-1} \mathbf{T}_{\ell} \rightarrow \mathbf{K}_{\ell}}^{\mathbf{K}_{\ell-1} \mathbf{T}_{\ell} \rightarrow \mathbf{K}_{\ell}} \Gamma_{\mathbf{K}_{\ell-1} \mathbf{T}_{\ell} \rightarrow \mathbf{K}_{\ell}}^{\mathbf{K}_{\ell-1} \mathbf{T}_{\ell} \rightarrow \mathbf{K}_{\ell}} \cdot \Gamma_{\mathbf{n}_{\ell} \mathbf{T}_{\ell}^{\prime} \rightarrow \mathbf{m}_{\ell}}^{\mathbf{n}_{\ell} \mathbf{T}_{\ell}^{\prime} \rightarrow \mathbf{m}_{\ell}} \Gamma_{\mathbf{n}_{\ell}^{\prime(z)} \mathbf{T}_{\ell}^{\prime(z)} \rightarrow \mathbf{m}_{\ell}^{\prime(z)}}^{\mathbf{n}_{\ell} \mathbf{T}_{\ell}^{\prime} \rightarrow \mathbf{m}_{\ell}^{\prime(z)}} \\ &= \sum_{\substack{\mathbf{T}_{\ell}, \mathbf{T}_{\ell}^{\prime}, \\ \mathbf{T}_{\ell}^{(z)}, \mathbf{T}_{\ell}^{\prime(z)}}} \Gamma_{\mathbf{K}_{\ell-1} \mathbf{T}_{\ell} \rightarrow \mathbf{K}_{\ell}}^{\mathbf{K}_{\ell-1} \mathbf{T}_{\ell} \rightarrow \mathbf{K}_{\ell}} \Gamma_{\mathbf{n}_{\ell} \mathbf{T}_{\ell}^{\prime} \rightarrow \mathbf{m}_{\ell}}^{\mathbf{n}_{\ell} \mathbf{T}_{\ell}^{\prime} \rightarrow \mathbf{m}_{\ell}} \\ & \quad \cdot \sum_{\substack{\mathbf{k}_{\ell-1}, \mathbf{l}_{\ell-1}, \\ \mathbf{k}_{\ell}, \mathbf{l}_{\ell}, \mathbf{o}_{\ell}, \\ \mathbf{t}_{\ell}, \mathbf{x}_{\ell}}} \frac{(2\mathbf{T}_{\ell} + 1)(2\mathbf{T}_{\ell}^{\prime} + 1)}{(2\mathbf{m}_{\ell} + 1)(2\mathbf{K}_{\ell} + 1)} \cdot \overline{U}^{[t_{\ell}]}(\ell)_{\mathbf{k}_{\ell-1} \mathbf{m}_{\ell}}^{\mathbf{k}_{\ell} \mathbf{o}_{\ell}} \overline{V}^{[x_{\ell}]}(\ell)_{\mathbf{l}_{\ell-1} \mathbf{o}_{\ell}}^{\mathbf{l}_{\ell} \mathbf{n}_{\ell}} \langle\langle \mathbf{K}_{\ell-1} \| \mathbf{k}_{\ell-1}; \mathbf{l}_{\ell-1} \rangle\rangle \langle\langle \mathbf{k}_{\ell}; \mathbf{l}_{\ell} \| \mathbf{K}_{\ell} \rangle\rangle \\ & \quad \cdot \sum_{\substack{\mathbf{k}_{\ell-1}, \mathbf{l}_{\ell-1}, \\ \mathbf{k}_{\ell}, \mathbf{l}_{\ell}, \mathbf{o}_{\ell}, \\ \mathbf{t}_{\ell}, \mathbf{x}_{\ell}, \\ \mathbf{n}_{\ell}^{\prime(z)}, \mathbf{m}_{\ell}^{\prime(z)}, \\ \mathbf{K}_{\ell-1}^{(z)}, \mathbf{K}_{\ell}^{\prime(z)}}} \Gamma_{\mathbf{k}_{\ell-1} \mathbf{l}_{\ell-1} \rightarrow \mathbf{K}_{\ell-1}}^{\mathbf{k}_{\ell-1} \mathbf{l}_{\ell-1} \rightarrow \mathbf{K}_{\ell-1}} \Gamma_{\mathbf{k}_{\ell} \mathbf{l}_{\ell} \rightarrow \mathbf{K}_{\ell}}^{\mathbf{k}_{\ell} \mathbf{l}_{\ell} \rightarrow \mathbf{K}_{\ell}} \Gamma_{\mathbf{n}_{\ell}^{\prime(z)} \mathbf{T}_{\ell}^{\prime(z)} \rightarrow \mathbf{m}_{\ell}^{\prime(z)}}^{\mathbf{n}_{\ell} \mathbf{T}_{\ell}^{\prime} \rightarrow \mathbf{m}_{\ell}} \Gamma_{\mathbf{K}_{\ell-1} \mathbf{T}_{\ell} \rightarrow \mathbf{K}_{\ell}}^{\mathbf{K}_{\ell-1} \mathbf{T}_{\ell} \rightarrow \mathbf{K}_{\ell}} \cdot \Gamma_{\mathbf{k}_{\ell-1} \mathbf{t}_{\ell} \rightarrow \mathbf{k}_{\ell}}^{\mathbf{k}_{\ell-1} \mathbf{t}_{\ell} \rightarrow \mathbf{k}_{\ell}} \Gamma_{\mathbf{o}_{\ell} \mathbf{t}_{\ell} \rightarrow \mathbf{m}_{\ell}}^{\mathbf{o}_{\ell} \mathbf{t}_{\ell} \rightarrow \mathbf{m}_{\ell}} \Gamma_{\mathbf{l}_{\ell-1} \mathbf{x}_{\ell} \rightarrow \mathbf{l}_{\ell}}^{\mathbf{l}_{\ell-1} \mathbf{x}_{\ell} \rightarrow \mathbf{l}_{\ell}} \Gamma_{\mathbf{n}_{\ell} \mathbf{x}_{\ell} \rightarrow \mathbf{o}_{\ell}}^{\mathbf{n}_{\ell} \mathbf{x}_{\ell} \rightarrow \mathbf{o}_{\ell}} \end{aligned}$$

$$\begin{aligned}
& \text{Inserting } 1 = \sum_{\substack{\mathbf{t}'_\ell, \mathbf{x}'_\ell \\ \mathbf{t}_\ell, \mathbf{x}_\ell}} \delta_{\mathbf{t}'_\ell, \mathbf{t}_\ell} \delta_{\mathbf{x}'_\ell, \mathbf{x}_\ell} = \sum_{\substack{\mathbf{T}'_\ell, \mathbf{T}''_\ell, \\ \mathbf{t}'_\ell, \mathbf{x}'_\ell}} \Gamma_{\substack{\mathbf{t}_\ell \ \mathbf{x}_\ell \rightarrow \mathbf{T}'_\ell \\ \mathbf{t}^{(z)}_\ell \ \mathbf{x}^{(z)}_\ell \rightarrow \mathbf{T}''_\ell}} \Gamma_{\substack{\mathbf{t}_\ell \ \mathbf{x}_\ell \rightarrow \mathbf{T}'_\ell \\ \mathbf{t}'_\ell \ \mathbf{x}'_\ell \rightarrow \mathbf{T}''_\ell}} : \\
= & \sum_{\substack{\mathbf{T}_\ell, \mathbf{T}'_\ell, \mathbf{T}''_\ell, \\ \mathbf{T}^{(z)}_\ell, \mathbf{T}'^{(z)}_\ell, \mathbf{T}''^{(z)}_\ell}} \Gamma_{\mathbf{K}_{\ell-1} \mathbf{T}_\ell \rightarrow \mathbf{K}_\ell} \Gamma_{\mathbf{n}_\ell \mathbf{T}'_\ell \rightarrow \mathbf{m}_\ell} \Gamma_{\mathbf{n}_\ell \mathbf{T}^{(z)}_\ell \rightarrow \mathbf{m}_\ell^{(z)}} \\
& \cdot \sum_{\substack{\mathbf{k}_{\ell-1}, \mathbf{l}_{\ell-1}, \\ \mathbf{k}_\ell, \mathbf{l}_\ell, \mathbf{o}_\ell, \\ \mathbf{t}_\ell, \mathbf{x}_\ell}} \frac{(2\mathbf{T}_\ell + 1)(2\mathbf{T}'_\ell + 1)}{(2\mathbf{m}_\ell + 1)(2\mathbf{K}_\ell + 1)} \cdot \bar{U}[\mathbf{t}_\ell](\ell)_{\mathbf{k}_{\ell-1} \mathbf{o}_\ell}^{\mathbf{k}_\ell} \bar{V}[\mathbf{x}_\ell](\ell)_{\mathbf{l}_{\ell-1} \mathbf{o}_\ell}^{\mathbf{l}_\ell} \langle \mathbf{K}_{\ell-1} | \mathbf{k}_{\ell-1}; \mathbf{l}_{\ell-1} \rangle \langle \mathbf{k}_\ell; \mathbf{l}_\ell | \mathbf{K}_\ell \rangle \\
& \cdot \sum_{\substack{\mathbf{t}_\ell^{(z)}, \mathbf{x}_\ell^{(z)}, \\ \mathbf{k}_{\ell-1}^{(z)}, \mathbf{k}_\ell^{(z)}, \\ \mathbf{l}_{\ell-1}^{(z)}, \mathbf{l}_\ell^{(z)}, \\ \mathbf{K}_{\ell-1}^{(z)}, \mathbf{K}_\ell^{(z)}}} \Gamma_{\mathbf{k}_{\ell-1}^{(z)} \mathbf{l}_{\ell-1}^{(z)} \rightarrow \mathbf{K}_{\ell-1}^{(z)}} \Gamma_{\mathbf{k}_{\ell-1}^{(z)} \mathbf{t}_\ell^{(z)} \rightarrow \mathbf{k}_\ell^{(z)}} \Gamma_{\mathbf{k}_\ell^{(z)} \mathbf{l}_\ell^{(z)} \rightarrow \mathbf{K}_\ell^{(z)}} \Gamma_{\mathbf{K}_{\ell-1}^{(z)} \mathbf{T}_\ell^{(z)} \rightarrow \mathbf{K}_\ell^{(z)}} \Gamma_{\mathbf{K}_{\ell-1}^{(z)} \mathbf{T}'_\ell^{(z)} \rightarrow \mathbf{K}_\ell^{(z)}} \Gamma_{\mathbf{l}_{\ell-1}^{(z)} \mathbf{x}_\ell^{(z)} \rightarrow \mathbf{l}_\ell^{(z)}} \Gamma_{\mathbf{t}_\ell^{(z)} \ \mathbf{x}_\ell^{(z)} \rightarrow \mathbf{T}'_\ell^{(z)}} \\
& \cdot \sum_{\substack{\mathbf{t}'_\ell, \mathbf{x}'_\ell, \\ \mathbf{o}_\ell, \mathbf{n}'_\ell, \mathbf{m}'_\ell}} \Gamma_{\mathbf{n}'_\ell \mathbf{T}'_\ell \rightarrow \mathbf{m}'_\ell} \Gamma_{\mathbf{o}_\ell \mathbf{t}'_\ell \rightarrow \mathbf{m}'_\ell} \Gamma_{\mathbf{n}'_\ell \mathbf{x}'_\ell \rightarrow \mathbf{o}_\ell} \Gamma_{\mathbf{t}'_\ell \ \mathbf{x}'_\ell \rightarrow \mathbf{T}''_\ell}.
\end{aligned}$$

The last two rows can be contracted separately:

$$\begin{aligned}
& \sum_{\substack{\mathbf{t}'_\ell, \mathbf{x}'_\ell, \\ \mathbf{o}_\ell^{(z)}, \mathbf{n}_\ell^{(z)}, \mathbf{m}_\ell^{(z)}}} \Gamma_{\mathbf{n}'_\ell \mathbf{T}'_\ell \rightarrow \mathbf{m}'_\ell} \Gamma_{\mathbf{o}_\ell \mathbf{t}'_\ell \rightarrow \mathbf{m}'_\ell} \Gamma_{\mathbf{n}'_\ell \mathbf{x}'_\ell \rightarrow \mathbf{o}_\ell} \Gamma_{\mathbf{t}'_\ell \ \mathbf{x}'_\ell \rightarrow \mathbf{T}''_\ell} \\
= & \sum_{\substack{\mathbf{t}'_\ell, \mathbf{x}'_\ell, \\ \mathbf{o}_\ell^{(z)}, \mathbf{n}_\ell^{(z)}, \mathbf{m}_\ell^{(z)}}} (-1)^{\mathbf{m}_\ell - \mathbf{o}_\ell - \mathbf{t}_\ell} \Gamma_{\mathbf{t}'_\ell \ \mathbf{o}_\ell \rightarrow \mathbf{m}'_\ell} \cdot (-1)^{\mathbf{n}_\ell - \mathbf{n}_\ell^{(z)}} \sqrt{\frac{2\mathbf{m}_\ell + 1}{2\mathbf{T}'_\ell + 1}} \Gamma_{\mathbf{m}_\ell^{(z)} - \mathbf{n}_\ell^{(z)} \rightarrow \mathbf{T}'_\ell} \\
& \cdot (-1)^{\mathbf{n}_\ell - \mathbf{n}_\ell^{(z)}} \sqrt{\frac{2\mathbf{o}_\ell + 1}{2\mathbf{x}_\ell + 1}} \Gamma_{\mathbf{o}_\ell^{(z)} - \mathbf{n}_\ell^{(z)} \rightarrow \mathbf{x}_\ell} \cdot \Gamma_{\mathbf{t}'_\ell \ \mathbf{x}'_\ell \rightarrow \mathbf{T}''_\ell} \\
= & (-1)^{\mathbf{m}_\ell - \mathbf{o}_\ell - \mathbf{t}_\ell} \sqrt{\frac{(2\mathbf{m}_\ell + 1)(2\mathbf{o}_\ell + 1)}{(2\mathbf{T}'_\ell + 1)(2\mathbf{x}_\ell + 1)}} \sum_{\substack{\mathbf{t}'_\ell, \mathbf{x}'_\ell, \\ \mathbf{o}_\ell^{(z)}, \mathbf{n}_\ell^{(z)}, \mathbf{m}_\ell^{(z)}}} \Gamma_{\mathbf{t}'_\ell \ \mathbf{o}_\ell \rightarrow \mathbf{m}'_\ell} \cdot \Gamma_{\mathbf{m}_\ell^{(z)} \mathbf{n}_\ell^{(z)} \rightarrow \mathbf{T}'_\ell} \cdot \Gamma_{\mathbf{o}_\ell^{(z)} \mathbf{n}_\ell^{(z)} \rightarrow \mathbf{x}_\ell} \cdot \Gamma_{\mathbf{t}'_\ell \ \mathbf{x}'_\ell \rightarrow \mathbf{T}''_\ell} \\
= & (-1)^{\mathbf{m}_\ell - \mathbf{o}_\ell - \mathbf{t}_\ell} \sqrt{\frac{(2\mathbf{m}_\ell + 1)(2\mathbf{o}_\ell + 1)}{(2\mathbf{T}'_\ell + 1)(2\mathbf{x}_\ell + 1)}} \langle \mathbf{T}''_\ell(\mathbf{t}_\ell, \mathbf{x}_\ell(\mathbf{o}_\ell, \mathbf{n}_\ell)), \mathbf{T}'_\ell \rangle \left| \mathbf{T}'_\ell(\mathbf{m}_\ell(\mathbf{t}_\ell, \mathbf{o}_\ell), \mathbf{n}_\ell), \mathbf{T}'_\ell \right\rangle \\
= & (-1)^{\mathbf{m}_\ell - \mathbf{o}_\ell - \mathbf{t}_\ell} \sqrt{\frac{(2\mathbf{m}_\ell + 1)(2\mathbf{o}_\ell + 1)}{(2\mathbf{T}'_\ell + 1)(2\mathbf{x}_\ell + 1)}} \cdot \delta_{\mathbf{T}'_\ell \mathbf{T}''_\ell} \delta_{\mathbf{T}'_\ell \mathbf{T}''_\ell} \sqrt{(2\mathbf{m}_\ell + 1)(2\mathbf{x}_\ell + 1)} (-1)^{\mathbf{t}_\ell + \mathbf{o}_\ell + \mathbf{n}_\ell + \mathbf{T}'_\ell} \left\{ \begin{array}{ccc} \mathbf{t}_\ell & \mathbf{o}_\ell & \mathbf{m}_\ell \\ \mathbf{n}_\ell & \mathbf{T}'_\ell & \mathbf{x}_\ell \end{array} \right\} \\
= & (-1)^{\mathbf{m}_\ell + \mathbf{n}_\ell + \mathbf{T}'_\ell} (2\mathbf{m}_\ell + 1) \sqrt{\frac{2\mathbf{o}_\ell + 1}{2\mathbf{T}'_\ell + 1}} \delta_{\mathbf{T}'_\ell \mathbf{T}''_\ell} \delta_{\mathbf{T}'_\ell \mathbf{T}''_\ell} \left\{ \begin{array}{ccc} \mathbf{n}_\ell & \mathbf{x}_\ell & \mathbf{o}_\ell \\ \mathbf{t}_\ell & \mathbf{m}_\ell & \mathbf{T}'_\ell \end{array} \right\} \\
= & \frac{2\mathbf{m}_\ell + 1}{2\mathbf{T}'_\ell + 1} \cdot \delta_{\mathbf{T}'_\ell \mathbf{T}''_\ell} \delta_{\mathbf{T}'_\ell \mathbf{T}''_\ell} \left[\begin{array}{ccc} \mathbf{n}_\ell & \mathbf{x}_\ell & \mathbf{o}_\ell \\ \mathbf{t}_\ell & \mathbf{m}_\ell & \mathbf{T}'_\ell \end{array} \right],
\end{aligned}$$

as well as

$$\begin{aligned}
 & \sum_{\substack{t_\ell^{(z)}, x_\ell^{(z)}, \\ k_{\ell-1}^{(z)}, k_\ell^{(z)}, \\ l_{\ell-1}^{(z)}, l_\ell^{(z)}, \\ K_{\ell-1}^{(z)}, K_\ell^{(z)}}} \Gamma_{k_{\ell-1}^{(z)} l_{\ell-1}^{(z)} \rightarrow K_{\ell-1}^{(z)}} \Gamma_{k_{\ell-1}^{(z)} t_\ell^{(z)} \rightarrow k_\ell^{(z)}} \Gamma_{k_\ell^{(z)} l_\ell^{(z)} \rightarrow K_\ell^{(z)}} \Gamma_{K_{\ell-1}^{(z)} T_\ell^{(z)} \rightarrow K_\ell^{(z)}} \Gamma_{l_{\ell-1}^{(z)} x_\ell^{(z)} \rightarrow l_\ell^{(z)}} \Gamma_{t_\ell^{(z)} x_\ell^{(z)} \rightarrow T_\ell^{(z)}} \\
 &= \sum_{\substack{t_\ell^{(z)}, x_\ell^{(z)}, \\ k_{\ell-1}^{(z)}, k_\ell^{(z)}, \\ l_{\ell-1}^{(z)}, l_\ell^{(z)}, \\ K_{\ell-1}^{(z)}, K_\ell^{(z)}}} \Gamma_{k_{\ell-1}^{(z)} l_{\ell-1}^{(z)} \rightarrow K_{\ell-1}^{(z)}} \cdot (-1)^{k_\ell + l_\ell - K_\ell} \Gamma_{k_\ell^{(z)} l_\ell^{(z)} \rightarrow K_\ell^{(z)}} \cdot (-1)^{K_{\ell-1}^{(z)} - K_{\ell-1}} \sqrt{\frac{2K_\ell + 1}{2T_\ell + 1}} \Gamma_{K_{\ell-1}^{(z)} K_\ell^{(z)} \rightarrow T_\ell^{(z)}} \\
 & \cdot (-1)^{k_{\ell-1} - k_{\ell-1}^{(z)}} \sqrt{\frac{2k_\ell + 1}{2t_\ell + 1}} \Gamma_{k_{\ell-1}^{(z)} k_\ell^{(z)} \rightarrow t_\ell^{(z)}} (-1)^{l_{\ell-1} - l_{\ell-1}^{(z)}} \sqrt{\frac{2l_\ell + 1}{2x_\ell + 1}} \Gamma_{l_{\ell-1}^{(z)} l_\ell^{(z)} \rightarrow x_\ell^{(z)}} (-1)^{t_\ell + x_\ell - T_\ell} \Gamma_{t_\ell^{(z)} x_\ell^{(z)} \rightarrow T_\ell^{(z)}}
 \end{aligned}$$

Using $K_{\ell-1}^{(z)} = k_{\ell-1}^{(z)} + l_{\ell-1}^{(z)}$, and inserting $1 = (-1)^{2(K_{\ell-1} + K_\ell + T_\ell)}$:

$$\begin{aligned}
 &= (-1)^{k_{\ell-1} + l_{\ell-1} + K_{\ell-1} + k_\ell + l_\ell + K_\ell + t_\ell + x_\ell + 2T_\ell - T_\ell''} \sqrt{\frac{(2K_\ell + 1)(2k_\ell + 1)(2l_\ell + 1)}{(2T_\ell + 1)(2t_\ell + 1)(2x_\ell + 1)}} \\
 & \cdot \sum_{\substack{t_\ell^{(z)}, x_\ell^{(z)}, \\ k_{\ell-1}^{(z)}, k_\ell^{(z)}, \\ l_{\ell-1}^{(z)}, l_\ell^{(z)}, \\ K_{\ell-1}^{(z)}, K_\ell^{(z)}}} \Gamma_{k_{\ell-1}^{(z)} l_{\ell-1}^{(z)} \rightarrow K_{\ell-1}^{(z)}} \Gamma_{k_{\ell-1}^{(z)} k_\ell^{(z)} \rightarrow k_\ell^{(z)}} \Gamma_{K_{\ell-1}^{(z)} K_\ell^{(z)} \rightarrow T_\ell^{(z)}} \Gamma_{k_{\ell-1}^{(z)} k_\ell^{(z)} \rightarrow t_\ell^{(z)}} \Gamma_{l_{\ell-1}^{(z)} l_\ell^{(z)} \rightarrow x_\ell^{(z)}} \Gamma_{t_\ell^{(z)} x_\ell^{(z)} \rightarrow T_\ell^{(z)}} \\
 &= (-1)^{k_{\ell-1} + l_{\ell-1} + K_{\ell-1} + k_\ell + l_\ell + K_\ell + t_\ell + x_\ell + 2T_\ell - T_\ell''} \sqrt{\frac{(2K_\ell + 1)(2k_\ell + 1)(2l_\ell + 1)}{(2T_\ell + 1)(2t_\ell + 1)(2x_\ell + 1)}} \\
 & \cdot \delta_{T_\ell T_\ell''} \delta_{T_\ell^{(z)} T_\ell^{(z)}} \left\langle T_\ell(K_{\ell-1}(k_{\ell-1}, l_{\ell-1}), K_\ell(k_\ell, l_\ell)), T_\ell^{(z)} \middle| T_\ell''(t_\ell(k_{\ell-1}, k_\ell), x_\ell(l_{\ell-1}, l_\ell)), T_\ell^{(z)} \right\rangle \\
 &= (-1)^{k_{\ell-1} + l_{\ell-1} + K_{\ell-1} + k_\ell + l_\ell + K_\ell + t_\ell + x_\ell + T_\ell''} \sqrt{\frac{(2K_\ell + 1)(2k_\ell + 1)(2l_\ell + 1)}{(2T_\ell + 1)(2t_\ell + 1)(2x_\ell + 1)}} \\
 & \cdot \delta_{T_\ell T_\ell''} \delta_{T_\ell^{(z)} T_\ell^{(z)}} \sqrt{(2K_{\ell-1} + 1)(2K_\ell + 1)(2t_\ell + 1)(2x_\ell + 1)} \left\{ \begin{array}{ccc} k_{\ell-1} & l_{\ell-1} & K_{\ell-1} \\ k_\ell & l_\ell & K_\ell \\ t_\ell & x_\ell & T_\ell \end{array} \right\} \\
 &= (2K_\ell + 1) \sqrt{\frac{(2k_\ell + 1)(2l_\ell + 1)(2K_{\ell-1} + 1)}{2T_\ell'' + 1}} \cdot \delta_{T_\ell T_\ell''} \delta_{T_\ell^{(z)} T_\ell^{(z)}} \left\{ \begin{array}{ccc} k_{\ell-1} & l_{\ell-1} & K_{\ell-1} \\ t_\ell & x_\ell & T_\ell \\ k_\ell & l_\ell & K_\ell \end{array} \right\} \\
 &= \frac{2K_\ell + 1}{2T_\ell + 1} \cdot \delta_{T_\ell T_\ell''} \delta_{T_\ell^{(z)} T_\ell^{(z)}} \left[\begin{array}{ccc} k_{\ell-1} & l_{\ell-1} & K_{\ell-1} \\ t_\ell & x_\ell & T_\ell \\ k_\ell & l_\ell & K_\ell \end{array} \right].
 \end{aligned}$$

This can be used to evaluate the expression for the MPO tensors:

$$W(\ell)_{\mathbf{K}_{\ell-1}\mathbf{K}_{\ell-1}^{(z)}\mathbf{m}_{\ell}\mathbf{m}_{\ell}^{(z)}}^{\mathbf{K}_{\ell}\mathbf{K}_{\ell}^{(z)}\mathbf{n}_{\ell}\mathbf{n}_{\ell}^{(z)}} = \sum_{\mathbf{T}_{\ell}, \mathbf{T}_{\ell}^{(z)}} \Gamma_{\mathbf{K}_{\ell-1}^{(z)}\mathbf{T}_{\ell}^{(z)} \rightarrow \mathbf{K}_{\ell}^{(z)}}^{\mathbf{K}_{\ell-1} \mathbf{T}_{\ell} \rightarrow \mathbf{K}_{\ell}} \Gamma_{\mathbf{n}_{\ell}^{(z)}\mathbf{T}_{\ell}^{(z)} \rightarrow \mathbf{m}_{\ell}^{(z)}}^{\mathbf{n}_{\ell} \mathbf{T}_{\ell} \rightarrow \mathbf{m}_{\ell}} \overline{W}^{[\mathbf{T}_{\ell}]}(\ell)_{\mathbf{K}_{\ell-1}\mathbf{m}_{\ell}}^{\mathbf{K}_{\ell}\mathbf{n}_{\ell}}$$

where

$$\overline{W}^{[\mathbf{T}_{\ell}]}(\ell)_{\mathbf{K}_{\ell-1}\mathbf{m}_{\ell}}^{\mathbf{K}_{\ell}\mathbf{n}_{\ell}} = \sum_{\substack{\mathbf{k}_{\ell-1}, \mathbf{l}_{\ell-1}, \\ \mathbf{k}_{\ell}, \mathbf{l}_{\ell}, \mathbf{o}_{\ell}, \\ \mathbf{t}_{\ell}, \mathbf{x}_{\ell}}} \overline{U}^{[\mathbf{t}_{\ell}]}(\ell)_{\mathbf{k}_{\ell-1}\mathbf{m}_{\ell}}^{\mathbf{k}_{\ell}\mathbf{o}_{\ell}} \overline{V}^{[\mathbf{x}_{\ell}]}(\ell)_{\mathbf{l}_{\ell-1}\mathbf{o}_{\ell}}^{\mathbf{l}_{\ell}\mathbf{n}_{\ell}} \langle\langle \mathbf{K}_{\ell-1} \parallel \mathbf{k}_{\ell-1}; \mathbf{l}_{\ell-1} \rangle\rangle \langle\langle \mathbf{k}_{\ell}; \mathbf{l}_{\ell} \parallel \mathbf{K}_{\ell} \rangle\rangle$$

$$\cdot \begin{bmatrix} \mathbf{n}_{\ell} & \mathbf{x}_{\ell} & \mathbf{o}_{\ell} \\ \mathbf{t}_{\ell} & \mathbf{m}_{\ell} & \mathbf{T}_{\ell} \end{bmatrix} \begin{bmatrix} \mathbf{k}_{\ell-1} & \mathbf{l}_{\ell-1} & \mathbf{K}_{\ell-1} \\ \mathbf{t}_{\ell} & \mathbf{x}_{\ell} & \mathbf{T}_{\ell} \\ \mathbf{k}_{\ell} & \mathbf{l}_{\ell} & \mathbf{K}_{\ell} \end{bmatrix}.$$

The sums over the indices $\mathbf{k}_{\ell-1}$, $\mathbf{l}_{\ell-1}$, \mathbf{k}_{ℓ} and \mathbf{l}_{ℓ} contribute only for a fixed value because $\langle\langle \mathbf{K}_{\ell-1} \parallel \mathbf{k}_{\ell-1}; \mathbf{l}_{\ell-1} \rangle\rangle$, $\langle\langle \mathbf{k}_{\ell}; \mathbf{l}_{\ell} \parallel \mathbf{K}_{\ell} \rangle\rangle \in \{0, 1\}$. Which summand contributes depends on the values of \mathbf{K}_{ℓ} and $\mathbf{K}_{\ell-1}$. All in all, the reduced MPO tensors of the product of two irreducible tensor operators can be calculated easily just from the reduced MPO tensors of the individual operators. The only thing one has to consider is an additional rescaled Wigner 6j-symbol and an additional rescaled Wigner 9j-symbol, which take care of the angular momentum coupling.

A.6 – Localized Magnons

For the antiferromagnetic Heisenberg model of L quantum spins $S = 1/2$,

$$\widehat{H}_J = \sum_{i,j} J_{ij} \widehat{\mathbf{S}}_i \widehat{\mathbf{S}}_j \quad \text{with } J_{ij} = \begin{cases} J > 0 & \text{if there is a bond between } i \text{ and } j, \\ 0 & \text{otherwise,} \end{cases} \quad (\text{A.19})$$

the fully polarized state $|\Psi_{\text{FM}}\rangle = |\uparrow, \dots, \uparrow\rangle$ is an eigenstate. In the presence of a homogenous magnetic field,

$$\widehat{H}_B = -B \sum_i \widehat{S}_i^{(z)}, \quad (\text{A.20})$$

this state even becomes the ground state for a sufficiently strong B , with energy $E_{\text{FM}} = \frac{J \cdot N_b}{4} - \frac{B \cdot L}{2}$, where N_b is the total number of bonds between two sites in the given geometry, and $\frac{L}{2} = M_{\text{max}}$ is the maximum value for the magnetization. In terms of notation, $\langle i, j \rangle$ marks that there is a spin-coupling bond between the sites i and j . If this is used as a condition on the range of a sum, double-countings have to be taken care of:

$$\widehat{H}_J = J \sum_{\langle i, j \rangle} \widehat{\mathbf{S}}_i \widehat{\mathbf{S}}_j = \frac{J}{2} \sum_{i, j} \widehat{\mathbf{S}}_i \widehat{\mathbf{S}}_j.$$

Under certain circumstances, a magnon (i. e., an excitation that reduces the magnetization by one) can be confined to a localized domain \mathcal{D} . A subset \mathcal{D} of $L_{\mathcal{D}}$ sites with the following conditions

- The domain is bipartite, i. e., the sites can be divided into two partitions in such a way that bonds inside the domain only connect sites from different partitions. This gives rise to the definition of a staggered prefactor ϵ_i , which is $+1$ for one part and -1 for the other. In particular, when two sites $i, j \in \mathcal{D}$ are connected, this yields $\epsilon_i \epsilon_j = -1$.
- Each site outside \mathcal{D} is connected to an equal number of sites inside \mathcal{D} of both partitions.
- Each site in \mathcal{D} has the same amount of bonds which cross the domain border and connect to sites outside \mathcal{D} (this number shall be called $n_{b, X}$).
- Each site in \mathcal{D} has the same amount of bonds inside the domain which do not cross the domain border (this number shall be called $n_{b, \mathcal{D}}$).

allows for the definition of this magnon excitation operator:

$$\widehat{M}_{\mathcal{D}} = \frac{1}{\sqrt{L_{\mathcal{D}}}} \sum_{i \in \mathcal{D}} \epsilon_i \widehat{S}_i^{(-)}. \quad (\text{A.21})$$

If this operator is applied onto the fully polarized state, one obtains a normalized state

$$\begin{aligned} \langle \Psi_{\text{FM}} | \widehat{M}_{\mathcal{D}}^\dagger \widehat{M}_{\mathcal{D}} | \Psi_{\text{FM}} \rangle &= \frac{1}{L_{\mathcal{D}}} \sum_{i, j \in \mathcal{D}} \epsilon_i \epsilon_j \langle \uparrow, \dots, \uparrow | 2\delta_{ij} \widehat{S}_i^{(z)} - \widehat{S}_j^{(-)} \widehat{S}_i^{(+)} | \uparrow, \dots, \uparrow \rangle \\ &= \frac{1}{L_{\mathcal{D}}} \sum_{i, j \in \mathcal{D}} \epsilon_i \epsilon_j (\delta_{ij} + 0) = \frac{1}{L_{\mathcal{D}}} \sum_{i \in \mathcal{D}} \epsilon_i^2 = 1, \end{aligned} \quad (\text{A.22})$$

with a reduced magnetization:

$$M = \langle \Psi_{\text{FM}} | \widehat{M}_{\mathcal{D}}^\dagger \sum_i \widehat{S}_i^{(z)} \widehat{M}_{\mathcal{D}} | \Psi_{\text{FM}} \rangle = M_{\text{max}} - 1. \quad (\text{A.23})$$

To investigate the action of this operator further, the commutator with the Hamilton operator is considered:

$$\begin{aligned}
\left[\widehat{H}_J, \widehat{M}_{\mathcal{D}} \right] &= \frac{J}{2\sqrt{L_{\mathcal{D}}}} \left(\frac{1}{2} \sum_{\substack{\langle i,j \rangle \\ i \notin \mathcal{D}, \\ j \notin \mathcal{D}}} + \sum_{\substack{\langle i,j \rangle \\ i \in \mathcal{D}, \\ j \notin \mathcal{D}}} + \frac{1}{2} \sum_{\substack{\langle i,j \rangle \\ i \in \mathcal{D}, \\ j \in \mathcal{D}}} \right) \sum_{k \in \mathcal{D}} \epsilon_k \left[\widehat{S}_i^{(+)} \widehat{S}_j^{(-)} + \widehat{S}_i^{(-)} \widehat{S}_j^{(+)} + 2\widehat{S}_i^{(z)} \widehat{S}_j^{(z)}, \widehat{S}_k^{(-)} \right] \\
&= 0 + \frac{J}{2\sqrt{L_{\mathcal{D}}}} \sum_{\substack{\langle i,j \rangle \\ i \in \mathcal{D}, \\ j \notin \mathcal{D}}} \left(2\epsilon_i \widehat{S}_i^{(z)} \widehat{S}_j^{(-)} + 0 - 2\epsilon_i \widehat{S}_i^{(-)} \widehat{S}_j^{(z)} \right) \\
&\quad + \frac{J}{4\sqrt{L_{\mathcal{D}}}} \sum_{\substack{\langle i,j \rangle \\ i \in \mathcal{D}, \\ j \in \mathcal{D}}} \left(2\epsilon_i \widehat{S}_i^{(z)} \widehat{S}_j^{(-)} + 0 + 2\epsilon_j \widehat{S}_i^{(-)} \widehat{S}_j^{(z)} + 0 - 2\epsilon_i \widehat{S}_i^{(-)} \widehat{S}_j^{(z)} - 2\epsilon_j \widehat{S}_i^{(z)} \widehat{S}_j^{(-)} \right) \\
&= \frac{J}{\sqrt{L_{\mathcal{D}}}} \sum_{\substack{\langle i,j \rangle \\ i \in \mathcal{D}, \\ j \notin \mathcal{D}}} \epsilon_i \left(\widehat{S}_i^{(z)} \widehat{S}_j^{(-)} - \widehat{S}_i^{(-)} \widehat{S}_j^{(z)} \right) + \frac{J}{\sqrt{L_{\mathcal{D}}}} \sum_{\substack{\langle i,j \rangle \\ i \in \mathcal{D}, \\ j \in \mathcal{D}}} \epsilon_i \left(\widehat{S}_i^{(z)} \widehat{S}_j^{(-)} - \widehat{S}_i^{(-)} \widehat{S}_j^{(z)} \right)
\end{aligned}$$

Acting with this on the fully polarized state yields:

$$\begin{aligned}
\left[\widehat{H}_J, \widehat{M}_{\mathcal{D}} \right] |\Psi_{\text{FM}}\rangle &= \frac{J}{2\sqrt{L_{\mathcal{D}}}} \left(\sum_{\substack{\langle i,j \rangle \\ i \in \mathcal{D}, \\ j \notin \mathcal{D}}} \epsilon_i \left(\widehat{S}_j^{(-)} - \widehat{S}_i^{(-)} \right) + \sum_{\substack{\langle i,j \rangle \\ i \in \mathcal{D}, \\ j \in \mathcal{D}}} \epsilon_i \left(\widehat{S}_j^{(-)} - \widehat{S}_i^{(-)} \right) \right) |\uparrow, \dots, \uparrow\rangle \\
&= \frac{J}{2\sqrt{L_{\mathcal{D}}}} \left(\sum_{j \notin \mathcal{D}} \widehat{S}_j^{(-)} \sum_{i \in \mathcal{D}} \epsilon_i - \sum_{i \in \mathcal{D}} \epsilon_i \widehat{S}_i^{(-)} \sum_{j \notin \mathcal{D}} 1 - 2 \sum_{i \in \mathcal{D}} \epsilon_i \widehat{S}_i^{(-)} \sum_{j \in \mathcal{D}} 1 \right) |\uparrow, \dots, \uparrow\rangle \\
&= \frac{J}{2} \left(0 - n_{b,X} \widehat{M}_{\mathcal{D}} - 2n_{b,\mathcal{D}} \widehat{M}_{\mathcal{D}} \right) |\uparrow, \dots, \uparrow\rangle = -\frac{J}{2} \cdot (n_{b,X} + 2n_{b,\mathcal{D}}) \widehat{M}_{\mathcal{D}} |\Psi_{\text{FM}}\rangle.
\end{aligned}$$

The summed ϵ_i values for all sites that are connected to a fixed site $j \notin \mathcal{D}$ have to vanish, since by assumption each such site has an equal number of connected sites within both partitions of the domain. The trivial sums over j in the latter two terms result in the number of crossing and non-crossing bonds. The commutator with the magnetic field part gives:

$$\left[\widehat{H}_B, \widehat{M}_{\mathcal{D}} \right] = -\frac{B}{\sqrt{L_{\mathcal{D}}}} \sum_i \sum_{j \in \mathcal{D}} \epsilon_j \left[\widehat{S}_i^{(z)}, \widehat{S}_j^{(-)} \right] = +\frac{B}{\sqrt{L_{\mathcal{D}}}} \sum_{i \in \mathcal{D}} \epsilon_i \widehat{S}_i^{(-)} = B \widehat{M}_{\mathcal{D}}.$$

From this follows that $\widehat{M}_{\mathcal{D}} |\Psi_{\text{FM}}\rangle$ again is an eigenstate of the Hamilton operator:

$$\begin{aligned}
\left(\widehat{H}_J + \widehat{H}_B \right) \widehat{M}_{\mathcal{D}} |\Psi_{\text{FM}}\rangle &= \widehat{M}_{\mathcal{D}} \left(\widehat{H}_J + \widehat{H}_B \right) |\Psi_{\text{FM}}\rangle + \left[\widehat{H}_J + \widehat{H}_B, \widehat{M}_{\mathcal{D}} \right] |\Psi_{\text{FM}}\rangle \\
&= (E_{\text{FM}} + \Delta E_{\text{magnon}}) \widehat{M}_{\mathcal{D}} |\Psi_{\text{FM}}\rangle,
\end{aligned}$$

$$\text{with } \Delta E_{\text{magnon}} = -\frac{J}{2} (n_{b,X} + 2n_{b,\mathcal{D}}) + B. \quad (\text{A.24})$$

This magnetization-decreasing excitation on top of the fully polarized state is strictly confined to the sites in the domain \mathcal{D} . Thus, if there is another domain \mathcal{D}' which has no overlap with \mathcal{D} and which fulfills the same conditions as above, another localized magnon not interfering with the previous one can be confined to that domain, yielding a state with a magnetization $M = M_{\text{max}} - 2$.

In the specific example of the sodalite cage geometry with $L = 60$ spins and $N_b = 144$ bonds, two types of faces meet the conditions to host localized magnons. The squares and hexagons and their surroundings are shown in Figure 48. Irrespective of whether the localized domain is a hexagon or a square, the bond numbers

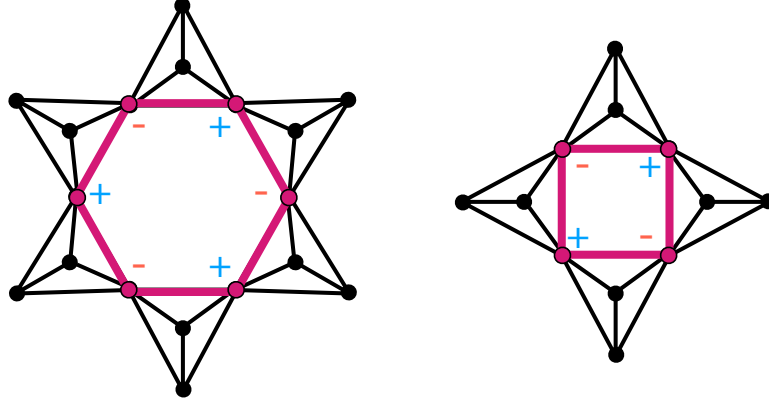


Figure 48: Visualization of the hexagon and square faces in the sodalite cage geometry together with their adjacent sites. The sites that make up the domain are equipped with a staggered sign factor. Figure taken from [CP2].

are $n_{b,X} = 4$ and $n_{b,D} = 2$, so that the energy of a magnon is $\Delta E_{\text{magnon}} = B - 4J$. Since in the sodalite cage geometry, the six squares have no overlapping sites, one can place up to six localized magnons $\widehat{M}_1, \dots, \widehat{M}_6$ on these square domains. The energy of a state with N_{magnon} magnonic excitations is then:

$$E(N_{\text{magnon}}) = E_{\text{FM}} + N_{\text{magnon}} \cdot \Delta E_{\text{magnon}} = 36J - 30B + (B - 4J)N_{\text{magnon}}. \quad (\text{A.25})$$

With $M = M_{\text{max}} - N_{\text{magnon}}$, Equation (A.25) gives an upper bound to the energetically lowest state for a given magnetization in the range of $M = M_{\text{max}}$ to $M = M_{\text{max}} - 6$:

$$E_0(M) \leq E_{\text{FM}} + (M_{\text{max}} - M) \cdot \Delta E_{\text{magnon}} = -84J + 4MJ - BM. \quad (\text{A.26})$$

A.7 – Calculations for Perturbation Theory in J around the BCS Groundstate

The action of local spin operators on the BCS groundstate can be evaluated as follows:

$$\begin{aligned}
\hat{s}_i^{(+)} |\Psi_0\rangle &= e^0 \sum_{n,n'} \left(v_{i\uparrow}^{(n,+)} \hat{b}_{n,+}^\dagger + v_{i\uparrow}^{(n,-)} \hat{b}_{n,-}^\dagger \right) \left(v_{i\downarrow}^{(n',+)} \hat{b}_{n',+}^\dagger + v_{i\downarrow}^{(n',-)} \hat{b}_{n',-}^\dagger \right) |\Psi_0\rangle \\
&= \sum_{n,n'} v_{i\uparrow}^{(n,+)} v_{i\downarrow}^{(n',+)} \hat{b}_{n,+}^\dagger \hat{b}_{n',+}^\dagger |\Psi_0\rangle \\
&= \sum_{n,n'} \frac{\sin(ik_n) \sin(ik_{n'})}{L+1} \sqrt{\left(1 - \frac{2t \cos(k_n)}{\varepsilon_n}\right) \left(1 + \frac{2t \cos(k_{n'})}{\varepsilon_{n'}}\right)} \hat{b}_{n,+}^\dagger \hat{b}_{n',+}^\dagger |\Psi_0\rangle, \\
\hat{s}_i^{(-)} |\Psi_0\rangle &= e^0 \sum_{n,n'} \left(v_{i\downarrow}^{(n,+)} \hat{b}_{n,+} + v_{i\downarrow}^{(n,-)} \hat{b}_{n,-} \right) \left(v_{i\uparrow}^{(n',+)} \hat{b}_{n',+} + v_{i\uparrow}^{(n',-)} \hat{b}_{n',-} \right) |\Psi_0\rangle \\
&= \sum_{n,n'} v_{i\downarrow}^{(n,-)} v_{i\uparrow}^{(n',-)} \hat{b}_{n,-} \hat{b}_{n',-} |\Psi_0\rangle \\
&= - \sum_{n,n'} \frac{\sin(ik_n) \sin(ik_{n'})}{L+1} \sqrt{\left(1 - \frac{2t \cos(k_n)}{\varepsilon_n}\right) \left(1 + \frac{2t \cos(k_{n'})}{\varepsilon_{n'}}\right)} \hat{b}_{n,-} \hat{b}_{n',-} |\Psi_0\rangle, \\
\hat{s}_i^{(z)} |\Psi_0\rangle &= \frac{e^0}{2} \sum_{n,n'} \left(\left(v_{i\uparrow}^{(n,+)} \hat{b}_{n,+}^\dagger + v_{i\uparrow}^{(n,-)} \hat{b}_{n,-}^\dagger \right) \left(v_{i\uparrow}^{(n',+)} \hat{b}_{n',+} + v_{i\uparrow}^{(n',-)} \hat{b}_{n',-} \right) \right. \\
&\quad \left. - \left(v_{i\downarrow}^{(n,+)} \hat{b}_{n,+} + v_{i\downarrow}^{(n,-)} \hat{b}_{n,-} \right) \left(v_{i\downarrow}^{(n',+)} \hat{b}_{n',+}^\dagger + v_{i\downarrow}^{(n',-)} \hat{b}_{n',-}^\dagger \right) \right) |\Psi_0\rangle \\
&= \frac{1}{2} \sum_{n,n'} \left(v_{i\uparrow}^{(n,+)} v_{i\uparrow}^{(n',-)} \hat{b}_{n,+}^\dagger \hat{b}_{n',-} + v_{i\uparrow}^{(n,-)} v_{i\uparrow}^{(n',-)} \delta_{nn'} - v_{i\downarrow}^{(n,-)} v_{i\downarrow}^{(n',+)} \hat{b}_{n,-} \hat{b}_{n',+}^\dagger - v_{i\downarrow}^{(n,+)} v_{i\downarrow}^{(n',+)} \delta_{nn'} \right) |\Psi_0\rangle \\
&= \frac{1}{2} \sum_{n,n'} \left(v_{i\uparrow}^{(n,+)} v_{i\uparrow}^{(n',-)} + v_{i\downarrow}^{(n',-)} v_{i\downarrow}^{(n,+)} \right) \hat{b}_{n,+}^\dagger \hat{b}_{n',-} |\Psi_0\rangle + \frac{1}{2} \sum_n \left(\left(v_{i\uparrow}^{(n,-)} \right)^2 - \left(v_{i\downarrow}^{(n,+)} \right)^2 \right) |\Psi_0\rangle \\
&= \sum_{n,n'} \frac{\sin(ik_n) \sin(ik_{n'})}{2(L+1)} \left(\sqrt{\left(1 - \frac{2t \cos(k_n)}{\varepsilon_n}\right) \left(1 + \frac{2t \cos(k_{n'})}{\varepsilon_{n'}}\right)} - \sqrt{\left(1 + \frac{2t \cos(k_n)}{\varepsilon_n}\right) \left(1 - \frac{2t \cos(k_{n'})}{\varepsilon_{n'}}\right)} \right) \\
&\quad \hat{b}_{n,+}^\dagger \hat{b}_{n',-} |\Psi_0\rangle + \sum_n \frac{\sin^2(ik_n)}{2(L+1)} \left(1 - \frac{2t \cos(k_n)}{\varepsilon_n} - 1 + \frac{2t \cos(k_n)}{\varepsilon_n} \right) |\Psi_0\rangle. \tag{A.27}
\end{aligned}$$

In particular, the groundstate expectation values are given by

$$\langle \Psi_0 | \hat{s}_i^{(+)} | \Psi_0 \rangle = \langle \Psi_0 | \hat{s}_i^{(-)} | \Psi_0 \rangle = \langle \Psi_0 | \hat{s}_i^{(z)} | \Psi_0 \rangle = 0. \tag{A.28}$$

The action of the total spin operators can be computed with the help of Equation (4.15):

$$\sum_{i=1}^L \hat{s}_i^{(+)} |\Psi_0\rangle = \frac{1}{2} \sum_n \sqrt{1 - \frac{4t^2 \cos^2(k_n)}{\varepsilon_n^2}} \hat{b}_{n,+}^\dagger \hat{b}_{n,+}^\dagger |\Psi_0\rangle = 0,$$

$$\sum_{i=1}^L \hat{s}_i^{(-)} |\Psi_0\rangle = -\frac{1}{2} \sum_n \sqrt{1 - \frac{4t^2 \cos^2(k_n)}{\varepsilon_n^2}} \hat{b}_{n,-} \hat{b}_{n,-} |\Psi_0\rangle = 0,$$

$$\sum_{i=1}^L \widehat{s}_i^{(z)} |\Psi_0\rangle = \frac{1}{4} \sum_n \left(\sqrt{1 - \frac{4t^2 \cos^2(k_n)}{\varepsilon_n^2}} - \sqrt{1 - \frac{4t^2 \cos^2(k_n)}{\varepsilon_n^2}} \right) \widehat{b}_{n,+}^\dagger \widehat{b}_{n,-} |\Psi_0\rangle = 0. \quad (\text{A.29})$$

Thus, the BCS groundstate is a spin singlet.

Concerning the charge-pseudospin, analogous calculations can be performed:

$$\begin{aligned} \widehat{\eta}_i^{(+)} |\Psi_0\rangle &= \epsilon_i e^{i\varphi} \sum_{n,n'} \left(v_{i\uparrow}^{(n,+)} \widehat{b}_{n,+}^\dagger + v_{i\uparrow}^{(n,-)} \widehat{b}_{n,-}^\dagger \right) \left(v_{i\downarrow}^{(n',+)} \widehat{b}_{n',+} + v_{i\downarrow}^{(n',-)} \widehat{b}_{n',-} \right) |\Psi_0\rangle \\ &= \epsilon_i e^{i\varphi} \sum_{n,n'} v_{i\uparrow}^{(n,+)} v_{i\downarrow}^{(n',-)} \widehat{b}_{n,+}^\dagger \widehat{b}_{n',-} |\Psi_0\rangle + \epsilon_i e^{i\varphi} \sum_n v_{i\uparrow}^{(n,-)} v_{i\downarrow}^{(n,-)} |\Psi_0\rangle \\ &= -\epsilon_i e^{i\varphi} \sum_{n,n'} \frac{\sin(ik_n) \sin(ik_{n'})}{L+1} \sqrt{\left(1 - \frac{2t \cos(k_n)}{\varepsilon_n}\right) \left(1 - \frac{2t \cos(k_{n'})}{\varepsilon_{n'}}\right)} \widehat{b}_{n,+}^\dagger \widehat{b}_{n',-} |\Psi_0\rangle \\ &\quad - \epsilon_i e^{i\varphi} \sum_n \frac{\sin^2(ik_n)}{L+1} \sqrt{1 - \frac{4t^2 \cos^2(k_n)}{\varepsilon_n^2}} |\Psi_0\rangle, \\ \widehat{\eta}_i^{(-)} |\Psi_0\rangle &= \epsilon_i e^{-i\varphi} \sum_{n,n'} \left(v_{i\downarrow}^{(n,+)} \widehat{b}_{n,+}^\dagger + v_{i\downarrow}^{(n,-)} \widehat{b}_{n,-}^\dagger \right) \left(v_{i\uparrow}^{(n',+)} \widehat{b}_{n',+} + v_{i\uparrow}^{(n',-)} \widehat{b}_{n',-} \right) |\Psi_0\rangle \\ &= \epsilon_i e^{-i\varphi} \sum_{n,n'} v_{i\downarrow}^{(n,+)} v_{i\uparrow}^{(n',-)} \widehat{b}_{n,+}^\dagger \widehat{b}_{n',-} |\Psi_0\rangle + \epsilon_i e^{-i\varphi} \sum_n v_{i\downarrow}^{(n,-)} v_{i\uparrow}^{(n,-)} |\Psi_0\rangle \\ &= \epsilon_i e^{-i\varphi} \sum_{n,n'} \frac{\sin(ik_n) \sin(ik_{n'})}{L+1} \sqrt{\left(1 + \frac{2t \cos(k_n)}{\varepsilon_n}\right) \left(1 + \frac{2t \cos(k_{n'})}{\varepsilon_{n'}}\right)} \widehat{b}_{n,+}^\dagger \widehat{b}_{n',-} |\Psi_0\rangle \\ &\quad - \epsilon_i e^{-i\varphi} \sum_n \frac{\sin^2(ik_n)}{L+1} \sqrt{1 - \frac{4t^2 \cos^2(k_n)}{\varepsilon_n^2}} |\Psi_0\rangle, \\ \widehat{\eta}_i^{(z)} |\Psi_0\rangle &= \frac{e^0}{2} \sum_{n,n'} \left(\left(v_{i\uparrow}^{(n,+)} \widehat{b}_{n,+}^\dagger + v_{i\uparrow}^{(n,-)} \widehat{b}_{n,-}^\dagger \right) \left(v_{i\uparrow}^{(n',+)} \widehat{b}_{n',+} + v_{i\uparrow}^{(n',-)} \widehat{b}_{n',-} \right) \right. \\ &\quad \left. - \left(v_{i\downarrow}^{(n,+)} \widehat{b}_{n,+}^\dagger + v_{i\downarrow}^{(n,-)} \widehat{b}_{n,-}^\dagger \right) \left(v_{i\downarrow}^{(n',+)} \widehat{b}_{n',+} + v_{i\downarrow}^{(n',-)} \widehat{b}_{n',-} \right) \right) |\Psi_0\rangle \\ &= \frac{1}{2} \sum_{n,n'} \left(v_{i\uparrow}^{(n,+)} v_{i\uparrow}^{(n',-)} \widehat{b}_{n,+}^\dagger \widehat{b}_{n',-} + v_{i\uparrow}^{(n,-)} v_{i\uparrow}^{(n',-)} \delta_{nn'} - v_{i\downarrow}^{(n,+)} v_{i\downarrow}^{(n',-)} \widehat{b}_{n,+}^\dagger \widehat{b}_{n',-} - v_{i\downarrow}^{(n,-)} v_{i\downarrow}^{(n',-)} \delta_{nn'} \right) |\Psi_0\rangle \\ &= \frac{1}{2} \sum_{n,n'} \left(v_{i\uparrow}^{(n,+)} v_{i\uparrow}^{(n',-)} - v_{i\downarrow}^{(n,-)} v_{i\downarrow}^{(n',+)} \right) \widehat{b}_{n,+}^\dagger \widehat{b}_{n',-} |\Psi_0\rangle + \frac{1}{2} \sum_n \left(\left(v_{i\uparrow}^{(n,-)} \right)^2 - \left(v_{i\downarrow}^{(n,+)} \right)^2 \right) |\Psi_0\rangle \\ &= \sum_{n,n'} \frac{\sin(ik_n) \sin(ik_{n'})}{2(L+1)} \left(\sqrt{\left(1 - \frac{2t \cos(k_n)}{\varepsilon_n}\right) \left(1 + \frac{2t \cos(k_{n'})}{\varepsilon_{n'}}\right)} - \sqrt{\left(1 + \frac{2t \cos(k_n)}{\varepsilon_n}\right) \left(1 - \frac{2t \cos(k_{n'})}{\varepsilon_{n'}}\right)} \right) \\ &\quad \widehat{b}_{n,+}^\dagger \widehat{b}_{n',-} |\Psi_0\rangle + \sum_n \frac{\sin^2(ik_n)}{2(L+1)} \left(1 + \frac{2t \cos^2(k_n)}{\varepsilon_n^2} - 1 + \frac{2t \cos^2(k_n)}{\varepsilon_n^2} \right) |\Psi_0\rangle. \quad (\text{A.30}) \end{aligned}$$

Again with the help of Equation (4.15), here in the form

$$\begin{aligned} \sum_{i=1}^L \epsilon_i \sin(ik_n) \sin(ik_{n'}) &= -\epsilon_1 \sum_{i=1}^L (-1)^i \sin(ik_n) \sin(ik_{n'}) = -\epsilon_1 \sum_{i=1}^L (\sin(i\pi) \cos(ik_n) + \cos(i\pi) \sin(ik_n)) \sin(ik_{n'}) \\ &= -\epsilon_1 \sum_{i=1}^L \sin(ik_{L+1+n}) \sin(ik_{n'}) = \frac{\epsilon_1(L+1)}{2} \cdot \delta_{n+n',L+1}, \quad (\text{A.31}) \end{aligned}$$

the action of the total pseudospin operators can be calculated using $\cos(k_{L+1-n}) = -\cos(k_n)$ and $\varepsilon_{L+1-n} = \varepsilon_n$:

$$\begin{aligned}
\sum_{i=1}^L \widehat{\eta}_i^{(+)} |\Psi_0\rangle &= -\frac{\epsilon_1 e^{i\varphi}}{2} \sum_n \sqrt{1 - \frac{4t^2 \cos^2(k_n)}{\varepsilon_n^2}} \widehat{b}_{n,+}^\dagger \widehat{b}_{L+1-n,-} |\Psi_0\rangle - \frac{\epsilon_1 e^{i\varphi}}{2} \sum_n \delta_{n, \frac{L+1}{2}} \sqrt{1 - \frac{4t^2 \cos^2(k_n)}{\varepsilon_n^2}} |\Psi_0\rangle \\
&= -\frac{\epsilon_1 e^{i\varphi}}{2} \sum_n \frac{|\Delta|}{\varepsilon_n} \widehat{b}_{n,+}^\dagger \widehat{b}_{L+1-n,-} |\Psi_0\rangle - \frac{\epsilon_1 e^{i\varphi}}{4} (1 - (-1)^L) |\Psi_0\rangle, \\
\sum_{i=1}^L \widehat{\eta}_i^{(-)} |\Psi_0\rangle &= \frac{\epsilon_1 e^{-i\varphi}}{2} \sum_n \sqrt{1 - \frac{4t^2 \cos^2(k_n)}{\varepsilon_n^2}} \widehat{b}_{n,+}^\dagger \widehat{b}_{L+1-n,-} |\Psi_0\rangle - \frac{\epsilon_1 e^{-i\varphi}}{2} \sum_n \delta_{n, \frac{L+1}{2}} \sqrt{1 - \frac{4t^2 \cos^2(k_n)}{\varepsilon_n^2}} |\Psi_0\rangle \\
&= \frac{\epsilon_1 e^{-i\varphi}}{2} \sum_n \frac{|\Delta|}{\varepsilon_n} \widehat{b}_{n,+}^\dagger \widehat{b}_{L+1-n,-} |\Psi_0\rangle - \frac{\epsilon_1 e^{-i\varphi}}{4} (1 - (-1)^L) |\Psi_0\rangle, \\
\Rightarrow \sum_{i=1}^L \frac{e^{-i\varphi} \widehat{\eta}_i^{(+)} + e^{i\varphi} \widehat{\eta}_i^{(-)}}{2} |\Psi_0\rangle &= \frac{-\epsilon_1 (1 - (-1)^L)}{4} |\Psi_0\rangle. \tag{A.32}
\end{aligned}$$

In particular, for $\Delta \in \mathbb{R}$ and $\epsilon_1 = +1$, the BCS groundstate is an eigenstate of the operator $\widehat{\eta}_{\text{tot}}^{(x)}$, and the pseudospin charge is given by the eigenvalue $Q_\eta = -1/2 \cdot \epsilon_1$ for odd system sizes L and $Q_\eta = 0$ for even system sizes.

A.8 – Diagonalization of the 3-Site Toy Model

The Hamilton operator of an open chain of $L = 3$ lattice sites with BCS superconductivity and two quantum spin-1/2 impurities attached to the sites $i_1 = 1$ and $i_2 = 3$ reads:

$$\begin{aligned} \widehat{H} = & -t \left(\widehat{c}_{1\uparrow}^\dagger \widehat{c}_{2\uparrow} + \widehat{c}_{2\uparrow}^\dagger \widehat{c}_{1\uparrow} + \widehat{c}_{2\uparrow}^\dagger \widehat{c}_{3\uparrow} + \widehat{c}_{3\uparrow}^\dagger \widehat{c}_{2\uparrow} + \widehat{c}_{1\downarrow}^\dagger \widehat{c}_{2\downarrow} + \widehat{c}_{2\downarrow}^\dagger \widehat{c}_{1\downarrow} + \widehat{c}_{2\downarrow}^\dagger \widehat{c}_{3\downarrow} + \widehat{c}_{3\downarrow}^\dagger \widehat{c}_{2\downarrow} \right) \\ & + \left(\Delta_1 \widehat{c}_{1\uparrow}^\dagger \widehat{c}_{1\downarrow} + \Delta_1 \widehat{c}_{1\downarrow} \widehat{c}_{1\uparrow} + \Delta_2 \widehat{c}_{2\uparrow}^\dagger \widehat{c}_{2\downarrow} + \Delta_2 \widehat{c}_{2\downarrow} \widehat{c}_{2\uparrow} + \Delta_3 \widehat{c}_{3\uparrow}^\dagger \widehat{c}_{3\downarrow} + \Delta_3 \widehat{c}_{3\downarrow} \widehat{c}_{3\uparrow} \right) \\ & + \frac{J}{2} \left(\widehat{S}_1^{(+)} \widehat{c}_{1\downarrow}^\dagger \widehat{c}_{1\uparrow} + \widehat{S}_1^{(-)} \widehat{c}_{1\uparrow}^\dagger \widehat{c}_{1\downarrow} + \widehat{S}_1^{(z)} \left(\widehat{c}_{1\uparrow}^\dagger \widehat{c}_{1\uparrow} - \widehat{c}_{1\downarrow}^\dagger \widehat{c}_{1\downarrow} \right) \right. \\ & \left. + \widehat{S}_2^{(+)} \widehat{c}_{3\downarrow}^\dagger \widehat{c}_{3\uparrow} + \widehat{S}_2^{(-)} \widehat{c}_{3\uparrow}^\dagger \widehat{c}_{3\downarrow} + \widehat{S}_2^{(z)} \left(\widehat{c}_{3\uparrow}^\dagger \widehat{c}_{3\uparrow} - \widehat{c}_{3\downarrow}^\dagger \widehat{c}_{3\downarrow} \right) \right). \end{aligned} \quad (\text{A.33})$$

Here, the pairing strength is not necessarily taken uniform for the three sites, but it is assumed that their phase relation is the same (and then, without loss of generality, the pairing strengths are chosen real), so that the external pseudospin field is aligned in the x direction.

The total Hilbert space is of dimension $\dim(\mathcal{H}) = 4^3 \cdot 2^2 = 256$. Due to the presence of $\text{SU}(2)_{\text{spin}}$ and $\text{U}(1)_{\text{charge}}$, the Hilbert space can be decomposed into subspaces which are invariant under the action of the Hamilton operator:

$$\begin{aligned} \mathcal{H} = & \underbrace{\mathcal{H}(S_{\text{tot}} = 0, Q_\eta = -3/2)}_{\# 1 \cdot 1} \oplus \underbrace{\mathcal{H}(S_{\text{tot}} = 0, Q_\eta = -1/2)}_{\# 1 \cdot 9} \oplus \underbrace{\mathcal{H}(S_{\text{tot}} = 0, Q_\eta = +1/2)}_{\# 1 \cdot 9} \oplus \underbrace{\mathcal{H}(S_{\text{tot}} = 0, Q_\eta = +3/2)}_{\# 1 \cdot 1} \\ & \oplus \underbrace{\mathcal{H}(S_{\text{tot}} = 1/2, Q_\eta = -1)}_{\# 2 \cdot 6} \oplus \underbrace{\mathcal{H}(S_{\text{tot}} = 1/2, Q_\eta = 0)}_{\# 2 \cdot 17} \oplus \underbrace{\mathcal{H}(S_{\text{tot}} = 1/2, Q_\eta = +1)}_{\# 2 \cdot 6} \\ & \oplus \underbrace{\mathcal{H}(S_{\text{tot}} = 1, Q_\eta = -3/2)}_{\# 3 \cdot 1} \oplus \underbrace{\mathcal{H}(S_{\text{tot}} = 1, Q_\eta = -1/2)}_{\# 3 \cdot 12} \oplus \underbrace{\mathcal{H}(S_{\text{tot}} = 1, Q_\eta = +1/2)}_{\# 3 \cdot 12} \oplus \underbrace{\mathcal{H}(S_{\text{tot}} = 1, Q_\eta = +3/2)}_{\# 3 \cdot 1} \\ & \oplus \underbrace{\mathcal{H}(S_{\text{tot}} = 3/2, Q_\eta = -1)}_{\# 4 \cdot 3} \oplus \underbrace{\mathcal{H}(S_{\text{tot}} = 3/2, Q_\eta = 0)}_{\# 4 \cdot 10} \oplus \underbrace{\mathcal{H}(S_{\text{tot}} = 3/2, Q_\eta = +1)}_{\# 4 \cdot 3} \\ & \oplus \underbrace{\mathcal{H}(S_{\text{tot}} = 2, Q_\eta = -1/2)}_{\# 5 \cdot 3} \oplus \underbrace{\mathcal{H}(S_{\text{tot}} = 2, Q_\eta = +1/2)}_{\# 5 \cdot 3} \oplus \underbrace{\mathcal{H}(S_{\text{tot}} = 5/2, Q_\eta = 0)}_{\# 6 \cdot 1}. \end{aligned} \quad (\text{A.34})$$

Finding orthonormal basis states for these subspaces is straightforward, but not very insightful. Therefore, it is not reproduced here. However, some general remarks can be concluded. If $\mathbf{H}(S_{\text{tot}}, Q_\eta)$ is the matrix representation of the Hamilton operator in a given subspace with an orthonormal basis $|\psi_n\rangle$, i. e., $H(S_{\text{tot}}, Q_\eta)_{nm} = \langle \psi_n | \widehat{H} | \psi_m \rangle$, then a rotation by π around the z axis brings the basis states with pseudocharge Q_η into orthonormal states with $-Q_\eta$ which span $\mathcal{H}(S_{\text{tot}}, -Q_\eta)$:

$$\begin{aligned} \widehat{\eta}_{\text{tot}}^{(x)} \exp\left(i\pi \widehat{\eta}_{\text{tot}}^{(z)}\right) |\psi_n\rangle &= \exp\left(i\pi \widehat{\eta}_{\text{tot}}^{(z)}\right) \exp\left(-i\pi \widehat{\eta}_{\text{tot}}^{(z)}\right) \widehat{\eta}_{\text{tot}}^{(x)} \exp\left(i\pi \widehat{\eta}_{\text{tot}}^{(z)}\right) |\psi_n\rangle \\ &= \exp\left(i\pi \widehat{\eta}_{\text{tot}}^{(z)}\right) \left(-\widehat{\eta}_{\text{tot}}^{(x)}\right) |\psi_n\rangle = -Q_\eta \exp\left(i\pi \widehat{\eta}_{\text{tot}}^{(z)}\right) |\psi_n\rangle. \end{aligned} \quad (\text{A.35})$$

With this choice of basis states one finds:

$$H(S_{\text{tot}}, -Q_\eta)_{nm} = \langle \psi_n | \exp\left(-i\pi \widehat{\eta}_{\text{tot}}^{(z)}\right) \widehat{H} \exp\left(i\pi \widehat{\eta}_{\text{tot}}^{(z)}\right) |\psi_m\rangle = \langle \psi_n | \widehat{H}' | \psi_m \rangle, \quad (\text{A.36})$$

where \widehat{H}' is the Hamilton operator with inverted pairing strengths $\Delta_i \rightarrow -\Delta_i$. Therefore, the matrix representation on the subspace $\mathcal{H}(S_{\text{tot}}, -Q_\eta)$ can be obtained from $\mathbf{H}(S_{\text{tot}}, Q_\eta)$ by simply replacing the pairing strengths with their negatives.

The numerical diagonalization of the Hamilton matrices yields the lowest eigenvalues in the three subspaces $\mathcal{H}(S_{\text{tot}} = 0, Q_\eta = +1/2)$, $\mathcal{H}(S_{\text{tot}} = 0, Q_\eta = -1/2)$ or $\mathcal{H}(S_{\text{tot}} = 1/2, Q_\eta = 0)$. For completeness, the corresponding Hamilton matrices are stated here:

$$\mathbf{H}(S_{\text{tot}} = 0, Q_\eta = \pm 1/2) =$$

$$\begin{pmatrix} \mp \Delta_1 & -t & 0 & \sqrt{2}t & & -\sqrt{2}t & 0 & -\frac{\sqrt{3}J}{4} & 0 & 0 \\ -t & \pm \Delta_2 & -t & 0 & & 0 & 0 & 0 & -\frac{\sqrt{3}J}{2} & 0 \\ 0 & -t & \mp \Delta_3 & \sqrt{2}t & & 0 & -\sqrt{2}t & 0 & 0 & -\frac{\sqrt{3}J}{4} \\ \sqrt{2}t & 0 & \sqrt{2}t & \mp \Delta_1 \mp \Delta_2 \mp \Delta_3 & & 0 & 0 & 0 & 0 & 0 \\ -\sqrt{2}t & 0 & 0 & 0 & & \mp \Delta_1 \pm \Delta_2 \pm \Delta_3 & 0 & 0 & 0 & 0 \\ 0 & 0 & -\sqrt{2}t & 0 & & 0 & \pm \Delta_1 \pm \Delta_2 \mp \Delta_3 & 0 & 0 & 0 \\ -\frac{\sqrt{3}J}{4} & 0 & 0 & 0 & & 0 & 0 & \mp \Delta_1 - \frac{J}{2} & -t & 0 \\ 0 & -\frac{\sqrt{3}J}{2} & 0 & 0 & & 0 & 0 & -t & \pm \Delta_2 - J & -t \\ 0 & 0 & -\frac{\sqrt{3}J}{4} & 0 & & 0 & 0 & 0 & -t & \mp \Delta_3 - \frac{J}{2} \end{pmatrix},$$

$$\mathbf{H}(S_{\text{tot}} = 1/2, Q_\eta = 0) =$$

$$\begin{pmatrix} \Delta_1 + \Delta_2 & 0 & -t & 0 & 0 & 0 & -\frac{t}{\sqrt{2}} & \sqrt{\frac{3}{2}}t & -\frac{\sqrt{3}J}{4} & \dots \\ 0 & -\Delta_1 - \Delta_2 & 0 & -t & 0 & 0 & \frac{t}{\sqrt{2}} & -\sqrt{\frac{3}{2}}t & 0 & \dots \\ -t & 0 & \Delta_1 - \Delta_3 & 0 & -t & 0 & 0 & 0 & 0 & \dots \\ 0 & -t & 0 & -\Delta_1 + \Delta_3 & 0 & -t & 0 & 0 & 0 & \dots \\ 0 & 0 & -t & 0 & -\Delta_2 - \Delta_3 & 0 & \frac{t}{\sqrt{2}} & \sqrt{\frac{3}{2}}t & 0 & \dots \\ 0 & 0 & 0 & -t & 0 & \Delta_2 + \Delta_3 & -\frac{t}{\sqrt{2}} & -\sqrt{\frac{3}{2}}t & 0 & \dots \\ -\frac{t}{\sqrt{2}} & \frac{t}{\sqrt{2}} & 0 & 0 & \frac{t}{\sqrt{2}} & -\frac{t}{\sqrt{2}} & 0 & 0 & 0 & \dots \\ \sqrt{\frac{3}{2}}t & -\sqrt{\frac{3}{2}}t & 0 & 0 & \sqrt{\frac{3}{2}}t & -\sqrt{\frac{3}{2}}t & 0 & 0 & 0 & \dots \\ -\frac{\sqrt{3}J}{4} & 0 & 0 & 0 & 0 & 0 & 0 & 0 & \Delta_1 + \Delta_2 - \frac{J}{2} & \dots \\ 0 & -\frac{\sqrt{3}J}{4} & 0 & 0 & 0 & 0 & 0 & 0 & 0 & \dots \\ 0 & 0 & 0 & 0 & 0 & 0 & 0 & 0 & -t & \dots \\ 0 & 0 & 0 & 0 & 0 & 0 & 0 & 0 & 0 & \dots \\ 0 & 0 & 0 & 0 & \frac{\sqrt{3}J}{4} & 0 & 0 & 0 & 0 & \dots \\ 0 & 0 & 0 & 0 & 0 & \frac{\sqrt{3}J}{4} & 0 & 0 & 0 & \dots \\ 0 & 0 & 0 & 0 & 0 & 0 & 0 & \frac{J}{2} & -\frac{t}{\sqrt{2}} & \dots \\ 0 & 0 & 0 & 0 & 0 & 0 & \frac{J}{2} & 0 & \sqrt{\frac{3}{2}}t & \dots \\ 0 & 0 & 0 & 0 & 0 & 0 & -\frac{J}{\sqrt{2}} & 0 & 0 & \dots \end{pmatrix}$$

$$\begin{pmatrix}
 \cdots & 0 & 0 & 0 & 0 & 0 & 0 & 0 & 0 \\
 \cdots & -\frac{\sqrt{3}J}{4} & 0 & 0 & 0 & 0 & 0 & 0 & 0 \\
 \cdots & 0 & 0 & 0 & 0 & 0 & 0 & 0 & 0 \\
 \cdots & 0 & 0 & 0 & 0 & 0 & 0 & 0 & 0 \\
 \cdots & 0 & 0 & 0 & \frac{\sqrt{3}J}{4} & 0 & 0 & 0 & 0 \\
 \cdots & 0 & 0 & 0 & 0 & \frac{\sqrt{3}J}{4} & 0 & 0 & 0 \\
 \cdots & 0 & 0 & 0 & 0 & 0 & 0 & \frac{J}{2} & -\frac{J}{\sqrt{2}} \\
 \cdots & 0 & 0 & 0 & 0 & 0 & \frac{J}{2} & 0 & 0 \\
 \cdots & 0 & -t & 0 & 0 & 0 & -\frac{t}{\sqrt{2}} & \sqrt{\frac{3}{2}}t & 0 \\
 \cdots & -\Delta_1 - \Delta_2 - \frac{J}{2} & 0 & -t & 0 & 0 & \frac{t}{\sqrt{2}} & -\sqrt{\frac{3}{2}}t & 0 \\
 \cdots & 0 & \Delta_1 - \Delta_3 & 0 & -t & 0 & 0 & 0 & 0 \\
 \cdots & -t & 0 & -\Delta_1 + \Delta_3 & 0 & -t & 0 & 0 & 0 \\
 \cdots & 0 & -t & 0 & -\Delta_2 - \Delta_3 - \frac{J}{2} & 0 & \frac{t}{\sqrt{2}} & \sqrt{\frac{3}{2}}t & 0 \\
 \cdots & 0 & 0 & -t & 0 & \Delta_2 + \Delta_3 - \frac{J}{2} & -\frac{t}{\sqrt{2}} & -\sqrt{\frac{3}{2}}t & 0 \\
 \cdots & \frac{t}{\sqrt{2}} & 0 & 0 & \frac{t}{\sqrt{2}} & -\frac{t}{\sqrt{2}} & 0 & 0 & 0 \\
 \cdots & -\sqrt{\frac{3}{2}}t & 0 & 0 & \sqrt{\frac{3}{2}}t & -\sqrt{\frac{3}{2}}t & 0 & -\frac{2J}{3} & \frac{J}{3\sqrt{2}} \\
 \cdots & 0 & 0 & 0 & 0 & 0 & 0 & \frac{J}{3\sqrt{2}} & -\frac{5J}{6}
 \end{pmatrix} \otimes \mathbf{1}_2. \tag{A.37}$$

In the case of a translationally invariant $\Delta_1 = \Delta_2 = \Delta_3 := \Delta$, the relevant subspaces can be decomposed even further by using the spatial parity. In this case, one finds that in $\mathcal{H}(S_{\text{tot}} = 0, Q_\eta = +1/2)$ and $\mathcal{H}(S_{\text{tot}} = 0, Q_\eta = -1/2)$, the groundstate has negative parity, and in $\mathcal{H}(S_{\text{tot}} = 1/2, Q_\eta = 0)$, the groundstate has positive parity. Therefore, the relevant Hamilton matrices are given by

$$\begin{aligned}
 \mathbf{H}(S_{\text{tot}} = 0, Q_\eta = \pm 1/2, P = -) &= \begin{pmatrix}
 \mp\Delta & -\sqrt{2}t & -\frac{\sqrt{3}J}{4} & -\sqrt{2}t & 2t & 0 \\
 -\sqrt{2}t & \pm\Delta & 0 & 0 & 0 & 0 \\
 -\frac{\sqrt{3}J}{4} & 0 & \mp\Delta - \frac{J}{2} & 0 & 0 & -\sqrt{2}t \\
 -\sqrt{2}t & 0 & 0 & \pm\Delta & 0 & -\frac{\sqrt{3}J}{2} \\
 2t & 0 & 0 & 0 & \mp 3\Delta & 0 \\
 0 & 0 & -\sqrt{2}t & -\frac{\sqrt{3}J}{2} & 0 & \pm\Delta - J
 \end{pmatrix}, \\
 \mathbf{H}(S_{\text{tot}} = 1/2, Q_\eta = 0, P = +) &= \begin{pmatrix}
 2\Delta & 0 & -t & \sqrt{3}t & -\frac{\sqrt{3}J}{4} & 0 & 0 & 0 \\
 0 & -2\Delta & t & -\sqrt{3}t & 0 & -\frac{\sqrt{3}J}{4} & 0 & 0 \\
 -t & t & 0 & 0 & 0 & 0 & 0 & 0 \\
 \sqrt{3}t & -\sqrt{3}t & 0 & 0 & 0 & 0 & 0 & \frac{J}{2} \\
 -\frac{\sqrt{3}J}{4} & 0 & 0 & 0 & 2\Delta - \frac{J}{2} & 0 & -t & -t \\
 0 & -\frac{\sqrt{3}J}{4} & 0 & 0 & 0 & -2\Delta - \frac{J}{2} & -t & t \\
 0 & 0 & 0 & 0 & -t & -t & 0 & 0 \\
 0 & 0 & 0 & \frac{J}{2} & -t & t & 0 & 0
 \end{pmatrix} \otimes \mathbf{1}_2. \tag{A.38}
 \end{aligned}$$

Bibliography

- [1] P. W. Anderson, “More is different”, *Science*, vol. **177**, no. 4047, 393–396, Aug 1972.
- [2] R. L. Greene, P. R. Mandal, N. R. Poniatowski, and T. Sarkar, “The strange metal state of the electron-doped cuprates”, *Annual Review of Condensed Matter Physics*, vol. **11**, 213–229, Mar 2020.
- [3] S. F. Edwards and P. W. Anderson, “Theory of spin glasses”, *Journal of Physics F: Metal Physics*, vol. **5**, no. 5, 965–974, May 1975.
- [4] N. F. Mott, “Metal-insulator transition”, *Reviews of Modern Physics*, vol. **40**, 677–683, Oct 1968.
- [5] Y. Takabayashi and K. Prassides, “Unconventional high- T_c superconductivity in fullerides”, *Philosophical Transactions of the Royal Society A*, vol. **374**, 20150320, Sep 2016.
- [6] M. Capone, M. Fabrizio, C. Castellani, and E. Tosatti, “Colloquium: Modeling the unconventional superconducting properties of expanded A_3C_{60} fullerides”, *Reviews of Modern Physics*, vol. **81**, 943–958, Jun 2009.
- [7] M. Kim, Y. Nomura, M. Ferrero, P. Seth, O. Parcollet, and A. Georges, “Enhancing superconductivity in A_3C_{60} fullerides”, *Physical Review B*, vol. **94**, 155152, Oct 2016.
- [8] M. Mitrano, A. Cantaluppi, D. Nicoletti, S. Kaiser, A. Perucchi, S. Lupi, P. Di Pietro, D. Pontiroli, M. Riccò, S. R. Clark, D. Jaksch, and A. Cavalleri, “Possible light-induced superconductivity in K_3C_{60} at high temperature”, *Nature*, vol. **530**, no. 7591, 461–464, Feb 2016.
- [9] M. Budden, T. Gebert, M. Buzzi, G. Jotzu, E. Wang, T. Matsuyama, G. Meier, Y. Laplace, D. Pontiroli, M. Riccò, F. Schlawin, D. Jaksch, and A. Cavalleri, “Evidence for metastable photo-induced superconductivity in K_3C_{60} ”, *Nature Physics*, vol. **17**, 611–618, May 2021.
- [10] D. Fausti, R. I. Tobey, N. Dean, S. Kaiser, A. Dienst, M. C. Hoffmann, S. Pyon, T. Takayama, H. Takagi, and A. Cavalleri, “Light-induced superconductivity in a stripe-ordered cuprate”, *Science*, vol. **331**, 189–191, Jan 2011.
- [11] N. Bohr, “Studier over metallernes elektrontheori”, in *Early Work (1905–1911), II. The Doctor’s Dissertation (Text and Translation)*, L. Rosenfeld and J. R. Nielsen, Eds., vol. **1** of *Niels Bohr Collected Works*, 163–393. Elsevier, 1972.
- [12] H. J. Van Leeuwen, “Problèmes de la théorie électronique du magnétisme”, *Journal de Physique et Le Radium*, vol. **2**, no. 12, 361–377, Dec 1921.
- [13] W. Nolting and A. Ramakanth, *Quantum Theory of Magnetism*, Springer Berlin, Heidelberg, 2009.
- [14] J. Hubbard, “Electron correlations in narrow energy bands”, *Proceedings of the Royal Society*, vol. **276**, 238–257, Nov 1963.
- [15] W. Heisenberg, “Zur Theorie des Ferromagnetismus”, *Zeitschrift für Physik*, vol. **49**, 619–636, Sep 1928.
- [16] P. W. Anderson, “Localized magnetic states in metals”, *Physical Review*, vol. **124**, 41–53, Oct 1961.
- [17] J. R. Schrieffer and P. A. Wolff, “Relation between the Anderson and Kondo Hamiltonians”, *Physical Review*, vol. **149**, 491–492, 1966.

- [18] J. Kondo, “Resistance minimum in dilute magnetic alloys”, *Progress of Theoretical Physics*, vol. **32**, no. 1, 37–49, Jul 1964.
- [19] M. A. Ruderman and C. Kittel, “Indirect exchange coupling of nuclear magnetic moments by conduction electrons”, *Physical Review*, vol. **96**, 99–102, Oct 1954.
- [20] T. Kasuya, “A theory of metallic ferro- and antiferromagnetism on Zener’s model”, *Progress of Theoretical Physics*, vol. **16**, no. 1, 45–57, Jul 1956.
- [21] K. Yosida, “Magnetic properties of Cu-Mn alloys”, *Physical Review*, vol. **106**, 893–898, Jun 1957.
- [22] N. Bloembergen and T. J. Rowland, “Nuclear spin exchange in solids: Tl²⁰³ and Tl²⁰⁵ magnetic resonance in thallium and thallic oxide”, *Physical Review*, vol. **97**, 1679–1698, Mar 1955.
- [23] P. Coleman, “Heavy fermions: Electrons at the edge of magnetism”, in *Handbook of Magnetism and Advanced Magnetic Materials*, vol. **1**, 95–148. John Wiley & Sons, Ltd, 2007.
- [24] P. Fulde, “Introduction to the theory of heavy fermions”, *Journal of Physics F: Metal Physics*, vol. **18**, no. 4, 601, Apr 1988.
- [25] D. R. Hartree, “The wave mechanics of an atom with a non-Coulomb central field. Part II. Some results and discussion”, *Proceedings of the Cambridge Philosophical Society*, vol. **24**, no. 1, 111–132, Jan 1928.
- [26] V. Fock, “Näherungsmethode zur Lösung des quantenmechanischen Mehrkörperproblems”, *Zeitschrift für Physik*, vol. **61**, 126–148, Jan 1930.
- [27] P. Hohenberg and W. Kohn, “Inhomogeneous electron gas”, *Physical Review*, vol. **136**, B864–B871, Nov 1964.
- [28] W. Kohn and L. J. Sham, “Self-consistent equations including exchange and correlation effects”, *Physical Review*, vol. **140**, A1133–A1138, Nov 1965.
- [29] R. O. Jones and O. Gunnarsson, “The density functional formalism, its applications and prospects”, *Reviews of Modern Physics*, vol. **61**, 689–746, Jul 1989.
- [30] N. Metropolis and S. Ulam, “The Monte Carlo method”, *Journal of the American Statistical Association*, vol. **44**, no. 247, 335–341, Sep 1949.
- [31] D. M. Ceperley and B. J. Alder, “Ground state of the electron gas by a stochastic method”, *Physical Review Letters*, vol. **45**, 566–569, Aug 1980.
- [32] E. Gull, A. J. Millis, A. I. Lichtenstein, A. N. Rubtsov, M. Troyer, and P. Werner, “Continuous-time Monte Carlo methods for quantum impurity models”, *Reviews of Modern Physics*, vol. **83**, 349–404, May 2011.
- [33] J. Gubernatis, N. Kawashima, and P. Werner, *Quantum Monte Carlo Methods: Algorithms for Lattice Models*, Cambridge University Press, 2016.
- [34] W. Metzner and D. Vollhardt, “Correlated lattice fermions in $d = \infty$ dimensions”, *Physical Review Letters*, vol. **62**, no. 3, 324–327, Jan 1989.
- [35] A. Georges, G. Kotliar, W. Krauth, and M. J. Rozenberg, “Dynamical mean-field theory of strongly correlated fermion systems and the limit of infinite dimensions”, *Reviews of Modern Physics*, vol. **68**, 13–125, Jan 1996.

- [36] A. Georges and G. Kotliar, “Hubbard model in infinite dimensions”, *Physical Review B*, vol. **45**, 6479–6483, Mar 1992.
- [37] F. J. Dyson, “The S matrix in quantum electrodynamics”, *Physical Review*, vol. **75**, 1736–1755, Jun 1949.
- [38] N. N. Bogoljubov, “On a new method in the theory of superconductivity”, *Il Nuovo Cimento (1955-1965)*, vol. **7**, 794–805, Mar 1958.
- [39] J. G. Valatin, “Comments on the theory of superconductivity”, *Il Nuovo Cimento (1955-1965)*, vol. **7**, 843–857, Mar 1958.
- [40] G. C. Wick, “The evaluation of the collision matrix”, *Physical Review*, vol. **80**, 268–272, Oct 1950.
- [41] C. E. Shannon, “A mathematical theory of communication”, *The Bell System Technical Journal*, vol. **27**, no. 3, 379–423, Jul 1948.
- [42] E. Schmidt, “Zur Theorie der linearen und nichtlinearen Integralgleichungen”, *Mathematische Annalen*, vol. **63**, no. 4, 433–476, Dec 1907.
- [43] C. K. Majumdar, “Antiferromagnetic model with known ground state”, *Journal of Physics C: Solid State Physics*, vol. **3**, no. 4, 911–915, Apr 1970.
- [44] C. K. Majumdar and D. K. Ghosh, “On next-nearest-neighbor interaction in linear chain. I”, *Journal of Mathematical Physics*, vol. **10**, 1388–1398, Sep 1967.
- [45] I. Affleck, T. Kennedy, E. H. Lieb, and H. Tasaki, “Rigorous results on valence-bond ground states in antiferromagnets”, *Physical Review Letters*, vol. **59**, 799–802, Aug 1987.
- [46] S. R. White, “Density matrix formulation for quantum renormalization groups”, *Physical Review Letters*, vol. **69**, 2863–2866, Nov 1992.
- [47] S. R. White, “Density-matrix algorithms for quantum renormalization groups”, *Physical Review B*, vol. **48**, 10345–10356, Oct 1993.
- [48] U. Schollwöck, “The density-matrix renormalization group”, *Reviews of Modern Physics*, vol. **77**, 259–315, Apr 2005.
- [49] U. Schollwöck, “The density-matrix renormalization group in the age of matrix product states”, *Annals of Physics*, vol. **326**, no. 1, 96–192, Jan 2011, Special Issue.
- [50] C. Eckart and G. Young, “The approximation of one matrix by another of lower rank”, *Psychometrika*, vol. **1**, 211–218, Sep 1936.
- [51] L. Mirsky, “Symmetric gauge functions and unitarily invariant norms”, *The Quarterly Journal of Mathematics*, vol. **11**, no. 1, 50–59, Jan 1960.
- [52] W. Wirtinger, “Zur formalen Theorie der Funktionen von mehr komplexen Veränderlichen”, *Mathematische Annalen*, vol. **97**, no. 1, 357–375, Dec 1927.
- [53] C. Lanczos, “An iteration method for the solution of the eigenvalue problem of linear differential and integral operators”, *Journal of Research of the National Bureau of Standards*, vol. **45**, 255–282, Oct 1950.
- [54] M. B. Hastings, “An area law for one-dimensional quantum systems”, *Journal of Statistical Mechanics: Theory and Experiment*, vol. **2007**, no. 08, P08024, Aug 2007.

- [55] J. Eisert, M. Cramer, and M. B. Plenio, “Colloquium: Area laws for the entanglement entropy”, *Reviews of Modern Physics*, vol. **82**, 277–306, Feb 2010.
- [56] F. Verstraete and J. I. Cirac, “Matrix product states represent ground states faithfully”, *Physical Review B*, vol. **73**, 094423, Mar 2006.
- [57] G. Vidal, “Efficient simulation of one-dimensional quantum many-body systems”, *Physical Review Letters*, vol. **93**, 040502, Jul 2004.
- [58] S. R. White and A. E. Feiguin, “Real-time evolution using the density matrix renormalization group”, *Physical Review Letters*, vol. **93**, 076401, Aug 2004.
- [59] J. Haegeman, J. I. Cirac, T. J. Osborne, I. Pižorn, H. Verschelde, and F. Verstraete, “Time-dependent variational principle for quantum lattices”, *Physical Review Letters*, vol. **107**, 070601, Aug 2011.
- [60] A. J. Daley, C. Kollath, U. Schollwöck, and G. Vidal, “Time-dependent density-matrix renormalization-group using adaptive effective Hilbert spaces”, *Journal of Statistical Mechanics: Theory and Experiment*, vol. **2004**, no. 04, P04005, Apr 2004.
- [61] J. Haegeman, C. Lubich, I. Oseledets, B. Vandereycken, and F. Verstraete, “Unifying time evolution and optimization with matrix product states”, *Physical Review B*, vol. **94**, 165116, Oct 2016.
- [62] A. E. Feiguin and S. R. White, “Finite-temperature density matrix renormalization using an enlarged Hilbert space”, *Physical Review B*, vol. **72**, 220401, Dec 2005.
- [63] F. Verstraete, J. J. García-Ripoll, and J. I. Cirac, “Matrix product density operators: Simulation of finite-temperature and dissipative systems”, *Physical Review Letters*, vol. **93**, 207204, Nov 2004.
- [64] S. Östlund and S. Rommer, “Thermodynamic limit of density matrix renormalization”, *Physical Review Letters*, vol. **75**, 3537–3540, Nov 1995.
- [65] I. P. McCulloch, “Infinite size density matrix renormalization group, revisited”, *arXiv preprint*, 0804.2509, Apr 2008.
- [66] V. Zauner-Stauber, L. Vanderstraeten, M. T. Fishman, F. Verstraete, and J. Haegeman, “Variational optimization algorithms for uniform matrix product states”, *Physical Review B*, vol. **97**, 045145, Jan 2018.
- [67] J. Jordan, R. Orús, G. Vidal, F. Verstraete, and J. I. Cirac, “Classical simulation of infinite-size quantum lattice systems in two spatial dimensions”, *Physical Review Letters*, vol. **101**, 250602, Dec 2008.
- [68] P. Corboz, R. Orús, B. Bauer, and G. Vidal, “Simulation of strongly correlated fermions in two spatial dimensions with fermionic projected entangled-pair states”, *Physical Review B*, vol. **81**, 165104, Apr 2010.
- [69] G. Vidal, “Class of quantum many-body states that can be efficiently simulated”, *Physical Review Letters*, vol. **101**, 110501, Sep 2008.
- [70] A. Messiah, *Quantum Mechanics Volume II*, Elsevier Science B.V., 1961.
- [71] A. Weichselbaum, “Non-abelian symmetries in tensor networks: A quantum symmetry space approach”, *Annals of Physics*, vol. **327**, no. 12, 2972–3047, Jul 2012.
- [72] L. C. Biedenharn and J. D. Louck, *Angular Momentum in Quantum Physics: Theory and Application*, Encyclopedia of Mathematics and its Applications. Cambridge University Press, 1984.

- [73] I. P. McCulloch, “From density-matrix renormalization group to matrix product states”, *Journal of Statistical Mechanics: Theory and Experiment*, vol. **2007**, no. 10, P10014, Oct 2007.
- [74] M. Galassi et al., *GNU Scientific Library Reference Manual (3rd Ed.)*, Release 2.7, 2021.
- [75] C. Hubig, I. P. McCulloch, and U. Schollwöck, “Generic construction of efficient matrix product operators”, *Physical Review B*, vol. **95**, 035129, Jan 2017.
- [76] D. E. Parker, X. Cao, and M. P. Zaletel, “Local matrix product operators: Canonical form, compression, and control theory”, *Physical Review B*, vol. **102**, 035147, Jul 2020.
- [77] G. Guennebaud, B. Jacob, et al., “Eigen v3”, <http://eigen.tuxfamily.org>, 2010.
- [78] A. J. Stace and P. O’Brien, “Fullerenes: past, present and future, celebrating the 30th anniversary of Buckminster fullerene”, *Philosophical Transactions of the Royal Society A*, vol. **374**, 20160278, Sep 2016.
- [79] L. Bergomi, J.-P. Blaizot, T. Jolicoeur, and E. Dagotto, “Generalized spin-density-wave state of the Hubbard model for C₁₂ and C₆₀ clusters”, *Physical Review B*, vol. **47**, 5539–5542, Mar 1993.
- [80] W. Marshall, “Antiferromagnetism”, *Proceedings of the Royal Society London*, vol. **232**, 48–68, Oct 1955.
- [81] S. L. Altmann and P. Herzig, *Point-group Theory Tables*, Oxford science publications. Clarendon Press, 1994.
- [82] Y. Wang, T. Han, Y.-S. Ding, Z. Zheng, and Y.-Z. Zheng, “Sodalite-like rare-earth carbonates: a study of structural transformation and diluted magnetism”, *Dalton Transactions*, vol. **45**, 1103–1110, Jan 2016.
- [83] L. Qin, G.-J. Zhou, Y.-Z. Yu, H. Nojiri, C. Schröder, R. E. P. Winpenny, and Y.-Z. Zheng, “Topological self-assembly of highly symmetric lanthanide clusters: A magnetic study of exchange-coupling “fingerprints” in giant gadolinium(III) cages”, *Journal of the American Chemical Society*, vol. **139**, no. 45, 16405–16411, Nov 2017.
- [84] E. Cuthill and J. McKee, “Reducing the bandwidth of sparse symmetric matrices”, in *Proceedings of the 1969 24th National Conference*, New York, 1969, ACM ’69, 157–172, Association for Computing Machinery.
- [85] M. Oshikawa, “Commensurability, excitation gap, and topology in quantum many-particle systems on a periodic lattice”, *Physical Review Letters*, vol. **84**, 1535–1538, Feb 2000.
- [86] J. Richter, “Localized-magnon states in strongly frustrated quantum spin lattices”, *Low Temperature Physics*, vol. **31**, no. 8, 695–703, Aug 2005.
- [87] R. D. Woods and D. S. Saxon, “Diffuse surface optical model for nucleon-nuclei scattering”, *Physical Review*, vol. **95**, 577–578, Jul 1954.
- [88] V. Zelevinsky and A. Volya, *Physics of Atomic Nuclei*, Wiley-VCH Verlag GmbH & Co. KGaA, 2017.
- [89] N. Schwierz, I. Wiedenhover, and A. Volya, “Parameterization of the Woods-Saxon potential for shell-model calculations”, *arXiv preprint*, 0709.3525 [nucl-th], Sep 2007.
- [90] A. Holt, T. Engeland, M. Hjorth-Jensen, and E. Osnes, “Effective interactions and shell model studies of heavy tin isotopes”, *Nuclear Physics A*, vol. **634**, 41–56, May 1998.
- [91] W. Huang, M. Wang, F. G. Kondev, G. Audi, and S. Naimi, “The AME 2020 atomic mass evaluation (I). Evaluation of input data, and adjustment procedures”, *Chinese Physics C*, vol. **45**, no. 3, 030002, Jan 2021.

- [92] S. Doniach, “The Kondo lattice and weak antiferromagnetism”, *Physica B+C*, vol. **91**, 231–234, Jul 1977.
- [93] I. Titvinidze, A. Schwabe, and M. Potthoff, “Ferromagnetism of magnetic impurities coupled indirectly via conduction electrons: Insights from various theoretical approaches”, *Physical Review B*, vol. **90**, 045112, Jul 2014.
- [94] H. Tsunetsugu, M. Sigrist, and K. Ueda, “The ground-state phase diagram of the one-dimensional Kondo lattice model”, *Reviews of Modern Physics*, vol. **69**, 809–864, Jul 1997.
- [95] A. C. Hewson, *The Kondo Problem to Heavy Fermions*, Cambridge Studies in Magnetism. Cambridge University Press, 1993.
- [96] H. Schmid, J. F. Steiner, K. J. Franke, and F. von Oppen, “Quantum Yu-Shiba-Rusinov dimers”, *Physical Review B*, vol. **105**, 235406, Jun 2022.
- [97] P. Schlottmann, “Magnetic and thermal properties of nanoscale heavy-fermion particles”, *Physical Review B*, vol. **65**, 024431, Dec 2001.
- [98] P. Schlottmann, “Charge- and spin-excitation gaps for a magnetic Anderson impurity embedded in a nanoscale metallic sphere”, *Physical Review B*, vol. **65**, 174407, Apr 2002.
- [99] P. Simon and I. Affleck, “Finite-size effects in conductance measurements on quantum dots”, *Physical Review Letters*, vol. **89**, 206602, Oct 2002.
- [100] G. Franzese, R. Raimondi, and R. Fazio, “Parity-dependent Kondo effect in ultrasmall metallic grains”, *Europhysics Letters*, vol. **62**, no. 2, 264–270, Apr 2003.
- [101] E. Rossi and D. K. Morr, “Spatially dependent Kondo effect in quantum corrals”, *Physical Review Letters*, vol. **97**, 236602, Dec 2006.
- [102] F. Eickhoff, B. Lechtenberg, and F. B. Anders, “Effective low-energy description of the two-impurity Anderson model: RKKY interaction and quantum criticality”, *Physical Review B*, vol. **98**, 115103, Sep 2018.
- [103] A. Schwabe, D. Gütersloh, and M. Potthoff, “Competition between Kondo screening and indirect magnetic exchange in a quantum box”, *Physical Review Letters*, vol. **109**, 257202, Dec 2012.
- [104] A. Schwabe, M. Hänsel, M. Potthoff, and A. K. Mitchell, “Screening mechanisms in magnetic nanostructures”, *Physical Review B*, vol. **92**, 155104, Oct 2015.
- [105] J. Bardeen, L. N. Cooper, and J. R. Schrieffer, “Microscopic theory of superconductivity”, *Physical Review*, vol. **106**, 162–164, Apr 1957.
- [106] J. Bardeen, L. N. Cooper, and J. R. Schrieffer, “Theory of superconductivity”, *Physical Review*, vol. **108**, 1175–1204, Dec 1957.
- [107] N. Y. Yao, C. P. Moca, I. Weymann, J. D. Sau, M. D. Lukin, E. A. Demler, and G. Zaránd, “Phase diagram and excitations of a Shiba molecule”, *Physical Review B*, vol. **90**, 241108, Dec 2014.
- [108] K. G. Wilson, “The renormalization group: Critical phenomena and the Kondo problem”, *Reviews of Modern Physics*, vol. **47**, 773–840, Oct 1975.
- [109] R. Žitko, O. Bodensiek, and T. Pruschke, “Effects of magnetic anisotropy on the subgap excitations

- induced by quantum impurities in a superconducting host”, *Physical Review B*, vol. **83**, 054512, Feb 2011.
- [110] F. von Oppen and K. J. Franke, “Yu-Shiba-Rusinov states in real metals”, *Physical Review B*, vol. **103**, 205424, May 2021.
- [111] E. Liebhaber, L. M. Rütten, G. Reecht, J. F. Steiner, S. Rohlf, K. Rossnagel, F. von Oppen, and K. J. Franke, “Quantum spins and hybridization in artificially-constructed chains of magnetic adatoms on a superconductor”, *Nature Communications*, vol. **13**, no. 1, 2160, Apr 2022.
- [112] J. F. Steiner, C. Mora, K. J. Franke, and F. von Oppen, “Quantum magnetism and topological superconductivity in Yu-Shiba-Rusinov chains”, *Physical Review Letters*, vol. **128**, 036801, Jan 2022.
- [113] M. Ruby, B. W. Heinrich, Y. Peng, F. von Oppen, and K. J. Franke, “Wave-function hybridization in Yu-Shiba-Rusinov dimers”, *Physical Review Letters*, vol. **120**, 156803, Apr 2018.
- [114] L. Yu, “Bound state in superconductors with paramagnetic impurities”, *Acta Physica Sinica*, vol. **21**, 75–91, Apr 1965.
- [115] H. Shiba, “Classical spins in superconductors”, *Progress of Theoretical Physics*, vol. **40**, no. 3, 435–451, Sep 1968.
- [116] A. I. Rusinov, “Superconductivity near a paramagnetic impurity”, *Journal of Experimental and Theoretical Physics Letters (English Translation)*, vol. **9**, 85, Jan 1969.
- [117] S. Nadj-Perge, I. K. Drozdov, B. A. Bernevig, and A. Yazdani, “Proposal for realizing Majorana fermions in chains of magnetic atoms on a superconductor”, *Physical Review B*, vol. **88**, 020407, Jul 2013.
- [118] O. Deb, S. Hoffman, D. Loss, and J. Klinovaja, “Yu-Shiba-Rusinov states and ordering of magnetic impurities near the boundary of a superconducting nanowire”, *Physical Review B*, vol. **103**, 165403, Apr 2021.
- [119] J. von Neumann and E. P. Wigner, “Über das Verhalten von Eigenwerten bei adiabatischen Prozessen”, *Physikalische Zeitschrift*, vol. **30**, 467–470, May 1929.
- [120] F. H. L. Essler, H. Frahm, F. Göhmann, A. Klümper, and V. E. Korepin, *The One-Dimensional Hubbard Model*, Cambridge University Press, 2005.
- [121] I. Titvinidze and M. Potthoff, “Boundary and finite-size effects in the competition between indirect magnetic exchange and Kondo screening”, *Journal of the Korean Physical Society*, vol. **62**, no. 10, 1434–1439, May 2013.
- [122] A. Schwabe, I. Titvinidze, and M. Potthoff, “Inverse indirect magnetic exchange”, *Physical Review B*, vol. **88**, 121107, Sep 2013.
- [123] L. N. Cooper, “Bound electron pairs in a degenerate fermi gas”, *Physical Review*, vol. **104**, 1189–1190, Nov 1956.
- [124] H.-C. Jiang and S. Kivelson, “Electronic pair binding and Hund’s rule violations in doped C_{60} ”, *Physical Review B*, vol. **93**, 165406, Apr 2016.
- [125] P.-G. Reinhard and E. Otten, “Transition to deformed shapes as a nuclear Jahn-Teller effect”, *Nuclear Physics A*, vol. **420**, no. 2, 173–192, May 1984.

- [126] C. A. Büsser, G. B. Martins, and A. E. Feiguin, “Lanczos transformation for quantum impurity problems in d -dimensional lattices: Application to graphene nanoribbons”, *Physical Review B*, vol. **88**, 245113, Dec 2013.
- [127] G. W. Semenoff, “Condensed-matter simulation of a three-dimensional anomaly”, *Physical Review Letters*, vol. **53**, 2449–2452, Dec 1984.
- [128] A. V. Balatsky, I. Vekhter, and J.-X. Zhu, “Impurity-induced states in conventional and unconventional superconductors”, *Reviews of Modern Physics*, vol. **78**, 373–433, May 2006.
- [129] A. Kamlapure, L. Cornils, R. Žitko, M. Valentyuk, R. Mozara, S. Pradhan, J. Fransson, A. I. Lichtenstein, J. Wiebe, and R. Wiesendanger, “Correlation of Yu–Shiba–Rusinov states and Kondo resonances in artificial spin arrays on an s-wave superconductor”, *Nano Letters*, vol. **21**, no. 16, 6748–6755, Aug 2021.
- [130] F. Eickhoff and F. B. Anders, “Strongly correlated multi-impurity models: The crossover from a single-impurity problem to lattice models”, *Physical Review B*, vol. **102**, 205132, Nov 2020.
- [131] L. Schneider, S. Brinker, M. Steinbrecher, J. Hermenau, T. Posske, M. dos Santos Dias, S. Lounis, R. Wiesendanger, and J. Wiebe, “Controlling in-gap end states by linking nonmagnetic atoms and artificially-constructed spin chains on superconductors”, *Nature Communications*, vol. **11**, no. 1, 4707, Sep 2020.
- [132] C. Mier, D.-J. Choi, and N. Lorente, “Calculations of in-gap states of ferromagnetic spin chains on s-wave wide-band superconductors”, *Physical Review B*, vol. **104**, 245415, Dec 2021.
- [133] A. Y. Kitaev, “Unpaired majorana fermions in quantum wires”, *Physics-Uspekhi*, vol. **44**, no. 10S, 131, Oct 2001.
- [134] B. Braunecker and P. Simon, “Interplay between classical magnetic moments and superconductivity in quantum one-dimensional conductors: Toward a self-sustained topological Majorana phase”, *Physical Review Letters*, vol. **111**, 147202, Oct 2013.
- [135] J. Klinovaja, P. Stano, A. Yazdani, and D. Loss, “Topological superconductivity and Majorana fermions in RKKY systems”, *Physical Review Letters*, vol. **111**, 186805, Nov 2013.
- [136] F. Pientka, L. I. Glazman, and F. von Oppen, “Topological superconducting phase in helical Shiba chains”, *Physical Review B*, vol. **88**, 155420, Oct 2013.
- [137] K. Flensberg, F. von Oppen, and A. Stern, “Engineered platforms for topological superconductivity and Majorana zero modes”, *Nature Reviews Materials*, vol. **6**, no. 10, 944–958, Jul 2021.

This thesis was typeset in L^AT_EX. The graphics and visualizations were created using the Matplotlib Python package and Keynote by Apple Inc. The DeepL language tool was employed to enhance the language style. For the captions, the font **TheSans UHH / LucasFonts** was utilized.

List of Publications

- [CP1] R. Rausch, C. Plorin, and M. Peschke, “The antiferromagnetic $S = 1/2$ Heisenberg model on the C_{60} fullerene geometry”, *SciPost Physics*, vol. **10**, 087, Apr 2021.
- [CP2] R. Rausch, M. Peschke, C. Plorin, and C. Karrasch, “Magnetic properties of a capped kagome molecule with 60 quantum spins”, *SciPost Physics*, vol. **12**, 143, May 2022.
- [CP3] R. Rausch, M. Peschke, C. Plorin, J. Schnack, and C. Karrasch, “Quantum spin spiral ground state of the ferrimagnetic sawtooth chain”, *SciPost Physics*, vol. **14**, 052, Mar 2023.
- [CP4] R. Rausch, C. Plorin, M. Peschke, and C. Karrasch, “Matrix-product state approach to the generalized nuclear pairing Hamiltonian”, *Annalen der Physik*, vol. **536**, no. 6, 2300436, Jun 2024.
- [CP5] C. Plorin and M. Potthoff, “Kondo screening and indirect magnetic exchange through a conventional superconductor studied by the density matrix renormalization group”, *Physical Review B*, vol. **110**, 085119, Aug 2024.

Declaration of own contributions

Publication [CP1]: I am a co-author of this publication. I developed the MPO construction and compression algorithm necessary for this project, I engaged in physical discussions and assisted in the publication process. The VMPS computations were performed by R. Rausch and M. Peschke.

Publication [CP2]: I am a co-author of this publication. I developed the MPO construction and compression algorithm necessary for this project, I engaged in physical discussions, did analytical calculations and assisted in the publication process. The VMPS computations were performed by R. Rausch and M. Peschke.

Publication [CP3]: I am a co-author of this publication. I developed the MPO construction and compression algorithm necessary for this project and assisted in the publication process. The VMPS computations were performed by R. Rausch and M. Peschke.


Publication [CP4]: I am a co-author of this publication. I developed the MPO construction and compression algorithm necessary for this project, I engaged in physical discussions, did analytical calculations and assisted in the publication process. I also developed the code for comparison with self-consistent BCS theory. The VMPS computations were performed by R. Rausch and M. Peschke. This publication was featured on the cover of the June 2024 issue of *Annalen der Physik*.

Publication [CP5]: I am the main author of this publication. I developed the code based on an existing project from R. Rausch and M. Peschke, did the VMPS computations on the PHYSnet cluster, performed analytical calculations and interpreted the results. This project was conducted under the supervision of M. Potthoff, whose contributions I gratefully acknowledge.

Eidesstattliche Versicherung

Hiermit versichere ich an Eides statt, die vorliegende Dissertationsschrift selbst verfasst und keine anderen als die angegebenen Hilfsmittel und Quellen benutzt zu haben.

Hamburg, den 23.07.2024


Cassian Plorin